2020

EXPERIMENTAL EVALUATION OF AN RWD VEHICLE WITH PARAMETER EXTRACTION FOR ANALYTICAL MODELING AND EVALUATION

Jon Furlich
Michigan Technological University, jefurlic@mtu.edu

EXPERIMENTAL EVALUATION OF AN RWD VEHICLE WITH PARAMETER EXTRACTION FOR ANALYTICAL MODELING AND EVALUATION

By

Jon Einar Furlich

A DISSERTATION

Submitted in partial fulfillment of the requirements for the degree of

DOCTOR OF PHILOSOPHY

In Mechanical Engineering-Engineering Mechanics

MICHIGAN TECHNOLOGICAL UNIVERSITY

2020

This dissertation has been approved in partial fulfillment of the requirements for the Degree of DOCTOR OF PHILOSOPHY in Mechanical Engineering – Engineering Mechanics.

Department of Mechanical Engineering – Engineering Mechanics

Dissertation Advisor:	***Dr. Darrell L. Robinette***
Committee Member:	***Dr. Jason R. Blough***
Committee Member:	***Dr. Jeremy P. Bos***
Committee Member:	***Dr. James P. DeClerck***
Department Chair:	***Dr. William W. Predebon***

Table of Contents

Table of Figures

Table of Tables

Acknowledgements

"if I have seen further, it is by standing on the shoulders of giants." – Sir Isaac Newton

Throughout my journey I have stood on the shoulders of many giants and learned valuable lessons along the way. To thank everyone would be an impossible feat which I will foolishly attempt to summarize here. My journey began with a gentle nudge from Dr. William Shapton that I should seriously consider going to graduate school. Not only did he provide the initial push, Dr. Shapton was an inspirational teacher and immaculate storyteller I am grateful to have met. Chuck Van Karsen pushed me to think more (because it's not optional) but also see the forest for the trees. I learned so much about experimental testing and analytical predictions from Chuck, yet I don't think I could soak up all his teachings even if I had another decade of graduate school. Dr. Jason Blough has been a fountain of knowledge both in academics and in life. His tireless efforts allowed me to conduct research, travel to domestic and international conferences, and exemplified what it's like to balance family and academics together. Dr. Darrell Robinette has been a mentor since I was a Sophomore at Michigan Tech before he returned to become a professor. Through the years he has been an amazing teacher and inspiration which I have the pleasure to call my advisor and friend. Also, a thank you to all my other committee members for their patience and the MEEM staff for their support along the way.

Many people ask me how I could stand staying in school so long. The answer is easy, I had incredible friends and colleagues to keep me motivated and enjoy time outside of the lab. Weekend trips to the local brewery, winter broomball, summer softball, camping in the Keweenaw, and hiking Isle Royale allowed for much needed relaxation aside from work. Such events would not have been possible without the amazing friends I met while in graduate school to balance work and play.

Finally, I would be nowhere if it wasn't for the amazing family I was born into. Thank you to my mother and father for your endless support and love. Also, to my older siblings for providing encouragement and sanity through the years.

Definitions

2WD	Two Wheel Drive
4WD	Four Wheel Drive
BPF	Band Pass Filter
BSFC	Brake Specific Fuel Consumption
CAE	Computer Aided Engineering
DOF	Degree(s) of Freedom
EKF	Extended Kalman Filter
EPA	Environmental Protection Agency
FWD	Front Wheel Drive
ICE	Internal Combustion Engine
LVDT	Linear Variable Displacement Transducer
ODS	Operational Deflection Shape
ROM	Reduced Order Model
RPM	Revolutions Per Minute
RWD	Rear Wheel Drive
SB	Throttle Stab Event
ST	Seat Track
STFT	Short Time Fourier Transform
TC	Torque Converter
TCC	Torque Converter Closed
TCO	Torque Converter Open
Thr/r	Dyno Road Load Simulation Mode
Thr/v	Dyno Velocity Mode
TI	Tip In
TIS	Transmission Input Speed
TISS	Transmission Input Speed Sensor
TITO	Tip In Tip Out Testing
TO	Tip Out
TOS	Transmission Output Speed
TOSS	Transmission Output Speed Sensor
TOSSd	Transmission Output Speed Sensor Derivative
TWVDV	Torque Weighted Vibration Dose Value
VDV	Vibration Dose Value
WBV	Whole Body Vibration

Abstract

This study was conducted to perform experimental vibration testing on a light duty rear wheel drive vehicle. The vehicle is known to have excessive longitudinal acceleration response perceived after step changes in the driver torque command. The excessive response includes shuffle and clunk transients. Experimental testing was performed to understand the coupling between driver torque commands and peak shuffle oscillations. Data was also targeted to understand the coupling between driveline torsional oscillations and longitudinal vehicle vibrations. This data was also used to establish vehicle parameters for use in an analytical CAE model of the driveline and coupling. Driver applied tip-in and tip-out transients were captured with road testing on a rear wheel drive dynamometer test rig. Transducer signatures were captured during testing to estimate backlash size, shuffle frequency, and the influence of vehicle speed or gear. The data successfully extracted the shuffle frequency in 3^{rd}-6^{th} gear. Vehicle parameters extracted were used to assemble a CAE model with correlation <7.5% of measured data. It also indicated that there is a stiffness asymmetry contributing to the shuffle mode not explicitly documented and necessary for shuffle modeling. The data also extracted backlash size estimates for 3^{rd}-6^{th} gear within design specifications of tolerance stack-up. The estimates were derived from both static and in-situ testing. Experimental testing was used to understand coupling in the driveline torsional oscillations with longitudinal vibrations for improved model understanding and estimates for improved vehicle response to shuffle.

Body of Work

This dissertation is broken up into five major chapters. It begins with Chapter 1 outlining the introduction and motivation. This is followed by the four core chapters, each including the major contributions from this body of work. Chapter 2 will focus on a detailed analysis of shuffle excitation with clunk. It begins by analyzing data collected with an experimental test vehicle while driving on a controlled road segment. The chapter later transitions into a controlled lab environment where test maneuvers were replicated on a dynamometer test platform. Chapter 3 includes analysis of both the road and laboratory test data with an emphasis on estimating the shuffle frequency and overall vehicle backlash size in various fixed gear states. Chapter 4 details a new technique for vibration dosage based off ISO2631 for objective quantification of the shuffle transient severity. Finally, Chapter 5 concludes with development of an analytical model that was used to understand parameter modifications to the driveline and their implications in shuffle and clunk severity.

1. Introduction/Motivation

Passenger vehicles have many stakeholder needs including but not limited to passenger capacity, load haul capacity, acceleration requests, vehicle handling, vehicle comfort, and EPA fuel requirements. In efforts to meet this stakeholder needs, vehicles have been trending towards powertrain packages with higher energy densities with lower drivetrain inertia and body mass. The number of onboard sensors continues to increase to monitor vehicle health and manage these complex vehicle control processes. Manufacturers must

balance the use of onboard sensors and controls to improve vehicle handling and meet stakeholder needs.

Rear wheel drive (RWD) is a common vehicle architecture used for light duty passenger trucks. This architecture has a driveline consisting of a primary power source, primary drive ratio, driveshaft, final drive ratio, axle shafts, and wheels. The test vehicle in this study has an RWD architecture driven by an internal combustion engine (ICE). A recent trend in manufacturing includes downsizing ICE's to meet EPA fuel requirements along with forced air induction. The act of downsizing with forced air induction increases power output while decreasing overall mass and rotating inertia.

Downstream of the ICE is the primary gear ratio or transmission assembly. The transmission is paired with the ICE to keep the engine operating within its most efficient revolution per minute (RPM) range according to brake specific fuel consumption (BSFC) mapping. Multiple forward gear ratios are used to keep vehicles within this optimal range. These lead manufactures to use transmissions with upwards of 8-12 forward gear ratios packaged into one transmission assembly. Multiple rotating and braking clutch elements are necessary to couple an array of planetary gear sets to achieve such high number of forward gear ratios. The high number of onboard sensors are used to monitor internal stages as well as control the clutching elements for seamless shifting and improved vehicle vibration response.

The driveshaft is a necessary coupling element to traverse the length of the RWD vehicle. It is a critical element that must be stiff enough to handle high torque outputs from the engine and transmission while being light weight for improved efficiency. Similar requirements are observed in the axle shafts and wheels. The combined driveline from engine to wheels makes up the un-sprung mass of the vehicle while the vehicle body sits atop the suspension as the sprung mass of the vehicle.

During operation, drivers apply pressure to throttle or brake pedals. Application of the throttle pedal is a positive torque request while application of the brake pedal is a negative torque request. The onboard controllers interpret the driver requests and convert them into control demands for the driveline components. Any change in torque will induce a transient response on the vehicle driveline. The transient response will propagate through driveline components and coupling elements between the un-sprung and sprung mass. The driver and passengers can hear and feel artifacts of the propagated transient response.

Humans perceive the vibration and acoustic signatures based on frequency and amplitude of the signature. Overall, the driver requests torque from the vehicle and perceives the response in a positive or negative manner based on the physical response of the vehicle. When viewed from the source-path-receiver paradigm; the engine and/or road are *sources* that transfer through driveline and suspension components as the *path* before being absorbed by the driver and/or passengers whom are *receivers.*

The increased power density of ICE's lead to high ramp rates in torque delivery. The onboard controller will taper driver requested torque to avoid excessive vibration generation in the engine. This in turn reduces source excitation of the vehicle modes such as shuffle, shudder, boom, moan, clunk, rattle, etc. Recent trends use reduced order control

models to mitigate such transient vibrations. This is achieved through anti-jerk control in a reduced order model which relies on physical vehicle parameters. The accuracy of the model will in turn correlate to the accuracy of the control. It is important that values for frequency, damping, and lash are measured and initialized in the model for each individual vehicle.

This study aims to fully investigate the transient phenomenon induced during changes in driver requested torque on a rear wheel drive vehicle. It experimentally captured transient events on road and transitioned into laboratory-controlled testing. The on-road testing was used to combine past measurement techniques into one assembly for a high-level understanding of shuffle with clunk. This was achieved with additional sensors supplementing onboard production vehicle transducers (i.e. wheel speed sensor, vehicle speed, etc.). All the measurements were combined into one data acquisition platform and used to evaluate the propagation and response of the system. The major aim of this high-fidelity data acquisition was to publish resulting transients at a combined level never documented before. The combined measurements also confirm coupling between torsional driveline response and the longitudinal body response attributed to shuffle. The data quantifies the torque ramp rates achieved due to ICE downsizing, changes in response due to variations in calibration as well as gear state to support the creation of a more effective control model.

An improved control model was achieved by extracting vehicle parameters such as the tip-in and tip-out shuffle frequency along with overall vehicle backlash size from the data. Previous studies have evaluated driveline models to estimate the shuffle frequency but make no note to the differences in tip-in or tip-out behavior. Past research also claims to evaluate backlash size but lack a rigorous discussion of signal processing and in-situ measurement of this parameter. Both the shuffle frequency and backlash size were measured with road and laboratory testing. The data proved there is a change in shuffle frequency from tip-in to tip-out excitation. This is understood as stiffness and damping asymmetries in the driveline. The in-situ data also proved useful in the extraction of driveline backlash size derived from in-situ data. These parameters were then used for tuning of a reduced order model. The tuning improves accuracy and performance of the ROM controller. The Vibration Dose Value metric is used to classify transient events as an industry standard [1]. This metric can be used to correlate transient events but lacks high correlation due to road/chassis noise inputs in the measurement. This study is interested in vibrations induced by ICE torque transients and thus an improved metric was developed to correlate these results. The improved metric applies a torque weighting to the VDV for improved correlation due to transient torque maneuvers. The new metric was evaluated in a simulation environment. The simulation allows for modeling of the system with perturbed vehicle parameters to observe improvements in the response quality based off the proposed dosage metric. Results of the parameter perturbation yielded an improved response to changes. The results are optimized with an increase in effective transmission stiffness with decreased torque converter clutch stiffness.

2. Transient Shuffle with Clunk Response

1. Literature Review

The passenger vehicle in this study is primarily concerned with shuffle and clunk excitation induced by changing driver torque requests. Shuffle and clunk are two of the common vehicle modes with frequency ranges shown in Figure 1 based on a compiled review of published values. Tip-in (TI), tip-out (TO), or consecutive tip-in followed by tip-out (TITO) induce torque requests which take the shape of step function inputs on the driveline. TITO maneuvers are understood to excite shuffle and consequential clunk if lash is traversed during a torque reversal Such a reversal indicates a change in contact region of the geared components [2-7]. Clunk is defined by two categories, both with broadband frequency response. Each range is caused by lash component impacts; the lower range relating to booming within the vehicle cabin while the higher range consists of metallic impact on geared components. These two modes are studied together because clunk is excited by shuffle events such that the two are in lock step with one another. Therefore, the mitigation of shuffle or damped lash crossing is aimed at reducing clunk as well.

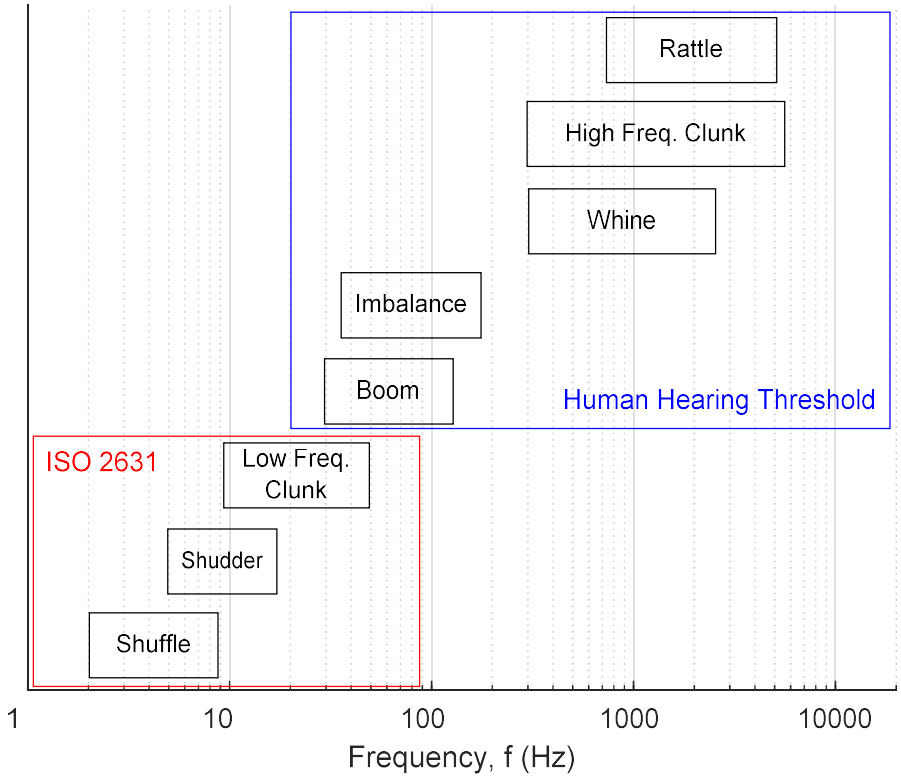

Figure 1: Common Vehicle Modes and Frequency Ranges According to Literature [2-4, 6-41]

The study of shuffle has been performed with multiple degree of freedom models to identifying the mode shape [4, 42-44], run analytical sensitivity studies [2, 6, 13], evaluate contact friction between tire and road surface [42], and torque shaping [6]. In the past,

literature agrees that shuffle is considered the lowest frequency non-rigid body mode of a lumped driveline system [2-5, 7, 13, 45]. The mode shape is depicted as a damped torsional mode of the driveline with peak oscillation at the lumped engine element getting smaller in amplitude progressing towards the wheels show in [4, 5, 44]. Further examination of the mode shape shows the engine, transmission, driveshaft, differential, half-shafts are all in phase while the wheel/tire lumped element has a phase lag relative to the rest of the driveline [4, 5].

It has been identified that the shuffle mode damping is dominated by torque converter slip in vehicles equipped with an automatic transmission [4] or controlled clutch slip in a manual transmission (MT) vehicle [2]. This is intuitive when examining the shuffle mode shape noting that the highest relative twist occurs near the engine and transmission lumped components. Therefore, higher relative velocity of such components leads to additional damping in the system. Slipping the MT clutch or torque converter (TC) clutch has a negative impact on vehicle fuel economy, albeit temporarily. Thus, controlled slip is desired to mitigate shuffle excitation while optimizing for fuel economy.

Past literature also notes that the shuffle mode is responsible or accompanied with fore-aft or longitudinal vibrations in the vehicle body [2, 4, 7, 13, 45]. The longitudinal direction complies with SAE Standard J670 as the X-axis of the vehicle [46-48]. Any further reference of longitudinal or X-axis will be used interchangeably in the document. One study argues that shuffle is only related to driveline torsional oscillations whereas the longitudinal motion is considered shunt. Most of the literature assume the torsional and longitudinal acceleration are combined. Many studies note that driver perception of such a longitudinal vibration can be analyzed by capturing seat track vibration [3, 7, 13, 49]. The use of seat track vibration for passenger evaluation presents a lack of physics involved in previous shuffle modeling. Previous studies have limited to no coupling of torsional oscillations of a driveline model into linear oscillations of the seat track. Some studies verify correlation in the vibration response between driveline components and seat track acceleration however, current models lack a compliance mechanism between the two.

Recent studies focus on utilizing similar torsional models for reduced order modeling to perform model based control [32, 50-54]. The utilization of a plant model for control assumes that the torsional model captures all necessary physics. Therefore, components may be reflected and summed into a lower number of lumped elements. There will be questionable accuracy if the torsional driveline model is indeed missing an important compliance element between torsion and linear displacement. Recent models mitigate this error by using an extended Kalman filter (EKF) to update lumped system parameters for improved model performance. The author notes that the need for EKF and parameter updating can be improved if the initial system model captures all relevant physics and will converge to low errors sooner with updated elements. Such a convergence study is outside the scope of this document but can followed up in future experiments.

There is disagreement in the literature whether coupling exists between torsional oscillations and longitudinal vibration during shuffle. This study will use the high-fidelity data acquisition with multiple transducers to measure and observe this correlation. The data will also expand on the shuffle response with respect to a tip-in or tip-out induced shuffle

event. It will further observe the influence of a slipping TC clutch and peak acceleration amplitude to draw conclusions on driveline damping. It will finish by using an experimental test apparatus to confirm the results observed on road. The on-road results contain controlled slip and will be compared to a binary locked or unlocked TC clutch analysis.

2. Road Test Apparatus and Procedures

Current literature describes shuffle as the first torsional mode of the driveline that couples with longitudinal vibration of the vehicle body. This coupled modal response is excited by a torque transient requested by the vehicle controller. An assortment of transducers was used to experimentally capture the source and response of shuffle in a fashion like previous studies but with a higher number of measurement locations. These locations are observed in Figure 2 with accelerometers depicted as red triangles, strain gauges depicted as blue diamonds, speed sensors depicted as yellow lightning bolts, and green rectangles depicting microphones. Figure 2 shows an image of the rear wheel drive passenger vehicle used for testing in this study. It has an outline of the vehicle frame with the driveline inside. Two brown boxes overlaid depict locations inside the vehicle body where measurements were taken. Images of the experimental vehicle(s) are found in Appendix A: Test Vehicle and Instrumentation Figures.

The excitation, or source, is captured by measuring the driver requested throttle position and corresponding controller output torque estimate. Both of these signals are measured on the vehicle CAN bus system in accordance with SAE J1939 [55]. The influence of torque input rate and magnitude is studied by capturing the driver requested and controller interpretation of output torque. The shuffle and clunk response were captured by measuring reaction torque on the propeller shaft. This measurement was used to observe torque propagation and estimate when lash components make contact. Rotating speed was measured on the flexplate (representing engine speed), transmission input, output and intermediate gears, the differential ring gear, and rotating speed of the wheels. Measurement of these rotating speeds was used to study how shuffle propagates, initiates clunk, and the phase relationship between different rotating components. The body vibration response was measured with accelerometers mounted on the transmission, differential, frame, seat track, and seat pad. The seat track measurement captures how the driver feels vibration. It also is used to show correlation between rotating oscillations in the driveline and vibrations in the vehicle components. The acoustic response was measured in the differential and in the body of the vehicle. This measurement observes the clunk impact response when gears in the differential impact one another during lash traversal.

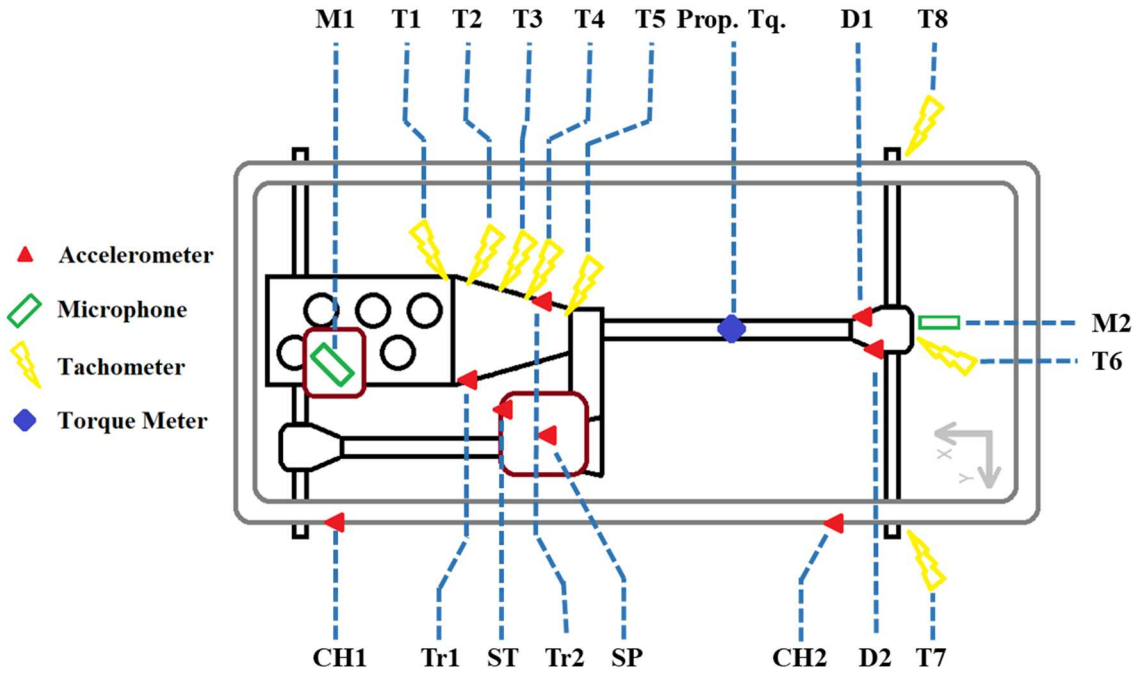

Figure 2: On Road Experimental Test Vehicle Measurement Locations

Table 1: Road Experimental Sensor Descriptions

Abbreviation	Measurement	Transducer
Tr1	Accelerometer	PCB356A15
Tr2	Accelerometer	PCB 356A15
D1	Accelerometer	PCB 356A15
D2	Accelerometer	PCB 356A15
CH1	Accelerometer	PCB 356A15
CH2	Accelerometer	PCB 356A15
ST	Accelerometer	PCB 356B41
M1	Microphone	PCB 130D20
M2	Microphone	PCB 130D20
T1	Tachometer	Honeywell 3015A17
T2	Tachometer	Ford P# DY1400
T3	Tachometer	Ford P# 7M183
T4	Tachometer	Ford P# DY1406
T5	Tachometer	Ford P# DY1379
T6	Tachometer	Honeywell 3015A17
T7	Tachometer	Ford P# BRAB412
T8	Tachometer	Ford P# BRAB532
Prop. Tq.	Strain	VPG CEA-13-062UV-350 *See Appendix A

Signals available on the CAN bus contain poor signal quality with regards to supplemental signals installed with the data acquisition. They lack anti-aliasing filters, have no absolute time synchronization, have lower quantization bit numbers, and are measured at a slower sample rate [56]. All other signals mentioned and shown in Figure 2 were sampled at 8192 Hz while the CAN signals were sampled at 248 Hz. These sample frequencies are high enough to measure clunk and shuffle frequencies depicted in Figure 1. Given Shannon's sampling criteria, the data sampled at 248 Hz is not capable of capturing the high frequency clunk response and was not processed for the influence of clunk. A description of the sensors available and used in Figure 2 are available in Table 1

The test vehicle was driven on a straight test track during various operating conditions. The testing profile included a sequence of consecutive tip-in (TI), tip-out (TO) and throttle stabs (a rapid tip-in and tip-out within one second of each other). The tip-in, tip-out (TITO) maneuvers were used to excite shuffle and clunk in the vehicle. They were conducted in various fixed gear states and centered around a target vehicle speed described in Table 2. There are ten combinations created with the target speed and gear number. The document will further refer to these ten combinations as runs 1-10. The run numbering starts with the top left working down each row before proceeding to the next column.

The center target vehicle speed means that during testing the vehicle velocity dropped below the target velocity a set amount before TI. Once the vehicle accelerated to an equivalent amount above the target velocity, the throttle was tipped-out and coasting followed. At the target velocity an SB event was excited before coasting again to the set amount below target speed. This maneuver can be observed in Figure 3.

Table 2: Test Run Speeds and Corresponding Gear Ratio with (Forward Gear Number Sequence)

	Target Speed [kph]		
	[56]	[73]	[88]
Transmission Ratio (Gear #)	2.14 (3)	2.14 (3)	
	1.76 (4)	1.76 (4)	1.76 (4)
	1.52 (5)	1.52 (5)	1.52 (5)
		1.27 (6)	1.27 (6)

The vehicle was equipped with different calibration modes from the manufacturer. These two modes are referred to as Normal and Sport mode. The difference in these two calibrations is proprietary to the manufacturer and each mode was tested to measure the vehicle response and subsequent changes in each mode. The vehicle also had selectable four-wheel drive (4WD) which was engaged and tested in sport mode. An additional ~225 kg of payload was mounted in the bed of the vehicle and the corresponding response was measured. These four test conditions; Normal 2WD mode, Sport 2WD mode, 4WD Sport mode and Loaded 2WD Sport Mode, were all setup and used to conduct all 10 tests according to Table 2. Each test included upwards of one-minute worth of data with multiple TITO events in each gear state, target velocity, and mode. The various vehicle speeds are

analyzed to determine if there is a difference in shuffle/clunk response at different boundary conditions. The different calibration modes are used for the same purpose to understand their influence on the response with no changes to the hardware.

3. Road Transient Analysis

In-situ road data was collected for test conditions shown in Table 2. This includes data for all four vehicle calibration modes. An example result is shown in Figure 3 for third gear or a transmission ratio of 2.146, while targeting a center speed of 56 kph. The figure depicts a driver throttle input signal for % application with a dotted black line. The solid orange line denotes actual vehicle speed with the dashed black line indicating the target center speed. There are green and orange highlighted sections which highlight TITO and throttle stab events respectively. A throttle stab event is inherently a TITO event, with the distinction that it has a pulse width of less than one second.

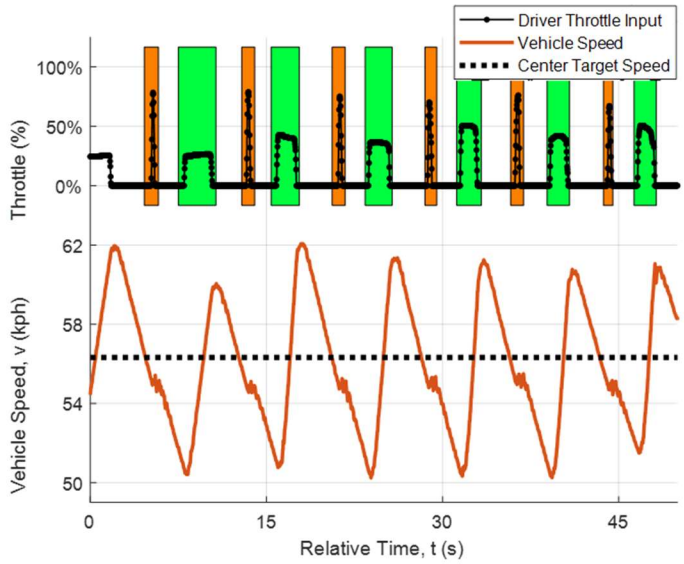

Figure 3: TITO Testing in Third Gear at Target 56 kph Center Speed, Normal Mode with 2WD

It is shown in Figure 3 that the vehicle increases in speed during TI events then begins to decrease in speed when the throttle is no longer applied. During the coast down event, pre and post throttle stab, the vehicle exhibits a similar linear decrease in speed. It exhibits a short transient reaction to the throttle stab that will be further investigated along with the tip-in and tip-out locations. The overall vehicle response is understood with the generalized road load equation represented by Equation 1. In Equation 1, F_0, F_1, and F_2 represent the vehicle mass, rolling resistance with drivetrain losses, and drag coefficients respectively. m is the vehicle mass, g is the acceleration due to gravity, φ is the road grade $I_{eff}$is the effective inertia, $\ddot{\theta}$ is the axle acceleration, and $\ddot{x}$ is the vehicle acceleration.

$$m\ddot{x} = F_0 + F_1\dot{x} + F_2\dot{x}^2 + mg\sin\varphi + I_{eff}\ddot{\theta} \qquad \text{Equation 1}$$

A truncated time trace of the vehicle velocity is shown in Figure 4 which breaks down the TITO maneuver into sections. Each section is enclosed with a letter above with grey dashed

lines on either side. An increase in vehicle velocity is shown for section A and is referred to as a drive event. There are two drive sections denoted with the letter A and it is observed that each share a similar positive slope. After the drive events there is a consecutive TO of the throttle or drive to coast maneuver. This happens where the slope of the velocity transitions from positive to negative. During this transition, all the driveline lash components transition from the drive contact side to the opposing coast contact side. In section C, the vehicle is decelerating due to the vehicle road loads, grade, and inertias according to Equation 1. Next is the throttle stab event in section D that appears to flatten out the slope of the velocity momentarily. The last section is E corresponding to a coast to drive transition, or TI, which flattens out the velocity slope for a short duration. The relative time for TI is shorter than the TO time. This is observed by comparing the delta time for transition in B to the delta time in transition E. In section B, the duration of time is reliant on the road grade along with effective inertia. The short duration of E is dependent on the driver requested torque. The relative magnitude of available driver requested torque (>300 Nm at the engine) is much greater than the road load torque during coasting (<40 Nm at the engine). Therefore, section E will be observed in shorter durations of time than B. This indicates that lash is crossed faster (in the time domain) as well. The rapid lash crossing in B, D, and E are controlled by the engine torque calibration. Understanding of these maneuvers are used to extract the system parameters for a ROM to control this lash crossing.

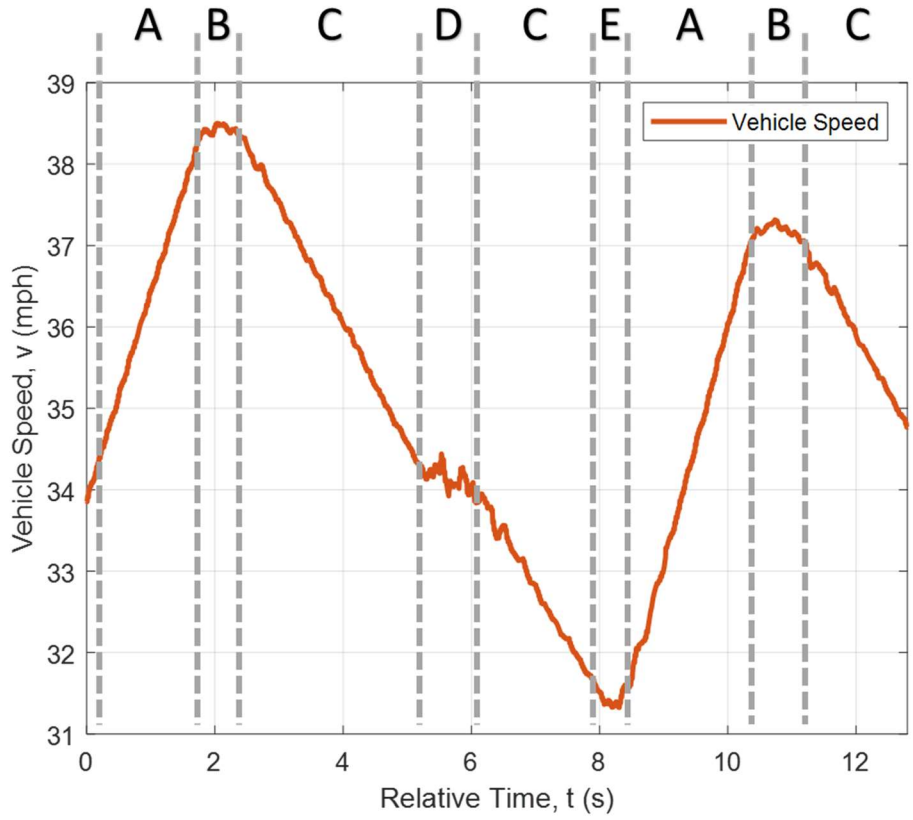

Figure 4: Vehicle Velocity Sections for A - Drive, B - Drive to Coast (or TO), C – Coast, D - Throttle Stab (or SB), and E - Coast to Drive (or TI)

The data is further discriminated in Figure 5 to show how the different driveline rotating components respond to a TITO and throttle stab event. It is common practice to compare the different rotating components on the same plane. This requires projecting or scaling the speed to match as if they were measured at the same location. This scaling is described in Equation 2 for n intermediate gear ratio elements i.

$$\omega_{projection} = \omega_{original} * \sum i_n \quad \text{Equation 2}$$

The experimental vehicle is equipped with ten forward transmission gear ratios and one final drive ratio, though only four of these gears identified as gears of interest by the sponsor will be analyzed in depth for this study. The wheel speeds and differential ring gear speeds (denoted as ω_{Road}) are all on the same relative plane. They each must be scaled by both the final drive ratio and transmission ratio to project onto the transmission input speed (TIS) plane as described by Equation 3.

$$\omega_{Road\ proj.\ TIS} = \omega_{Road} * \left(i_{transmission} + i_{final\ drive\ ratio}\right) \quad \text{Equation 3}$$

The transmission output speed is only scaled by the transmission gear ratio as described by Equation 4. Any intermediate transmission speeds are scaled by their kinematic intermediate ratio relative to the input speed in Equation 5.

$$\omega_{TOS\ proj.\ TIS} = \omega_{TOS} * i_{transmission} \quad \text{Equation 4}$$

$$\omega_{Int,\ proj.\ TIS} = \omega_{Int.} * i_{Int.} \quad \text{Equation 5}$$

The original shaft speeds are displayed in Figure 5 which depicts the engine and TIS speeds as blue and dashed red lines respectively. They lie on the same plane when the torque converter (TC) clutch is fully locked up. There are slight deviations in the two when controlled slip occurs in the TC clutch based on calibration of the system. This slip appears to occur only at transient events such as TITO or throttle stab locations. The Transmission Output Speed (TOS) is depicted as a solid yellow line and appears as an intermediate plane between the road plane and the TIS plane. The road plane contains the differential ring gear speed as a purple line with upward triangle markers, along with the driver wheel speed as a solid green line with circle markers, and passenger wheel speeds as a solid light blue line with diamond markers.

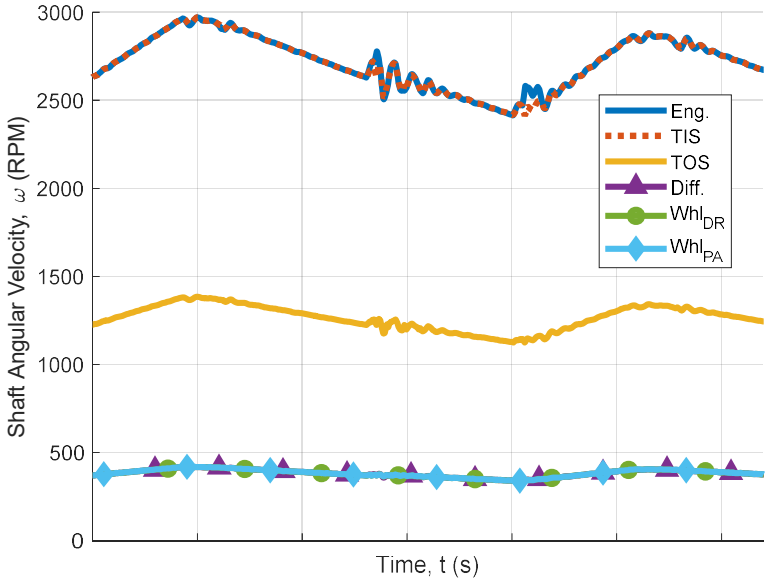

Figure 5: Rotating Driveline Response to TITO Testing in Third Gear at Target 56 kph Center Speed, Normal Mode with 2WD without Projection onto the Same Plane

After projecting each speed onto the same plane using Equation 3 & Equation 4, the result is shown in Figure 6. The line and marker type are the same as Figure 5 which makes all the speed sensors line up on top of one another during sustained positive or negative acceleration. The sensors deviate from one another during transient TITO or throttle stab events indicating shuffle.

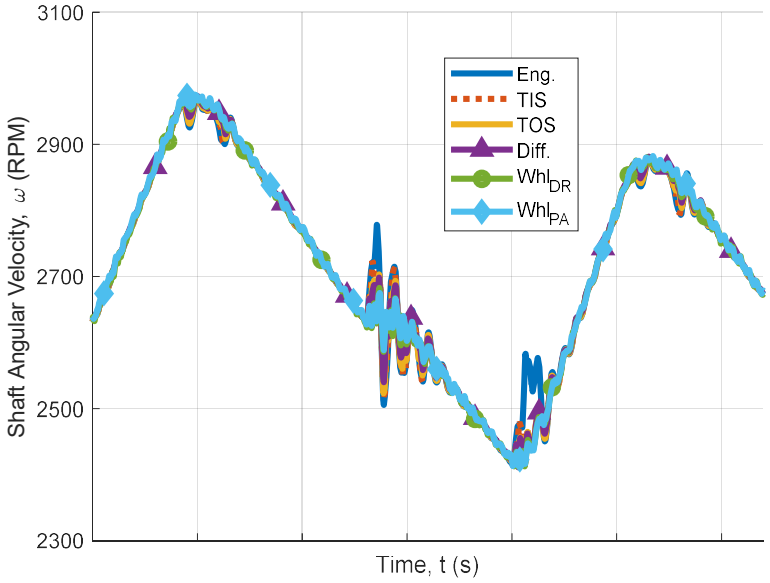

Figure 6: Rotating Driveline Response to TITO Testing in Third Gear at Target 56 kph Center Speed, Normal Mode with 2WD after Projection onto the TIS Plane

The literature review notes that shuffle is expected anywhere between 2-9 Hz as shown in Figure 1. Literature also notes that shuffle is the first torsional oscillating mode coupled with longitudinal vibration on the vehicle body. The shaft speeds should be in phase with one another with the exception of the wheel speeds as noted in [4, 5, 44]. To identify this mode, a Band Pass Filter (BPF) is applied to the data to remove the DC offset and high frequency noise from engine torque oscillations or road inputs into the shaft speed measurements. This BPF result is depicted in Figure 7 along with dashed boxes of dark red, dark blue and dark pink representing tip-in (TI), tip-out (TO), and throttle stab (SB) respectively. The relative time scale shows that for these maneuvers in third gear, 56 kph target, normal mode 2WD, the transient time for TI and TO decays is less than 1.5 seconds while the stab transient decays in less than 2.5 seconds.

The peak oscillating response is observed in the engine and transmission input speeds after a throttle stab excitation. The TI transient has a lower peak oscillation relative to the SB but is greater in amplitude than the TO transient.

It is also observed that the SB response appears as a single transient with rapid buildup of amplitude and logarithmic decay after the throttle is released. The TI event has three similar amplitude oscillations before a logarithmic decay. When cross referencing this TI event in Figure 6 it is shown that the engine speed is higher than the TIS indicating that the TC clutch is slipping during TI. The time of controlled slip corresponds with the three equal oscillation amplitudes followed by the peak at clutch lock up and decay following. The TO event is most interesting as it appears to exhibit two separate transient events. Referencing back to event B in Figure 4, it is understood that there is an initial release of the throttle followed by a slow lash transition from drive lash contact to coast lash contact. The slow

transition allows the first transient to occur at throttle release then the second transient corresponds to the lash impact.

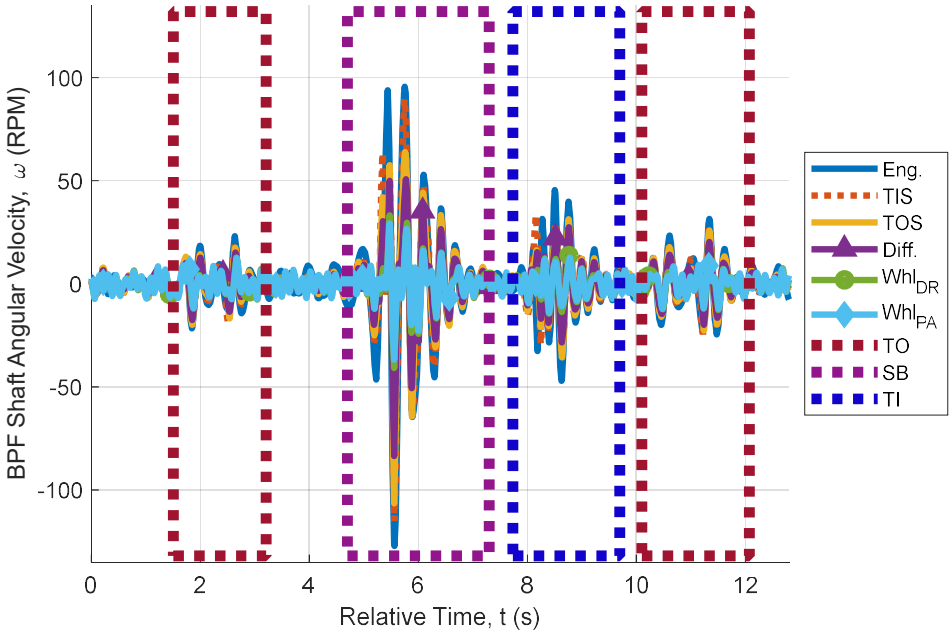

Figure 7: BPF Result of TITO Response with Truncated Sections Denoting TO, SB, and TI Trigger Indications

A short time Fourier transform (STFT) was applied to the time data to identify the instantaneous frequency content of each transient event, note any changes in peak frequency content amplitude, and look for broadband excitation indicative of clunk. The STFT is applied to different signals according to Equation 6 [57, 58]. The application of the STFT yields a spectrogram of frequency data G_g that is a function of both the time shift τ and the time period $N\Delta t$ or T windowed for the transform.

$$G_g(k\Delta f, \tau) = \frac{2}{N}\sum_{n=0}^{N-1} g(k\Delta t)w(k\Delta t - \tau)e^{-2j\pi kn/N} \quad \text{Equation 6}$$

The spectrogram for the TIS signal was calculated according to Equation 6 using a period of 0.75 seconds with overlapped averages following processing recommendations laid out in [59]. The criteria for the maximum number of consecutive overlaps to be averaged together should match the inequality given in Equation 7.

$$\#\ of\ avgs. = ceil\left(\frac{1}{1 - \%\ Overlap}\right) \quad \text{Equation 7}$$

The result is shown in Figure 8 which display's the shaft signal in dashed red along with the corresponding averaged spectrogram containing logarithmic frequency along the y-axis, relative time along the x-axis and dB re 1 RPM in the z-axis. Around 40 Hz there appears to be a solid line in the spectrogram increasing then decreasing like the shaft speeds

shown in Figure 6. This shows the first order line of TIS or Engine speed which is expected to be a dominant order observed in the frequency domain. The spectrogram also shows what was initially observed in the time domain with low frequency (<10 Hz) content induced by shuffle oscillations.

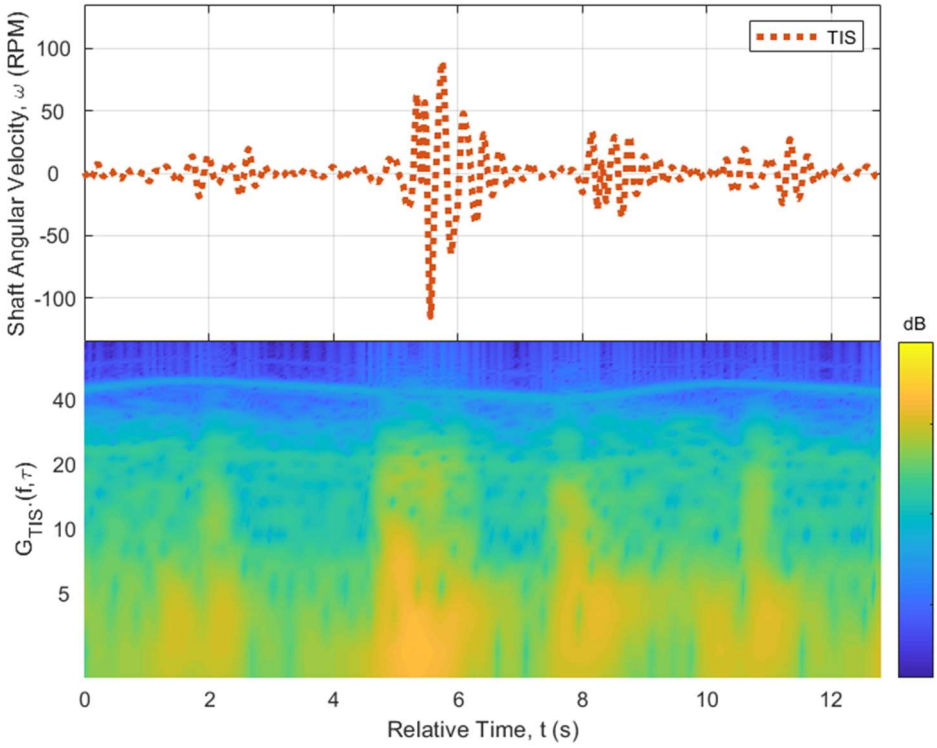

Figure 8: TIS Filtered Shaft Speed and Corresponding Averaged Auto Power Spectrogram

The TO events show two separated spikes in response in the 2-7 Hz range, once when the throttle is let off and the second follows when lash is crossed, and the vehicle enters a coast event. The second spike in amplitude with the TO event appears with more broadband content that is impulsive and expected for the impact created from lash crossing. The TI event around eight seconds shows an impulsive spike with low frequency content in the 2-7 Hz range following the transient decay. The SB event also shows similar behavior to the TI event but with a peak in amplitude around 3 Hz at the highest amplitude of all events as expected from the time domain observations. The peak frequency response shown in all the transient events is indicative of shuffle and the broadband spikes also indicate a low frequency clunk based off the shaft speed sensors.

As a function of Shannon's sampling criteria applied to the STFT, frequency resolution increases with larger time periods. If a larger time period was utilized with the STFT processing, the resulting spectrogram will be able to track the instantaneous frequencies at higher fidelity. This comes with a tradeoff due to the transients spaced together close in time, a larger time period will capture frequency content from two events. Therefore, windows are created around the TI, TO, and SB events of interest to separate from one

another according to the time boxes in Figure 7. By truncating separate events and evaluating the maximum observed or instantaneous frequency f while plotting at a relative time shift τ as done in Figure 9. The overlaid data-points represent the maximum frequency for TI, TO, and SB events as red circles, green stars, and black upper triangles respectively. Based on Figure 9 it appears that the peak frequency content during TI events has a higher frequency of oscillation compared with the TO transient. The SB event is dominated by low frequency content but shifts higher in frequency as the transient decays. These changes in frequency from TI to TO will be further evaluated in later sections. Overall, the frequency content is consistent with shuffle, but the mode shape and propagation of longitudinal acceleration must be confirmed.

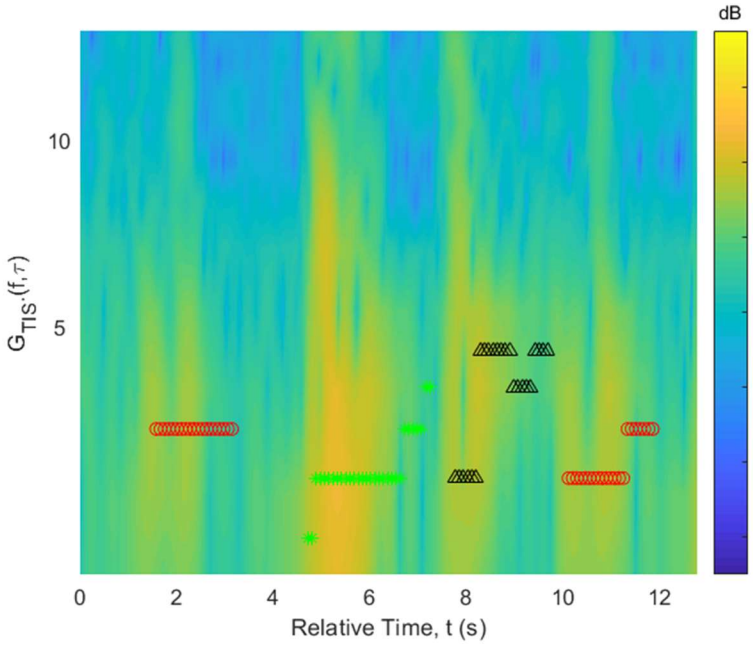

Figure 9: STFT of TIS with Overlaid Maximum Instantaneous Frequency for TI, TO, and SB events Represented as Black Upward Triangles, Red Circles, and Green Stars Respectively

The dataset is truncated around a single transient event to evaluate the corresponding relative mode shape of the transient response. This was done by setting a trigger condition for each of the three different transients observed. A trigger condition for TI and SB would indicate based on Figure 3 that the throttle pedal position goes from zero to a positive percentage application. During TO transients, the throttle pedal position does the opposite, traveling from a positive % application to zero. To further distinguish TI from SB, it was observed that a throttle stab transient occurs in less than one second. Therefore, if a consecutive TI and TO happen within one second it is considered an SB. This logic for selecting TI, TO and SB are depicted in Equation 8. The notation includes a signal f, sample n or m with time/sample shift k and truncating number of samples N for the signal x. These criteria were used to sift through data to find and truncate different transient events for triggered analysis.

$$\begin{Bmatrix} if\ f_{throttle}^{n+k} > \%_{threshold}\ \&\ \ f_{throttle}^{n} < \%_{threshold} \\ if\ f_{throttle}^{m+k} < \%_{threshold}\ \&\ \ f_{throttle}^{m} > \%_{threshold} \\ if\ TI\ \&\ TO\ \&\ n < m\ \&\ (n+T) > m \end{Bmatrix} \begin{matrix} x(n) - x(n+N) & TI \\ x(m) - x(m+N) & TO \\ x(n) - x(n+N) & SB \end{matrix} \quad \text{Equation 8}$$

Using the criteria in Equation 8, an SB event is identified in Figure 10 which depicts the BPF rotating shaft speeds. Also included in Figure 10 is a highlighted box of time that indicates where the TC clutch is slipping. This is determined by evaluating the un-filtered time domain response and recognizing when the Eng. and TIS signals are outside of 5% agreement with one another. The TC clutch must be slipping if these two signals are not within this threshold. The same BPF with upper and lower cutoff frequencies from Figure 7 was used in Figure 10. The signals appear to be at an equilibrium prior to the throttle pedal application and subsequent TC clutch slip and transient decay. The drivetrain components appear to oscillate in phase with one another after the SB event induces peak oscillations, except for the road speed signals (wheels and differential). It looks as though the shuffle mode is beating or superimposed with a higher frequency mode during this transient event. Based on the geometry of the rear axle, a rear axle torsional mode may be found in the 8-30 Hz range depending on suspension parameters.

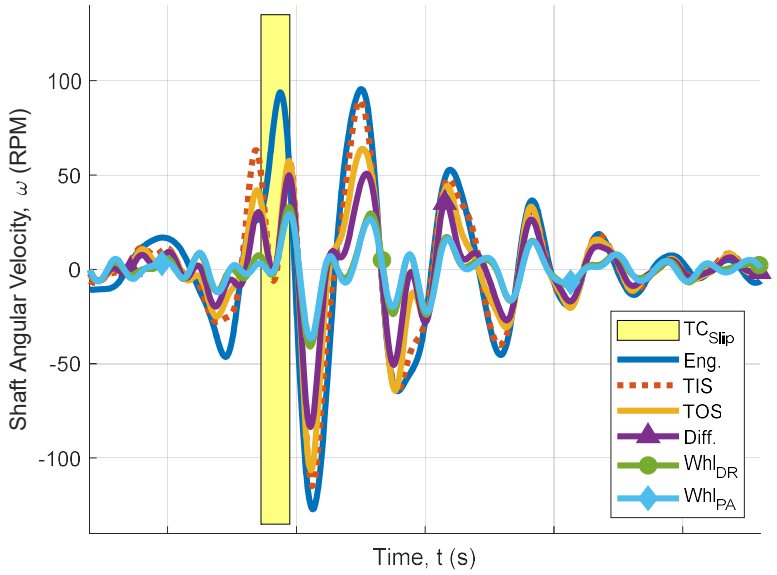

Figure 10: SB Transient Time Domain Mode Shape with 2-9 Hz BPF

It was shown in Figure 9 that the peak instantaneous response frequency during SB was ~3.5 Hz. This is also supported by applying cursors to the time domain peaks of the Eng. or TIS signals and calculating a similar frequency. The data also exhibits indicators that the dominant shuffle frequency can be extracted from the shaft rotational speed measurements of the engine with locked TC clutch and the TIS. The road speed measurements also exhibit behavior that could isolate and predict the shuffle mode.

A narrower BPF between 2.5-4.5 Hz is applied to the data to remove the beating mode and result is shown in Figure 11. The result shows a reduction in the overall amplitude of oscillations which means the total response is either attenuated by the filter or is a combination of the shuffle mode and other content superimposed. The narrower BPF removes the higher frequency mode from the time domain response and depicts the Eng., TIS, and TOS all in-phase with one another along with the road speeds slightly out of phase with the rest of the driveline. This is confirmed to be shuffle as noted in the literature based on the mode shape. It will be further analyzed for propagation of vibration in the body to confirm longitudinal acceleration coupling.

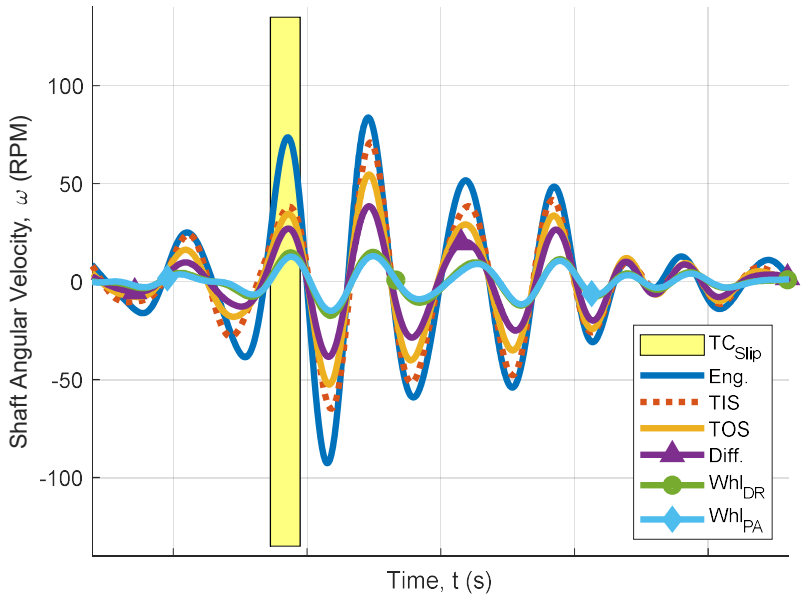

Figure 11: 2.5-5 Hz BPF Indicating Time Domain Mode Shape of Shuffle

The time domain response is a strong indicator of torsional oscillation linked to shuffle after a torque disturbance requested from the driver. The same response in 3rd gear for this transient is compared with the prop shaft torque in Figure 12 where the top dotted red line depicts the TIS speed and the bottom solid green trace denotes the shaft torque. This comparison depicts a slight phase lag in oscillation for the torque signal relative to the speed oscillations. The torque signal does show shuffle frequency content along with multiple crossings of zero relative torque. The torque signal appears to flatten out with a horizontal region around each zero crossing. The flat region indicates that there is no relative torque felt by the prop shaft and one or both ends of the shaft are in a lash transition zone.

There are five flat lash regions shown in Figure 12. Two are positive lash crossings, two are negative lash crossings, while the fifth does not observe a total lash crossing. Each total lash traversal will induce an impact in the geared components upon completion of the lash crossing. Four impacts are expected to be observed based on this torque trace.

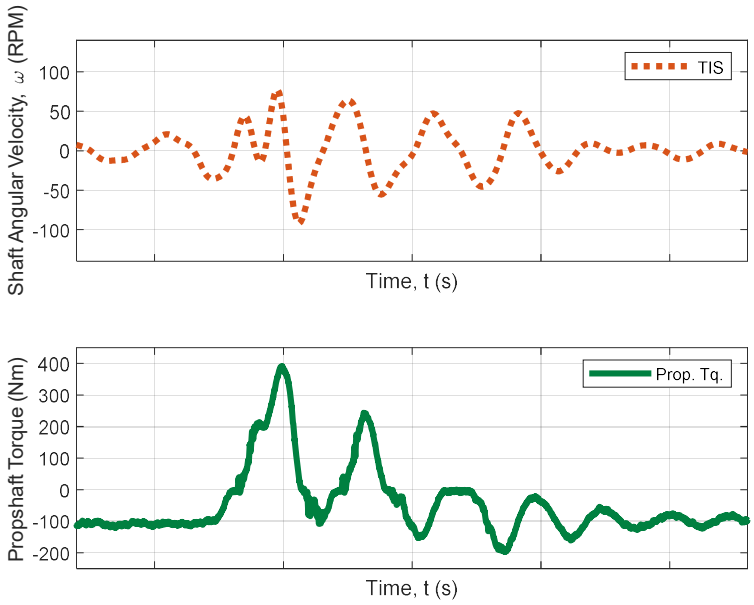

Figure 12: Top: TIS Shaft Speed, Bottom: Propeller Shaft Relative Torque after an SB Event in 3rd Gear Targeting a Center Velocity of 56 kph Resulting in Shuffle

The BPF longitudinal (+X) accelerometer response is also compared with the filtered shaft speed signal in Figure 13. The top plot again depicts the TIS in dotted red while the bottom plot shows the transmission, differential, chassis, and seat track longitudinal accelerometer responses with solid blue, red, orange, and purple traces respectively. Both the seat track and chassis accelerometers appear to be overlaid on one another and in phase. This behavior is expected with the front chassis accelerometer CH1 because the track is rigidly mounted to the cab. The cab is also rigidly mounted on the chassis. Therefore, at low frequency these components should react as one rigid body element.

The differential response appears lower in amplitude but leads (in phase) the reaction observed by the chassis and body accelerometers. This follows the reaction flow of the shuffle transient. First a torque change occurs at the engine which excites the torsional portion of the shuffle mode as previously recorded and noted in literature. The oscillation can include multiple lash crossings, as noted in Figure 12, which when impulsive are sources for body vibrations observed in Figure 13. Therefore, the initial impact in the differential was a source for vibration and propagated forward towards the chassis and seat track accelerometer appearing to lead the body accelerometers. The transmission accelerometer has lower amplitude than the other three longitudinal traces shown. As the shuffle mode decay's in the shaft speed it is also shown to decay in the longitudinal accelerometer traces. This indicates that there is coupling between the torsional oscillating mode and longitudinal body vibration noted in literature. There is a discrepancy with majority of literature in that the shuffle models used do not contain a linear oscillating component. If these two axes of motion are coupled to make an overall shuffle mode, the

predictive math models used must account for this physics. These concepts will be discussed further when developing the math model used in Chapter 5.

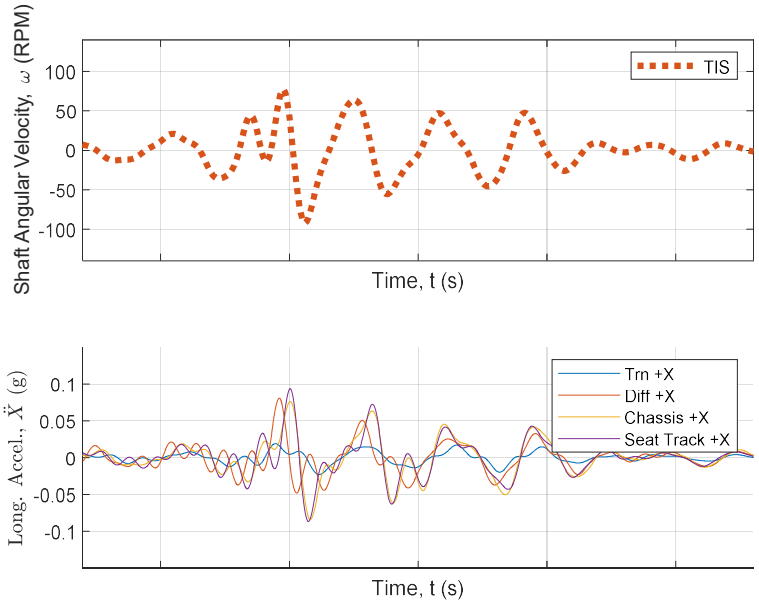

Figure 13: Top: TIS Shaft Speed, Bottom: BPF Accelerometer Measurements in 3rd Gear Targeting a 56 kph Velocity for SB Event

The BPF accelerometer result is useful to identify the shuffle participation, but clunk is also a concern during shuffle transients. The torque trace in Figure 12 depicted multiple lash crossings and depending on their severity, the crossings are known to induce clunk. By repeating the same figure but with no filtering of the accelerometer signals, the torque trace can be compared as done in Figure 14. There are five additional vertical lines overlaid on the torque signal and down onto the accelerometer subplot to indicate the same relative time in each dataset.

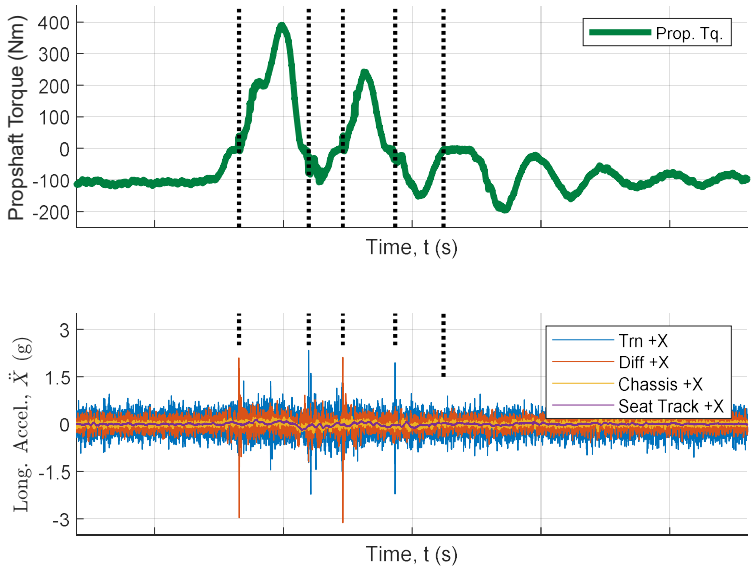

Figure 14: SB Event in 3rd Gear with 56 kph Target Center Velocity, Top: Experimental Torque at the Propeller Shaft, Bottom: Measured Longitudinal Acceleration of Various Measurement Locations Indicating Clunk at Zero Torque Crossings

In Figure 14 the longitudinal acceleration trace exhibits impulsive spikes indicative of clunk. These occur where the torque trace shows a reversal or zero crossing. The four leftmost dashed lines all correspond to impulses either observed at the transmission or differential accelerometer while the chassis and seat track accelerometers do not share similar high frequency content. The fifth dotted black line, furthest to the right, shows the torque holding near zero but never exhibiting a full lash reversal. This shows that the contact is free on one or both ends of the propeller shaft. When this is true, it cannot transfer any appreciable relative torque other than inertial reactions. With no contact, the measurement holds near zero relative torque. Figure 14 suggests that there are different responses in the accelerometer measurement depending on the slope of the torque reversal.

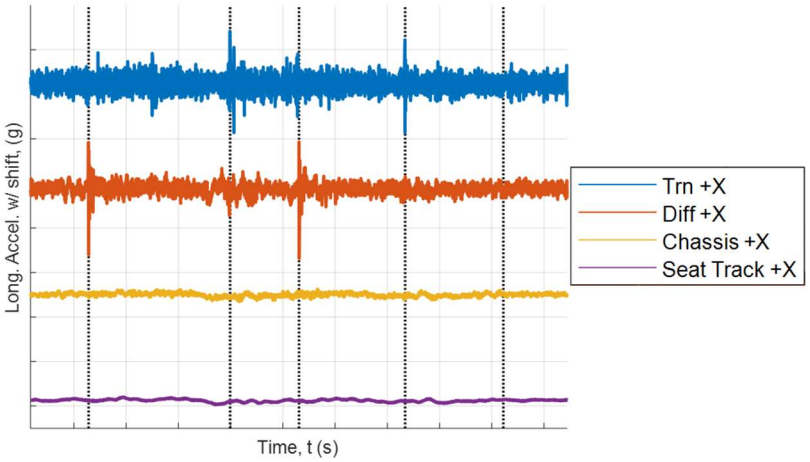

Figure 15: Detailed Accelerometer Response (Y-axis Shifted) to an SB Event in 3rd Gear for a Target Center Velocity of 56 kph with Zero Crossing Clunk Indicators

Figure 15 further truncates the relative time domain to observe all five of the impulsive events in detail. It does this by offsetting the four accelerometer traces while maintaining the same relative y-axis (g) scaling. The figure again confirms that the impulsive nature is shared in the transmission and differential while the chassis and seat track are less sensitive to the impact excitation. The shuffle response is shared by all four shown accelerometers consistent with the BPF results in Figure 13.

By adding the y-axis offset in Figure 15 the data shows that a positive torque crossing in the propeller shaft measurement (indicated by the first and third vertical dotted line from left to right) result in impacts on the differential. The negative torque crossing (indicated by the second and fourth vertical dotted line from left to right) shows an impulse in the transmission response. The fifth vertical dotted line corresponds to a lash entry, but no crossing occurs and therefore no impulsive event is observed. These results are understood that a positive torque crossing is most severe at the differential. This is because the inertia of the transmission and prop shaft (together ~1.5 kgm^2 reflected on the engine) are smaller in magnitude than the body on frame (~$0.5m_{vehicle}*r_{tire}^2$) combined with vehicle road load response. The relative magnitude allows lash to be taken up in the transmission during a positive torque crossing with low impact based on the impulse momentum equation depicted by Equation 9. The Equation 9 notation indicates the impulse magnitude I is equal to the sum of the initial mass m, and velocity v, with the final mass and velocity. Therefore, during the positive torque crossing, the relative mass of the body on frame and road loads are large and impact when lash is taken up in the differential.

The opposite occurs during a negative torque crossing through zero. The system takes up lash in the reverse direction and the intermediate inertia of the propeller shaft reflected onto the road speeds is small and doesn't initiate a large impact when lash is taken up in the differential. The inertia of the transmission and engine appears larger when reflected onto

the road speeds. Therefore, when lash is crossed in the transmission there is an impulse shown in the longitudinal direction as shown in Figure 14-Figure 15.

$$I = m_1 v_1 + m_2 v_2 \qquad \text{Equation 9}$$

Conclusion, damping devices in the transmission should be tuned to asymmetrically damp more during negative torque crossings (drive to coast event when shuffle is not present) and the differential damping device should be tuned asymmetrically to damp more during positive torque crossings (coast to drive event when shuffle is not present).

The influence and presence of impulsive behavior can also be observed by computing the Short Time Fourier Transform (STFT) from Equation 6. This processing technique was applied to the longitudinal acceleration of the transmission (Tr1 +X), differential (D1 +X), chassis (CH1 +X) and seat track (ST +X) as seen in Figure 16. This shows data time aligned with that in Figure 8 which included a sequential TO, SB, TI, and again TO. Both the transmission and differential traces indicate impulsive behavior from the TO, SB, and TI. The spectrogram further shows higher frequency content, up to thousands of hertz, indicative of high frequency metallic clunk according to the literature summarized in Figure 1. The STFT does not show clunk excitation in the chassis or seat track response. These two signals are dominated by low frequency content, primarily the shuffle mode.

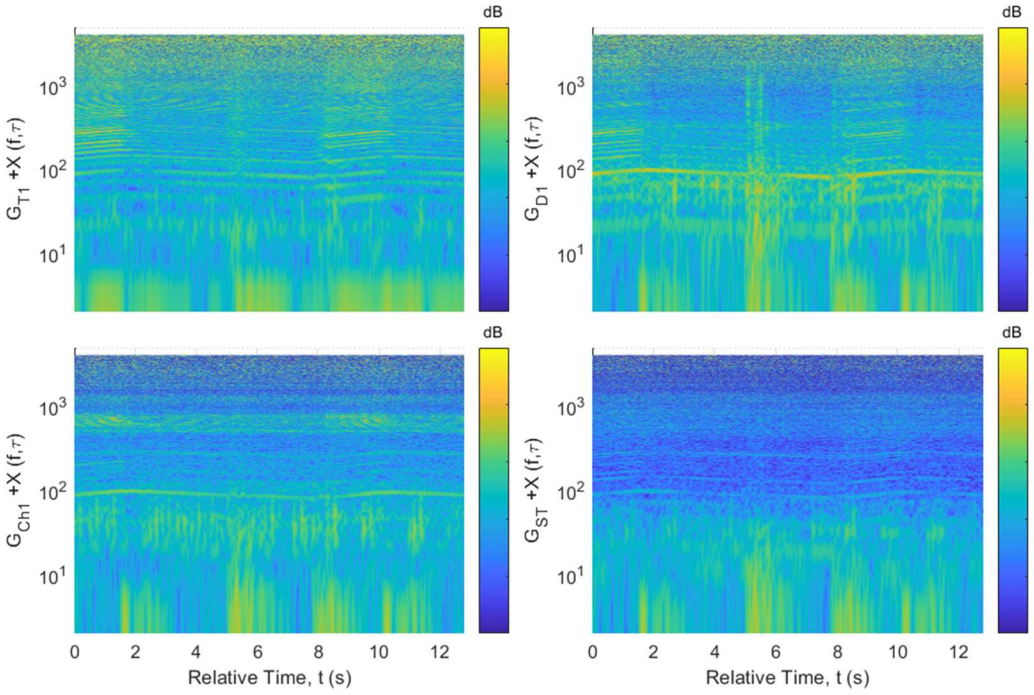

Figure 16: STFT for Top Left: Transmission, Top Right: Differential, Bottom Left: Chassis, Bottom Right: Seat Track all in the +X Direction with the Same Relative dB Scaling (re 1g) in 3rd gear for SB Event at a Target Center Velocity of 56 kph

Additional observation of the differential microphone shows results like Figure 14 where the top torque trace in green forces excitation in the accelerometer response below in blue.

The initial positive torque crossing was shown to be impulsive through the STFT and have greater amplitude response at the differential than the transmission.

The same five dotted black lines indicating impulse events from previous work in Figure 15 are preserved again and plotted over the top torque trace and bottom differential microphone in Figure 17. This is also done with the TIS speed on top and propeller shaft torque trace on bottom in Figure 18. The same lines that corresponded to impulses in the differential also appear impulsive in the microphone signature in Figure 17. They do not coincide with maximum and/or minimum shaft speeds on the TIS in Figure 18.

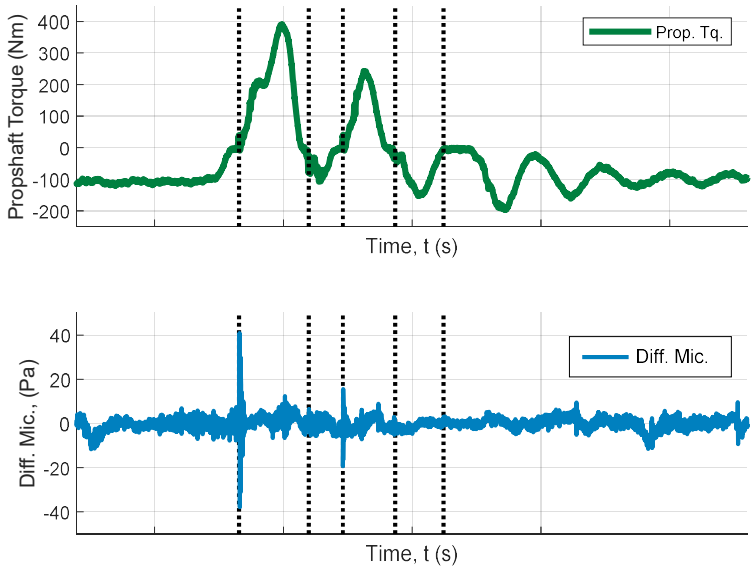

Figure 17: Detailed Torque and Differential Microphone Impulsive Measurement for 3rd Gear at a Target Center Velocity of 56 kph Indicating Clunk at Zero Torque Crossings

According to Figure 18, the local maximum values of the shaft speed lag the positive torque crossings and the local minimum values lead the negative torque crossing. The final line where lash is entered but never crossed does in fact lag the local maximum for TIS speed which would not be expected had a positive torque crossing occurred. This is an example where the torsional mode shape has entered a linear region and is no longer shifting in response where all main inertia elements have been coupled. After this brief zero relative torque hold, the propeller shaft once again exhibits free vibration with one observed decaying shuffle frequency.

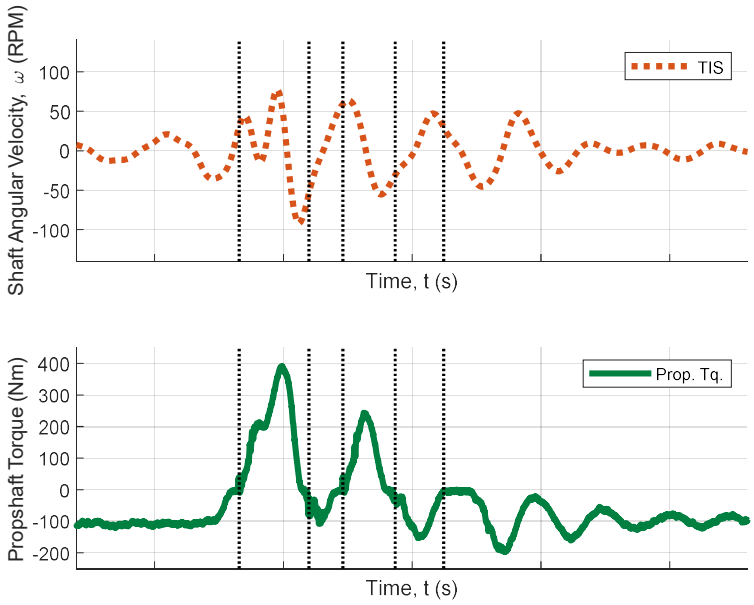

Figure 18: Detailed TIS Speed and Relative Propeller Shaft Torque Measurement Indicating TIS Oscillations Coupled with Torque Zero Crossings

The overall system response (shaft speeds, accelerometers, microphone, etc.) is depicted together with subplots in Figure 19. This combined response is the high-fidelity sensor coupling which has not been simultaneously published before. The top solid black line represents the driver applied throttle pedal input followed by; the TIS speed sensor in dashed red, the prop shaft torque in solid green, the differential longitudinal response in red, the differential microphone response in dashed blue, the transmission response in solid blue, and a solid purple line denoting the longitudinal seat track accelerometer response. The tip-in shown in Figure 19 is classified as a throttle stab, SB, and excites the impulsive clunk response at both the transmission and the differential. The impulses are induced by a torque reversal traversing through a lash zone before spiking once the total lash has been made. This progression first spikes in the differential accelerometer and microphone response followed by the transmission response. The seat track does not indicate impulsive behavior but instead shows the sustained low frequency body acceleration.

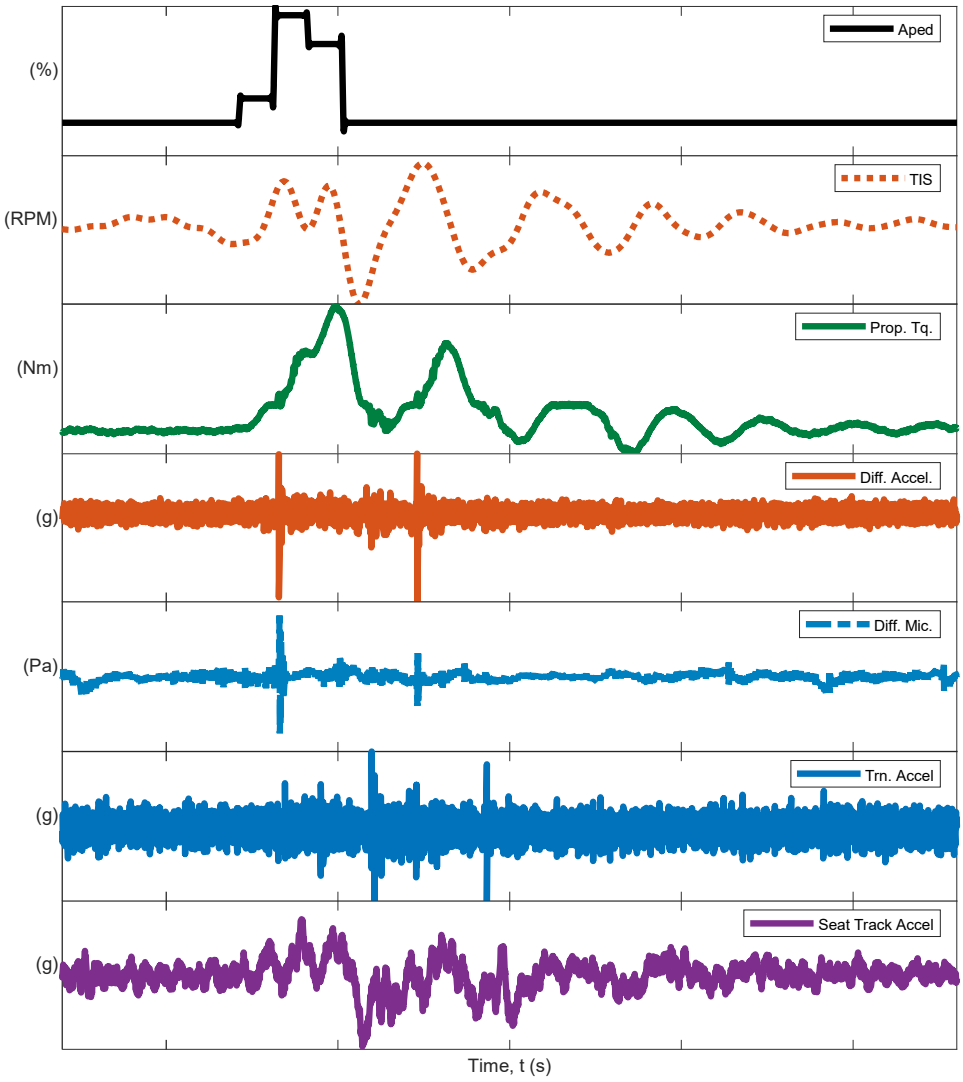

Figure 19: Top to Bottom: Throttle Pedal Apply, TIS Speed, Propeller Shaft Torque, Differential Acc., Differential Mic., Transmission Acc., and Seat Track Acc. during an SB Event Resulting in Shuffle During 3rd Gear SB Event at a Target Center Velocity of 56 kph

Further truncating the data and zooming in on the time domain was done in Figure 20. This further confirms these impulsive events occur after lash has been crossed indicated by a zero crossing in torque. The zero crossing further induces longitudinal acceleration as expected and verified here in Figure 19 and Figure 20. This once again confirms that the shuffle mode is a coupled torsional mode with longitudinal acceleration and will be included when developing the math model for Chapter 5.

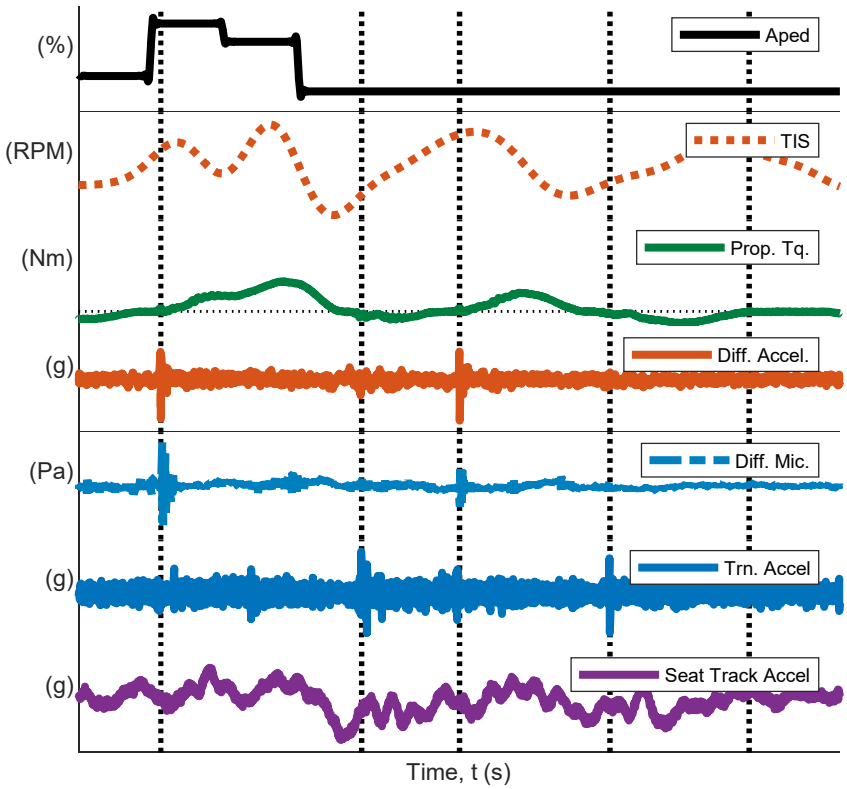

Figure 20: Top to Bottom: Throttle Pedal Apply, TIS Speed, Propeller shaft Torque, Differential Acc., Differential Mic., Transmission Acc., and Seat Track Acc during SB event resulting in Shuffle during 3rd Gear TI at a Target Center Velocity of 56 kph with Dotted Lines Indicating Impulse Events

Similar data for a sustained tip-in and tip-out event are depicted in Figure 21 and Figure 22 respectively. The sustained tip-in event in Figure 21 shows one single sided impact as lash is crossed from the coast to drive and occurs where the vertical dashed black line denotes where lash was fully crossed. This coincides with the propeller shaft experiencing a positive relative torque. The torque signal also does not exhibit significant oscillations, unlike the SB event, and therefore only had one impulse event observed on the longitudinal accelerometer signals. The TOSS data indicates shuffle oscillations, unlike the torque trace, and can be analyzed for shuffle amplitude and/or frequency. The seat track itself doesn't show a heavy impact but does indicate a rise in amplitude after the tip-in event that will be further analyzed for customer perception with the VDV in later sections. The differential microphone trace doesn't indicate an impulse event based on this tip-in scenario as was shown in the SB data for this sustained TI.

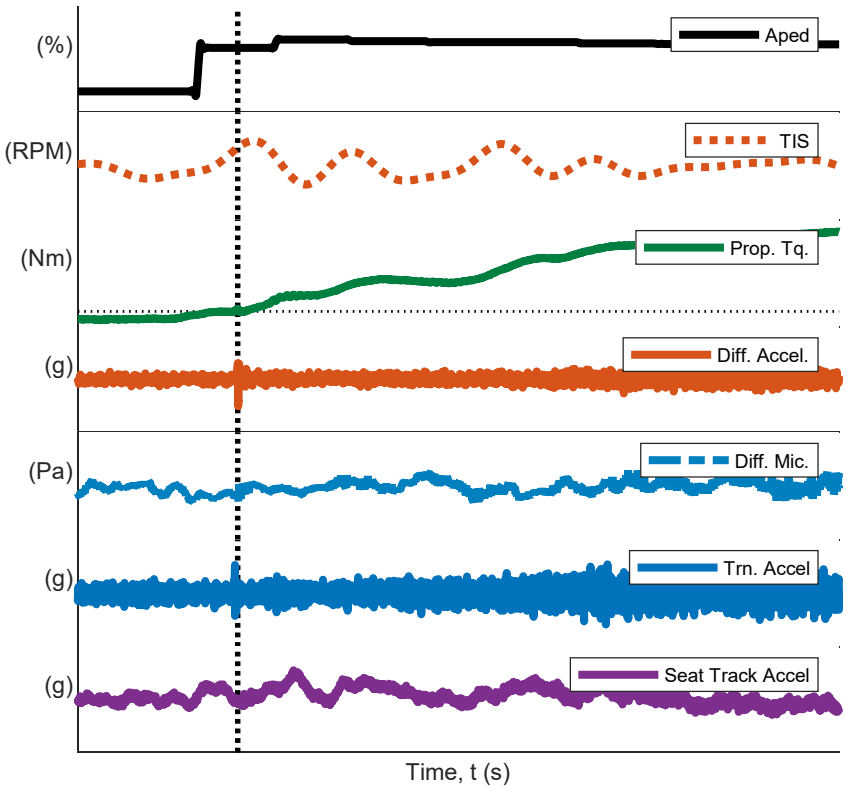

Figure 21: Top to Bottom: Throttle Pedal Apply, TIS Speed, Propeller shaft Torque, Differential Acc., Differential Mic., Transmission Acc., and Seat Track Acc during Sustained Tip-in Event for 3rd Gear at a Target Center Velocity of 56 kph Normal Mode.

The data shown in Figure 22 indicates a TO event where the throttle pedal goes from a positive request to zero. The propeller shaft torque slowly tapers off to a negative torque with a less aggressive decay ramp rate compared to TI. The decay and crossing appear slow such that no impulse events are observed. This is not fully representative of all TO events in other gears. It depicts that when torque ramp rates are low, the lash crossing velocity is also slow. This leads to lower or no impulse events observed and a better perception is expected from the VDV metrics.

To compare the different TI and TO events, there were a few metrics developed to understand differences in each. The torque ramp rate is of interest because it indicates how aggressive the acceleration event is and thus the amount of potential energy stored in the driveline due to the shaft twist angle. The peak acceleration and microphone response are an indication of how much clunk excitation was experienced during a transient event. These metrics and more will be used in later processing to contrast the different events and observe trends in the vehicle response.

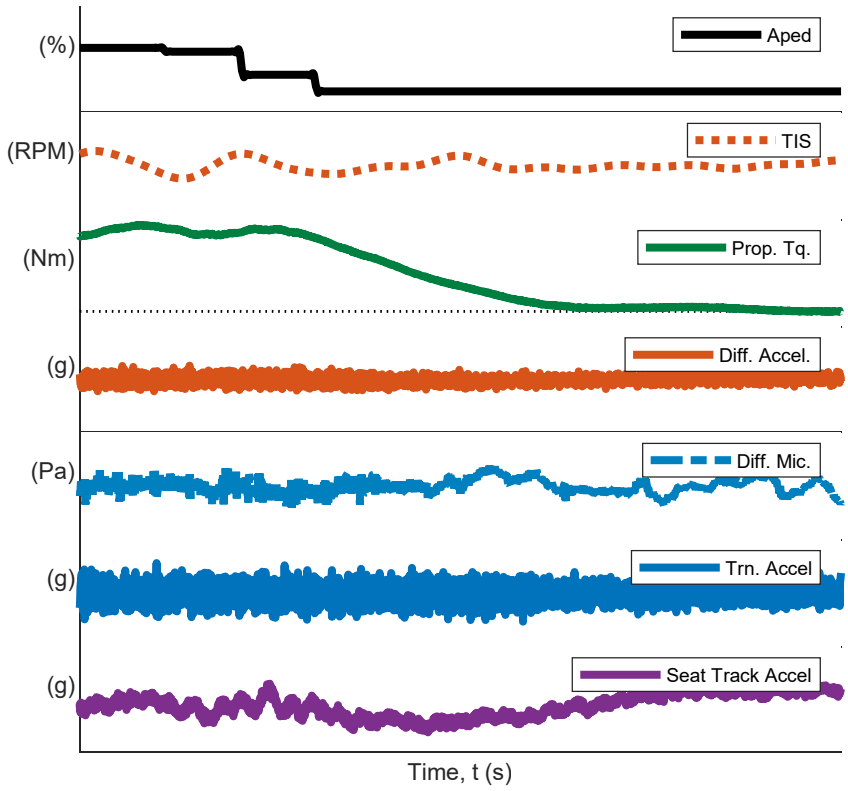

Figure 22: Top to Bottom: Throttle Pedal Apply, TIS Speed, Propeller shaft Torque, Differential Acc., Differential Mic., Transmission Acc., and Seat Track Acc during Sustained TO Event for 3rd Gear at a Target Center Velocity of 56 kph in Normal Mode.

Analyzing the response, or receiver of the system, indicates how the vehicle behaves to driver inputs but doesn't characterize the source. Figure 23 depicts how the ECU interprets a driver torque request in the vehicle. The figure overlays data from 3rd Gear at a target center velocity of 56 kph for several TI events (both sustained and SB). The top subplot indicates the driver requested torque as measured on the vehicle CAN bus while the bottom subplot denotes the measured propeller shaft torque. Each signal has been low pass filtered but show that the internal control strategy has two ramp rates used for sustained TI events. The control strategy is proprietary to the manufacture but is understood that the initial ramp rate is used to slow down the impact velocity during lash traversal and once lash is taken up, the torque request can increase to the maximum driver request at a steeper slope.

There are differences in the estimated driver torque request and the measured propeller shaft torque. The shuffle mode is superimposed on the propeller shaft torque as seen in the measured data as opposed to the CAN estimate. The measured estimates also show a difference in overall ramp rate and can be compared to one another based on each individual TI event. The torque ramp rate estimate is plotted vs. the measured torque ramp rate in Figure 23. A solid black diagonal line is included that indicates 1:1 measured vs. CAN estimate. If the estimate and engine control were perfect, then all measurements should lie on this line. However, the torque management is not perfect in this system and

have no clear trend of over or under delivering torque. What is clear from Figure 24 is that the actual and estimated torque differ for torque ramp rate in the data.

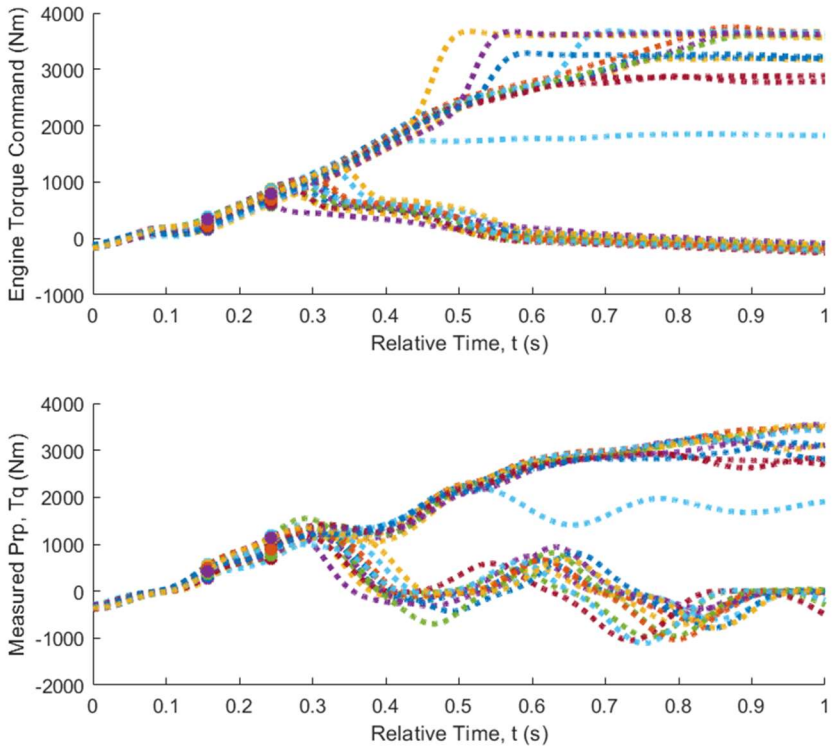

Figure 23: CAN Bus Driver Requested Torque vs. Time during TI event, including SB for 3rd gear at a target vehicle speed of 56 kph

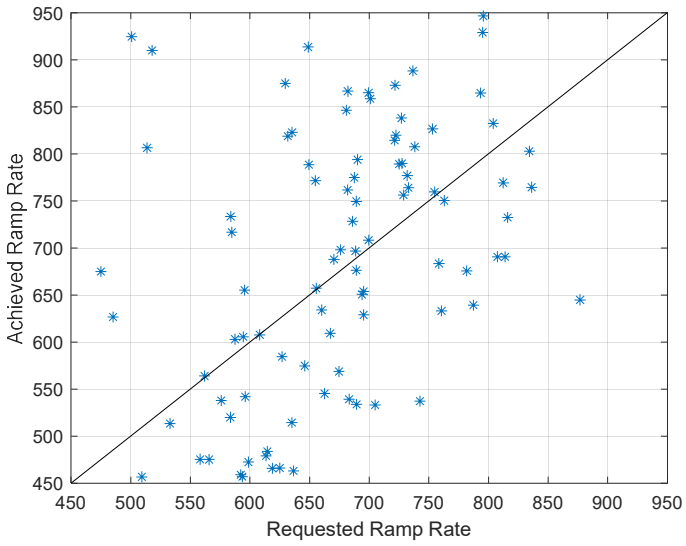

Figure 24: Measured Propeller Shaft Torque Ramp Rate vs. Requested CAN Estimated Torque Ramp Rate

The shuffle mode is understood to be within 1-10 Hz and therefore the shaft and accelerometer data is band pass filtered to remove the influence of other modes or frequencies participating in operating data. Peak-to-peak metrics were estimated from the truncated TI events for shaft oscillation and longitudinal acceleration and plotted vs. CAN torque ramp rate in Figure 25 and Figure 26 respectively.

In Figure 25 the metrics for engine, TISS, TOSS, and differential speeds are depicted with blue diamonds, red squares, yellow upper triangles, and purple circles respectively. The data is a combination of all ten run scenarios driven with 2WD in Normal calibration mode. A linear trendline was fit to all four transducers to note how the peak accelerometer response increases with increasing propeller shaft torque ramp rate. The correlation coefficient is low for all four comparisons when evaluating against the CAN torque estimates.

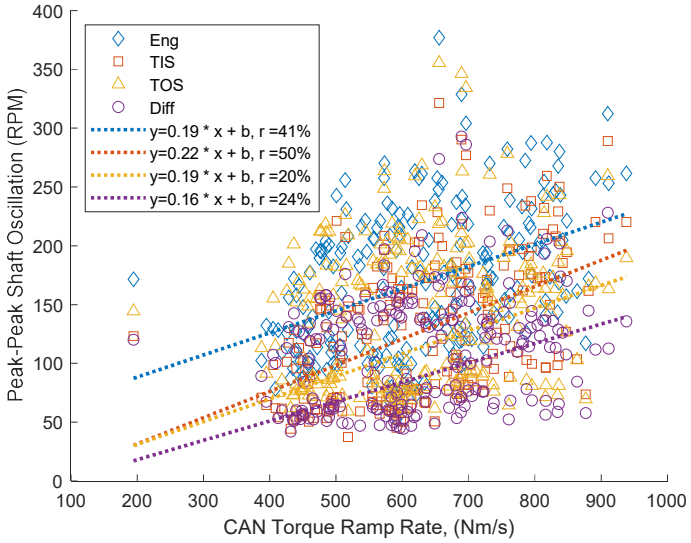

Figure 25: Peak-peak Shuffle Oscillation Response vs. CAN Estimated Torque Ramp Rate for TI Data from All Runs and Modes Combined with Correlation Coefficient

Figure 26 depicts a similar scenario by comparing the longitudinal transmission, differential, chassis, and seat track accelerometers with blue diamonds, red squares, yellow upper triangles, and purple circles respectively. The correlation coefficient is low for this data as well indicating the torque ramp rate is not a good predictor for the severity of clunk when measured from the CAN torque estimates. This could be due to CAN data errors as described in [56] or just low correlation based on shuffle response.

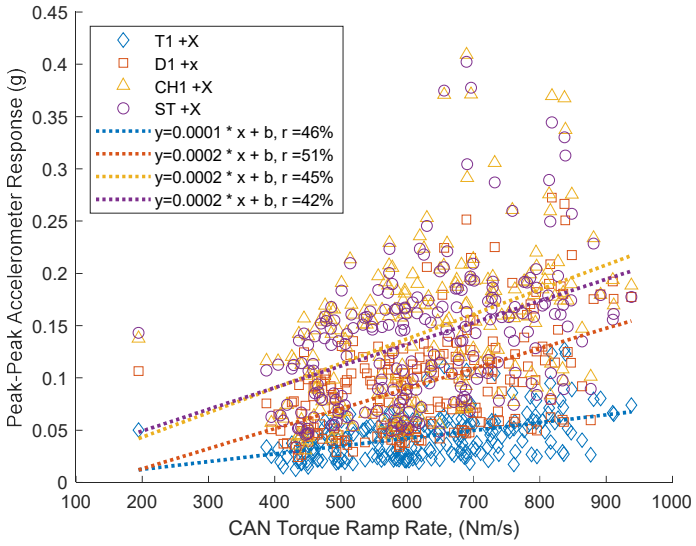

Figure 26: Peak Accelerometer Shuffle Response vs. CAN Estimated Torque Ramp Rate for TI Data from all Runs and Modes Combined with Correlation Coefficient

The same comparison is made with the measured propeller shaft torque from the Wheatstone bridge setup installed as shown in Appendix B: Propeller Shaft Strain Gauge Installation. The data is plotted vs shaft oscillations and accelerometer shuffle response in Figure 27 and Figure 28 respectively. The correlation coefficient increases for all eight-curve fit's shown compared to the CAN bus estimate. Overall, the correlation value is still low and does not indicate a strong relationship between torque ramp rate and peak shuffle response. This could be due to the non-linear nature of the lash crossings along with over fitting data from different gear states and operating speeds.

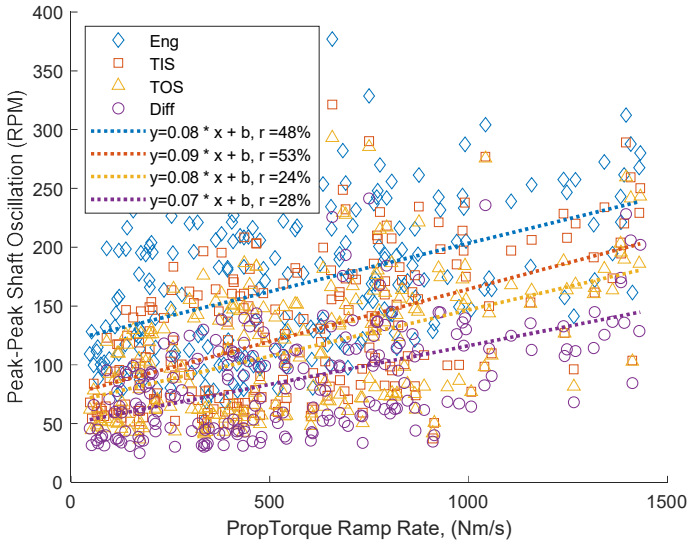

Figure 27: Peak Shuffle Oscillation Response vs. Wheatstone Bridge Measured Propeller Shaft Torque Ramp Rate for TI Data from all Runs and Modes Combined with Correlation Coefficient

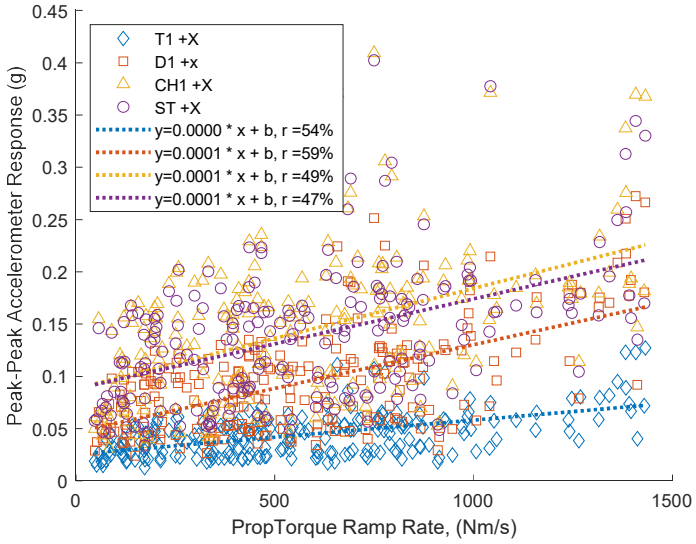

Figure 28: Peak Accelerometer Shuffle] Response vs. Wheatstone Bridge Measured Propeller Shaft Torque Ramp Rate for TI Data from all Runs and Modes Combined with Correlation Coefficient

The experimental vehicle has an automatic transmission and therefore torque converter to couple between the engine and transmission input. The torque converter is equipped with a lockup clutch to increase efficiency at highway driving speed but also allow for fluid churn and decoupling of the engine and transmission during zero vehicle speed events. During transient torque requests, the clutch may unlock according to control strategies. When the clutch unlocks, it allows for an amount of converter fluid shear, an additional damping element in the driveline. To estimate if the torque converter, TC, clutch is slipping

a slip factor metric was developed and described by Equation 10. The evaluation uses discrete integration of the relative engine and TISS speed signals. When the engine speed is faster than the transmission input speed, the slip factor will increase indicating that the TC clutch is in an unlocked and slipping state. This factor is plotted against peak accelerometer response data in Figure 29. The data depicts longitudinal transmission, differential, chassis, and seat track responses with blue diamonds, red squares, upper yellow triangles and purple circles respectively. Two distinct groupings can be observed in Figure 29, data with a slip factor less than 20000 RPM/s and data with a slip factor greater. The data less than this amount is in a locked or controlled slip state while data above 20000 RPM/s is an unlocked converter. The data are separated into these two regions by filled in markers for locked/controlled slip and the unlocked data is shown with un-filled markers.

The overall trend for an unlocked converter shows as the slip factor increases, peak accelerometer response decreases. This confirms the damping effects of the slipping torque converter aiding in reduced peak shuffle acceleration. While this additional damping is desirable for reduced shuffle response, it is not a desirable trait for overall fuel consumption, albeit at a very small fraction of overall vehicle drive time. An optimization study could be done in future works to balance this slip for improved damping with tradeoffs for fuel economy.

$$Slip\ Factor = \int_0^T \omega_{eng} - \omega_{tiss}\, dt \qquad \text{Equation 10}$$

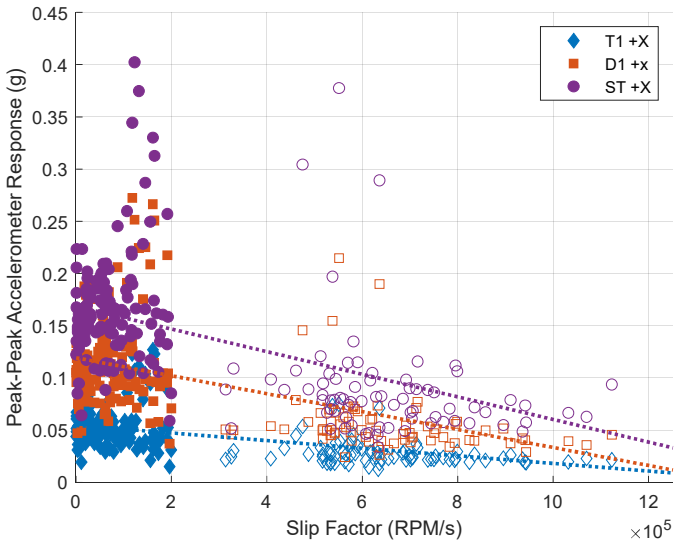

Figure 29: Peak Shuffle Longitudinal Acceleration vs. Torque Converter Estimated Slip Factor for all TI Data in Every Run and Mode

Data from Figure 27 and Figure 28 is further sorted by the slip factor metric into locked and unlocked data with filled and unfilled markers. The new distinction is shown in Figure 30 and Figure 31 for the shaft oscillation and acceleration shuffle response respectively.

The data once again confirms that slipping torque converter data has a lower peak response than locked torque converter data. There still is no strong correlation coefficient for the overall data set for each transducer with a linear fit trendline. The correlation reduces for peak differential and TOSS shuffle oscillation in a locked TC clutch state in relation to tip-in torque ramp rate. This shows that in a locked state the input torque ramp rate does not have a strong influence on the peak shuffle response at the TOSS and differential. The overall correlation is similar for the peak acceleration data when separated for slipping and locked torque converter but also shows that the slipping data is lower in amplitude than the locked TC clutch data.

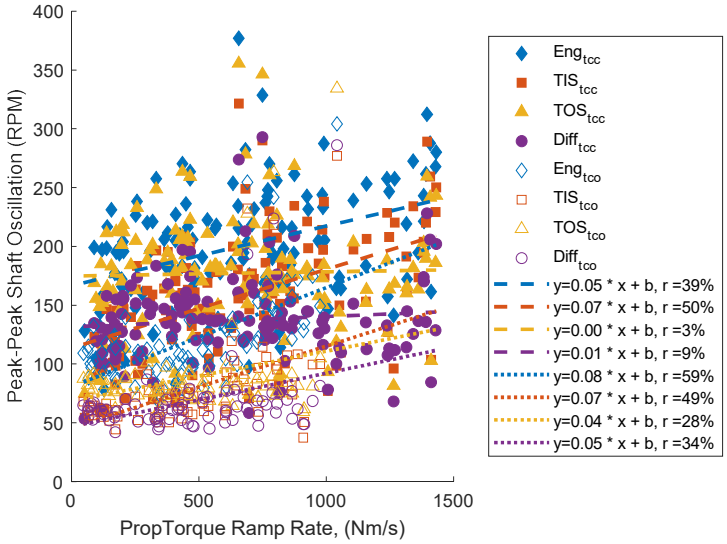

Figure 30: Peak Shuffle Oscillation vs. Measured Propeller shaft Torque Separated by Slipping and Non-Slipping TC Clutch Data for every Run and Mode with Correlation Coefficient

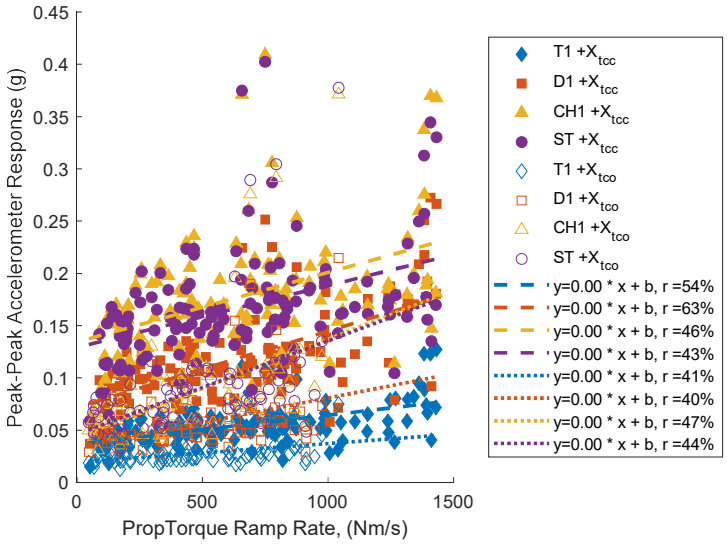

Figure 31: Peak Shuffle Acceleration vs. Measured Propeller shaft Torque Separated by Slipping and Non-Slipping TC clutch for TI Data in every Run and Mode with Correlation Coefficient

Torque ramp rate was not a significant indicator of peak shuffle oscillation or acceleration, so a similar processing was performed with the peak torque achieved during TI truncated around the torque trigger. This comparison is made in Figure 32 for the longitudinal transmission, differential, chassis, and seat track response with blue diamonds, red squares, yellow upper triangles, and purple circles respectively. The correlation coefficient is like that of torque ramp rate however the data appears to have distinct groupings of the locked and unlocked data with outliers considering the binary slipping vs locked TC clutch status. The locked TC clutch data with peak torque below 1800 Nm appears to be consistent in grouping but contain some above 1800 Nm.

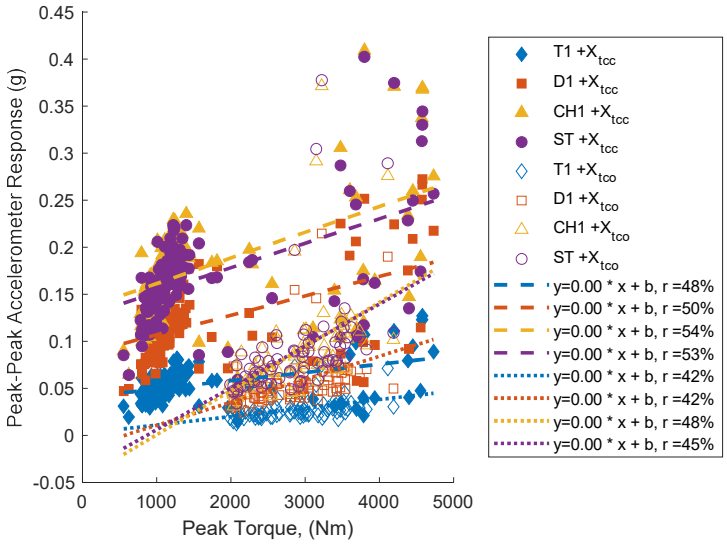

Figure 32: Peak torque vs. Accelerometer Response for Slipping and Non-Slipping with Correlation Coefficient

A 3D plot was generated in Figure 33 to observe and understand the outliers relative to the TC clutch state distinction. Only the longitudinal transmission response was included in Figure 33 and the same binary distinction was created for locked TC clutch data in solid markers and slipping TC clutch with unfilled markers. Six additional indicators were overlaid on the different groupings shown in the 3D data. The red pentagram and left triangle both denote data in the low slip low peak torque region. Within this region the pentagram shows the lower peak accelerometer data of this region while the left triangle denotes the upper accelerometer data of this region. The individual time data is plotted in Figure 34. The two green markers; a square and right triangle, denote the low slip high torque region of the plot for low and high peak acceleration respectfully. This individual time data is plotted in Figure 35. The two blue markers; an upper triangle and hexagram, denote the high slip data for low and high peak acceleration respectfully. This individual time data is plotted in Figure 36.

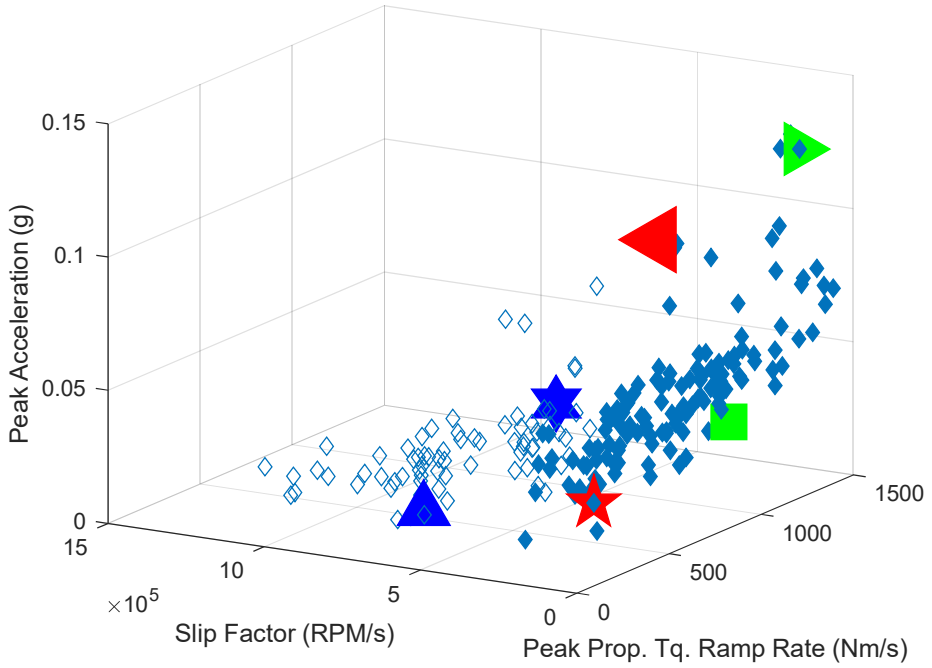

Figure 33: Longitudinal Acceleration in the Z-axis Plotted vs. Peak Torque Along the X-axis and Slip Factor along the Y-axis.

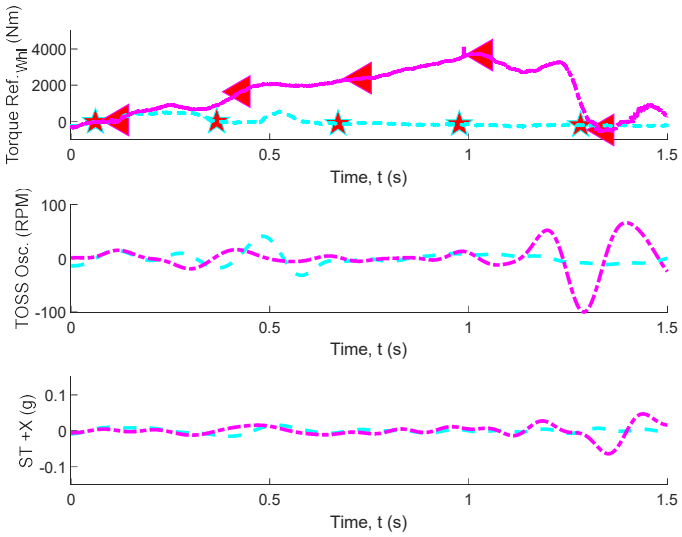

Figure 34: Torque, TOSS, and Longitudinal Seat Track Acceleration vs. Time for Two Individual Conditions of Low Peak Torque and Low Slip Factor.

Data in Figure 34 denotes the high and low peak-peak accelerometer data in dot-dashed magenta and dashed cyan respectively. Plotting the time data of high and low peak-peak accelerometer selected from Figure 33 reveals that the high accelerometer depicted in dot

dashed magenta shows a sustained TI event that is followed with a TO in the 1.5 second truncated data section. The peak accelerometer event doesn't pertain to the TI event but instead is a product of the TO maneuver. The large windup and release of torque in the driveline caused a release in potential energy that was dissipated after release or TO of the throttle pedal. This TI data appears more severe than the TO example from Figure 22 when comparing the peak accelerometer and TOSS shuffle amplitudes. The TO portion displays a steeper torque decay or ramp rate that has low correlation with peak-peak shuffle amplitude in the TOSS and longitudinal ST. The dashed cyan line also exhibits a TI and TO but the short duration of time for these inputs classifies the event as an SB.

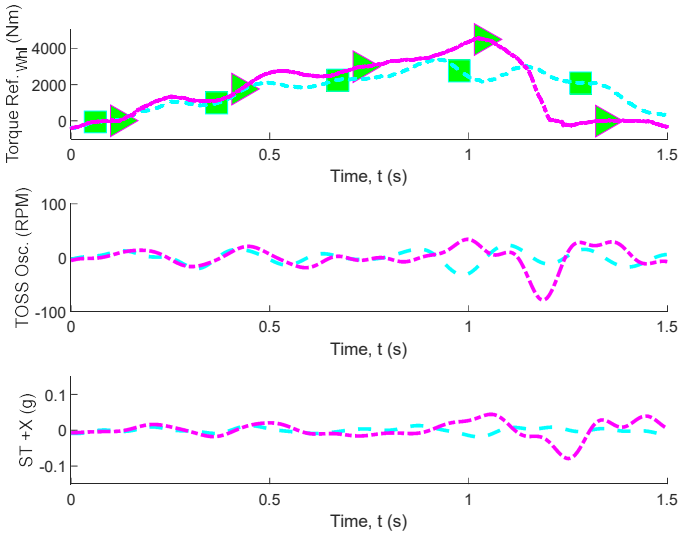

Figure 35: Torque, TOSS, and Longitudinal Seat Track Acceleration vs. Time for Two Individual Conditions of High Peak Torque and Low Slip Factor.

Figure 35 depicts the two green markers from Figure 33 but for high and low peak-peak accelerometer data in the low slip high torque region. Both traces fall into the locked TC clutch region due to a low slip factor and both traces exhibit a TI followed by TO within the 1.5 second truncated time data. The high peak-peak response data in dot-dashed magenta is similar to that shown in Figure 34 with an aggressive torque decay ramp rate followed by the peak shuffle response in TOSS and longitudinal seat track. This is the reason why these data points appear as outliers in the low slip factor, but high torque data based on TI truncation.

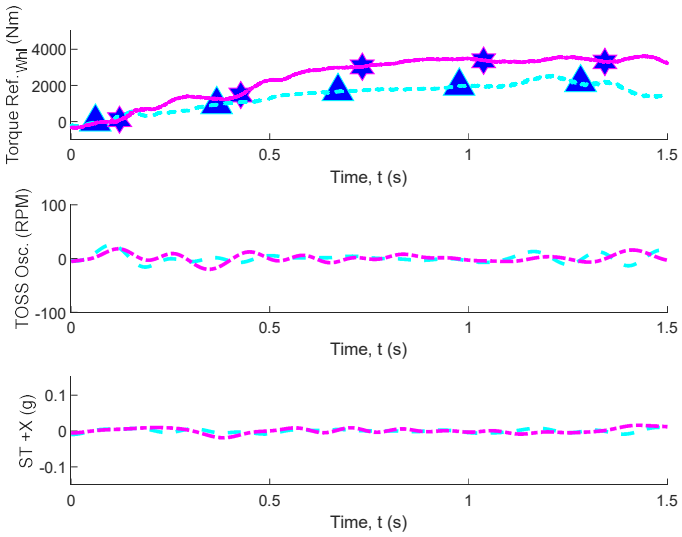

Figure 36: Torque, TOSS, and Longitudinal Seat Track Acceleration vs. Time for Two Individual Conditions of Various Peak Torque and High Slip Factor.

Both data traces depicted in Figure 36 are sustained TI events with no TO within the 1.5 second truncation period. The shuffle response is prominent in the TOSS signal as soon as the sustained torque increase begins but there is low longitudinal ST response as understood based on the damping from the slipping converter.

One of the major aims in this study was to confirm the relationship between shuffle driveline oscillations and longitudinal acceleration. If there is correlation, then previous literature is correct and analytical models should be updated to account for this coupling. The data was evaluated by band pass filtering both rotating speed and accelerometer signals for the shuffle response contribution. It was then processed together as accelerometer response vs. TOSS oscillation response in Figure 27.

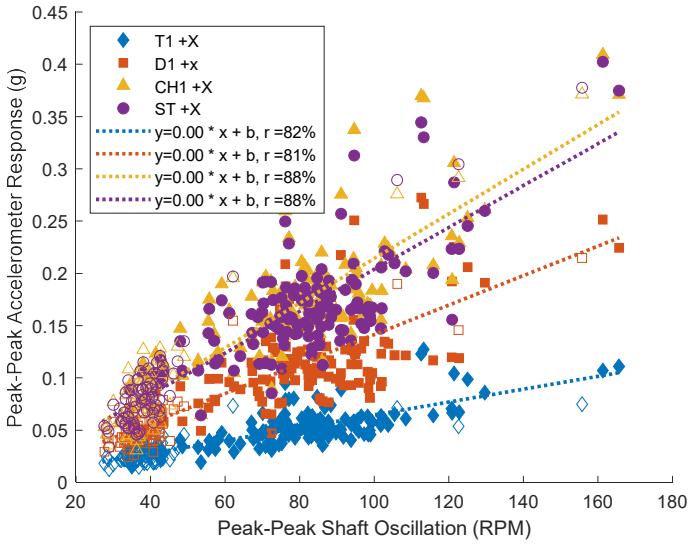

Figure 37: Shuffle Correlation Between TOSS Peak Oscillation and Longitudinal Accelerometer Response.

There is confirmed correlation in peak shaft oscillation to peak acceleration as depicted in Figure 37. The peak-peak shuffle response is strongly correlated with the peak-peak longitudinal acceleration. If the torsional oscillations (slipping TC clutch) are reduced in the driveline, there will be further reduction in the overall response. This correlation will be useful when comparing VDV values when no longitudinal acceleration is available as done in [60].

The frequency response function, FRF, with coherence was computed using the truncated operating data for all ten runs in 2WD normal mode averaged over all TI events. The averaged FRF is depicted in Figure 38 for the seat track accelerometer data over the propeller shaft torque bridge measurement. It depicts 3rd, 4th, 5th, and 6th gear data in blue, red, yellow, and purple respectively. Additional data for transmission and differential data are available in Appendix C: Additional Analysis and Figures. The FRF indicates a shifting shuffle frequency based on gear state for TI data. The shuffle response appears heavily damped during the TI response with higher coherence near shuffle for each gear state. This behavior is further analyzed later in Chapter 3.

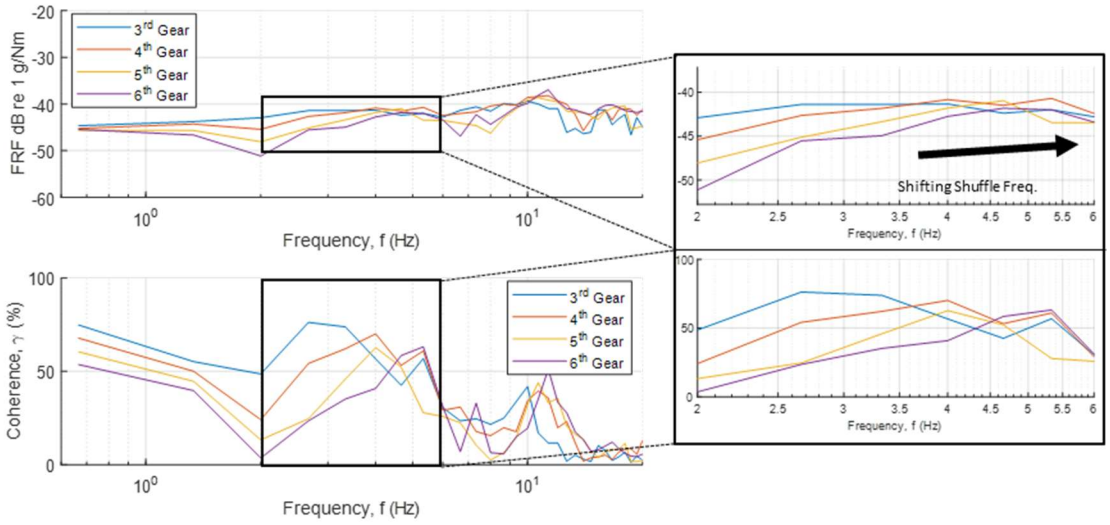

Figure 38: Averaged ST +X/Prop. Torque FRF for 3rd-6th gear for All Road Data in Normal Mode 2WD.

4. Laboratory Test Apparatus and Procedures

Experimental testing with the road vehicle was useful in understanding the baseline transients of the driveline. It allowed for baseline testing like what may be experienced by a customer or user of the vehicle. The torque inputs and wheel speeds were not constrained to a high degree, that is each torque tip-in did not achieve the exact same duration of application, the peak torque achieved was not consistent, the road grade was not kept perfectly level and the tire-road interaction induced uncorrelated vibration inputs. To obtain a higher level of control, another test vehicle was retrofitted to be installed in a laboratory dynamometer cell for testing.

The new dyno cell truncated model is depicted in Figure 39 as opposed to the full test vehicle depicted in Figure 2. The key differences show that the internal combustion engine was replaced with a BorgWarner, BW, HVH250 090SWM electric motor as a torque source. The installation and cradle FEA analysis performed is documented in Appendix E: Cradle Assembly Engine Swap Verification. There is no internal combustion engine used in the dyno test cell. Any speed reference to the engine is made off the flexplate which is the exact same measurement location used in road testing. An image of the magnetic pickup drilled through the transmission bellhousing may be observed in Appendix A: Test Vehicle and Instrumentation Figures.

A supplemental rotary torque disk was installed between the input electric motor and flexplate to measure torque input to the transmission TC pump. All other accelerometer and microphone locations were kept the same and are denoted in Figure 39. The rear wheels were removed from the vehicle and replaced with “floating hub” wheels. The floating hub allows the rear axle to spin freely on a bearing internal and independent of the wheel that is supporting it. It also has a through coupling so that an additional rotary torque meter and axle are coupled to the wheel output. This additional axle connects to an absorbing

dynamometer on both sides (passenger and driver). Additional sensor descriptions are available in Table 3.

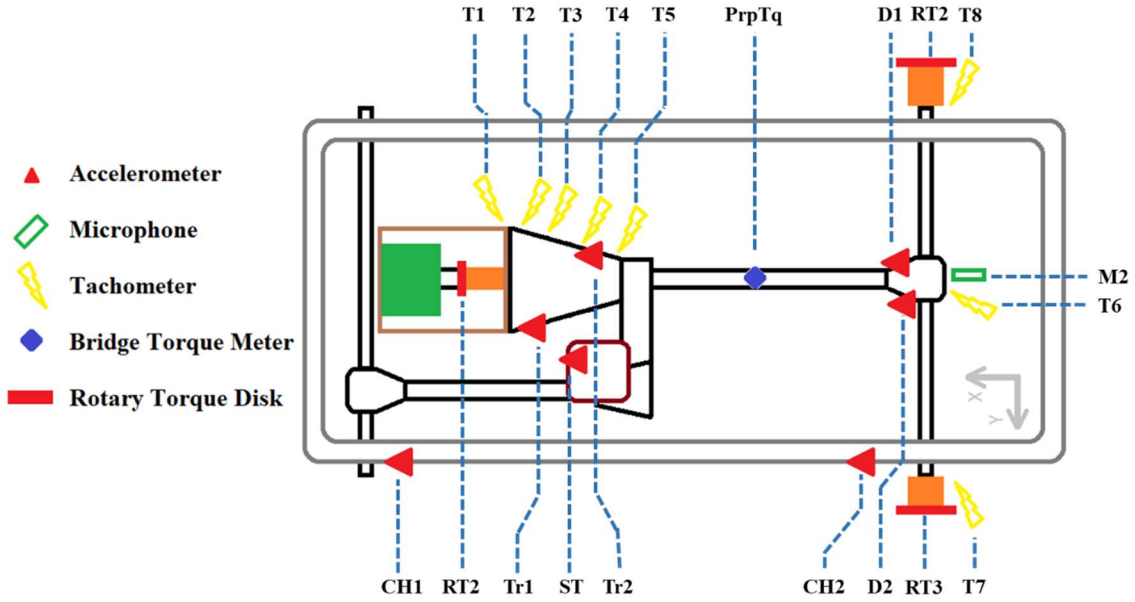

Figure 39: Fully Instrumented Dynamometer Test Rig Transducers and Locations

Table 3: Dynamometer Experimental Sensor Descriptions

Abbreviation	Measurement	Transducer
Tr1	Accelerometer	PCB 356A15
Tr2	Accelerometer	PCB 356A15
D1	Accelerometer	PCB 356A15
D2	Accelerometer	PCB 356A15
ST	Accelerometer	PCB 356B41
M2	Microphone	PCB 130D20
T1	Tachometer	Honeywell 3015A17
T2	Tachometer	Ford P# DY1400
T3	Tachometer	Ford P# 7M183
T4	Tachometer	Ford P# DY1406
T5	Tachometer	Ford P# DY1379
T6	Tachometer	Honeywell 3015A17
T7	Tachometer	Ford P# BRAB412
T8	Tachometer	Ford P# BRAB532
PrpTq	Strain	VPG CEA-13-062UV-350
RT1	Strain	PCB 5308D-01A
RT2	Strain	PCB 5308D-02A
RT3	Strain	PCB 5308D-02A

The combined input electric motor and two absorbing dynamometers allow for controlled transient testing in the laboratory that is used to simulate road loads referred to as Thr/r testing. This is achieved through a control strategy or road load simulation that estimates the tractive effort using Equation 1 to estimate the absorbing torque required at the dynamometers. The signal commands are shown in Figure 40 and dyno commands are calculated using Equation 11. Variables used in Equation 11 include $V^{i}_{cmd\,rpm}$, the commanded vehicle speed, in rpm, that is compared to the instantaneous dyno speed, $Dyno_{rpm}$, and used as error input to the PID controller. $V^{i-1}_{cmd\,kph}$, the previous commanded vehicle velocity in kph. dT is the delta time between calculations for discrete real time evaluation. Tq_{sum} is the sum of both wheel torques measured on the dyno. GR is the total gear ratio of the vehicle, a product of the transmission and final drive ratio. ef is the rated "efficiency" of the driveline (set to 100% for testing). r_{wheel} is the effective tire radius in meters. $m_{vehicle}$ is the mass of the simulated vehicle in kg.

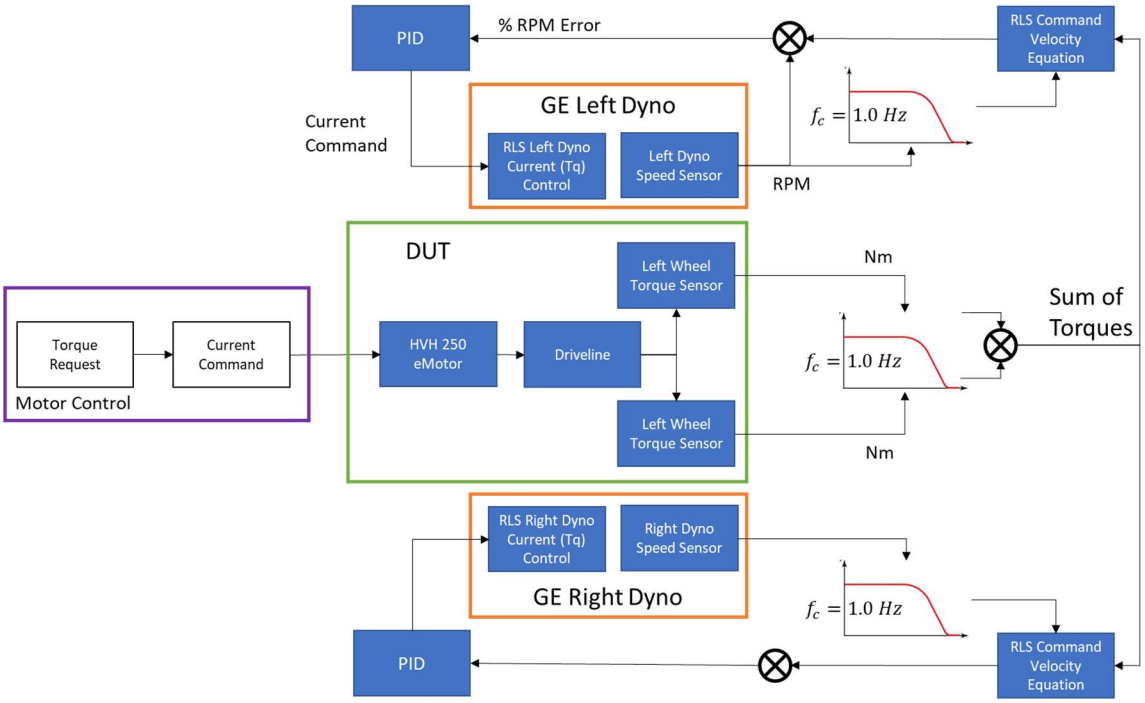

Figure 40: Dyno Thr/r (Road Load Simulator) Workflow and Processing

The workflow depicted in Figure 40 has three main components. The motor control (surrounded in purple), the device under test (DUT) which is the modified driveline depicted in Figure 39 (surrounded in green), and the absorbing dynamometers (surrounded in orange). A torque request is sent from the motor controller which becomes a current command delivered to the input HVH250 eMotor. This in turn delivers torque to the driveline which is measured by the left and right wheel rotary torque sensors. The sum of torques along with wheel speed signals are fed into the road load simulator, RLS, velocity equation. The dyno PID controller then compares the error from actual measured velocity to estimated RLS velocity and modifies the dyno current command to achieve the desired road loads.

$$V^{i}_{cmd\,rpm} = \left(V^{i-1}_{cmd\,kp} + \left[dT * \frac{\left(\begin{array}{c} \left\{ \frac{Tq_{sum} * GR * ef}{r_{wheel}} \right\} - \\ \left\{ F_0 + F_1 \left\langle \frac{Dyno_{rpm} * 30\pi r_{wheel}}{GR * 1000} \right\rangle + \right\} \\ F_2 \left\langle \frac{Dyno_{rpm} * 30\pi r_{wheel}}{GR * 1000} \right\rangle^2 \end{array} \right) * 3.6}{m_{vehicle}} \right] * GR * 1000 \right) \Big/ 30\pi r_{wheel} \quad \text{Equation 11}$$

Road testing consisted of consecutive tip-out, throttle stab, and tip-in maneuvers all while attempting to keep the vehicle speed near a target center speed as selected in Table 2. The dyno controller output's real time velocity estimates but controls on the wheel speed plane. Thus, it is desired to consider target speeds at the dyno as target wheel speed RPM converted in Table 4.

Table 4: Revised Test Run Speeds and Corresponding Gear Ratio for Dyno Testing with Wheel Speed and Torque Input Control

	Target Wheel Speed (RPM)		
	400	500	600
Transmission Ratio	2.14	2.14	1.76
	1.76	1.76	1.52
	1.52	1.52	1.27
		1.27	1.00

The dynamometer data was collected in the road load simulator mode to replicate driving conditions based on tractive effort estimates and measured wheel speeds and torques. While on the dynamometer, the modified vehicle driveline is missing some inertial elements. There is no engine inertia along with losses, no rotating tire inertia, and no reflected body inertia due to pitch as the vehicle accelerates. With these inertia elements removed, there is >55 kgm^2 of inertia missing relative to road testing and rolling chassis dyno testing. This reduction in mass and inertia will be considered when evaluating reactions to TI and TO in the lab. The dyno controller PID is used to control the RLS behavior according to the vehicle road load coefficients F_0, F_1, F_2, all available from EPA test results at www.epa.gov and implemented on the controller.

5. Laboratory Transient Analysis

Testing with the laboratory rig allows control over the torque converter clutch in two binary states; locked or unlocked. The control strategy for the converter lockup clutch is proprietary the manufacturer and partial slipping states were not the target of this research and therefore omitted from this study. Testing was conducted in the same four gear states identified and tested on road to evaluate differences and understand the influence of a locked or unlocked converter.

A sample dataset in 3rd gear, unlocked torque converter, with TI and TO event is depicted in Figure 41. Figure 41 shows the individual shaft speeds for the engine, TIS, TOS, Diff., driver side wheel, and passenger side wheel in solid blue, dashed red, solid yellow, solid purple with upper triangle markers, solid green with circle markers, and solid light blue with diamond markers respectively. The data reveals that the slipping torque converter allows the TIS to lag the engine speed during coast conditions after TO and the engine leads the TIS during drive or TI conditions. There are no SB events in the dyno RLS data because the current software architecture does not allow for such control. Future works are reviewing the implementation of such a strategy for comparison but were not available for this study.

The variations in speed once again are attributed to the gear ratio elements in the primary and final drive ratios. To compare on the same plane, the speeds are reflected by multiplying by the total gear ratio as done to reflect all the speeds onto the transmission input in Figure 42.

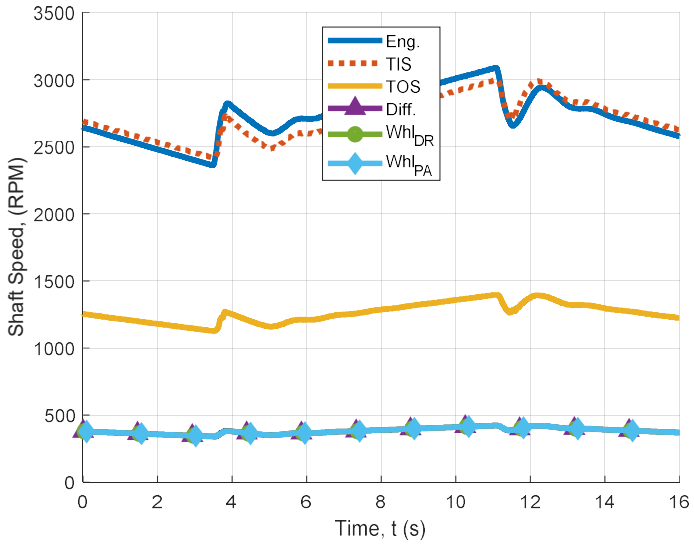

Figure 41: Dyno RLS Testing in 3rd Gear with TC Clutch Open Including a TI and TO event

The relative speed oscillations are observed in Figure 42 after the transient TI and TO events similar to those observed from the road data in Figure 6. The dyno RLS data shows a significant spike in all speed signals after a TI or TO event followed by a low <1 Hz oscillation. This low frequency oscillation occurs where the shuffle mode is assumed to be

excited but is not in-fact the shuffle mode and is a PID control mode based on the designated controller gain values. The controller gain values react to the change in measured wheel speed in RLS mode. The real time controller has latency in the discrete update rate. The latency paired with less aggressive gain values contribute to large overshoots but stable dyno control. The intermediate controller signals are depicted in Figure 43 and Figure 44 for a TI and TO event respectively. These provide an understanding of why the dyno control mode has large overshoots and dominates the TI and TO response.

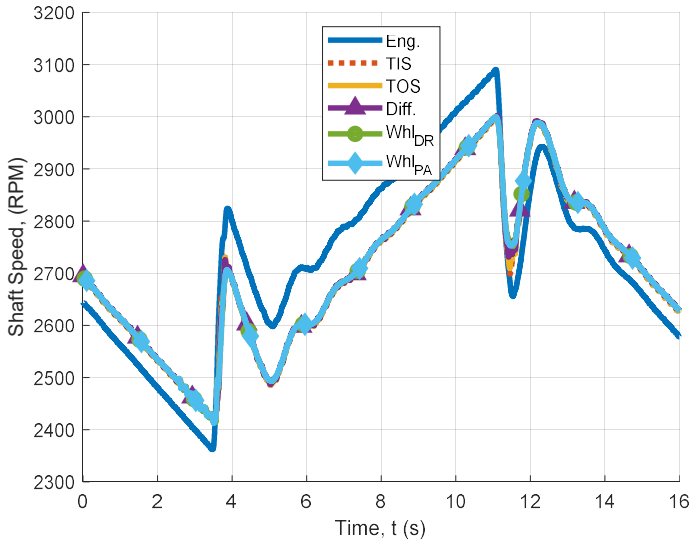

Figure 42: Dyno RLS Testing in 3rd gear with TC Clutch Open Including a TI and TO event with All Shaft Speeds Reflected onto the TISS Plane

Analyzing the intermediate controller RLS signals in Figure 43 & Figure 44 shows a few of the different feedback signals and formulas from Figure 40 and note their respective variable in Equation 11 when appropriate. The top subplot depicts the two filtered dyno speeds for left and right in dotted blue and dashed red respectively. The calculated RLS velocity from Equation 11 is in solid yellow, and the unfiltered left and right dyno speeds are in solid purple and dot-dashed green respectively. The second subplot in each figure depicts the torque measurements for driver side (left), passenger side (right), and sum of torques in dotted blue, dashed red, and solid yellow respectively. The third and bottom subplot denotes the resulting dyno control current from the PID controller for the left dyno in dotted blue and the right dyno in dashed red. In each plot there is a solid vertical black line that denotes the start of the TI or TO event.

At the start of the TI or TO event all the filtered, calculated, and instantaneous speeds in the top subplot are equal and stable. The TI event shows a positive spike in instantaneous dyno/wheel speed whose phase leads the filtered comparison used in the RLS command velocity equation. The resulting dyno command velocity lags the filtered comparison even further as a product of the discrete filter and discrete math delays in the software. As a

result, the commanded torque depicted in the bottom subplot stays positive for a TI and negative for a TO for a few milliseconds before switching signs and opposing the overshoot or spike in driveline speed. Thus, the driveline can accelerate beyond the RLS command velocity at a rapid rate before the PID controller reverses the control signal and oppose the overshoot. This results in a dyno control mode and transient data that does not resemble reactions observed in the road test data. Future improvements to this controller should be aimed at reducing the dyno control mode and possible implementation of a feed forward or similar strategy to reduce driveline speed overshoots during heavy TI and TO events.

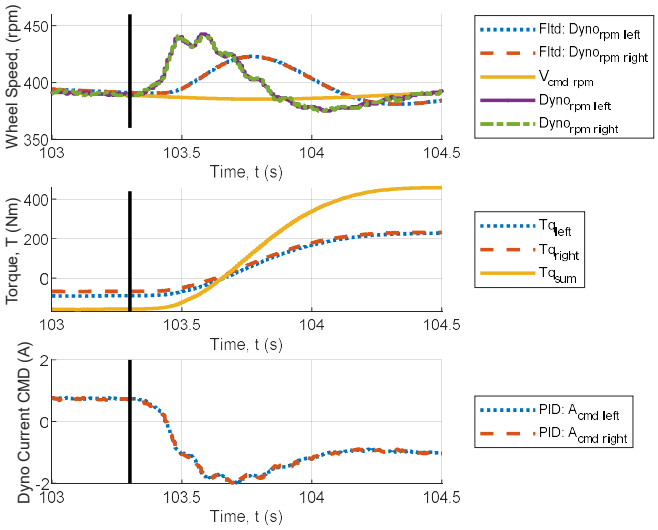

Figure 43: Dyno Thr/r Tip-In PID Low Frequency Mode

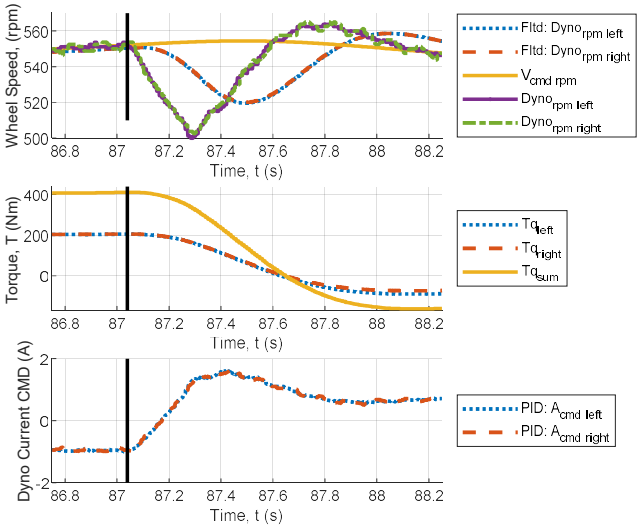

Figure 44: Dyno Thr/r Tip-Out PID Low Frequency Mode

Regardless of the dyno control strategy, the dyno mode (<1 Hz) is spaced far enough away in the frequency domain that it does not interact with the higher shuffle mode (expected to be >3 Hz based on road data in Table 5. Based on this frequency spacing, the dyno control mode can be removed along with other high frequency content with a band pass filter. BPF results for the example unlocked torque converter data is depicted in Figure 45. This data agrees with and is like the road data evaluated in Figure 7 with a dashed royal blue and magenta boxes outlining the TI and TO events respectively. Once again there are no SB events in the dyno RLS data due to limitations with the input motor control capabilities.

The dyno response with an open torque converter depicts a response like the road data shown in Figure 7. During the shuffle response, all the torsional shaft elements are in phase with one another with a slight lag in the wheel speed. Another similarity is during TI events, the peak shuffle oscillation is negative while the peak TO oscillation is positive. The open torque converter response differs from the road data showing one clear transient for the TI and TO events. Recall, in the road data for a TI event the shaft oscillation amplitude increases before a plateau followed by a subsequent decay. The TO event had two spaced transients in road data. The first when the throttle was released, and torque dropped and the second when lash is taken up and all the driveline lash components are in a coast contact region. The overall response is further compared in in Figure 46.

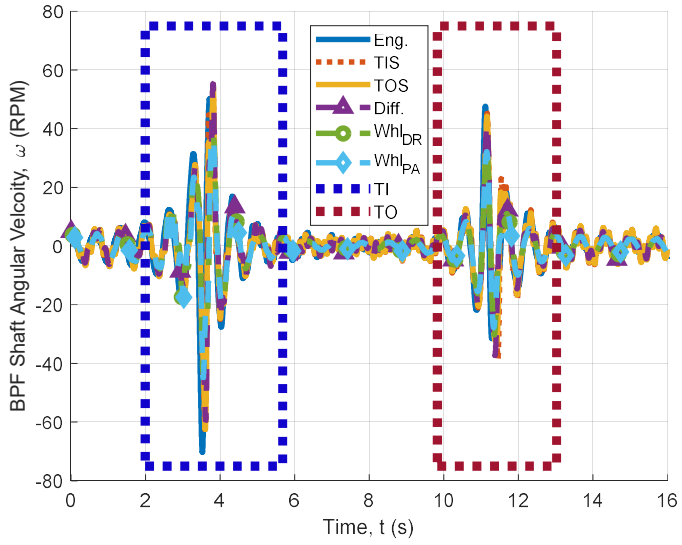

Figure 45: BPF Shaft Speeds During Dyno Thr/r Testing in 3rd Gear with TC Clutch Open

The overall response for an open torque converter TI and TO sequence shown in Figure 46 depicts from top subplot to bottom; the TIS speed in dashed red, the bridge measured propeller shaft torque in solid green, the longitudinal differential in solid red, the differential microphone in dashed blue, the longitudinal transmission acceleration in solid blue and the longitudinal seat track acceleration in solid purple. There is no throttle pedal position sensor in the dyno test cell because the engine has been removed and therefore no

throttle pedal exists. The remaining signals shown are comparable to the road data collected and analyzed in Figure 19-Figure 22.

By analyzing the data, it is observed that the propeller shaft torque display's a shape function like a step function or square wave. This exemplifies the input motor's capability to a near instantaneous step in torque request. This response is different to that from the ICE used for road testing. There is also a decrease in rotational inertia of the driveline on dyno. By observing the data, the torque level increases and holds flat at a peak torque before undergoing the low frequency dyno mode oscillation and settling at a lower torque level than the peak. The actual torque request is unchanged however and the higher torque is an artifact of the relative torque input to the eMotor counteracted by the dyno motor inputs after lash has been crossed in the driveline. The longitudinal differential and seat track accelerometers show an impulsive event induced by the TI but no high impulse after the TO like what was experienced in the road data. The differential microphone does not observe any impulse events based on the dyno data. The data was proven to show the shuffle response superimposed on the total response for shuffle frequency extraction. The propeller shaft torque signal is also available for processing to estimate the total lash and compare with the road data estimates.

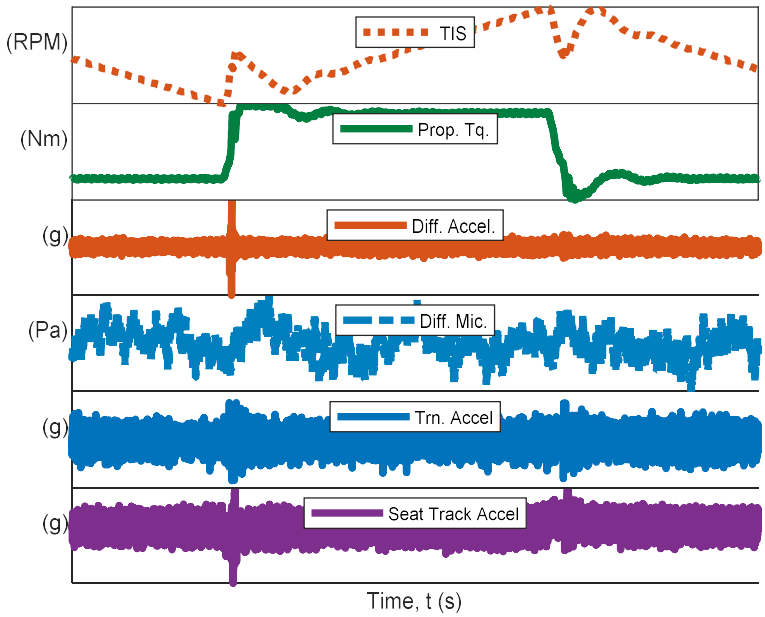

Figure 46: Summary of Dyno Thr/r Testing in 3rd Gear with TC Clutch Open from Top to Bottom; TIS Speed (RPM), Propeller Shaft Torque (Nm), D1 +X (g), M2 (Pa), Tr1 +X (g), and ST +X (g).

The same sequence was repeated for all ten runs from Table 4 with a locked torque converter to observe the differences in driveline response when locked vs. unlocked. The analysis can be found in Appendix C: Additional Analysis and Figures.

The peak-peak shuffle longitudinal accelerometer response and shaft oscillations are plotted in Figure 47 and Figure 48 respectively. They combine all the locked and unlocked

torque converter data from the dyno test vehicle. A large contrast in the dyno test data relative to the road data is that all the locked torque converter data has a very narrow window for slip factor that appears to be stacked atop one another in a column. This differs from the road data where the locked data had a range of slip ratios covered. The change comes from the internal control strategy allowing small amounts of controlled slip on road during TI and TO events. The dyno transmission controller does not allow for any controlled slip and is either fully locked or unlocked during testing.

In Figure 47 the longitudinal transmission, differential, and seat track accelerations are plotted in blue diamonds, red squares, and purple circles respectively. Once again, the filled in markers denote the low slip factor and therefore locked torque converter data while the unfilled markers denote the unlocked torque converter data. The trend for each accelerometer is like the road data whereas the slip factor increases, the longitudinal acceleration decreases. This once again indicates that the slipping torque converter has positive benefits to decreasing the longitudinal acceleration experienced during shuffle.

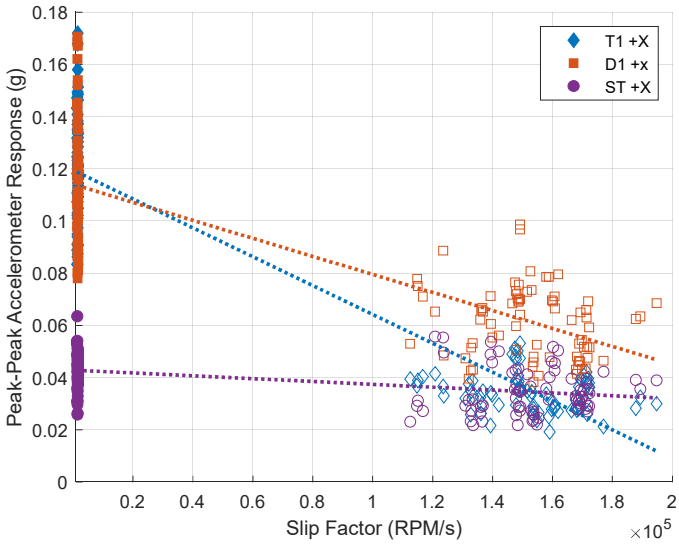

Figure 47: Peak Accelerometer Response vs. Torque Converter Estimated Slip Factor for All TI Data on the Dyno Test Vehicle Including Every Gear Combination and Test Speeds

In Figure 48 the peak-peak shuffle shaft oscillations are plotted vs slip factor. The engine, TIS, TOS, and Diff. speeds are denoted with blue diamonds, red squares, yellow upper triangles, and purple circles respectively. The filled and unfilled markers once again denote locked and unlocked torque converter data. The peak-peak shaft response in the dyno cell is much different than the road response trend. The amplitude increases with increasing slip factor instead of decreasing. This confirms the trend observed between the two example BPF data sets in Figure 45 and Figure 123. The reason for a lowered peak-peak oscillation is attributed to the locked state of the TC along with the dyno controller enforcing low oscillations relative to the unlocked state.

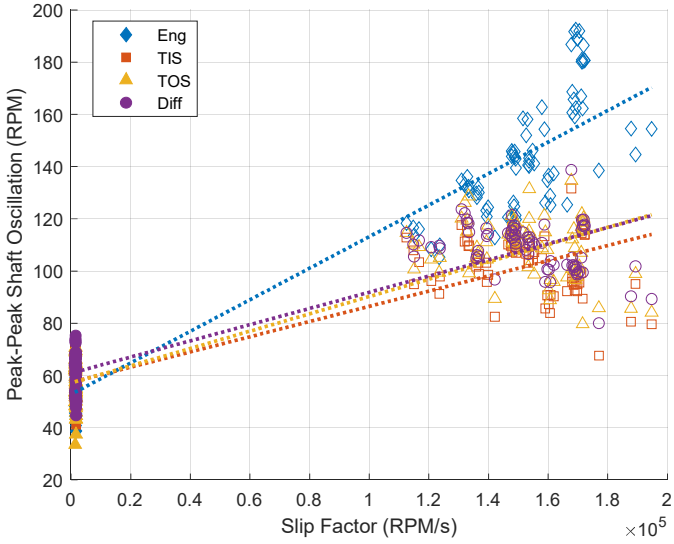

Figure 48: Peak Shuffle Oscillation vs. Torque Converter Estimated Slip Factor for all TI Data on the Dyno Test Vehicle Including Every Gear Combination and Test Speeds

The peak-peak responses for shuffle shaft oscillations and longitudinal acceleration are plotted in Figure 49 and Figure 50 respectively while separating the data for locked and unlocked classifiers. Figure 49 depicts the engine, TIS, TOS, and Diff. rotational speeds with blue diamonds, red squares, upper yellow triangles, and purple circles respectively. The linear fit trendlines are also superimposed on each data set with matching colors while the dashed and dotted trendlines are fit to the locked and unlocked data respectively. The data shows that as the torque ramp rate increases, the differential shuffle oscillation amplitude increases in both locked and unlocked scenarios. The only other trace to increase is the locked engine shuffle oscillation amplitudes. These three traces that have positive linear fit trendlines also have the highest correlation coefficients associated with the linear regression. The other negative slope trendlines have lower correlation and differ from the road data results.

The data in Figure 50 depicts the longitudinal acceleration for the transmission, differential, and seat track in blue diamonds, red squares, and purple circles respectively. The linear trend lines once again denote locked and unlocked torque converter clutch with dashed and dotted lines respectively. The correlation coefficient for all linear fits are very low and indicate poor linear correlation based on the data collected. The trend observed shows that in the locked torque converter state, the peak-peak accelerometer response is higher than when unlocked same as indicated in the slip rate plot from Figure 47. This data is all combined for a 3D view in Figure 51.

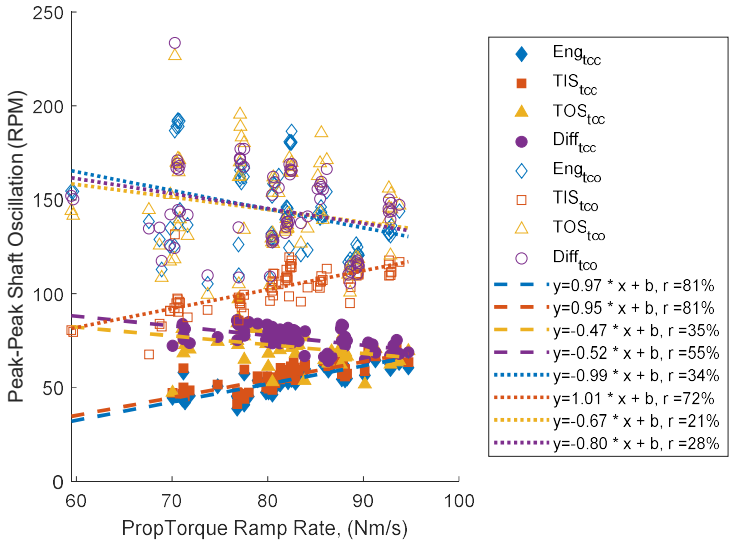

Figure 49: Dyno Data Peak Shuffle Oscillation vs. Measured Propeller Shaft Torque Separated for Slipping and Non-Slipping TC Clutch Data for all Test Gear States and Speeds with Correlation Coefficient

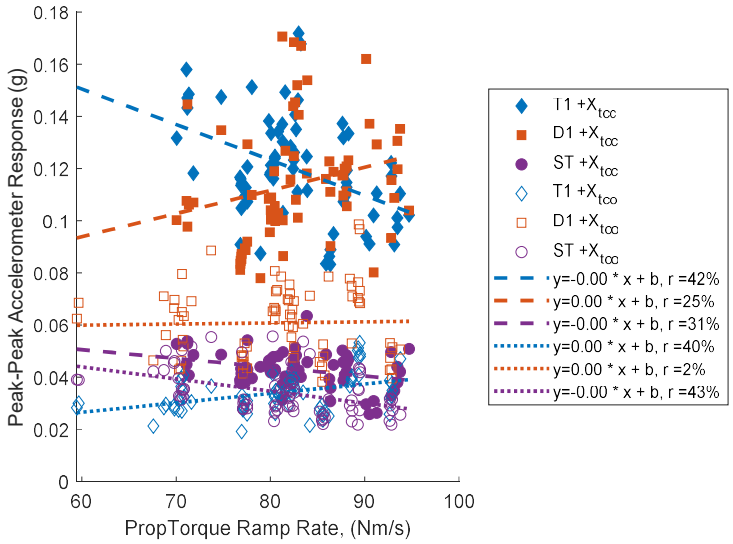

Figure 50: Dyno Data Peak Shuffle Acceleration vs. Measured Propeller Shaft Torque Separated by Slipping and Non-Slipping TC Clutch for TI Data in all Test Gear States and Speeds with Correlation Coefficient

Data shown in Figure 51 replicates the experimental road data compiled in Figure 33. The X-axis denotes the peak propeller shaft torque ramp rate, the Y-axis denotes the measured slip factor and the Z-axis denotes the peak-peak longitudinal seat track acceleration data. The controlled testing environment of the dyno generated two distinct groupings in Figure 51 that are separated for locked and unlocked TC clutch data with filled and unfilled markers. Six large markers are highlighted in the data, three in each group. The red star and left triangle indicate low and high peak torque data respectively for locked TC clutch

condition. The blue hexagram and upper blue triangle indicate low then high peak torque data respectively for the unlocked TC clutch testing condition on dyno. The green right triangle and square are used to contrast the differences in locked and unlocked peak torque data. The red, green, and blue marker time data is compared in Figure 52, Figure 53, and Figure 54 respectively. Note, the propeller shaft torque ramp rate is estimated much lower than the road data process. This is a limitation of the eMotor preset as a calibration value in the inverter software.

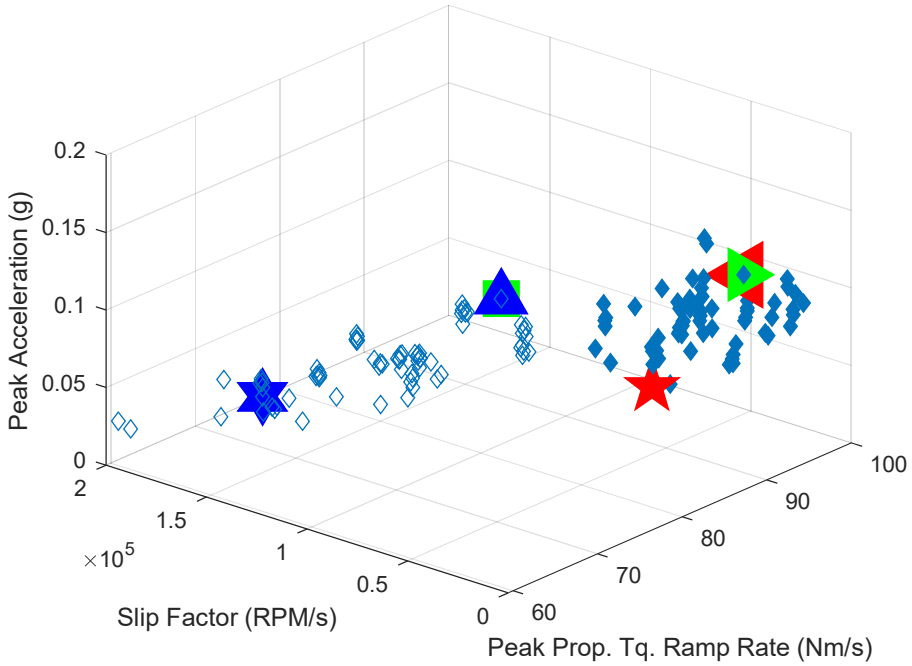

Figure 51: Dyno Data for Longitudinal Acceleration in the Z-axis plotted vs. Peak Torque ramp rate along the X-axis and slip factor along the Y-axis

Data in Figure 52 depicts a clear torque TI with a low frequency oscillation (~0.8 Hz) in the TOSS yet higher frequency shuffle oscillations (~8 Hz) on the seat track response. Adjustments to the BPF understand this low frequency TOSS oscillation to be an artifact of the low frequency dyno response's influence on the shaft speeds. The same higher frequency seat track response appears to be excited when comparing locked vs. unlocked data in Figure 53 however the unlocked data is at a much lower amplitude of oscillation. The two unlocked data traces in Figure 54 shows one big dyno influenced oscillation with higher frequency shuffle oscillations superimposed on the TOSS response. Overall, this shows that during a locked condition the longitudinal seat track amplitude increases while the dyno control mode induces a forced response on the driveline that reduces the influence of shuffle oscillations. This again depicts the influence that shuffle is not just a driveline oscillating mode but is coupled with the body response and should be modeled as such in any analytical study of shuffle.

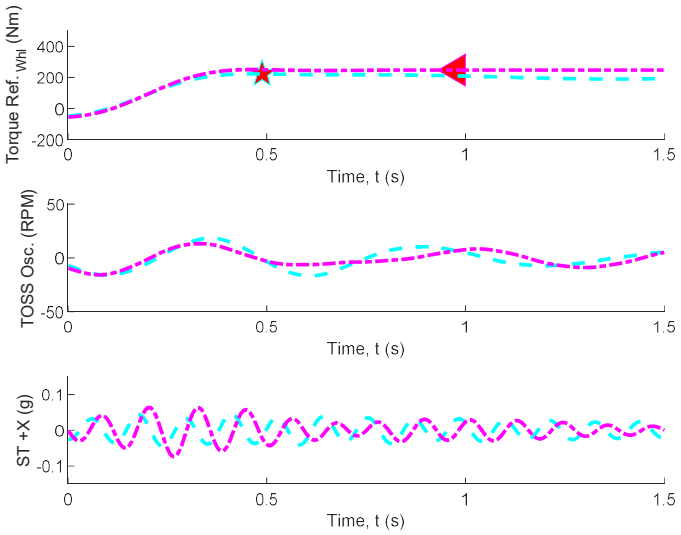

Figure 52: Locked torque converter data plotted from top to bottom; Torque, Toss, and Longitudinal seat track acceleration vs. time for low peak torque (light blue dashed line) and higher peak torque (dot dashed magenta line)

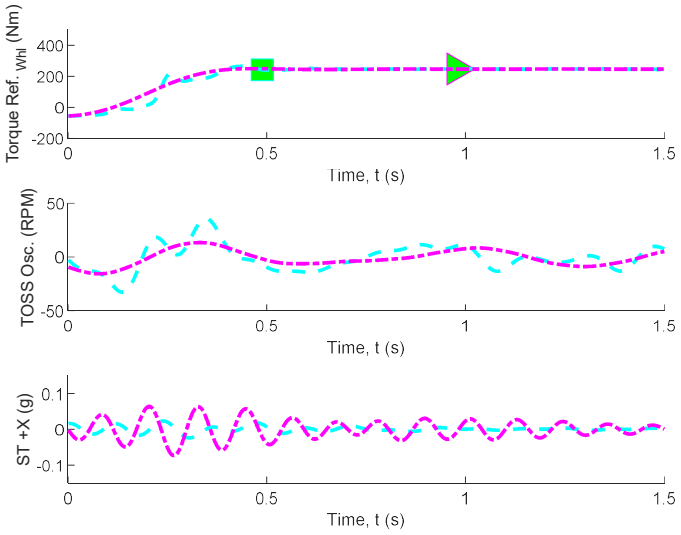

Figure 53: Locked (dot dashed magenta line) vs. Unlocked (light blue dashed line) torque converter data plotted from top to bottom; Torque, Toss, and Longitudinal seat track acceleration vs. time

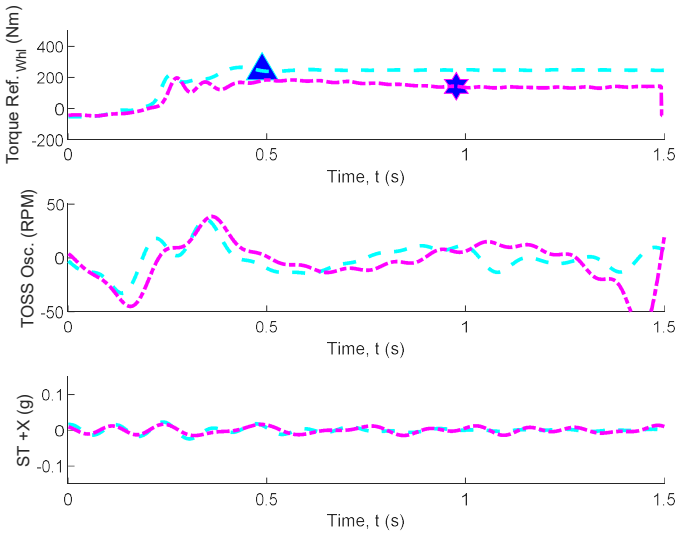

Figure 54: Unlocked torque converter data plotted from top to bottom; Torque, Toss, and Longitudinal seat track acceleration vs. time for low peak torque (dot dashed magenta line) and higher peak torque (light blue dashed line)

FRF data of the longitudinal seat track accelerometer over propeller shaft torque with coherence were plotted to compare with road data. They are depicted in Figure 55 and Figure 56 for the unlocked and locked TC clutch while on dyno respectively. The dyno FRF data is an order of magnitude greater than the road data due to a reduction in the sprung mass and un-sprung mass in the driveline. The disassembly for dyno testing included removal of the ~200 kg engine and peripheral components causing a reduction in inertia and mass. Another interesting observation is while on dyno, the T1 +X FRF is overall highest in amplitude while the ST +X was highest on road. This shows that the transmission pitch mode near ~11 Hz is dominating the response on dyno. Installation of the BorgWarner motor caused a forward shift in the powerplant center of gravity towards the front of the vehicle. The original engine mounts and spring rate did not change during this installation. Therefore, they are not tuned for this shift in CG and allow excessive pitching motion of the coupled transmission and BorgWarner assembly. Furthermore, there is a mode in the unlocked TC clutch data near ~4 Hz that is damped out and shifted down as shown by the low frequency peak in coherence when the TC is locked in Figure 56. This was caused by an increase in coupled inertia during lock up and forced response by the absorbing dyno motors. Once again coherence is highest near the shuffle frequency along with a frequency shift in each gear state that will be investigated in Chapter 3.

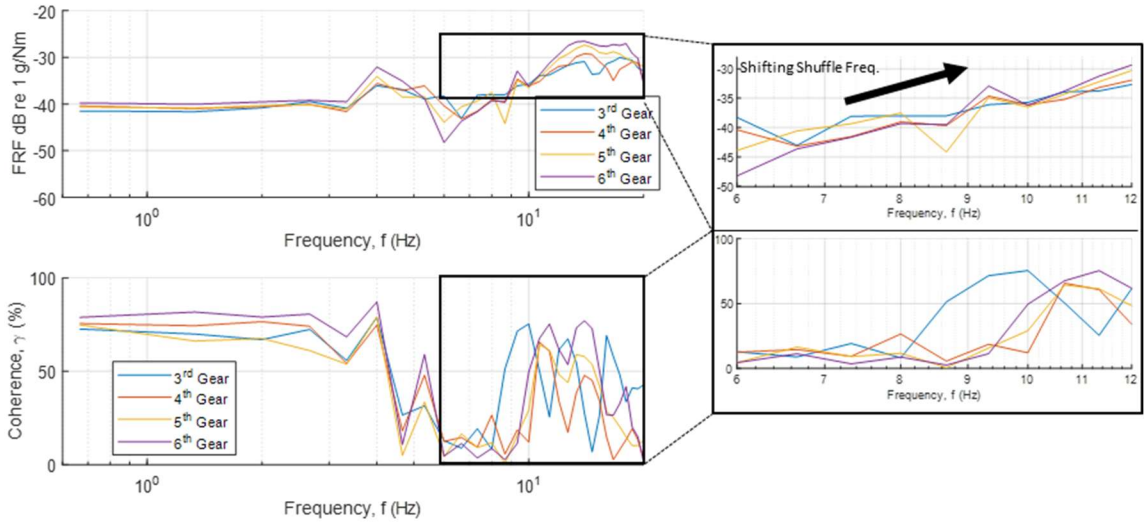

Figure 55: Averaged ST +X/Prop. Torque FRF for 3rd-6th gear on the ADAPT dyno testing in RLS mode with an Unlocked TC Clutch

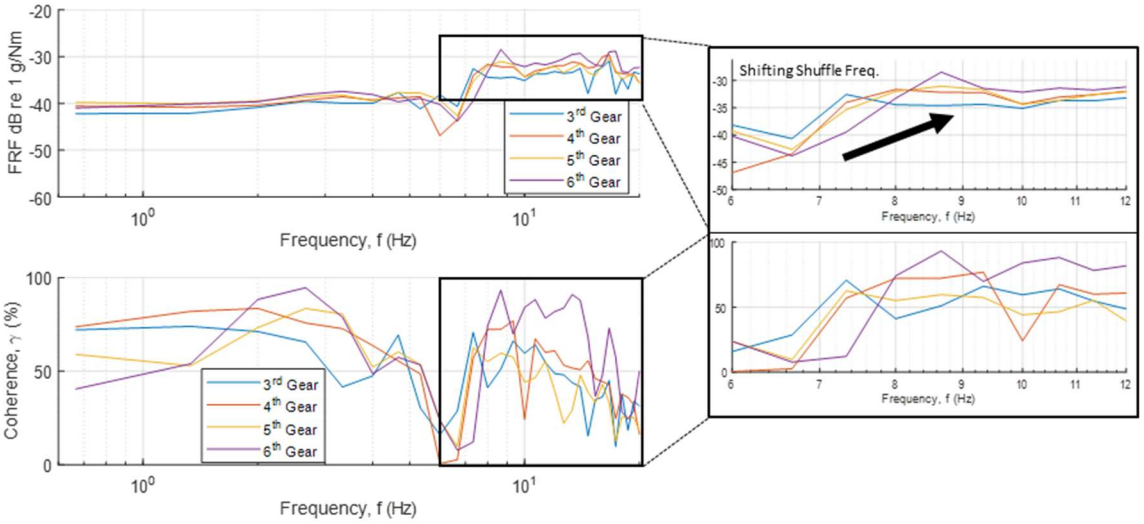

Figure 56: Averaged ST +X/Prop. Torque FRF for 3rd-6th gear on the ADAPT dyno testing in RLS mode with a Locked TC Clutch

Correlation between the driveline shuffle oscillation response and the longitudinal accelerometer response is depicted in Figure 57. This shows data from the dynamometer test vehicle and is shown to compare to results from the road data in Figure 37. The correlation coefficient for transmission and differential responses relative to the TOSS data is close in amplitude relative to the road data. This confirms again the correlation between shaft shuffle oscillations and the longitudinal coupling response. It is the longitudinal response that is be perceived by the driver and evaluated for vibration dosage. One contrast in the dyno data vs. road data shows how the locked torque converter data has higher peak

accelerometer responses but the shaft oscillations are lower on the dyno. The physics of this coupling are depicted in Figure 58.

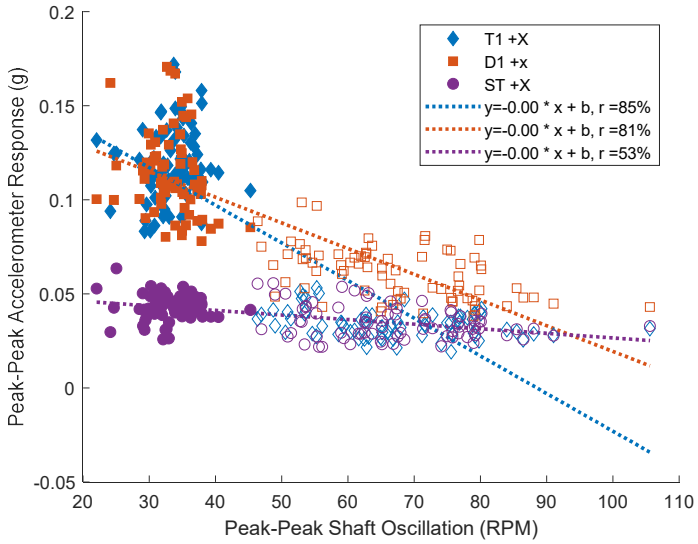

Figure 57: Shuffle correlation between TOSS peak oscillation and longitudinal accelerometer response on ADAPT dyno with correlation coefficient

Figure 58 depicts a differential ring and pinion gear representation boxed to the left along with the body reactions to the right. Reaction forces in the differential cause the rear axle to both pitch and roll. Roll about the y-axis generates a linear response in the x-axis due to reaction moments in the differential. The amount of longitudinal reaction force in the differential, $F_{Diff.}$, is proportional to the torque, $\tau_{Diff.}$, and equivalent suspension lever arm, $l_{Diff.}$, as described by Equation 12. The equivalent suspension lever arm is measured as the vertical distance from the pitch mode center to the rear suspension coupling plane.

$$F_{Diff.} \propto \frac{\tau_{Diff.}}{l_{Diff.}} \qquad \text{Equation 12}$$

A similar relationship is observed with the powerplant pitch mode reaction. This is due to the coupling of the propeller shaft inducing a reaction torque on the transmission output spline, τ_{spline}. The transmission output and propeller shaft do not lie on the same axis and intersect by angle α_{xz} thus, any translation of the propeller shaft induces pitching moment on the transmission. The torque reaction relationship at the transmission is simplified like the differential in Equation 13. The spline torque is proportional to the differential torque multiplied by an equivalent lever system through l_{Dnose} and $l_{T\ nose}$. In turn, the differential torque is proportional to the transmission output torque multiplied by the final drive ratio, FDR.

$$F_{Trn.} \propto \frac{\tau_{spline}}{l_{Trns.}} \propto \frac{\tau_{Diff.} * \frac{l_{T\,nose}}{l_{D\,nose}}}{l_{Trns.}} \propto \frac{\tau_{trn} * FDR * \frac{l_{T\,nose}}{l_{D\,nose}}}{l_{Trns.}}$$ Equation 13

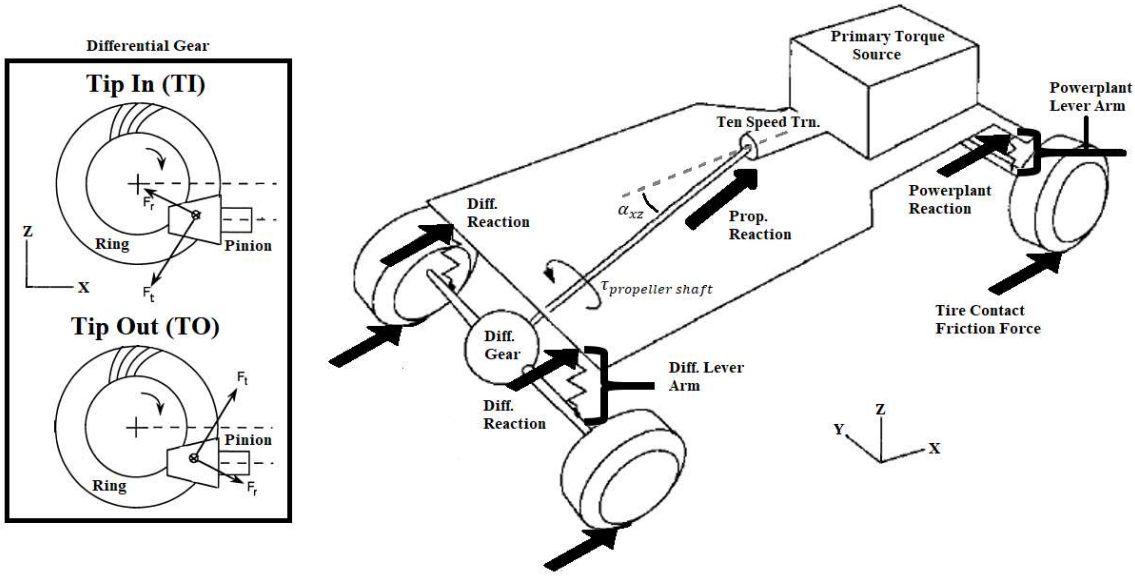

Figure 58: Coupled Reaction Torque to TI and TO Induced Longitudinal Vibration adapted with permission From [46, 61] as seen in Appendix G.

6. Conclusions

This study set out to understand the shuffle mode at a high fidelity combining many previous measurement metrics into one concrete analysis. This was done with a large assortment of transducers (tachometers, accelerometers, microphones, and strain gauges) retrofitted on a production test vehicle. The additional sensors were measured along with onboard CAN signals to compare ECU torque and speed estimates with high fidelity data acquisition. The response was then measured on another test vehicle but in a controlled laboratory dynamometer environment. The controlled test vehicle had many of the same sensors, minus the CAN bus signals. It also had additional torque input and output measurements with an electric motor used as the primary torque source replacing the ICE.

The results based on these two experimental setups concluded the following:

- Shuffle is the first torsional oscillation mode and confirms previous literature understanding. Further, this study showed that there is a difference in frequency based on a TI or TO event which should be captured in the ROM.
- The direction of torque reversal or lash crossing also dictates how severe the clunk response is. A positive lash crossing (coast to drive) event is highly impulsive on the differential while a negative lash crossing (drive to coast) peaks in the transmission longitudinal direction. This is due to the secondary location where lash is taken up due to a torque reversal and oscillation.

    - Thus, asymmetric damping should be higher in the transmission during negative torque loading and higher in the differential during positive torque loading.
- The torsional oscillations of the shuffle mode are coupled with the longitudinal oscillations and will be incorporated in the math model proportional to the first difference of shaft speed.
    - If the amplitude of torsional oscillations is reduced, the longitudinal acceleration is reduced and so should the VDV.
- A slipping TC clutch leads to reduced shuffle oscillation amplitude and accelerometer response. This in turn leads to a lower VDV metric.
- Low slip with high accelerometer response in the longitudinal direction for all measurement locations was shown to include a consecutive TI followed by TO but not classified as an SB event.
- High accelerometer response with low slip is due to the same behavior with consecutive TO late in the truncation window but at a very relaxed torque taper
- High slip with high accelerometer response was observed to be the result of a torque ramp rate and achieved peak torque at low gear with low vehicle velocity initial condition

3. Reduced Order Model Parameter Estimation

1. Literature Review

The test vehicle in this study has a high number of non-linear elements to control including backlash and asymmetric stiffnesses. The control strategy being investigated and supported by this work utilizes a reduced order model (ROM) for low computational cost of torque shaping and vehicle control. The reduced order model assigns real system parameters such as driveshaft inertia, stiffness, and damping, as inputs for the system they are controlling [51-53, 62]. The model must have these properties for each individual forward gear combination it is intending to control. Properties of interest in this study include the total system lash or gear backlash along with the shuffle frequency in a fixed gear state. The backlash represents the main non-linearity in the plant model to be used while the shuffle frequency is the target main oscillatory mode which the ROM is tuned to achieve and control.

Shuffle is understood to occur within the 2-10 Hz range for passenger vehicles. Analytical studies verify that the shuffle mode is in this range by calculating the first torsional mode of a torsional model of the driveline [4, 5]. Neither of these models include the coupling between driveline suspension components and the torsional body. Experimental studies such as the one done by Krenz used a time domain approach with peak picking in one tip-in dataset to conclude a shuffle frequency of 5.9 Hz based on an axle shaft torque measurement [2]. The result is only shown for one gear state and not compared or averaged over multiple tip in events so there is no clear indication if the frequency is changing in different gear states, loading conditions, or operating speed. Govindswamy et. al. concluded the shuffle frequency range based on ODS animations but does not publish the individual frequencies for each gear state, so no conclusion or trend is recognized based on

changes in the operating mode. This study used similar techniques to that of Krenz with a time-domain method as described in the shuffle frequency estimation section.

Lash (or gear backlash) is the amount of free play between two rotating components where one component may rotate a fixed amount of distance between two contact points in either a positive or negative rotation direction. The amount of lash can be experimentally measured and is typically done in a static fashion. In a study with Govindswamy et. al. they measured the final drive ratio lash in a static fashion by mechanically constraining driveline components but do not note how the measurement was made, just that a static technique was used [6]. Lash can also be measured in a dynamic fashion such as measuring the number of incremental rotations an input shaft achieves before the output shaft begins to rotate as well [63]. Another study done by Nordin et. al. iteratively updates a 2DOF control model until the resulting simulation matches that of a physical test model [50]. For an in-situ method, Krenz estimated angular displacement by integrating the relative shaft speeds but makes no mention how the total value was procured from this relative shaft displacement value. The study estimates lash at 8 degrees and verifies the system was designed to have 8 degrees of lash but makes no mention of manufacturing variances nor does it compare over several tip-in events for averaging and accuracy of the data. This study will use a similar technique to that of Krenz but will expand further to combine the relative shaft displacement with the shaft torque measurement as well.

2. Shuffle Frequency Estimation

To extract the response shuffle frequency for an individual transient event the data is first truncated into TI and TO data sets based on a positive or negative torque ramp rate while crossing a specified torque threshold. This is exemplified by the truncated data in Figure 19-Figure 22. The experimental data shows the shuffle frequency superimposed on the mean operating speed of the driveline and therefore a BPF is applied to remove the DC components and reject influence of higher frequency (>15 Hz) modes on the analysis.

Vibration theory for a free vibration system will oscillate at the system's natural frequency. The vibration response includes both a transient and steady state response, transient being the response to a change in force or torque input superimposed on the steady state. The steady state response is the system reaction to a constant forcing function. The TI or TO events are understood as transient inputs which yield a response as described by Equation 14 [57, 64, 65]. The equation denotes the system mass, m, the damped natural frequency, w_d, the damping ratio, ζ, the system natural frequency, w_n, and time, t.

$$h_{transient}(t) = \frac{1}{mw_d} e^{-\zeta w_n t} sin\,(w_d t) \qquad \text{Equation 14}$$

Based on this derivation, the carrier frequency contained in $sin\,(w_d t)$ is ignored and further post processing interrogates the logarithmic decrement rate according to the envelope of decay as described by Equation 15.

$$h_{Log.\ Dec.}(t) = \frac{1}{mw_d} e^{-\sigma t} \qquad \text{Equation 15}$$

The response data is analyzed, and curve fit with this single logarithmic decrement model to extract the damped natural frequency. More advanced but similar techniques could be further evaluated for use such as those are used in controlled modal analysis. These other time domain methods include the complex exponential, least squares complex exponential, Ibraham Time Domain or Eigensystem Realization. Future works could improve the estimation techniques by implementing such strategies. This research chose to curve fit the time data with Equation 14 in order to reduce the computational complexity. The future objective is to perform shuffle mode frequency extraction with real-time processing. Therefore, low computational expense is desired to reduce the needs of onboard computing in a production vehicle.

The curve fitting technique used for this analysis is depicted in Figure 59 by separating two events for TI and TO in accordance with the trigger conditions laid out in Equation 8. The figure depicts a curve fit and projection of the transient response for the lower envelope only. The actual algorithm utilized takes both the upper and lower envelope to curve fit and compare in the automated data processing algorithm.

It was previously shown that the frequency of shuffle oscillation appears to change for TI and TO response based on the STFT in Figure 9. The resulting frequencies estimated in Figure 59 confirm that TO has a lower response frequency than TI in the example dataset. This indicates that either the system is softening or loosing relative mass/inertia. However, this is one anecdotal case and additional measurements must be made to compare batch processing of these results.

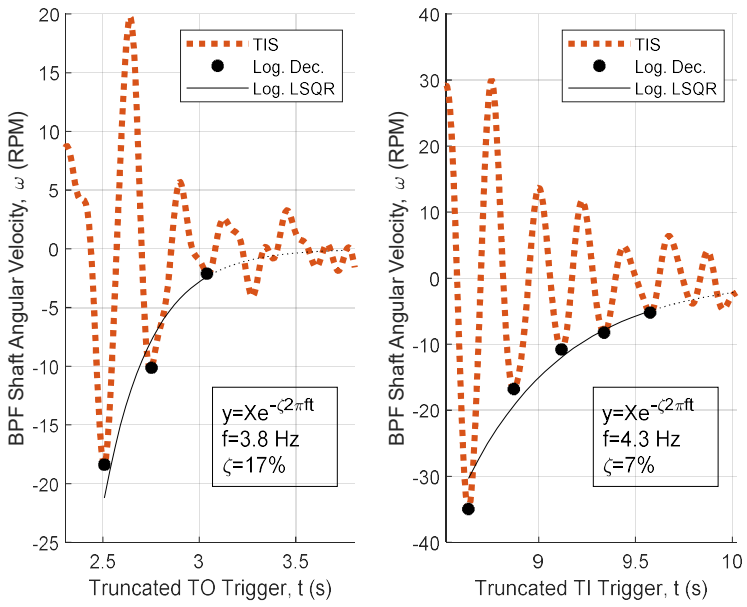

Figure 59: TI and TO Shuffle Frequency Differences for 3rd Gear at a Target Center Velocity of 56 kph

The experimental data was batch processed to estimate shuffle frequency based on the tip-in and tip-out data sets for all experimental run conditions; Normal Mode 2WD, Sport

Mode 2WD, Sport Mode 4WD, and Loaded [Sport] Mode 2WD. Two example sets of TI data are published in Table 5 and Table 6 for Normal and Sport calibration modes respectively. The data includes the average estimated shuffle frequency for fixed gear state ratio's and the target center velocity for all runs as outlined in Table 2. The experimental road data shows there are significant variations in estimated frequency depending on the fixed gear state but not significant variations as target center velocity increases. Therefore, further processing concatenates all data that is similar in fixed gear ratio when making further generalizations.

This observation is important to note because the ROM will need to consider the changes in different gear states but is not sensitive to changes in velocity. Therefore, no lookup table for shuffle frequency will be needed according to velocity & gear state. This observation is further verified by the analytical model in Chapter 5. Another note from Table 5 and Table 6 observes that the standard deviation is rather high in relation to the mean estimated frequency. This is on the magnitude of almost 25% of the estimated frequency. Such high deviation could further be refined by controlled testing in the dyno test cell or updated signal processing to eliminate noise variations in the data. Further comparison of the two vehicle control modes (Normal 2WD and Sport 2WD) observes a difference in shuffle frequency simply based on the calibration mode of the vehicle. The physical system parameters are not changing in different calibration modes other than engine mapping and torque delivery. These have no influence on effective stiffness or damping but may play a role in engine coupled inertia on the turbine shaft due to changing calibration. The lockup threshold and calibration of the torque converter clutch is also expected to change based on calibration modes of the vehicle. Based on the experimental results with open and closed TC clutch on dyno, these changes influence the shift in shuffle frequency based on calibration mode selection. This torque ramp rate and slipping TC clutch timing are highlighted in Figure 60.

Table 5: Normal 2WD Mode Average TI Shuffle Frequency Estimated from the TIS Sensor with Standard Deviation noted for all ten runs

Normal 2WD TIS. Shuffle Frequency [Hz] and (Std. Dev.)		Transmission Forward Gear Number			
		3	4	5	6
Target Center Velocity	56 kph	3.7 (0.9)	4.4 (0.4)	4.9 (0.7)	
	72 kph	3.9 (1.0)	4.8 (0.8)	5.0 (0.7)	4.8 (0.5)
	88 kph		4.8 (0.4)	5.3 (0.4)	5.3 (0.8)

Table 6: Sport 2WD Mode Average TI Shuffle Frequency Estimated from the TIS Sensor with Standard Deviation noted for all ten runs

Sport 2WD TIS. Shuffle Frequency [Hz] and (Std. Dev.)		Transmission Forward Gear Number			
		3	4	5	6
Target Center Velocity	56 kph	3.6 (0.7)	4.6 (0.8)	5.0 (0.5)	
	72 kph	3.7 (0.5)	4.4 (0.6)	4.8 (0.6)	5.1 (1.1)
	88 kph		4.4 (0.6)	4.9 (0.7)	5.2 (1.0)

The data in Figure 60 depicts data for Normal 2WD calibration in solid black and Sport 2WD calibration in solid grey. The top subplots both include all trigger condition data for a TI or SB event which both exhibit an increasing torque ramp rate. The bottom subplot includes the corresponding engine flare data. Engine flare is computed by subtracting the relative engine speed from the transmission input speed. This relative speed is the slip across the torque converter as described by Equation 16.

$$Engine\ Flare(t) = \omega_{engine}(t) - \omega_{TIS}(t) \qquad \text{Equation 16}$$

The resulting data observed in Figure 60 shows that the torque ramp rate is more aggressive in the grey Sport 2WD calibration data than the torque ramp rate observed in the Normal 2WD calibration data. This is indicated with a dashed blue and dotted red line overlaid on each plot of torque. The blue line fits close to the maximum Sport ramp rate while the red fits to the maximum Normal mode ramp rate. The Normal data in black appears to hit a threshold around 1700 Nm. At his point SB events bleed off torque while sustained TI events plateau then rise based on the vehicle calibration. This is denoted by the green arrow labeled A. The Sport mode data does not observe this threshold and appears to drive through the hang-up threshold all the way to peak torque. The slipping torque converter trace appears to sustain high amplitude slip early in each trace but peaks at the green arrow indicated by C much earlier in the Sport mode data than the peak in Normal Mode data at B.

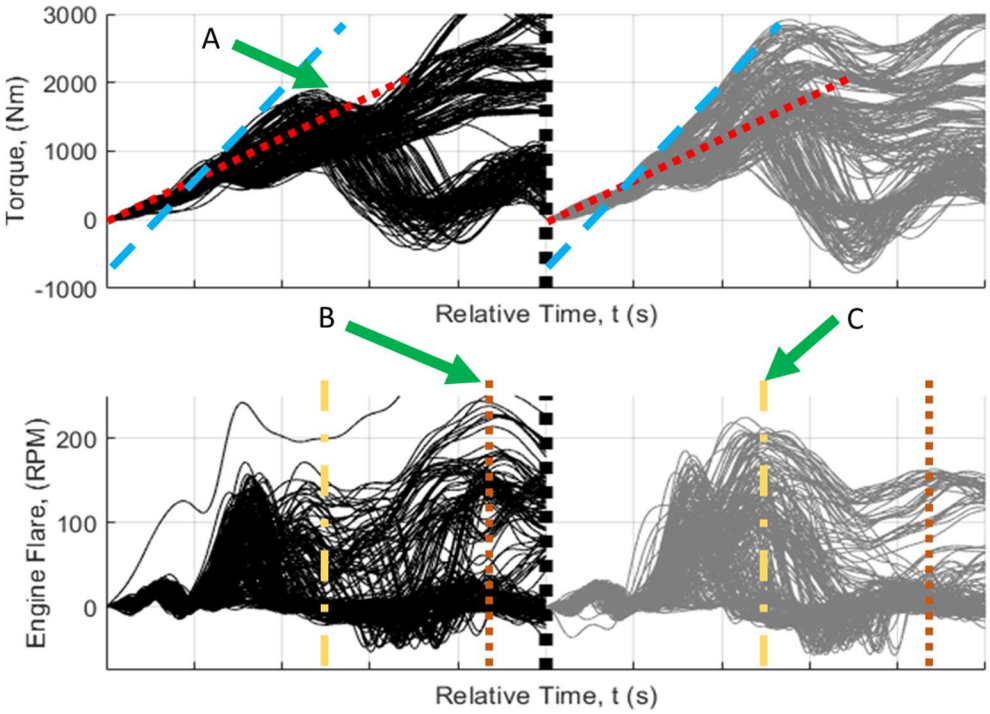

Figure 60: Truncated Torque (top) and Engine Flare Data (bottom) vs. Time for (left) Normal Mode 2WD Calibration and (right) Sport Mode 2WD Calibration

The normal mode calibration results shown in Figure 61 include data processed for the engine, TIS, TOS, and differential speed signals separated for TI (solid line with circle markers) and TO (dashed line with upper triangle markers) denoted with blue, red, yellow and purple lines respectively. The data combines all gear state runs together represented in each marker regardless of test target velocity. The data was processed as depicted in Figure 59 with the upper and lower envelopes. First, the trigger condition for tip-in or tip-out was determined based on a torque threshold crossing with positive or negative slope. Next the decay envelope was created by finding consecutive peak oscillations to curve fit the natural frequency and damping values of the envelope. The results for all 10 runs were collected and averaged together while rejecting any outlier greater than two standard deviations with respect to the shuffle frequency values. Outliers occur in the data due to noise on the signals either due to processing techniques or impulsive excitation due to secondary impacts in the data such as those observed in SB maneuvers.

The overall message from Figure 61 depicts a TI shuffle frequency analyzed to be higher than the TO shuffle frequency. This is on par with what was expected when reviewing the STFT from Figure 9 and confirms this shift in behavior from TI and TO. The anomaly in this behavior is observed in the top left subplot denoting data post processed from engine or flexplate speed data. This is upstream of the slipping TC clutch which explains this erroneous behavior and artificially lowers the shuffle mode observed at the engine. Otherwise, the shuffle frequency appears stable across the other sensors and gear states.

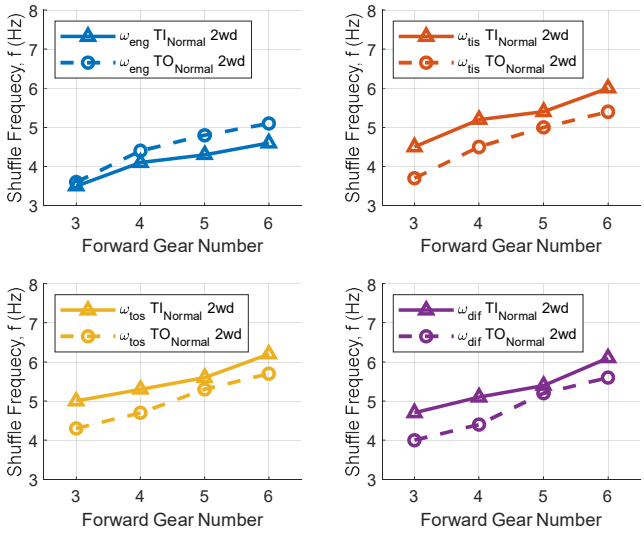

Figure 61: TI and TO Shuffle Response Estimated While Ignoring Outliers for the Engine, Transmission Input, Transmission Output, and Differential Speed During Normal 2WD Mode Testing

Data observed in Figure 62 is represented similar to that from Figure 61 but instead shows data analyzed from the sport mode calibration. The overall trend again shows TI at a higher frequency than TO shuffle but the differences become smaller when compared together. The resulting shuffle frequencies also appear lower than those calculated from the normal calibration mode. This graphically highlights the differences in calibration and their direct influence on the observed shuffle frequency without modification to the driveline itself. To compare changes in the driveline, the modified test modes are plotted against each other for all test conditions (Normal 2WD, Sport 2WD, Sport 4WD and Loaded Sport 2WD) in Figure 63 based on data from the TISS.

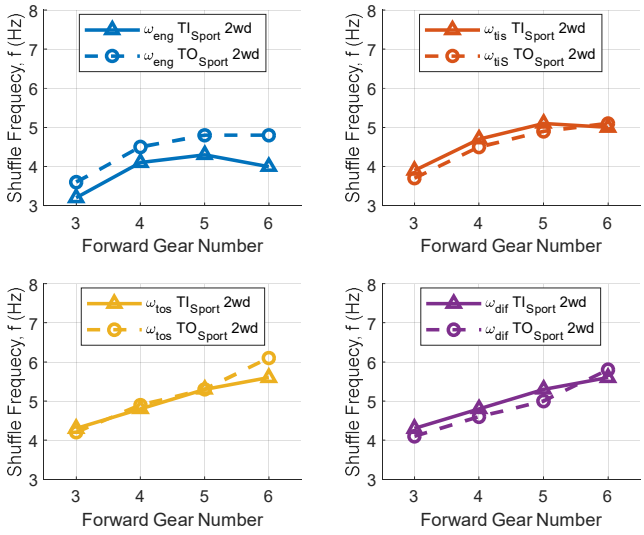

Figure 62: TI and TO Shuffle Response Estimated While Ignoring Outliers for the Engine, Transmission Input, Transmission Output, and Differential Speed During Sport 2WD Mode Testing

The resulting image in Figure 63 tracks the shift in shuffle frequency for TI (solid line with upper right triangle) vs. TO (dashed line with circle) in all vehicle test modes. The trend observes a decrease in shuffle frequency from Normal mode to Sport mode. It further shows a frequency increase from Sport mode 2WD to Sport mode 4WD. This is understood as the act of coupling another driveshaft, axle, and wheels which increased the effective driveline stiffness at a proportionally higher increment than the effective inertia. It further shows a slight decrease in shuffle frequency from 2WD Sport mode to Loaded 2WD Sport mode when weight was added to the center of the test vehicle truck bed. The added weight shows an increase in effective mass with little or no change in the effective stiffness. The results indicate further influence of the suspension coupling with the driveline that should be incorporated in shuffle analytical modeling during digital twin development.

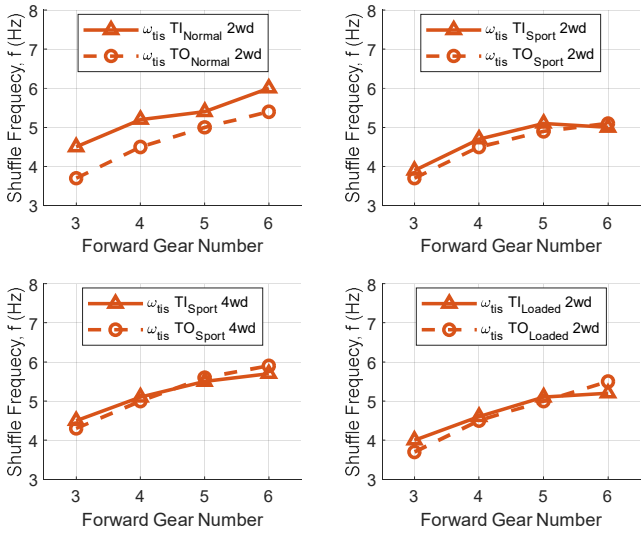

Figure 63: TI and TO Shuffle Frequency for All Four Testing Modes Estimated from TIS Sensor Data

Another way to compare the TI estimates across the different driveline modes and highlight the variability in data is to plot box and whiskers of the data with outliers as done for third gear data in Figure 64 and Figure 65. Additional data for fourth-sixth gear are found in Appendix C: Additional Analysis and Figures. Data in Figure 64 denotes curve fit solutions extracted from TISS data while data in Figure 65 represents curve fit solutions extracted from propeller shaft torque data. Each of these box and whisker comparisons has data for all four road testing modes; Normal 2WD (Norm), Sport 2WD (Sport), Sport 4WD (4WD), Loaded Sport 2WD (Load), and the two dyno control modes data; Thr/v and Thr/r. The dyno control data is differentiated by either fixing the dyno speed at a set velocity as done in Thr/v or allowing the dyno to operate in road load simulator, Thr/r, according to the control strategy in Figure 40 along with Equation 11. Thr/v is equivalent to Thr/r but replacing the output of Equation 11 with a set velocity that is then compared with the instantaneous wheel speed and the error is transferred to the PID. The data for each dyno mode analyzed is extracted from locked torque converter data. Each box and whisker depict outliers as a red "+" marker, two black whiskers at top and bottom for the maximum and minimum estimates, a blue box where the upper and lower edges define the 75th and 25th percentile respectively. The inner red line of the blue box denotes the median datapoint ignoring all outliers.

There appear to be several outliers in all the experimental road data solutions. This can be expected in experimental work while fitting a linear transient solution for free vibrations to a non-linear transient system. It is understood that the standard deviation of each road dataset appears to be high relative to the low frequency solution. There is not baseline available for how accurate the solution needs to be to have an effective ROM estimate. This could be the focus of future analysis but was not covered in this study.

The previous trends from Figure 63 relating the mean solution shifting in each control mode do not on first glance appear to translate to the solution shown in Figure 64 and Figure 65. This is because the box and whisker data show the median value in the middle red line and not the mean value as extracted in the previous TI and TO data comparisons from Figure 61-Figure 63.

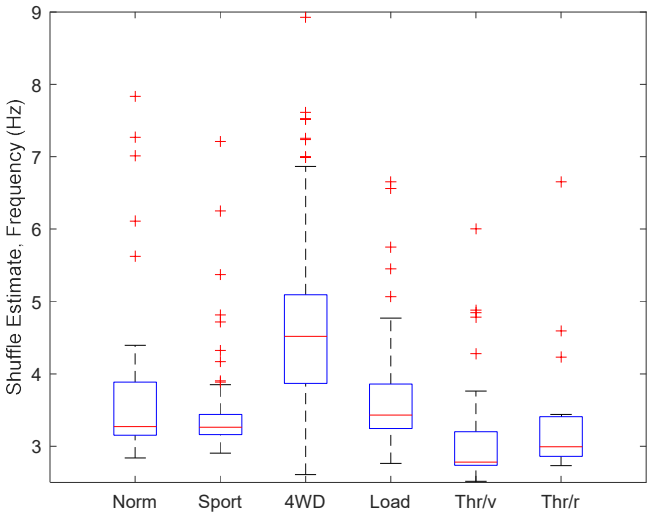

Figure 64: Third Gear TI Shuffle Frequency Estimates for Road (Normal Mode 2WD [Norm], Sport Mode 4WD [Sport], Sport Mode 4WD [4WD], Loaded Sport Mode 2WD [Load]) and Dyno Data (Thr/v and Thr/r) Extracted from TOSS Signal Data

Further observation shows the shuffle mode solution based on TISS data post processing is lower on dyno than the road data shuffle frequency in Figure 64. This indicates that the shuffle mode is shifting down when on dyno after removing inertial and stiffness elements. That solution indicates that the relative inertia has a larger proportional increase than the stiffness decrease. This is counter intuitive to the reality that inertia was removed, and the relative effective stiffness should sustain no change. The relative effective stiffness is expected to be unchanged due to shafts in series additive to the sum of the inverses and dominated by the softest spring in series. The only spring element removed is the tires and therefore no major stiffness effects are expected on dyno therefore this solution does not fit the physics. Another observation for the TISS processed data is that the range of each box and whisker is wider than the corresponding range when processed from the propeller shaft torque data.

The solution for shuffle frequency when post processing the propeller shaft torque data is presented in Figure 65 for third gear. Additional gears can be found in Appendix C: Additional Analysis and Figures. Trends observed from the torque extracted shuffle frequencies match the expectation for decreased inertia and unchanged relative stiffness. The higher frequency solution also matches with the observed higher frequency longitudinal response observed in the dyno time data response of Figure 52-Figure 54.

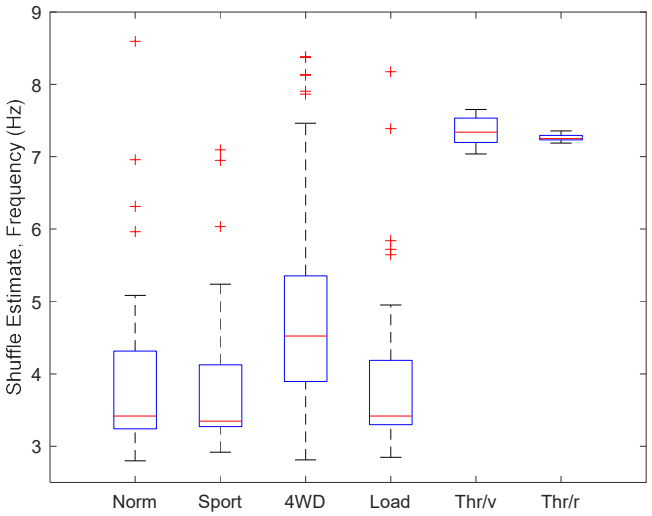

Figure 65: Third Gear TI Shuffle Frequency Estimates for Road (Normal Mode 2WD [Norm], Sport Mode 4WD [Sport], Sport Mode 4WD [4WD], Loaded Sport Mode 2WD [Load]) and Dyno Data (Thr/v and Thr/r) Extracted from Torque Signal Data

A similar comparison of TI and TO shuffle frequency changes based on gear state is made in Figure 66. The data was analyzed while the dyno controller was in Thr/r mode replicating road conditions. The data depicts TI and TO data by dashed lines with circle markers and solid lines with upper triangle markers respectively. The different colors indicate torque data with open TC clutch in blue, torque data with locked TC clutch in red, TISS data with open TC clutch in yellow, and TISS data with locked TC clutch in purple. The figure has three smaller subplots on the right-hand side to highlight the trend between TI and TO data but on different y-axes scales. The trend once again depicts that analysis of the TISS data observes a lower frequency solution but does indicate TI frequency to be higher than TO frequency. The propeller shaft torque data shows a mix of results where the TI frequency is lower than the TO frequency if the TC clutch is open in blue while the trend moves from lower to higher in different gear states for the locked TC clutch data in red.

Figure 66 further depicts the previous trend where estimates based on TISS data result in a lower shuffle frequency solution than experimental road data deemed counterintuitive to the stiffness and inertia adjustments made. The BPF used to post process data in Figure 66 has a lower cutoff frequency of 2.75 Hz which in turn is influencing the estimate. Changes to the BPF during post processing shift the low frequency solution of TISS estimates while the propeller shaft torque estimates remain unchanged. Therefore, the TISS data while on dyno is influenced by the dyno control while torque measurements still align with road data expectations.

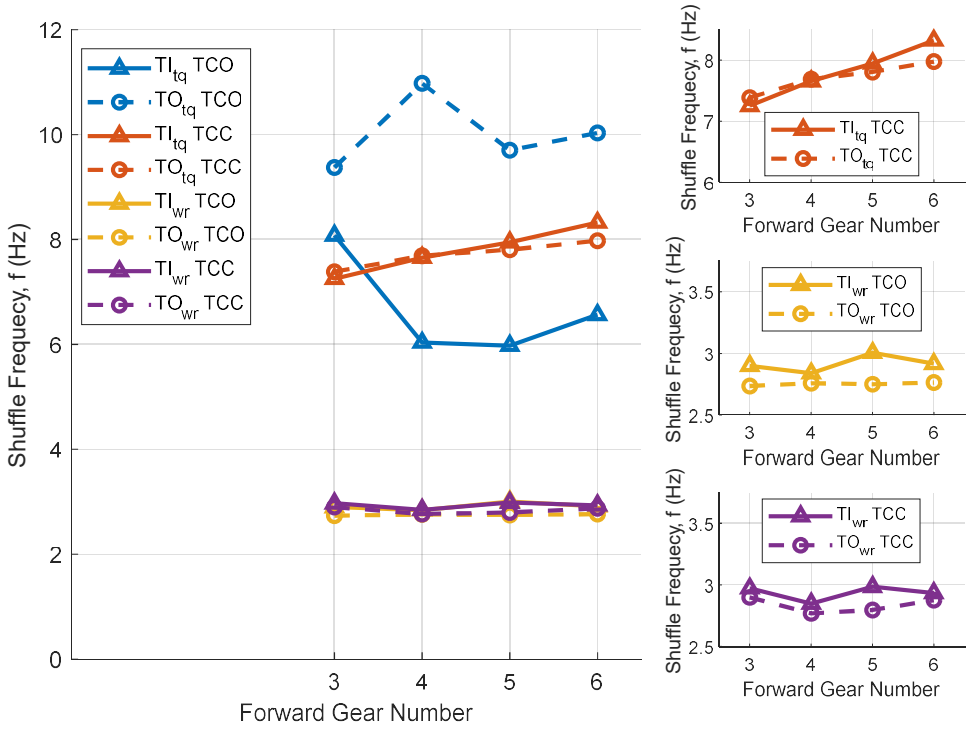

Figure 66: Dyno Data Estimates for Shuffle Frequency Based on Torque or TISS Data Analysis in Thr/r Dyno Control Mode with Locked (TCC) and Unlocked (TCO) Torque Converter Data.

3. System Lash Estimation

It is important to measure individual vehicle overall lash values to support the ROM for successful vehicle control and implementation. Each individual vehicle assembled is a combination of lash elements stacked together for one combined lash value in each fixed gear state. This value changes for every vehicle assembled due to manufacturing tolerances and assembly. Therefore, a technique is necessary to estimate a baseline overall lash value to assign in the ROM.

Lash is represented as a contact non-linearity and can be described mathematically in Equation 17. This equation denotes the angular displacement, θ, its two derivatives with respect to time $\dot{\theta}$ & $\ddot{\theta}$, the lash value, δ, the system inertia, J, system damping, d, system stiffness, k, and applied torque, τ. The stiffness and damping properties also denote positive and negative contact with the subscript p and n respectively. The simple system described by Equation 17 can also be interpreted as shown in Figure 67.

$$\begin{matrix} if\ \theta & > & \delta_{lash}/2 \\ if\ |\theta| & \geq & \delta_{lash}/2 \\ if\ \theta & < & -\delta_{lash}/2 \end{matrix} \begin{Bmatrix} J\ddot{\theta} + c_p\dot{\theta} + k_p\theta, \\ m\ddot{\theta}, \\ J\ddot{\theta} + c_n\dot{\theta} + k_n\theta, \end{Bmatrix} = \tau \qquad \text{Equation 17}$$

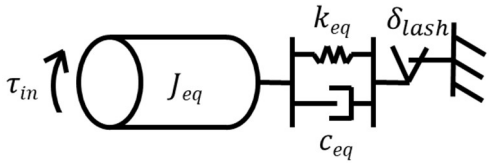

Figure 67: SDOF Oscillator with Backlash Representation

A truncated model of the test vehicle is observed in Figure 68 where the major lash components are denoted as the primary drive ratio boxed in blue (the transmission in a fixed gear state), and final drive ratio boxed in purple. These two lash elements were determined, based on CAE estimates provided, to be the largest lash elements of interest in the driveline. The primary drive ratio has green, red, and yellow boxes which denote the ring, planet and sun gears of each planetary gear set that make up the transmission. Also shown are five major inertial elements of the driveline, the engine, torque converter with lockup clutch, propeller shaft, and two absorbing shafts all denoted with grey boxes. There are ten clutching elements depicted in the truncated model, six grey clutches in the primary drive ratio, one black clutch in the torque converter, and three external yellow clutches. The external yellow clutches are not true physical elements of the driveline but instead are used to indicate portions of the driveline that are held fixed during static testing of sub-system components. Three different markers are noted on the truncated lash model including; speed sensors, torque sensors, and measurement locations denoted with blue diamonds, red hatched circles and purple pentagon markers respectively.

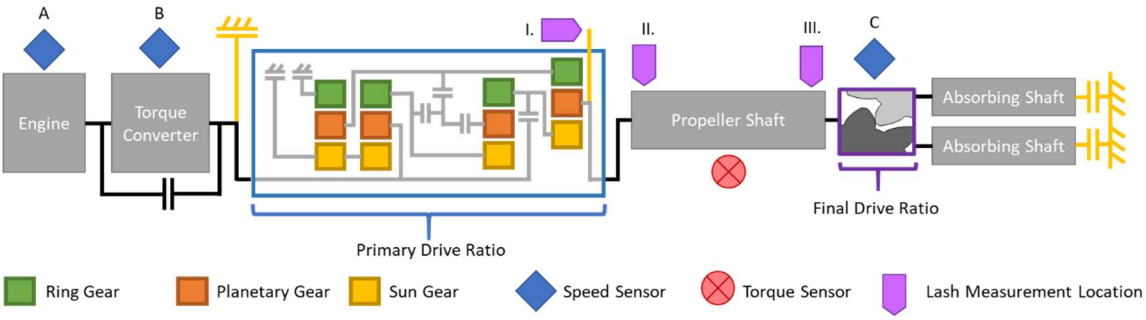

Figure 68: Truncated Driveline Lash Experimental Model Representation

The primary drive ratio is made up of four planetary gear elements with four rotating and two braking clutches. Selecting four clutches to engage within the transmission creates a fixed gear state during operation. The physical transmission relies on a rotating input to generate hydraulic pressure which in turn is used to pressurize each clutch through electronically controlled hydraulic solenoids. To "shift into" a fixed gear state in the absence of a rotating input to the transmission, each individual clutch pack can be removed and rigidly fixed together. A static gear state is then achieved by selecting, removing, rigidly fixing, and reinstalling four clutch packs. This process is repeated by removing and reinstalling fixed clutch packs for all gear states to be measured.

The output only rocking lash measurement was conducted by coupling or constraining the rotational degree of freedom at one end of the rotating lash component being tested while the opposing end is free to rotate. This is done in two stages to capture the two major lash components in the driveline. The first test on the primary drive ratio is done by creating the fixed gear state and constraining the transmission input shaft as depicted by the yellow clutch depicted to the left of the primary drive ratio in Figure 68. The output measurement was collected with a linear variable displacement transducer, LVDT, at measurement location I. on the output of the primary drive ratio. Since the output measure is linear, the rotational displacement is computed through multiplying by the offset measurement lever arm and assuming small angles. The small angle assumption was later verified to be true based on the resulting displacements. An example measurement is depicted in Figure 69 which shows the LVDT displacement as the output shaft is rocked back and forth against the two contact sides of lash. The total lash, δ_{lash}, is then computed by the average result of peak-peak displacement estimated by all the grey hexagrams shown in Figure 69. The left y-axis shows estimated measurement units according to the relative measurement displacement while the right y-axis shows displacement in accordance with the mathematical representation in Equation 17. Results of all measured gear states are later combined with the final drive element lash.

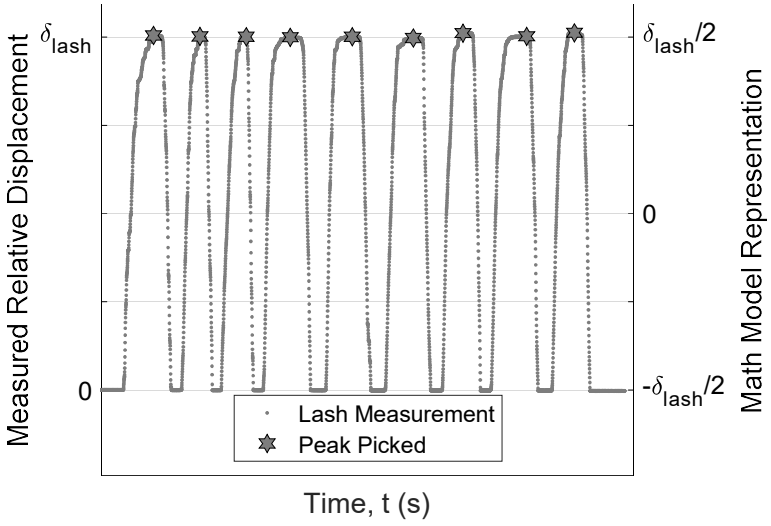

Figure 69: Output Only Static Rocking Lash Measurement Example Displacement vs. Time Dataset

The output only displacement measurements done on the transmission are a simplified test solution and assume that five degrees of freedom are fixed during testing. It also assumes that the positive and negative contact regions are infinitely stiff or that no elastic deformation occurs during the rocking measurement. It is recognized that if appreciable torque is applied then the total displacement measured will include elastic deformation according to Equation 18. In Equation 18, T denotes the applied torque, L denotes the shaft length, I denotes the mass moment of inertia, and G denotes the shear modulus of the shaft being tested.

$$\delta_{measured} = \delta_{lash} + \frac{TL}{IG} \qquad \text{Equation 18}$$

Both applied shaft torque and relative displacement are measured consecutively to account for the elastic deformation buildup due to torque loading. The relative torque applied is expected to be near zero during lash crossing because it only reacts against the inertial forces. Therefore, if the torque loading velocity is controlled to be slow or a cyclic application <1 Hz, the measured torque during lash should appear near zero.

An example of consecutive torque and displacement measurements was made and is shown in Figure 70. The top subplot shows the measured displacement in solid black while the bottom subplot depicts the measured torque in dot dashed black. Analyzing the torque measurement shows that the resulting signal appears to plateau near zero as the displacement measurement crosses relative zero displacement. It is also observed that both the torque and displacement measurements appear to be sinusoidal in nature due to the loading technique used for measurement. This loading leads to recognize there are two lash crossings during every one period of the sinusoidal function. One lash crossing during the negative slope or $0 - \pi$, assuming a cosine application starting at zero phase, and a second lash crossing in the positive slope region, $\pi - 2\pi$. Recognizing these two slopes for crossing regions leads into the data processing workflow used to extract the lash value from raw data depicted in Figure 71.

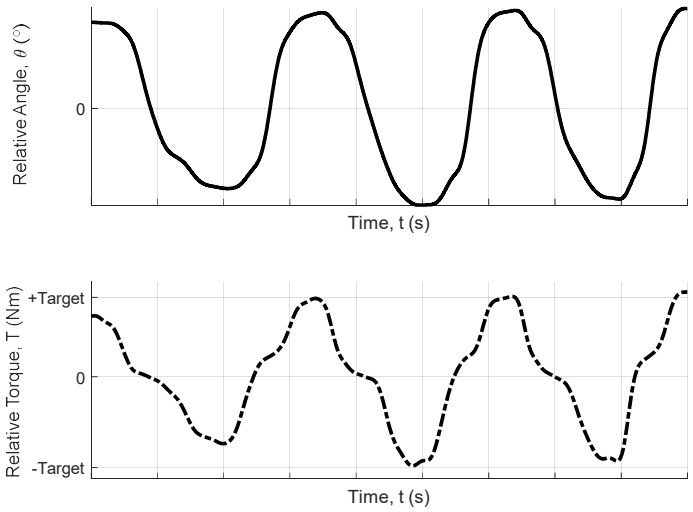

Figure 70: Static Rocking Lash Measurement Example for Relative Angle and Relative Torque Measurements vs. Time

The data processing workflow in Figure 71 is a generalization of how the data is processed to estimate lash. The raw data, as depicted in Figure 70, is separated into the positive and negative slope regions for different directional lash crossing events. The data is then filtered to remove any high frequency noise captured during the measurement. The data is further separated into three sections; the positive contact region $\theta > \delta_{lash}/2$, no contact

region $\theta \leq \delta_{lash}/2$, or negative contact region $\theta < -\delta_{lash}/2$, in accordance with Equation 17. After the regions have been separated, the lash is estimated for the relative displacement traversed between bisecting linear fit regions. A summary figure depicting the resulting bilinear curve fits and lash is shown in Figure 72.

Figure 71: Signal Processing Workflow for Rocking Backlash Data Post Processing

The resulting data in Figure 72 shows the hysteresis loop in dashed light grey achieved after filtering and plotting displacement vs. torque. The dark grey linear lines represent the linear fit trend lines for all six regions, three for the positive slope and three for the negative. Running along the backbone of all three regions is the bilinear curve fit where the center region runs along the near zero torque estimates. The drastic slope change and bilinear fit intersection points are crossed with horizontal red lines where the relative angular displacement between these two lines represents the estimated lash value, δ_{lash}.

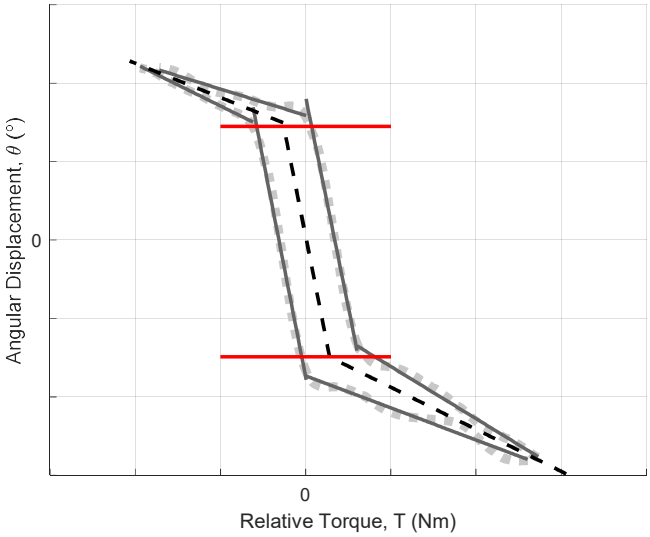

Figure 72: Resulting Backlash Data with overlaid Positive and Negative Sweep Curve Fits and Bisecting Linear Fit Lines with Resulting Lash Estimate

There are two additional lash measurement locations denoted in the truncated lash system depicted with Figure 68. These are the two measurement regions used for estimating lash in the final drive ratio (differential) of the vehicle. Each measurement was on the ring gear or input side of the differential, while the wheels or absorbing shaft was constrained allowing only rotation at the differential input. The two measurements upstream of the differential input are separated at each end of the propeller shaft. One was at the differential nose flange denoted as measurement location II and the other directly on the shaft just after the transmission output denoted as measurement location III. The difference and reason for

each was to incorporate the additional spline lash and examine the change in contact stiffness when adding the propeller shaft spring stiffness in series with the absorbing shafts.

The raw data for measurement location II and III are shown with red and black dots respectively in Figure 73. They are denoted differential and transmission estimate as a note for the proximity to which the measurement took place (II and III respectively). The positive and negative contact region stiffness is also estimated based on the bilinear curve fit trend line along with the non-contact region lash estimate. The results show that the positive and negative contact regions both exhibit different contact stiffnesses. This aligns with the changes in shuffle frequency in relation to a TI or TO shuffle event. The stiffness non-linearity is changing the effective stiffness which in turn shifts the response shuffle frequency according to a sustained TI or TO. The estimated lash value is also observed to be larger at the transmission location, II, due to the additional spline element. Some discrepancies are observed in the black transmission measurement data. Namely, the lower right quadrant of positive torque and negative displacement depicts two different hysteresis loops being followed. This is influenced by the torque amplitude inducing additional stiffness regions within the driveline elements. This is true to many drivelines but should be controlled during testing. Looking back at the example data in Figure 70 shows positive and negative target torque values used for the rocking backlash measurement differ in amplitude. The amplitude changes throughout the measurement which would account for the divergent hysteresis curves followed. The changes can also be achieved if the oscillating torque application frequency is changing throughout the measurement which should be controlled when and if possible. The data used for this processing was manually applied and therefore not controlled with any feedback loops nor structured positive or negative torque targets followed during application.

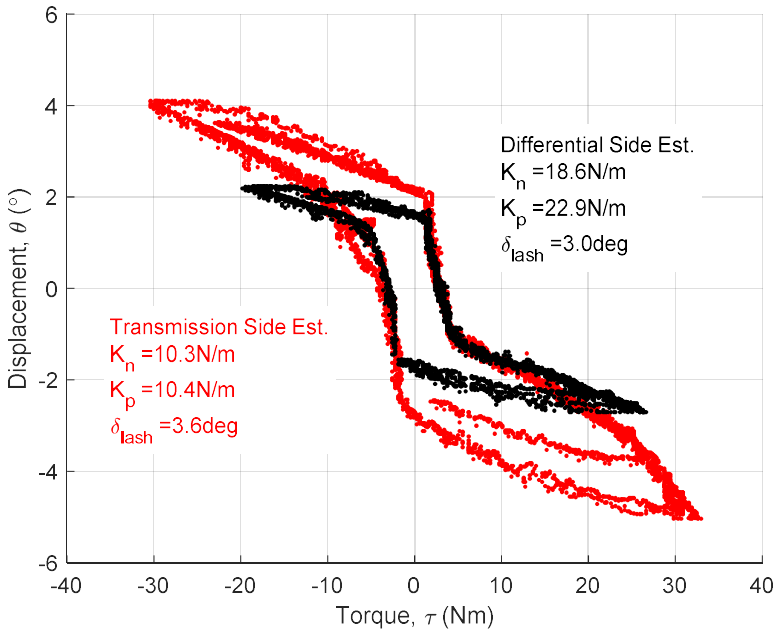

Figure 73: Final Drive Lash Estimate Results from Rocking Backlash Measurement

The static experimental results are a useful baseline measurement to compare with expected results but time consuming to achieve. They also require constrained measurements on the individual lash components based on the previously mentioned measurement sequences. The study desired to estimate lash with in-situ data for updating into the ROM and the static estimates are used as a comparison to analytical models as well as in-situ post processing accuracy.

Displacement is difficult to measure directly from a rotating shaft where only rotational speed is available from a single pulse train. It can be estimated by integrating the relative rotational speed as depicted in Equation 19. The discrete integration is skewed by high frequency noise in the rotational speed data and therefore must be filtered prior to integration. Continuous integration of the speed signals is also skewed by integrator windup and therefore a reset integration technique is used to mitigate the windup. These steps are taken before creating a torque vs. displacement curve like that done with the static measurement data. A block diagram is shown in Figure 74 of this workflow where the relative displacement is created by calculating the difference in rotational speed upstream of the major lash elements. This calculates relative displacement based on speed sensors A or B, to the rotational speed downstream of the lash element, speed sensor C. This formulation assumes only one torque source input to the driveline model.

$$\theta = \int \dot{\theta} dt + \theta_0 \qquad \text{Equation 19}$$

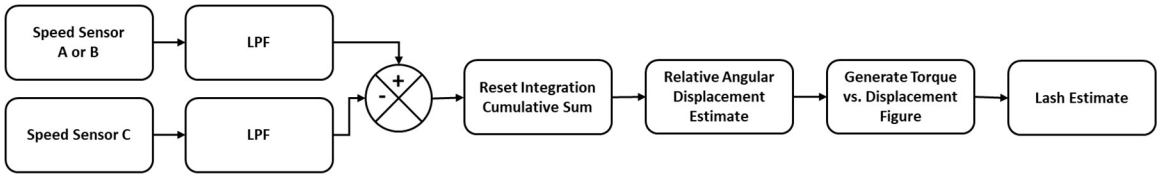

Figure 74: In-Situ Data Post Processing Workflow for Lash Estimation

The rest of the post processing workflow is like that done with the static lash measurements and is shown in Figure 75 for in-situ experimental data collected on the road test data in Normal 2WD calibration mode. The figure depicts upstream speed measurements of sensor A/B in blue along with downstream speed measurements of sensor C in red. These two are processed according to the workflow in Figure 74 with reset integration to achieve the relative displacement estimate according to Equation 19 in solid pink. Above that is the propeller shaft measured torque which is measured between the two major lash elements and should therefore measure near zero relative torque when one or both lash elements are not in complete contact. That same near zero torque estimate also assumes that there is only one primary torque source upstream of the propeller shaft, i.e. at the engine. The final subplot on the far right depicts the overall time trace resulting for torque vs. estimated relative displacement through reset integration in solid black. There is an additional truncated region overlaid in red that shows where the initial TI event occurs with consistent lash crossings near zero torque. The additional torque accumulation along with double lobed displacement windup is due to the sustained TI events with shuffle oscillations combined with slipping torque converter data. The additional lobes are not of interest and thus the data is truncated surrounding the TI events only for lash crossing estimates. The TO events do observe lash crossing behavior however torque management of the engine makes these trigger conditions less reliable to evaluate in-situ as observed in Figure 75.

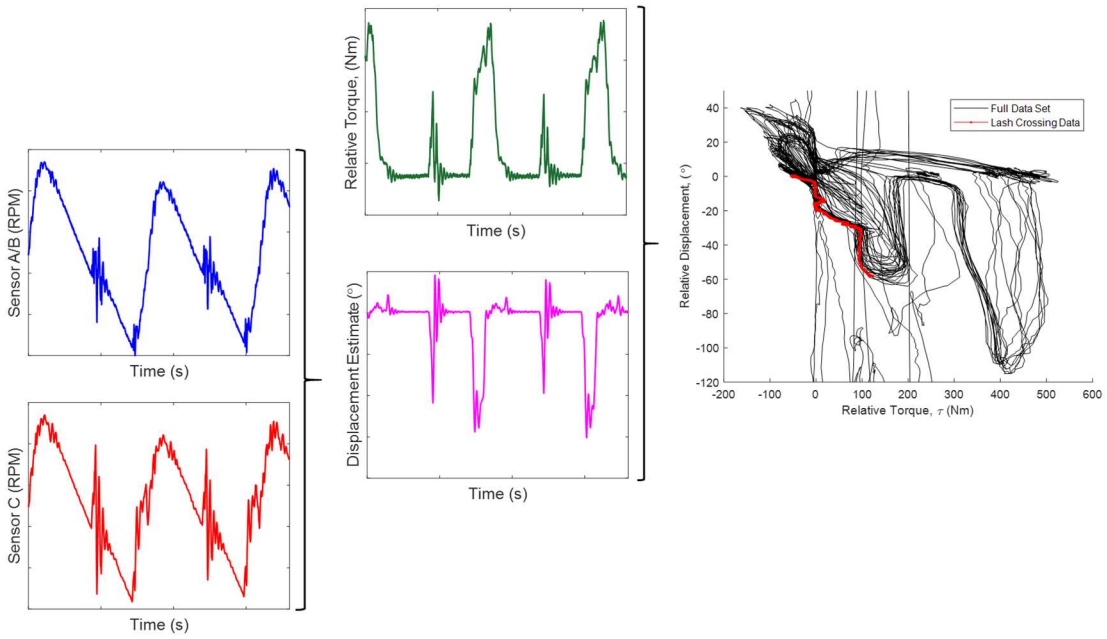

Figure 75: Backlash Post Processing Example with Truncated Data Depicting Graphical Workflow for Estimated Displacement Extraction

The data is truncated according to TI trigger conditions for each fixed gear run collected in accordance with Table 2 on road or Table 4 on dyno. An example of this truncation is depicted in Figure 76 where the truncated time selected is highlighted with magenta in the time domain torque and displacement traces denoted with green and pink respectively. The result from truncating according to TI criteria generates the consistent lash crossing data shown in the far right subplot of Figure 76 and was be used to estimate the lash just like the static torque vs. displacement lash estimate processing.

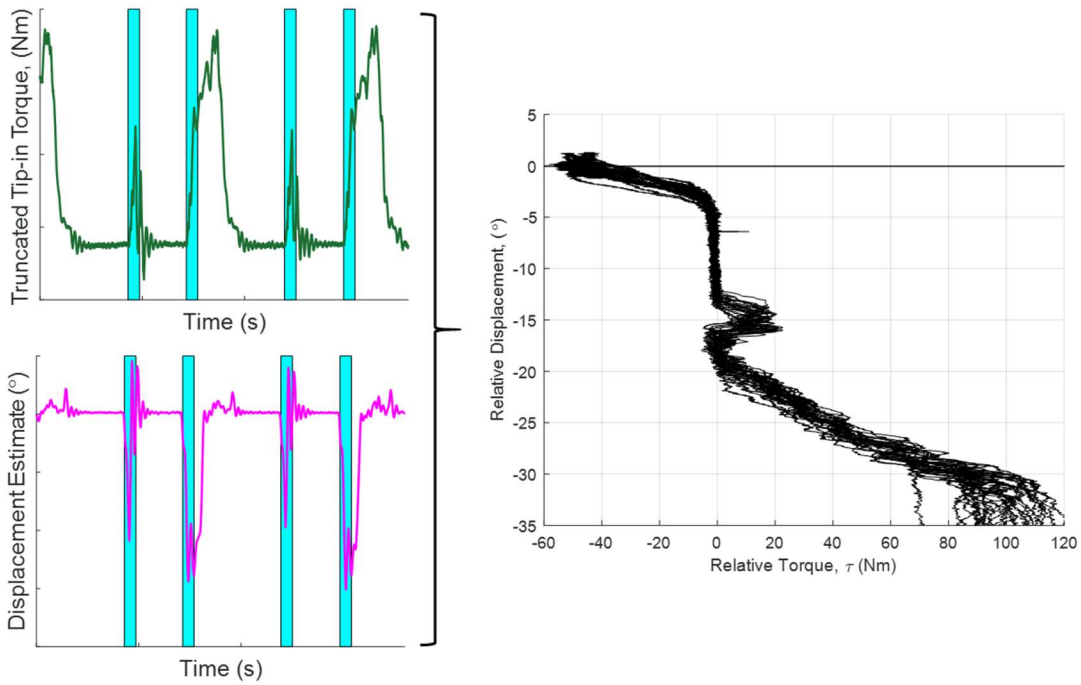

Figure 76: Truncated Torque (top-left) and Displacement (bottom-left) with Trigger Condition Highlighted Depicting Truncated Lash Crossing Data

An example dataset in third gear is plotted for the road data Normal 2W in Figure 77. Example data in third gear for Sport 2WD, Sport 4WD, and Loaded Sport 2WD in are found in Appendix C: Additional Analysis and Figures. Each dataset shows the raw data in solid black. There is also overlaid negative lash contact data in red with positive lash contact data in green. Unloading of the negative contact region during TI appears controlled and smooth in each of the 2WD datasets while the 4WD dataset is not as well behaved. The 2WD data also appears to cross lash as expected near zero measured torque in the propeller shaft. The 4WD trace appears to cross lash at a negative propeller shaft torque. Lash is known to cross because the torque appears vertical with slope changes indicating a lash crossing has occurred. The reason the 4WD data holds at a negative torque is because the torque splits between front and rear wheels upstream of the propeller shaft torque measurement and therefore the relative torque holds negative during the lash crossing due to the torque split between front and rear wheels. This torque split is attributed to errors in estimation of the driveline lash while in 4WD modes.

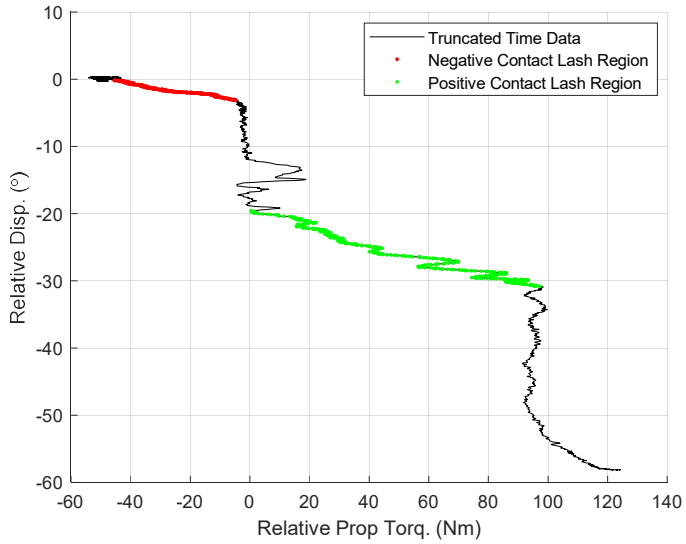

Figure 77: Normal 2WD Lash Estimation Data with Highlighted Negative Contact Lash Region in Red and Positive Contact Lash Region in Green

The same TI sequences were run on the dyno test vehicle as discussed in Chapter 2. Data was collected for TI and TO while the dyno was in thr/v and thr/r control modes and the resulting lash crossing events are shown in Figure 78 and Figure 79 respectively. Each figure separates into two distinct TC clutch modes, both unlocked and locked denoted by letters a) and b) respectively. The lash crossing data measured from the dyno testing results in a different response than observed in the experimental road test data. The trigger conditions for truncation are kept the same and initiated by the positive torque slope while crossing the same specified torque threshold. The period of truncated data is also kept the same and observes the relative displacement estimate starting near zero, dropping to a minimum before climbing back up to near zero. This is similar to the overall road data observed from the example in Figure 75 but occurs on a much faster time scale than the road data lash crossing. Another different feature in the dyno test data shows the lash crossing does not hold steady with a vertical line during the entire crossing event near zero. Instead the torque rises above zero, before decreasing below zero in all but the unlocked TC clutch Thr/v example in Figure 78 a). That very same data example has no clear indication of the completed lash crossing or positive contact stiffness engagement. Therefore, a spring stiffness value is unable to be extracted from this dyno data.

These differences are influenced by the torque reaction of the dyno. It was previously shown in Figure 43 and Figure 44 that in Thr/r the dyno torque opposes the input motor torque on the transmission. During a TI or TO event, there is a delay due to the PID tuning where dyno torque has not made a sign change to oppose the TI or TO torque. This means that momentarily, both the input motor and dyno motors are all inducing torque on the driveline in the same direction. This caused the spike in shaft speeds and accelerated lash crossing. Such behavior on dyno is why the lash crossing data does not mimic the on road

experimental test data and therefore the lash estimates have high error as shown in Figure 80.

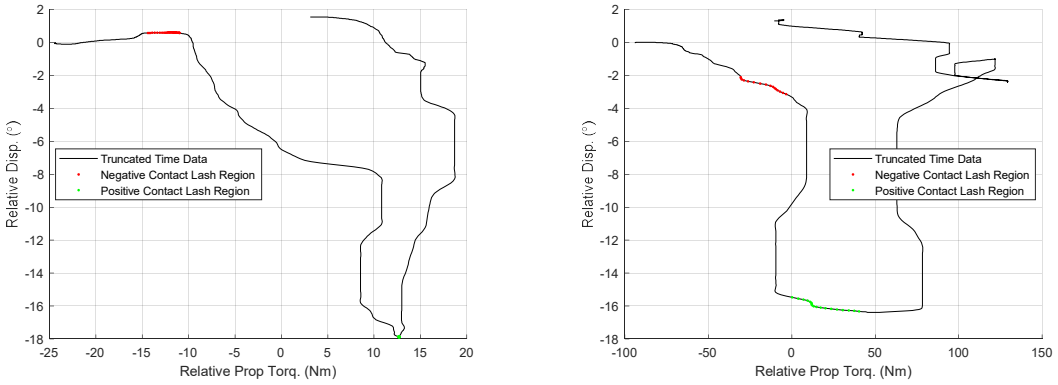

Figure 78: Dyno Control Mode Thr/v for a) Unlocked TC clutch and b) Locked TC clutch Lash Estimation Data with Highlighted Negative Contact Lash Region in Red and Positive Contact Lash Region in Green

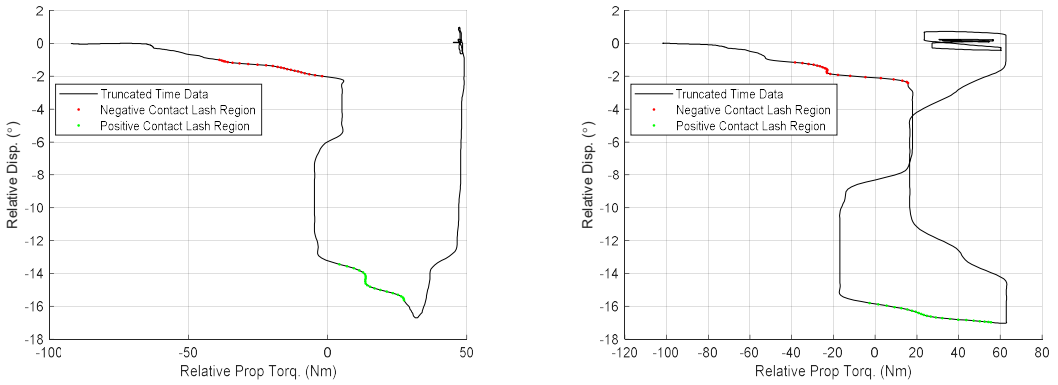

Figure 79: Dyno Control Mode Thr/r for a) Unlocked TC clutch and b) Locked TC clutch Lash Estimation Data with Highlighted Negative Contact Lash Region in Red and Positive Contact Lash Region in Green

The boxplot depicted in Figure 80 shows a series of post processed solutions for third gear while additional gear states can be found in Appendix C: Additional Analysis and Figures. It includes experimental data compared to the analytical estimate for lash tolerance as defined by the manufacturer. The y-axis shows lash value in degrees as reflected on the transmission input plane while the x-axis labels each boxplot according to the solution dataset. From left to right the data includes; analytical data based on CAE solid model stack-up, Normal 2WD mode (Norm), Sport 2WD mode (Sport), Sport 4WD mode (4WD), Loaded Sport 2WD mode (Load), dyno velocity mode with locked TC clutch (Thr/v), and dyno road simulator mode with locked TC clutch (Thr/r). Lastly, a red hexagram is overlaid

on the analytical boxplot to denote the combined estimate for lash based on static measurements estimated separately on the transmission and differential.

In each of the gear states analyzed, the static experimental lash value falls within the acceptable range defined by the manufacturer for tolerance stack-up. The estimate is consistently in the lower quartile but within 25% of the median expected value. This highlights that the experimental test methods are useful for estimating the overall lash value in a static measurement fashion for individual assembly tolerances.

The experimental road data solutions for 2WD (Normal Mode, Sport Mode, and Loaded Sport Mode) consistently lie within the analytical solutions as well. In 3rd gear, the lash estimates are in the lower quartiles while in 4th gear the solutions span the middle quartile ranges. Further 5th and 6th gear are shown in the upper quartiles. The solution trend does shift from underestimating the median to overestimating the median as gear ratio decreases but not to the extent that the estimate falls outside of the accepted tolerance range. The 4WD estimates do not always fall within the accepted lash range and is due to the coupling of additional driveshafts not accounted for in the analytical estimate. The shift into 4WD adds an additional gearbox element, driveshaft, and half shafts which in turn change the overall system lash. There were no static measurements done with the test vehicle for measuring the overall 4WD lash thus no comparison can be made in this study.

Solution for the dyno test data appears to underestimate lash in all four gear states analyzed. The change in boundary conditions and assumed single source of torque at the input of the transmission is the cause for discrepancy in the analysis. This along with the PID torque delay is reason for the underestimate. Future studies should revisit this calculation when a feed forward or similar control strategy is implemented.

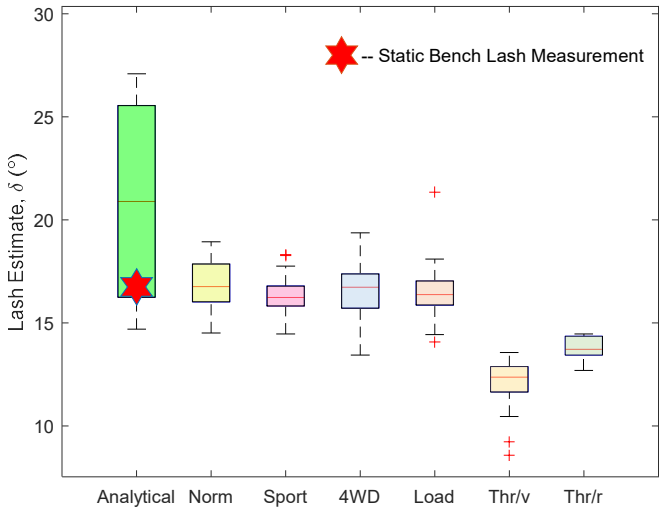

Figure 80: Lash Estimation Comparison in 3rd Gear for Road (Normal Mode 2WD [Norm], Sport Mode 4WD [Sport], Sport Mode 4WD [4WD], Loaded Sport Mode 2WD [Load]) and Dyno Data (Thr/v and Thr/r) Extracted from Torque and Relative Displacement Signal Data

4. Conclusions

The study evaluated in-situ data based on several different speed and torque sensors to estimate the effective shuffle frequency. The data showed differences based on the sensors used along with the calibration mode selected. Comparisons were further made on a dynamometer test vehicle with controlled inputs in a road load simulation mode. After shuffle was analyzed, the data was interrogated for overall backlash estimates. These estimates were made in a static fashion to understand behavior in the displacement vs. torque domain. These techniques were then pushed further with operating data. Results from the shuffle frequency extraction and lash estimates conclude;

- Shuffle frequency is a function of fixed gear state but does not change as a function of initial condition for vehicle speed. This will be verified in the digital twin as well.
- Simply changing the TC clutch-controlled slip has a change on the observed shuffle frequency as shown in differences with Normal 2WD and Sport 2WD frequency solutions. This is due to the amount of effective inertia and damping when coupling and uncoupling according to the TC clutch lockup schedule.
- Overall lash in the driveline can be estimated in each gear state based on TI maneuvers when torque measurements are available on the propeller shaft.
- Lash estimates for in-situ testing with 2WD are found within CAE tolerances but the additional coupling of 4WD driving conditions modifies the lash value due to changes in torque splitting to the wheels. These changes should be accounted for with the ROM controller
- Estimates of lash on the dyno test vehicle do not fall within CAE estimates due to additional torque sources (i.e. the absorbing dyno). Future works should revisit these test methods with implemented Feed Forward (or similar) control strategies.

4. Torque Weighted Vibration Dose Value

1. Literature Review

Engineers strive to make use of objective measurements to interpret and quantify subjective qualities such as ride comfort/discomfort. These quantitative values make it easier to compare different products, operating conditions, or maneuvers from one another with a single numerical metric. Studies have been conducted in the past to correlate perceived discomfort to vibrations induced on the body [66-75]. They have evaluated the effects of vibration amplitude [73, 74], forcing function (sinusoidal, random, burst random, sweep, etc.) [74, 76], duration [67, 68], direction/axis of motion [66, 73, 75], and frequency [67, 73, 74, 76]. These vibrations have been induced as whole-body vibration (WBV) [67, 70, 72, 74, 75] or localized on the body such as at the feet, seated surface, back rest, and/or hand contact surface [77]. A culmination of these studies and others influenced the formation of ISO2631 which aims to standardize human exposure metrics to vibration [1]. The most recent edition of this standard was published in 1997 and therefore all references to ISO2631 refer to this edition.

ISO2631 has several metrics of interest for human vibration. It is most well-known for the Vibration Dose Value (VDV) as a quantitative value engineers use to compare products as perceived by the end user. The VDV calculation is defined in Equation 20 where a_w represents the instantaneous frequency-weighted acceleration and T is the duration of the measurement. This formulation of the VDV takes on the form of an r.m.q. method because previous studies showed that rms formulations underestimate the influence of impulsive transients on the resulting summation [68]. Thus, it is recommended to use an r.m.q. method [76] as done in ISO2631:1997. Equation 20 also highlights that an arbitrary time duration can be used which is notable because this time duration can induce discrepancies between studies and the time scale used.

$$VDV = \left\{ \int_0^T [a_w(t)]^4 \, dt \right\}^{1/4} \qquad \text{Equation 20}$$

The instantaneous weighting curves can be found in Figures 2 and 3 of ISO2631 and defined in numeric form in Table 3 and 4 of the standards. These weighting curves correspond to the operator position; seated, standing, or recumbent based on Figure 1 of ISO2631 which are mapped to their corresponding weighting curves in Table 1 and 2 of the standards. The study conducted by this research evaluated a driver seated in a passenger vehicle looking at vibrations on the seat-track which corresponds to the driver's feet. The appropriate weighting scale for this condition with respect to comfort is scale k which was applied for all VDV calculations in this study.

Previous work has evaluated similar vehicles with the VDV to evaluate human perception to passenger vehicles. One such study [78] used jury testing with an FWD experimental test vehicle outfitted with displacement measurements of the front and rear right side suspension and displacement of the differential assembly. They also measured body longitudinal acceleration and output speed of the differential. They used the experimental data paired with jury evaluations of 1-2, 2-3, 3-4 and 4-5 upshifts based on the comfort level of each response on a scale of 1-10. The study concluded that vehicle body response was an indicator of comfort and did not find any actionable driveline dynamics that predicted subjective evaluation of the gearshift. Another study that uses their own metrics to evaluate the response to tip-in conditions was done in [79]. In this evaluation they took jury study results and compared the results with eight vehicle signals including; thumb rise rate, acceleration peak, response time, response delay, engine speed fluctuation, throttle change rate, kick, and jerk. From these eight signals they used fuzzy dynamic weighting logic to develop weighting scalars for each group to estimate the corresponding jury perceived value. The results showed high a relationship with a correlation coefficient of 0.89 with the jury results, however this and other studies lack an acceptable threshold for perceived comfort that is alluded to in ISO 2931 with the VDV.

Another study used to measure and calculate VDV metrics in their research include [71] where they apply the ISO standard to calculate VDV on a variety of cars, trucks, and tractors published in 1986. The study provides an extensive library of benchmarking data; however, the information is over 30 years old and might need to be revisited in techniques

and updated vehicle information. Many other studies include [80] which evaluates the susceptibility to spinal injury in railroad maintenance vehicles. [81] tested three different SUV's on open roads and a four-poster facility for VDV correlation but found that the VDV was not repeatable on open roads even for one vehicle on a single test strip. Similar results were also found in [81] that VDV results are not repeatable on the same section of road for the same vehicle. [82] calculated VDV based on analytical suspension parameters to select ideal spring stiffness for their mini-Baja car. [83] measured the VDV in different seating locations on a mass transportation bus for optimal passenger comfort and room. [84] calculated VDV metrics for an assortment of tractors in use in India as a health hazard to many local farmers.

In regard to similar torque maneuvers [60, 85] evaluated the VDV metric during a 1-2 upshift in passenger vehicles where [85] concluded that the VDV weighted with a 2^{nd} order Butterworth filter in the 1-32 Hz range correlated well with subjective jury testing. The results of [60] were able to correlate longitudinal acceleration of the vehicle with the first derivative of the transmission output speed. The correlated transmission output speed first difference was then able to adequately predict the VDV without need of a seat track accelerometer. This type of correlation would be useful for model prediction in the development phase where transmission output speeds may be obtained from simulation and VDV prediction.

The experimental data collected in this studies vehicle was setup in a way to replicate measured signals in [2, 6, 86]. This study incorporated all previously mentioned experimental techniques along with additional signals that had not been measured with relation to shuffle and clunk. The additional experimental data included a high number of CAN network signals collected to compare the differences in signals acquired in proper data acquisition with what the engine computers observe on the network. The VDV values are used to pursue a similar predictive tool based on [60] to predict dosage from transmission output speed signals.

The literature suggests that VDV is a common tool used as an objective measure to match subjective human evaluation of vibrations. A couple of the studies did remark that the results of this VDV are not repeatable on open road conditions. This speculates that the VDV metric is biased by road load inputs through the vehicle tires and chassis. Our study is interested in how drivers perceive clunk and shuffle therefore are less interested in the bias of road to tire interactions. An updated metric is desired that captures the human perception while also improving repeatability and correlation from driver torque request to vibration experience at the seat track. Furthermore, the updated metric should be actionable on a short time period to evaluate short transient events such as throttle tip-in, throttle tip-out, transmission up-shift and/or down-shift, or other driver inputs. The application of this metric can also aid in correlation from shaft speed to seat track acceleration similar to that done in [60] for engineering analysis on dynamometer rigs. This Chapter outlines the lack of correlation when predicting seat track VDV based on other measurements. This includes correlation to the differential, transmission, or shaft angular acceleration for longitudinal VDV estimation. The new metric proposed weights the traditional VDV with a torque

factor that was shown to increase correlation between all measurements. The use of this metric will be better used for correlation to driver requested torque demands as done in this study.

2. Experimental VDV Measurements

ISO2631 makes note that there is no pre-defined period of which the VDV metric is calculated. It does state that, "*The duration of measurement shall be sufficient to ensure reasonable statistical precision and that the vibration is typical of the exposures which are being assessed. The duration of measurement shall be reported*." [1]. The standard goes on to note a measurement duration of 108 and 227 seconds are required for 90% confidence of a 3-dB measurement error when the lower limiting frequency is 1 and 0.5 Hz respectively. The current language of the standard allows for deviations in processing from one study to the next when selecting a time period for processing. This is shown in Table 7 comparing the published times from different studies.

Table 7: Survey of Studies using ISO2631 Metrics and Their Published Time Duration(s)

Study Author [Reference]	Published Time Period, T
M. Griffin [71]	Various Times
K. Horste [85]	16 seconds
E. Johanning [80]	53 minutes to 5 hours and 16 minutes
D. Joshi et al. [81]	120 seconds or more
D. Robinette et al. [60]	16 seconds
F. Buarque et al. [82]	N/A
M. Walber et al. [83]	60 seconds
S. Pawar et al. [84]	7 minutes to 40 minutes
E. Little et al. [87]	N/A

It was observed from Table 7 that most of the studies do not adhere to the recommended 108 or 227 second time periods mentioned in ISO2631. It is further noted that some studies do not publish any time periods while others use multiple time periods within a single study. This is ambiguous and makes comparisons between studies not applicable. Even reviews such as the one published by S. Pawar [84] use various time periods and publish much different results for different tractors and road conditions.

It was shown in Chapter 2 Section 3 during the experimental data analysis of this test vehicle a typical shuffle event following a throttle stab, tip in, or tip out will decay within 1.5 seconds based on the transient events evaluated from the experimental data. Therefore, in this analysis, all metrics relevant to ISO2631 computed will use a period of 1.5 seconds. This deviates from the other studies referenced however many were evaluating overall comfort for long term events and less interested in short duration transient evaluation. This does deviate from ISO2631 recommendations but is done so due to the application for short duration events.

Data was processed for longitudinal accelerometer response and compared with the propeller shaft torque measurement along with estimated VDV metrics in Figure 81 for third gear data. Example data for 4^{th}-6^{th} gear are found in Appendix C: Additional Analysis

and Figures. The data was truncated to show a combination of TI, TO and SB events which are identified in the third subplot of VDV metric from Equation 21 with red diamonds, green circles, and magenta upper red triangle markers respectively.

The data reveals that all three of these transient events indicate an increase in VDV metric over coast condition values. The TI, TO, and SB response in the accelerometer trace shows elevated level responses as expected from the shuffle response characterized in Chapter 2. Another trend observed from the truncated time traces is that throttle stab events appear to have higher amplitude VDV response than the TI and TO data on average. There is an arrow shown around 42 seconds during a sustained coast VDV measure. It shows an increase in ST response and therefore VDV, but no torque input is observed. This alludes to an issue when using the VDV for powertrain specific analysis because chassis/road inputs can induce ST vibrations that are not correlated to the driver torque requests.

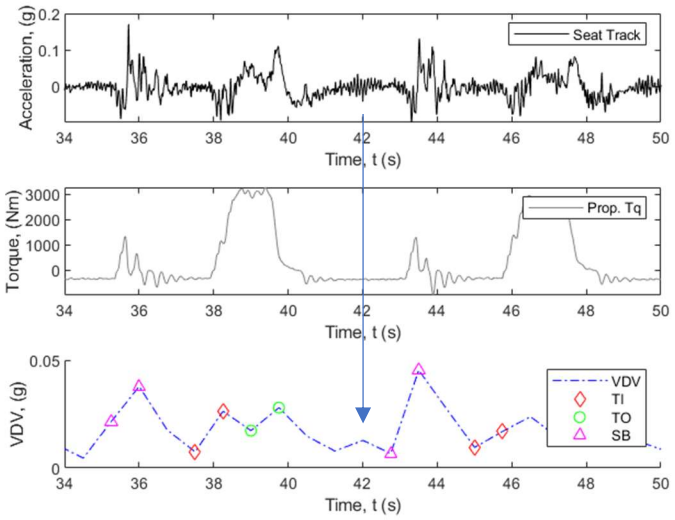

Figure 81: Third Gear Processed Data in Normal 2WD for Seat Track +X Acceleration vs. Time in Subplot 1, Propeller Shaft Torque Projected on the Transmission Input Plane in Subplot 2, and the Corresponding Shifted VDV Calculation vs. Time in Subplot 3 With Indicators for TI, TO, and SB.

There are additional considerations necessary when considering the transition from road data to dyno data. Along with the changes in vehicle mass and rotating driveline inertial changes, there is no driver apparent in the vehicle. This could be alleviated by placing a dummy in the driver's seat atop the seat pad accelerometer, but no dummy was available for testing in this study. Another consideration is different vehicle trim levels will offer changes in seat material and architecture. These changes modify the transfer path and resulting frequency response function when considering a source at the transmission or differential rotational elements. A few conclusions can be made by comparing longitudinal VDV metrics of the seat track vs. seat pad as done in Figure 82. This comparison was generated from data collected in Normal 2WD mode. It depicts elevated seat pad VDV relative to low seat track VDV, but the trend drops below the 1:1 threshold as seat track VDV increases. This confirms that the seat dynamics can play a role in the VDV metric. This study will only consider correlation and comparisons to the seat track to remove this

additional response. This will allow for better comparison of road data to dyno test data and be comparable across different vehicle trim lines.

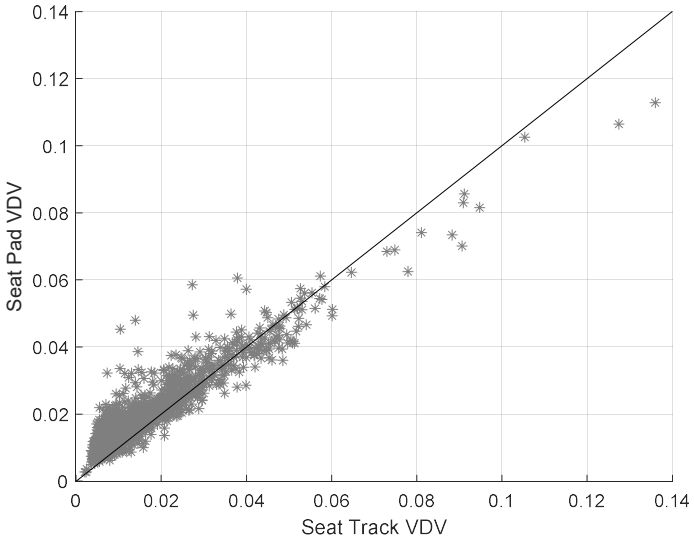

Figure 82: Longitudinal VDV Extracted from the Seat Pad Acceleration vs Seat Track Acceleration from All Runs and Gears in Normal 2WD Test Mode

As noted earlier, the two common locations in vehicles are the seat pad and seat track. Further analysis in this study is only interested in the seat track response. Furthermore, the analysis is interested in the longitudinal response when considering dosage due to shuffle transients. The following plots in Figure 83 and Figure 84 compare the calculated VDV metric at the seat track compared with the longitudinal transmission and differential VDV respectively. The transmission and differential are not common VDV measurement locations but are evaluated to look for correlation between the two. These comparisons could be used in analytical models to estimate seat track response if there is high correlation.

As reported in each, the transmission has a correlation coefficient of 0.38 to the seat track while the differential has a correlation coefficient of 0.54. These are low correlation values and do not lead to high confidence in their application to estimate seat track VDV dosage for transient events. Another option available is to estimate the seat track VDV dosage based off the transmission output speed sensor signal.

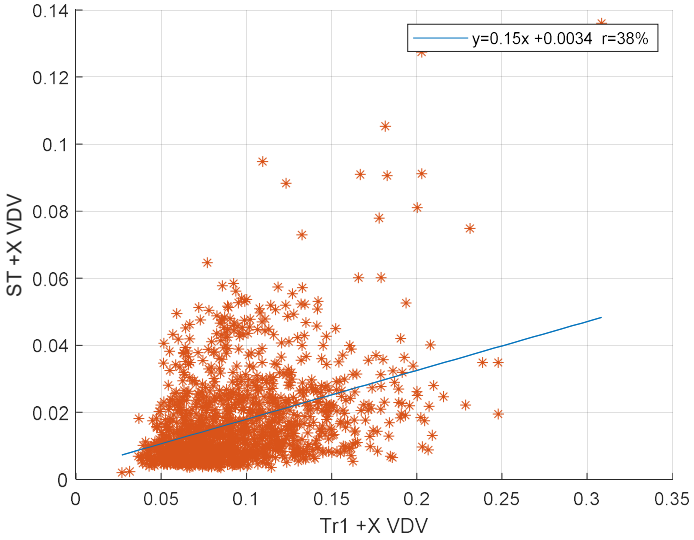

Figure 83: Seat Track VDV Metric vs. Transmission VDV Metric with Linear Curve Fit

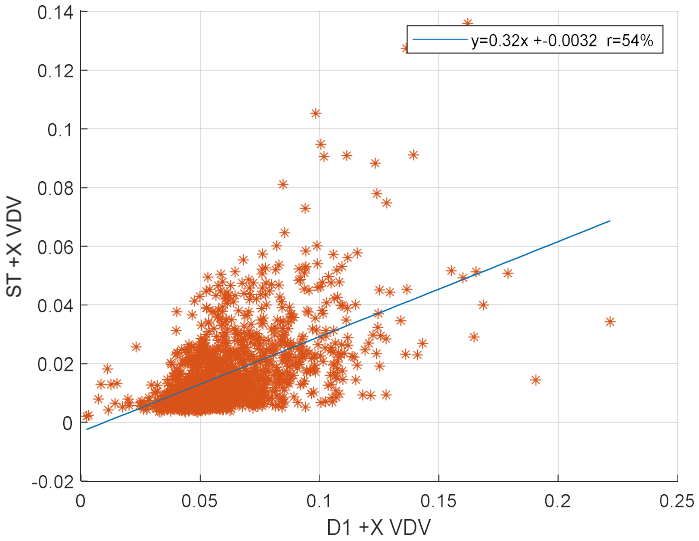

Figure 84: Seat Track VDV Metric vs. Differential VDV Metric with Linear Curve Fit

It was shown in [60] by Robinette et. al. that the vehicle VDV in the longitudinal direction could be estimated based off the transmission output speed signal. The study theorized that acceleration of the vehicle body is correlated to the driveshaft acceleration coupled to the ground through the tires. Therefore, longitudinal vehicle acceleration can be achieved by taking the derivative of the transmission output speed sensor, multiplying by the final drive ratio and reflecting across the torque arm of the tire as described in Equation 21. This study will further refer to this method as the TOSSd estimate which is shorthand for Transmission Output Speed Sensor derivative.

$$\ddot{x} = \frac{2\pi r_{tire\ eff}\dot{\omega}_{TOS}}{60\ i_{FDR}} \qquad \text{Equation 21}$$

This theory was shown to work for the vehicle tested by Robinette et. al. however, their test vehicle was a compact sedan as compared to the medium duty truck analyzed in this study. Additional notes are that the other study used signals available on the CAN bus along with integrated speed sensors in the transmission and vehicle acceleration based on the DC vehicle accelerometer. This study used higher sampling rates and time synchronized data acquisition channels but runs the same comparison as done by Robinette et. al. It is shown in Figure 85 that there is higher correlation when comparing the longitudinal seat track VDV to the TOSSd VDV. This is observed with a correlation coefficient of 0.90. This once again validates the TOSSd estimate to be a valid approach, but higher correlation is still desired.

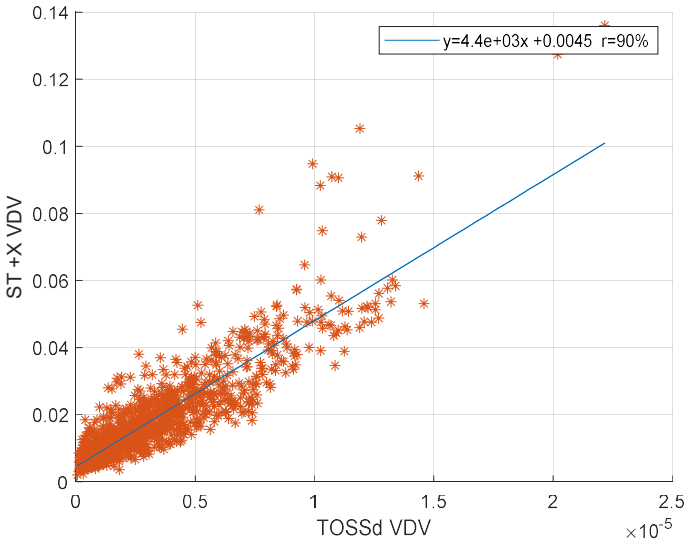

Figure 85: Seat Track VDV Metric vs. TOSS Derivative VDV Metric with Linear Curve Fit

3. Torque Weighting Formulation

It was shown in the previous section that correlation can be achieved between driveline components to estimate seat track response and thus driver comfort due to shuffle oscillations inducing longitudinal acceleration. There was room for improvement in the correlation coefficient to help predict the seat track response. It is noted that multiplication in time domain is equivalent to convolution in the frequency domain based on the Laplace transform. This realization leads to note that correlated signals in the frequency domain are additive and thus if a metric combined two correlated signals there should be better discrimination of events based on this metric.

Due to Newtons second law it is understood that force or torque is proportional to linear or rotational acceleration respectively. Therefore, the longitudinal acceleration should be proportional to the force applied at the tires. And the force applied at the tires is proportional to the torque applied on the driveline. This is similar logic to that used to formulate the longitudinal estimates of TOSSd in Equation 21. Because of these physics,

the torque measured across the driveshaft should be proportional to the angular acceleration and once again proportional to the longitudinal acceleration. By combining the torque and acceleration through multiplication in the time domain, their application with a Torque Weighted VDV metric is developed in Equation 22.

$$TWVDV = \left\{\int_0^T [a_w(t)]^4\, dt\right\}^{1/4} * \left\{\int_0^T [\tau_w(t)]^4\, dt\right\}^{1/4} \qquad \text{Equation 22}$$

Weighting for the TWVDV is applied the same as described in ISO2631. A sample signal processing workflow is shown in Figure 86. The two leftmost subplots depict a solid black line for the accelerometer and torque measurements on top and bottom left respectively. Moving right each signal is truncated into smaller overlapping periods of accelerometer and torque on top and bottom respectively before applying the weighting filter as defined by ISO2631. A comparison of the estimated TWVDV vs. the standard VDV is made in the top right subplot along with sample correlation between these two metrics applied for the longitudinal seat track acceleration vs. TOSSd estimate.

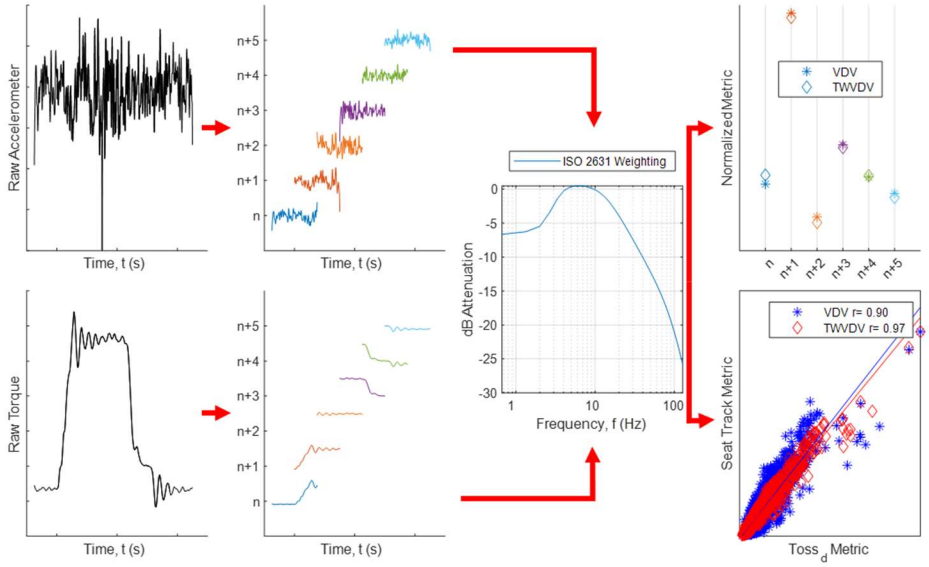

Figure 86: TWVDV Signal Processing Workflow with Raw Accelerometer (top left) and Torque (bottom left) Truncated as Time Progresses (Center Top and Bottom left) and Filtered (Center Middle Right) to Estimate VDV and TWVDV Metrics and Compared for Seat Track +X and TOSSd Comparisons with Correlation Coefficient.

Note, this is like applying a kernel function for a signal transform. The more a signal looks and acts like the kernel, the better the resulting metric will correlate. Essentially the kernel is the torque dose and the result is a torque weighted vibration dose. An example of how these sub calculations combine into the overall TWVDV is depicted in Figure 87. The figure shows overlapped and truncated torque sections in the top subplot along with the estimated VDV based on acceleration (VDV_{accel}), VDV based on torque (VDV_{torque}) which

is used as the weighting value or kernel, and finally the resulting TWVDV. These three metrics are shown in solid black, dot-dashed blue, and dotted red respectively. Once again, the dosage metrics increase when TI, TO, and SB are observed in the propeller shaft torque signal. It is further noted that during high torque inputs such as the TI and SB events, the torque weighting adds additional weighting while softening the metrics during coast conditions.

The application of the TWVDV vs. the VDV correlation is summarized in Table 8. The table shows the correlation coefficients of the transmission, differential, chassis and TOSSd estimated from Figure 83-Figure 85 for the VDV dosage. It further denotes the TWVDV correlation coefficient in the second row for all three estimates. The resulting correlation coefficients for TWVDV increase for all three comparisons making each one appears suitable for prediction of seat track response. There is an arrow overlaid on the data in Figure 87 indicating the benefit of the TWVDV metric. The torque trace indicates a coast condition but the VDV calculates a rise in dosage. This rise is not due to a torque input requested from the driver and must therefore be an artifact of road loading. Thus, the TWVDV smooths out the perceived dosage and only rises for TI, TO, or SB events.

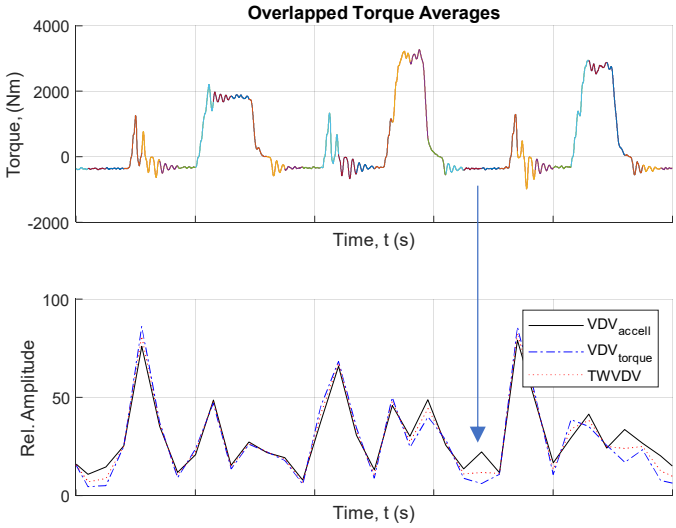

Figure 87: Normal 2WD Torque (Top Subplot) with Corresponding VDV Metrics (Bottom Subplot) vs. Time

Table 8: Normal 2WD mode VDV and TWVDV Correlation Coefficient for Longitudinal Accelerometers Tr1, D1, CH1, ST, and TOSSd

Correlation Coefficient r =		VDV					TWVDV				
		Tr1 +X	D1 +X	CH1 +X	ST +X	TOSSd	Tr1 +X	D1 +X	CH1 +X	ST +X	TOSSd
VDV	Tr1 +X	1.00	0.52	0.55	0.38	0.25	0.64	0.45	0.44	0.37	0.31
	D1 +X	0.52	1.00	0.58	0.54	0.53	0.61	0.74	0.56	0.54	0.54
	CH1 +X	0.55	0.58	1.00	0.90	0.76	0.89	0.86	0.94	0.89	0.82
	ST +X	0.38	0.54	0.90	1.00	0.90	0.90	0.92	0.97	0.99	0.95
	TOSSd	0.25	0.53	0.76	0.90	1.00	0.84	0.91	0.90	0.93	0.98
TWVDV	Tr1 +X	0.64	0.61	0.89	0.90	0.84	1.00	0.94	0.95	0.92	0.90
	D1 +X	0.45	0.74	0.86	0.92	0.91	0.94	1.00	0.95	0.94	0.94
	CH1 +X	0.44	0.56	0.94	0.97	0.90	0.95	0.95	1.00	0.99	0.95
	ST +X	0.37	0.54	0.89	0.99	0.93	0.92	0.94	0.99	1.00	0.97
	TOSSd	0.31	0.54	0.82	0.95	0.98	0.90	0.94	0.95	0.97	1.00

This analysis is again repeated while on the dynamometer test vehicle and depicted in Figure 88 while operating in Thr/r mode with an unlocked TC clutch in third gear. Once again, the data does not observe any SB events but the TI and TO transients are observed to have high VDV dosage values in normalized relative amplitudes. A similar but truncated version of the correlation between VDV and TWVDV is made for the longitudinal transmission, differential, and TOSSd estimate vs. the seat track accelerometer in Table 9. The coefficients are again higher in the TWVDV comparison relative to the VDV correlation. This gives more confidence that the TWVDV metric is a better discriminant for seat track comfort and may be suitable for analytical predictions in early stage vehicle development. There are two arrows overlaid in Figure 88 that highlight the increased correlation due to the TWVDV. These arrows occur at TO events and observe that there is no notable increase in the VDV metric. The addition of the torque weighting shows a rise and subsequent increase in TWVDV. This results in a higher perceived dosage as expected during a torque transient.

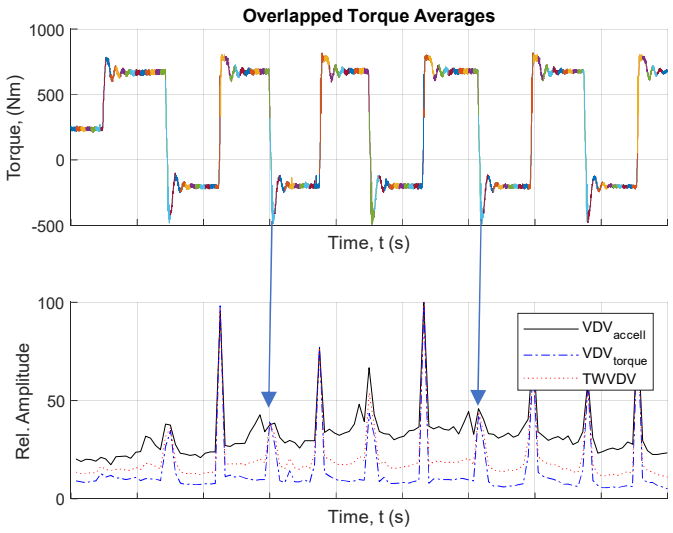

Figure 88: Dyno Thr/r with Unlocked TC Clutch Torque (Top Subplot) with Corresponding VDV Metrics (Bottom Subplot) vs. Time

Table 9: Dosage Values on Dyno Thr/r with Unlocked Clutch VDV and TWVDV correlation coefficients for seat track vs. transmission, differential, and TOSSd estimates.

Correlation Coefficient		Tr1 +x	D1 +x	TOSSd
VDV	ST +X	**0.71**	**0.78**	**0.37**
TWVDV	ST +X	**0.97**	**0.96**	**0.91**

The dyno data is also compared while in a locked TC clutch state while in Thr/r mode as shown in Figure 89. This sample data shows the truncated propeller shaft torque data in the top subplot with dosage values for VDV of the accelerometer (VDV_{accell}), VDV of the torque signal (VDV_{torque}), and combined TWVDV. The locked TC clutch data shows higher normalized relative amplitudes during coast conditions than the unlocked clutch data. It also shows that again the TI and TO events have increased dosage values which are emphasized by the torque weightings. The results are summarized in Table 10 comparing the correlation coefficients between longitudinal seat track acceleration to the transmission, differential, and TOSSd estimates.

It is observed that both Table 9 and Table 10 show lower correlation for the TOSSd estimate to seat track response than the differential or transmission response. This is reverse from the results shown for experimental road data in Table 8. Once again, the dyno controller behavior is attributed to this behavior in adding another torque source that modifies the boundary conditions during TI and TO due to controller delay. Overall, the TWVDV dosage metric correlates better in all cases and will be further used for analytical modeling and prediction of seat track behavior to TI and TO transients. Two additional arrows are superimposed on Figure 89 where the TWVDV once again reduces the perceived dosage observed in the VDV metric but not attributed to a torque change.

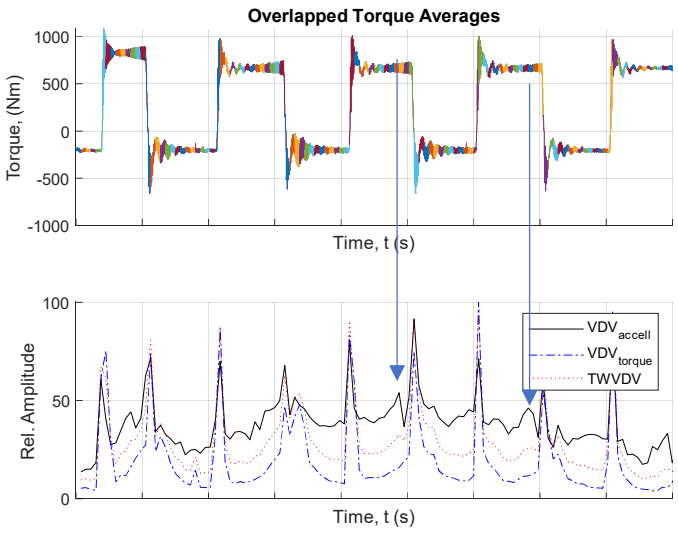

Figure 89: Dyno Thr/r with Locked TC Clutch Torque (Top Subplot) with Corresponding VDV Metrics (Bottom Subplot) vs. Time

Table 10: Dosage Values on Dyno Thr/r with Locked Clutch VDV and TWVDV Correlation Coefficients for Seat Track vs. Transmission, Differential, and TOSSd Estimates.

Correlation Coefficient		Tr1 +x	D1 +x	TOSSd
VDV	ST +X	**0.51**	**0.73**	**0.13**
TWVDV	ST +X	**0.94**	**0.96**	**0.75**

4. Conclusions

The evaluation of Seat Track response is used to estimate customer perception of good or bad ride quality. This is done in industry using the vibration dose value (VDV) which is a root mean quad metric defined for sensitivity to peak transient events. The drawback to the VDV metric is that any road imperfection inducing road vibrations on the tires propagates to the passenger and is included in the VDV dosage. This study is not interested in road inputs and therefore a metric was desired to correlate only driveline induced vibrations from the primary torque source, i.e. ICE. The result is the torque weighted vibration dose value or TWVDV. This metric allows correlation of the torque and seat track vibrations to superimpose for a combined higher discriminant metric of torque source induced vibrations. Key conclusions from this analysis include:

- TI, TO and SB events all show increased VDV over sustained drive or coast events. SB VDV are shown to have the highest amplitude over all other events.
- The VDV is sensitive to road loads and during coast events the estimated metric can rival the amplitude of the TI or TO events.

- The TWVDV formulation is successful in improving correlation between seat track response and other signals. It can therefore be used as an actionable metric for improvements in driveline properties relating to perceived comfort.

5. CAE Lumped Parameter Modeling and Analysis

1. Literature Review

CAE models are becoming commonplace in engineering design and analysis. They are useful for predicting loads for design optimization or predicting the natural frequencies of complex structures. Along with CAE modeling, there is an increasing trend to use "Digital Twin" models to estimate performance due to perturbation of model properties, estimate damage to a physical system, or estimate measurements on a system with no physical sensor. The concept of a digital twin mode has been rising in recent years for use in engineering. A search of the keyword "digital twin" results in an increasing trend of results based on the search database as shown in Figure 90. The figure was created by evaluating the number of search results per year that are found in five popular databases. The year of publication is along the x-axis while the number of scaled results per year are on the y-axis. Five different search databases were used and scaled such that a similar trend is observed. The scaling for SAE Mobilus for instance means that for every one hit found per year on the database, three hits are plotted on the y-axis in Figure 90. These results were compiled as of 03/18/2019.

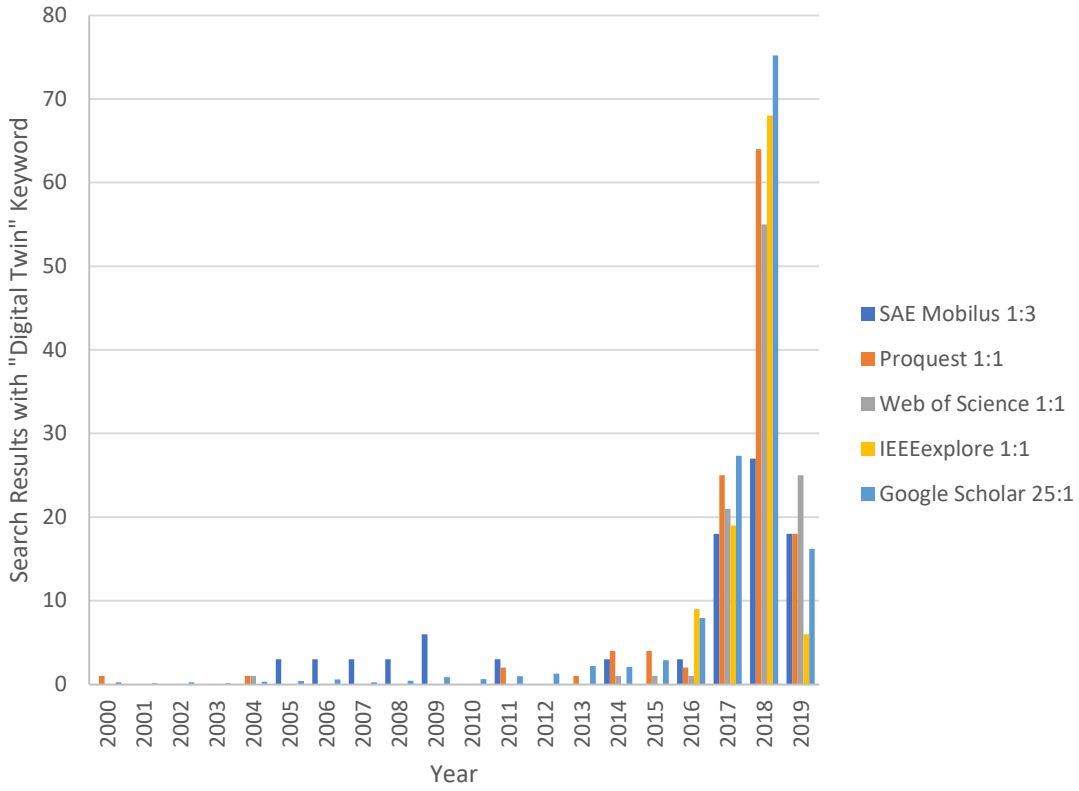

Figure 90: Digital Twin Keyword Search Result Trends as Indication of Prominent Use in Industry

Following the increasing trend, this study wishes to use a digital twin model for perturbation of physical properties along with estimating measurements on the vehicle that are not physically being measured. The aim of Chapter 4 was to develop an objectionable metric useful for discriminating vibration dosage at the seat track correlated to engine torque inputs as opposed to road inputs. This was done by expanding the VDV formulation to include a torque weighting. The test vehicles both on road and in the lab dyno had torque sensors installed on the propeller shaft to measure torque. This measurement is not available on all vehicles and therefore a digital twin can perform the calculation to estimate propeller shaft torque for use in the TWVDV. The study also used an additional accelerometer installed on the seat track for monitoring, but that measurement is also not available on a production vehicle. There are body accelerometers mounted like those used in [60] but there is additional dynamics between the seat track and body mounted accelerometer that may cause changes to the VDV metric similar to what was observed in Figure 82.

This study will use a lumped parameter model for lower computational cost. This research is focused on reducing the computational cost with a lumped parameter model but not too low fidelity that high frequency transient responses are lost. Examples of lumped parameter models include but are not limited to work done in [5, 6, 44, 86, 88-94]. A large majority of these analytical simulations include key driveline components such as engine,

transmission with gear reduction, driveshaft, differential gear reduction and tires. Some of the simulations include more advanced features such as non-linear clutch components with hysteresis, spline/CVJ/gear lash elements, reflected engine inertias, and reflected vehicle body inertia onto the wheels. Most of the studies can easily capture shuffle dynamics as the first torsional mode and track clunk as lash elements traverse from one boundary condition to the next. It was observed in Chapter 2 that the shuffle mode is coupled with the longitudinal for-aft motion of the body. This coupling is not mimicked in any of the other studies and techniques are proposed to include the driveline reaction torques to induce longitudinal reaction in the vehicle body.

Review of literature notes that the differential stiffness non-linearities are influenced by several factors. Contact non-linearity is the most common representation used and was implemented in the analytical model with backlash spring elements. Studies show that there is a variation in stiffness due to mesh variations in the number of gear teeth in contact at a given instance. This representation means that stiffness fluctuates as a function of speed and relative angle [95, 96]. Variations in mesh stiffness are also attributed to loading of the gear teeth and shows an increase in stiffness with increase in torque loading [97]. These influences were simplified by a single change in stiffness and was implemented in the model. This variation captures the loading change in coast vs. drive which models the change in effective stiffness to achieve asymmetry in TI and TO shuffle frequencies.

This study will correlate the model and then use the results to evaluate parameter perturbation based on the analytical TWVDV. Correlation of the model will target a shuffle frequency within 10% of the experimental results. This includes a shift in TI and TO solutions. The model will also include an estimate for seat track response based on the physics outlined in Chapter 2. Previous studies such as [93] had similar objectives to create a CAE model with seat track prediction. This study will expand on this task to use that seat track response for TWVDV evaluation. It will use the metrics as an objective value for improved system response due to parameter changes.

2. Digital Twin Model

The lumped parameter or digital twin model was developed in LMS Amesim. It includes a combination of rotational and linear elements to represent the physical parameters of the driveline. The key parameters that must be included based on previous studies include inertia and stiffness/damping of the engine, transmission, propeller shaft, half shafts, and tires. Values for inertia and stiffness were provided by the research sponsor while damping estimates were made and assigned based on a proportional damping application. Values for component backlash were provided based on tolerance stack up of CAD models. As noted in Chapter 3, these values are a guideline but variable for the exact vehicle tested. Values extracted in Chapter 3 are instead applied to the digital twin model. The shuffle frequency is also used as a correlation metric of the digital twin to the experimental test vehicle. The lumped parameter model also implements coupling of the transmission and differential sprung mass components to interact with and induce longitudinal vibration into the vehicle body. This coupling is used to generate an estimate of the seat track vibration

in the lumped parameter model. A screenshot overview is provided in Figure 91 that depicts the fully populated digital twin.

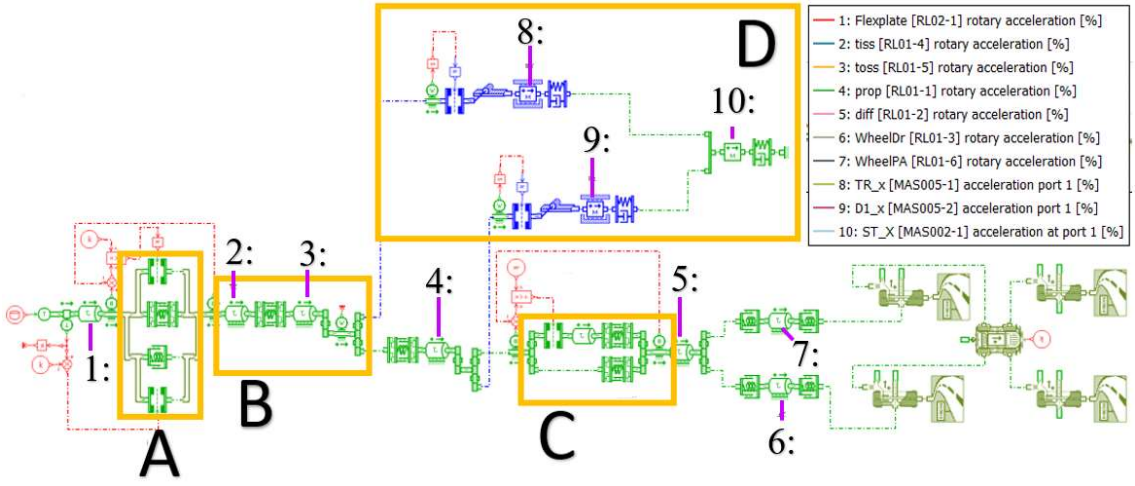

Figure 91: Lumped Parameter Digital Twin Graphical Programing Model Representation

There are four key features highlighted in the digital twin model with orange boxes surrounding them with an alphabet letter assigned to each box. The first key feature is A which surrounds the modeling representation of the torque converter clutch. The main aim of this study is not to control the effects of the torque converter but instead to understand the dynamics when the torque converter clutch is fully locked. Therefore, the locked clutch is modeled with hysteresis and asymmetric damping as specified by the sponsoring organization as shown in Figure 92. The hysteresis curve in Figure 92 was generated by isolating the clutch damper system enclosed in A. A low frequency (<0.5 Hz) sinusoidal displacement was input to the clutch while measuring torque and displacement. The result is depicted in Figure 92 with torque along the x-axis and displacement along the y-axis.

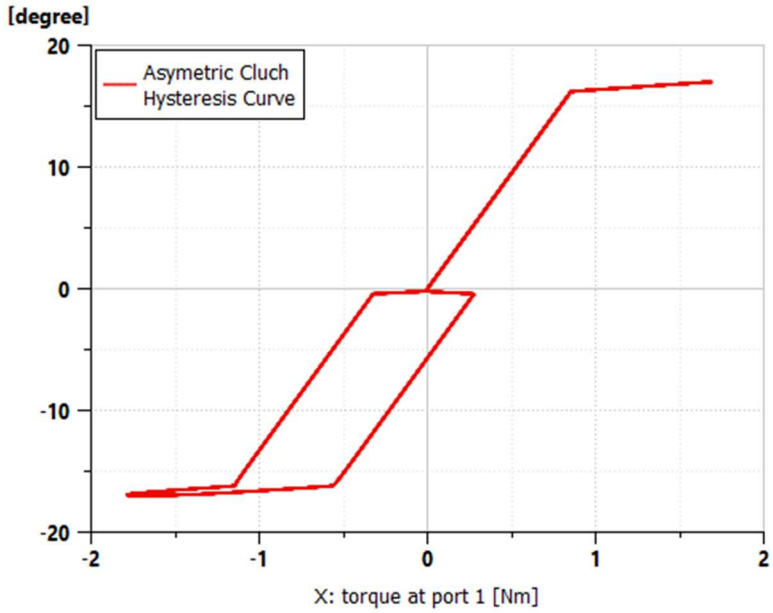

Figure 92: TC Clutch Hysteresis Model with Multi-Stage Backlash Stiffness for Input Clutch Displacement (Degrees) vs. Reaction Torque (Nm) Based on Cyclic Loading

Downstream of the TC clutch is B which surrounds the torque converter gear reduction with backlash and variable stiffness. The model recognizes changes in backlash and transmission reflected stiffness based on the forward gear state selected. These changes are assigned from a lookup table and modified if a new gear state is simulated. The backlash is assigned values measured in Chapter 3 by subtracting the amount of differential backlash from the overall backlash estimated from experimental data. The amount subtracted for the differential is applied in box C which depicts the asymmetric differential stiffness and lash. The stiffness asymmetry is expected for hypoid gearing which is used in this vehicle differential and modeled with parallel springs. The logic loop setup checks for positive or negative relative contact and will remove one spring when contact reverses.

The final box D represents the integration of driveline reaction torques which induce longitudinal vibrations from the un-sprung to sprung mass components. This represents the physics hypothesized in Figure 58. These reactions are the pitching motion of the differential during TI and TO. Based on observations during dyno testing, the pitching motion is accompanied with propeller shaft translation as the differential nose rotates up and down. This forces the slip flange on the transmission to plunge in and out. The angle of the transmission output spline does not match the angle of the propeller shaft. This along with vertical suspension travel are reasons for universal joints on each end of the propeller shaft. Because these two planes meet at an angle, the differential pitch pushes and pulls on the propeller shaft which plunges the spine coupling in and out of the transmission. Due to the angle offset, this plunging action also induces a moment on the powertrain assembly generating additional pitching oscillations. Therefore, there are two moments connected to the sprung mass or body. One at the differential/axle assembly and one on the powerplant

assembly. These two are coupled in the lumped parameter model by an equivalent torque and lever arm pushing on the driveline assemblies. These in turn are coupled to the body via springs where they combine to meet the frame and push in the longitudinal direction for seat track acceleration. This response is like the TOSSd formulation in Equation 21 where the reaction torque induced on the pitching mode is proportional to the angular acceleration of the shaft speeds multiplied by the pitch inertia.

Lever arm values for the transmission and differential were based off physical measurements of the test vehicle. A transmission lever arm was measured from the transmission output shaft in the vertical direction to the upper transmission mount. This is effectively the torque arm between the plunging transmission spline and powerplant mounts. The same procedure was followed for the differential when measuring from the differential input flange to the rear suspension leaf spring mounts. Target oscillation frequencies for the transmission and differential pitching modes were set at 11 Hz and 41 Hz while the body on frame mode was targeted at 1.1 Hz based on data from [98].

Simulation with the digital twin includes inputting the measured transmission input torque into the analytical model and observing the resulting reaction. This was done for each gear state to check for correlation of TI and TO shuffle frequencies. Then perturbation of parameters was applied to study modification in the VDV and TWVDV response. The verification of model estimates for shuffle frequency are compiled in Table 11. The table claims shuffle frequency targets based on the mean shuffle frequency found with TISS data for Normal Mode 2WD. The results conclude that the digital twin model can compute the shuffle frequency with <10% error at TI and TO maneuvers. The model achieved these results with only a 5% change in differential stiffness from coast to drive which is realistic and well within variations studied in literature [99].

Table 11: Shuffle Frequency Solution for Digital Twin (AME) Model for TI and TO Linearization

Gear	Shuffle Frequency Target TI	AME Shuffle Frequency	Error	Shuffle Frequency Target TO	AME Shuffle Frequency	Error
	Hz	Hz	%	Hz	Hz	%
1		1.94			1.92	
2		2.71			2.67	
3	3.42	3.64	6.58%	3.38	3.55	5.08%
4	4.34	4.37	0.56%	4.33	4.20	2.93%
5	4.90	4.96	1.06%	4.94	4.73	4.26%
6	5.51	5.72	3.72%	5.49	5.38	2.07%
7		6.85			6.30	
8		7.68			6.95	
9		8.91			7.82	
10		9.40			8.14	

An example of the analytical vs. experimental data is shown in Figure 93 for TOSS correlation in 3rd gear. Additional gear states are found in Appendix C: Additional Analysis and Figures. The experimental (Exp) and analytical (Ana) TOSS signals are depicted in solid red and blue respectively. The analytical signal first goes through a startup transient. This is due to non-zero initial conditions that need to settle at the start of the simulation. Once the startup transient dies out, the analytical signal tracks close to the experimental result for TOSS given the corresponding torque input on the driveline model. The mean analytical result tracks well with the experimental data but deviations during sustained TI and TO are due to imperfections in road grade modeling. There is not road grade data available from the experimental vehicle and future works would benefit from this measurement if available. However, the current simulation correlation deviates due to lack of road grade inputs on the vehicle model.

The digital twin shows shuffle induced by the SB, TI, and TO events as expected relative to the experimental baseline. By focusing on the SB event, there is the initial transient followed by a secondary transient as the simulation moved from a successive drive to coast condition and lash is crossed twice. At the onset of coast when lash is taken up, a secondary high frequency mode is observed to participate in the digital twin signal not seen in the experimental model. This is one advantage of the digital twin that isn't picked up by the other model due to low fidelity pulse train and signal smoothing during tachometer post processing algorithms. Another error in the analytical simulation after the SB event is a secondary harsh clunk transient. This is not apparent in the experimental data and is due to the torque input signal based on CAN bus torque estimates fed to the digital twin transmission input. Previous data in Chapter 2 showed errors associated with CAN torque estimates and this once again highlights those errors with added transients not observed on the experimental response.

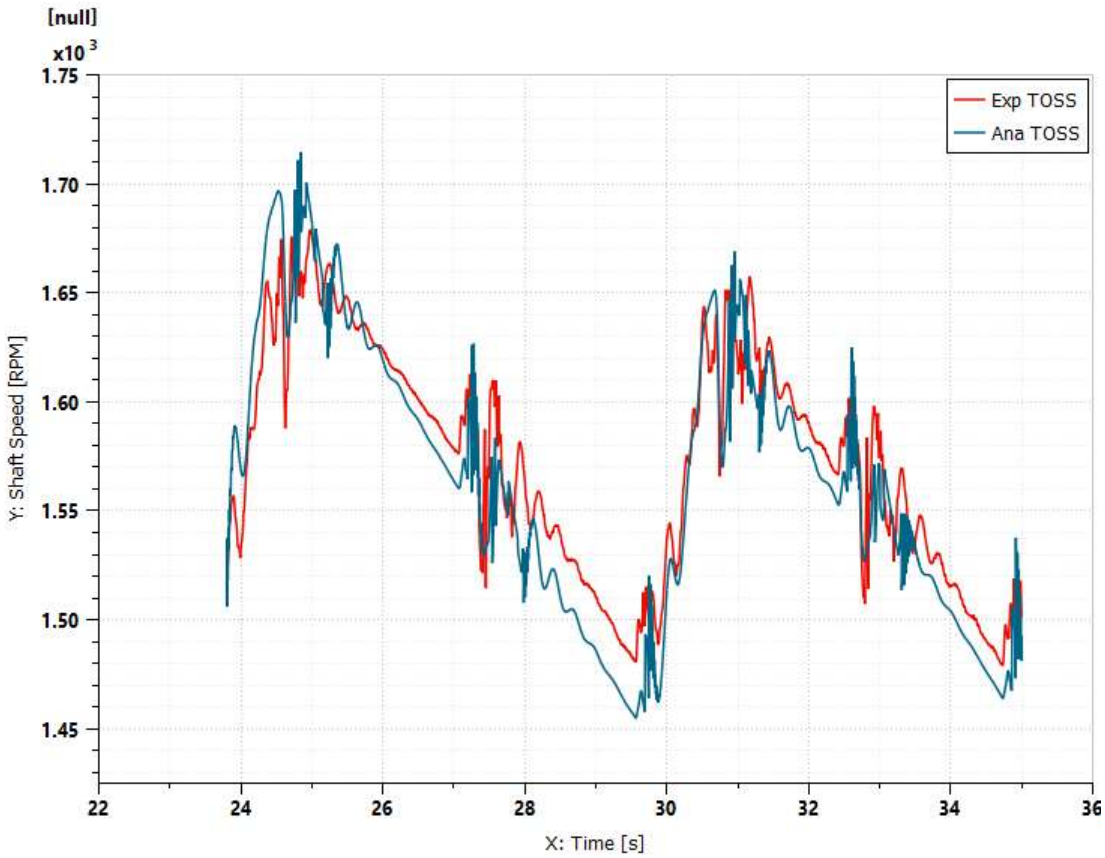

Figure 93: Experimental (Solid Red) vs. Analytical (Solid Blue) TOS Signal Results from TITO Testing in 3rd Gear

The analytical mode shape solutions for shuffle are shown in Figure 94 for TI and Figure 95 for TO and are similar to those found in [4, 5, 44]. The red bars denote the relative amplitude in % of modal response. The numbers 1-10 correlate with the lumped inertia and/or mass item represented by the legend at right of each figure. The following Figure 96 depicts the body on frame solution for longitudinal oscillations. The results verify that an asymmetric stiffness in the differential can shift the shuffle frequency for TI and TO events. The trend follows the experimental results as concluded in Table 11.

The shuffle modes respond as expected for the first torsional mode of the driveline. Highest relative oscillation occurs at the engine and decreases in amplitude traveling down the driveline components to the tires. It is important to note that these relative amplitudes are not reflected onto the same plane. Even if the reflection were considered, the maximum amplitude is still observed at the engine, tiss, and toss inertia elements. The mode shape shows that to target additional damping into the shuffle mode, there is high displacement and therefore relative velocity changes in the upstream driveline components. It is known that damping is proportional to shear or relative velocity and therefore should be targeted in those components. This also indicates additional tire damping would have minimal effect on the shuffle mode if torsional damping were modified in the tire.

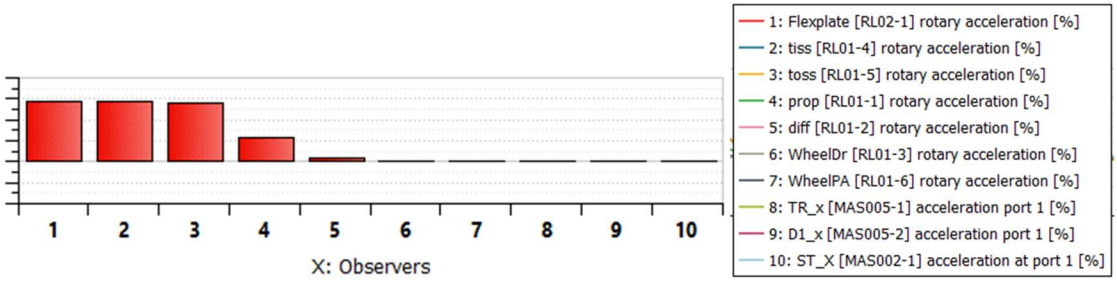

Figure 94: Digital Twin 3rd Gear TI Linearization Shuffle Mode Shape Solution with Relative Participation Amplitude

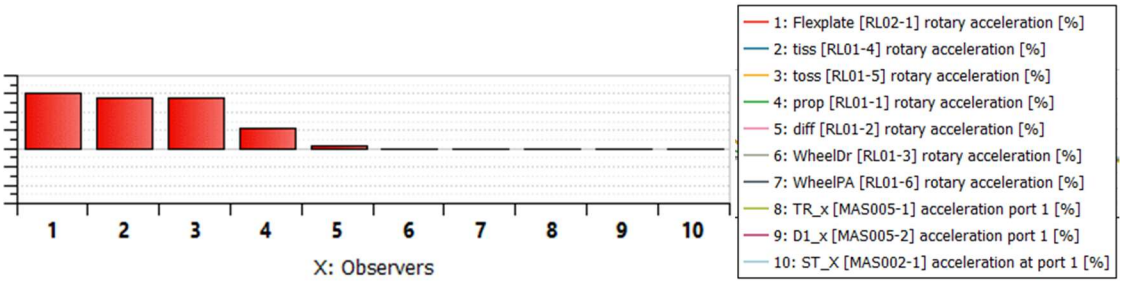

Figure 95: Digital Twin 3rd Gear TO Linearization Shuffle Mode Shape Solution with Relative Participation Amplitude

Another benefit of the digital twin with coupled longitudinal reaction forces is solving for the body on frame mode that has been noted in literature as part of the shuffle mode. The results for first driveline torsional bending in Figure 94 and Figure 95 have minimal response in the differential, transmission, or seat track response. The opposite is shown in Figure 96 where only these driveline assemblies are participating. This simulated result shows that indeed the shuffle mode and body on frame longitudinal response are two different modes but are close enough in frequency that they may be modally coupled. The author also notes that shuffle leads to impulsive excitation of the driveline assemblies due to impact excitation of lash components. The impulsive force will excite broadband frequency content and is therefore reason why shuffle excites the longitudinal body motion during TI or TO transients.

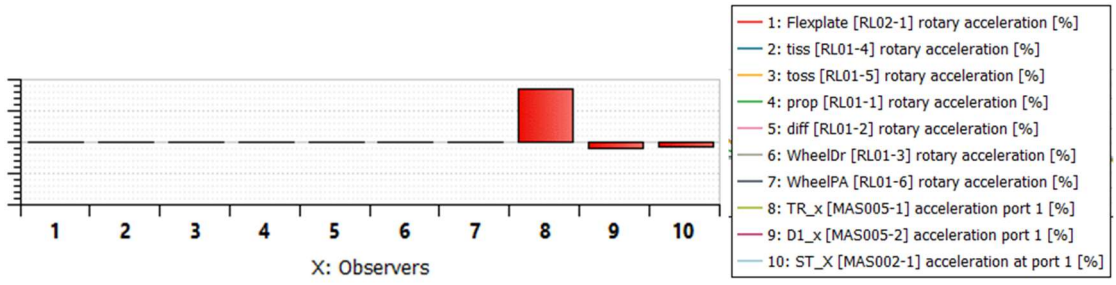

Figure 96: Digital Twin 3rd Gear Body on Frame Longitudinal Mode for TI and TO Linearization with Relative Participation Amplitude

The digital twin was used to verify shuffle behavior due to step input TI and TO and observed in all of the rotational speed sensors shown in Figure 97. All six of the shaft speeds are reflected onto the same plane at the transmission input. The analytical data follows the torsional mode shape expectation with highest relative velocity on the Eng., TISS, and TOSS. Downstream components show low oscillations. This is the same response observed experimentally in Chapter 2. A deviation in the TO behavior does not show two transients in the digital twin model. This is due to the torque loading and input to the model. Instead of a slow taper as the engine lets off torque and the driveline transfers from drive to coast, the analytical simulation has a step function input from positive to negative torque instantaneously. The step function excites the shuffle mode with clunk shown as higher frequency content but without a longer delay in the lash crossing. The overall behavior and frequency response match the expectation for a correlated model.

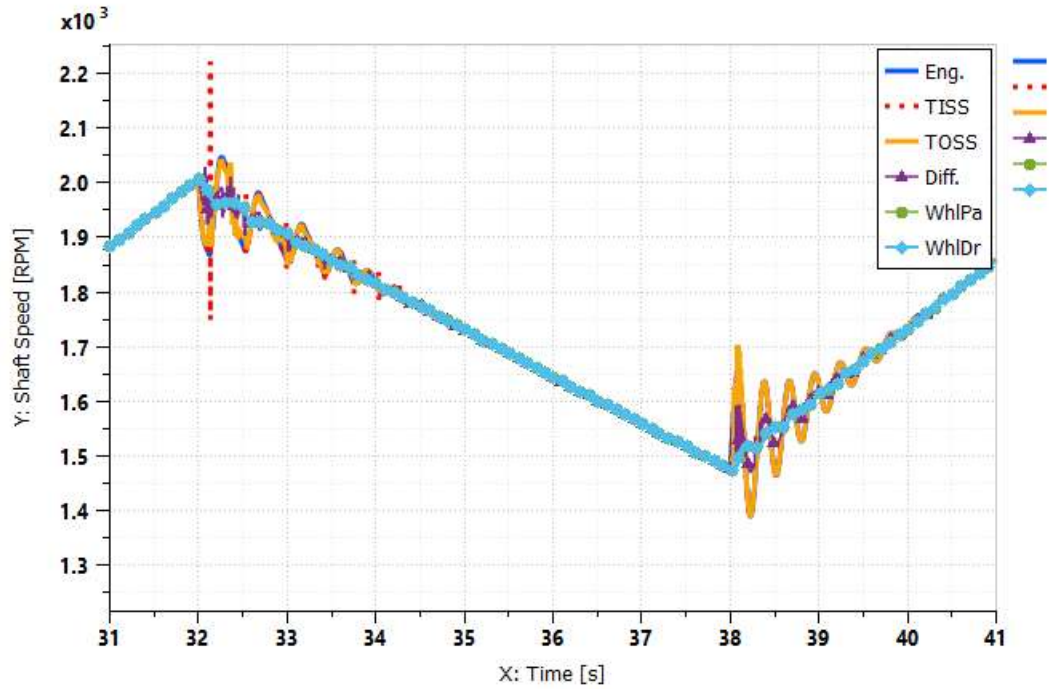

Figure 97: Analytical Shuffle Oscillation Observed for TI and TO for All Shaft Signal's Reflected onto the TISS Plane

The digital twin can further be used to evaluate the backlash traversal theories hypothesized based on experimental data. Recall from Figure 14 that during the SB event there were changes in clunk response based on the slope of the zero-torque lash crossing. The data showed that a reversal from negative to positive depicted peak clunk in the differential first while a positive to negative reversal had a peak in the transmission accelerometer response first. It was hypothesized that this behavior is due to the lash traversal propagating in different directions based on the TI or TO maneuver. The backlash can be tracked for a TI and TO in Figure 98. The simulated data depicts a step torque input signal in dashed green

with three backlash signals; the transmission, propeller shaft spline, and differential in solid red, dotted blue, and double dot dashed yellow respectively.

The time domain response of backlash clearance is observed for simulated step function TI and TO in Figure 98. The data shows the input torque step function in dashed green. The torque is plotted above the backlash clearances for the transmission, propeller shaft, and rear differential in solid red, dotted blue, and double dot-dashed orange respectively. Each backlash element is also a lumped spring element of the respective parameter and therefore includes shuffle oscillatory behavior post TI and TO. During TI, the torque is applied and sustained thus forcing contact to remain on the positive side of backlash for all three lash elements. After TO, the backlash is reversed in all three lash elements however, the time domain signal indicates multiple backlash traversals. These would be classified as double-sided impact events and have a negative perception on performance due to the multiple clunk excitations as noted by Crowther et. al. [100]. The multiple crossings are only shown in the TO and not in the TI. This is affected by the magnitude of the sustained torque application after TI whereas the TO torque is lower in amplitude allowing for the response to appear closer to a damped free vibration response with multiple lash crossings. Another benefit of the analytical model is that this time domain representation can be used to observe the propagation of overall system backlash. It was hypothesized in Chapter 2 that the direction of lash crossing corresponded to the peak accelerometer excitation due to clunk. The detailed lash crossing for TI and TO are observed in Figure 99 and Figure 100 respectively.

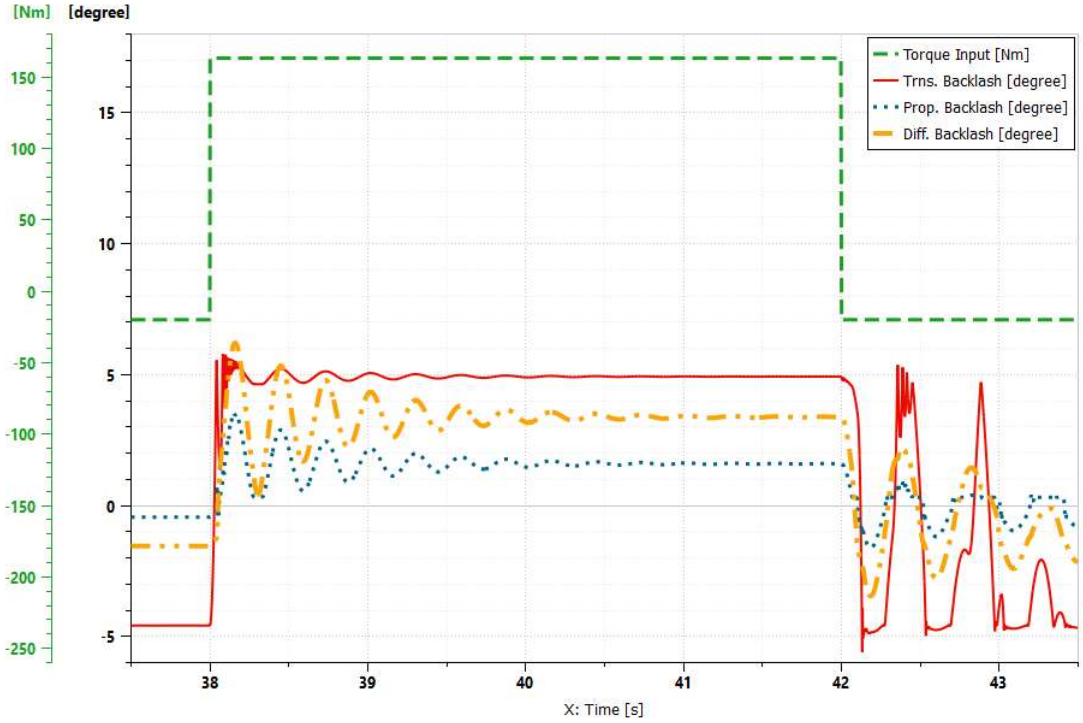

Figure 98: Backlash Traversal for TI and TO event on the Digital Twin Model Depicting Torque and Backlash Degrees vs. Time

The lash crossing for TI in Figure 99 depicts the torque step at 38 seconds. There is a delay after the torque step before the transmission element displacement begins to cross lash. A full lash crossing is considered when the displacement surpasses the backlash value which is overlaid as a dotted line denoted with the same color as the backlash displacement curve. Both positive and negative contact locations are shown. Number indicators show that lash is crossed 1 for the transmission element, 2 for the propeller shaft and lastly 3 is the differential element. This progression confirms what was hypothesized in Chapter 2 for a TI event. The opposite order of crossing and contact is confirmed in Figure 100. When the final element crosses lash, the full reflected driveline inertia is coupled at that time. The total lumped reflected inertia now coupled causes the accelerometer spike indicated in respective elements of Figure 14 relative to the direction of torque crossing. A peak in the transmission for TI and peak in the differential for TO.

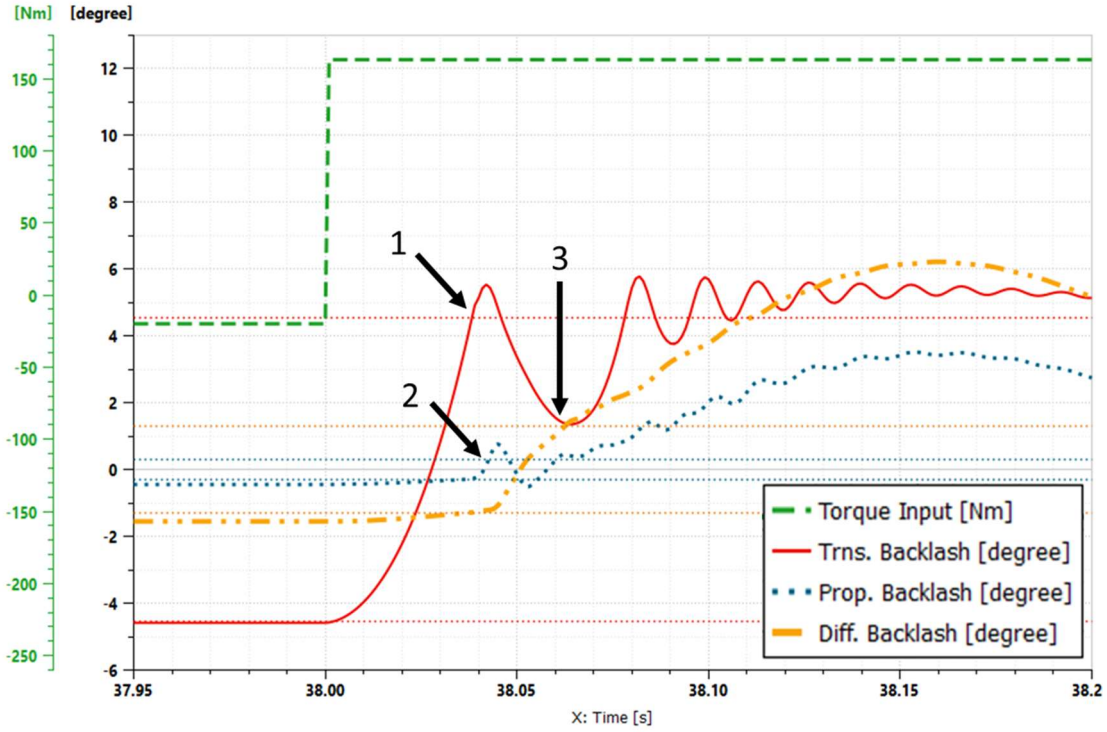

Figure 99: Detailed view of TI Backlash Traversal for Digital Twin Simulation vs. Time

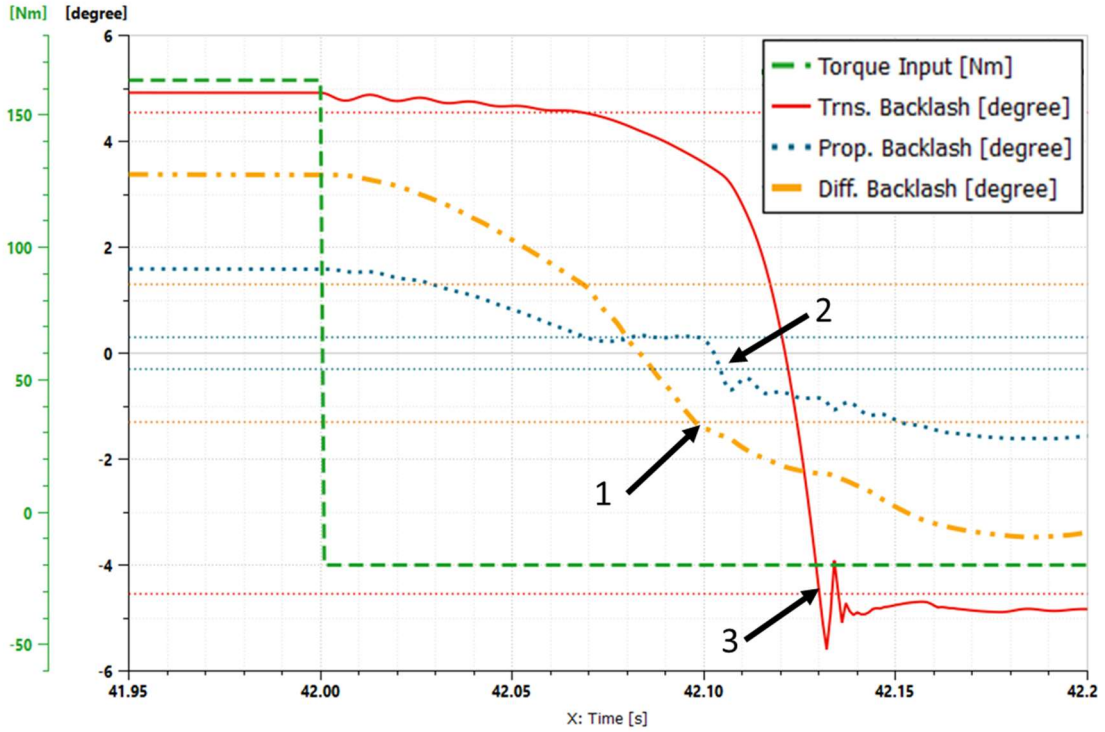

Figure 100: Detailed View of TO Backlash Traversal for Digital Twin Simulation vs. Time

The resulting ST accelerometer output based on Digital Twin replication for TITO analysis is shown in Figure 101 for 3rd gear. Additional gear states can be found in Appendix C: Additional Analysis and Figures. In each dataset, the digital twin model was input the measured CAN bus torque input estimate at the transmission. This torque input resulted in the estimated ST response based on the rack and pinion suspension coupling representation of Figure 91. The time domain response is plotted in each top subplot, experimental data corresponding to the experimental torque input in red and the digital twin estimate in dashed blue. The bottom subplot depicts the linear spectra of each signal for the truncated time shown in the top subplot.

The time domain representation is high in absolute error. This indicates that high accuracy of the ST response based on the simplified physical representation has further room for improvement. The frequency content observed in each lower subplot indicate peak response at the low <2 Hz region with a secondary peak near 11 Hz. These match up with expectation of the body on frame mode extracted from the step relaxation data in [98] and the powerplant pitching mode. The differential pitching mode is higher in content and when considered from the TWVDV filtering, it's response will be attenuated and outside the scope of the calculation.

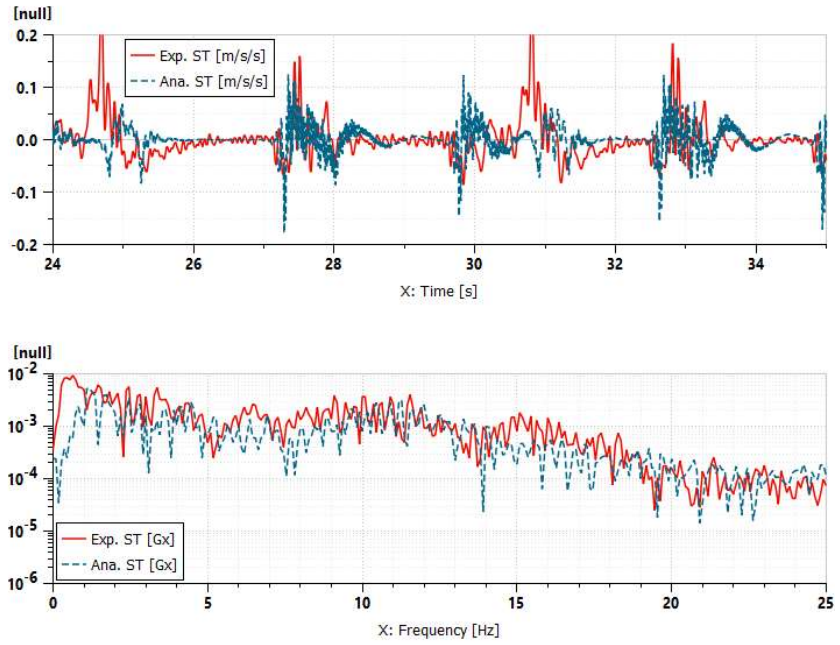

Figure 101: Third Gear ST +X from Experimental Data (Solid Red) and Analytical Estimate (Dashed Blue) for Digital Twin Estimate in Top Subplot and Linear Spectra in Bottom Subplot

3. Parameter Perturbation with TWVDV Analysis

The following figure depicts digital twin TITO maneuvers. The solid red trace depicts propeller shaft torque, the dashed blue trace depicts TIS speed changes with shuffle oscillations along with a solid yellow curve depicting longitudinal ST +X response. The bottom subplot shows implementation of the VDV and TWVDV in the digital twin model with red and dashed blue lines respectively. The value is depicted as a peak hold estimate because each calculation is the summation of 1.5 seconds worth of data. As expected, the VDV and TWVDV values increase at transient events as previously noted with the experimental data shown in Figure 87-Figure 89. Each metric is sensitive to the transient events, but the TWVDV value decay's faster than the VDV post transient. The use of a TWVDV is key for operating data to understand ST response dosage due to torque inputs requested from the driver as opposed to uncorrelated road inputs. The use in a digital twin simply confirms increased perception at step input events. The metric can further be used to gauge how perturbations in the digital twin model will correlate in perception to TI events.

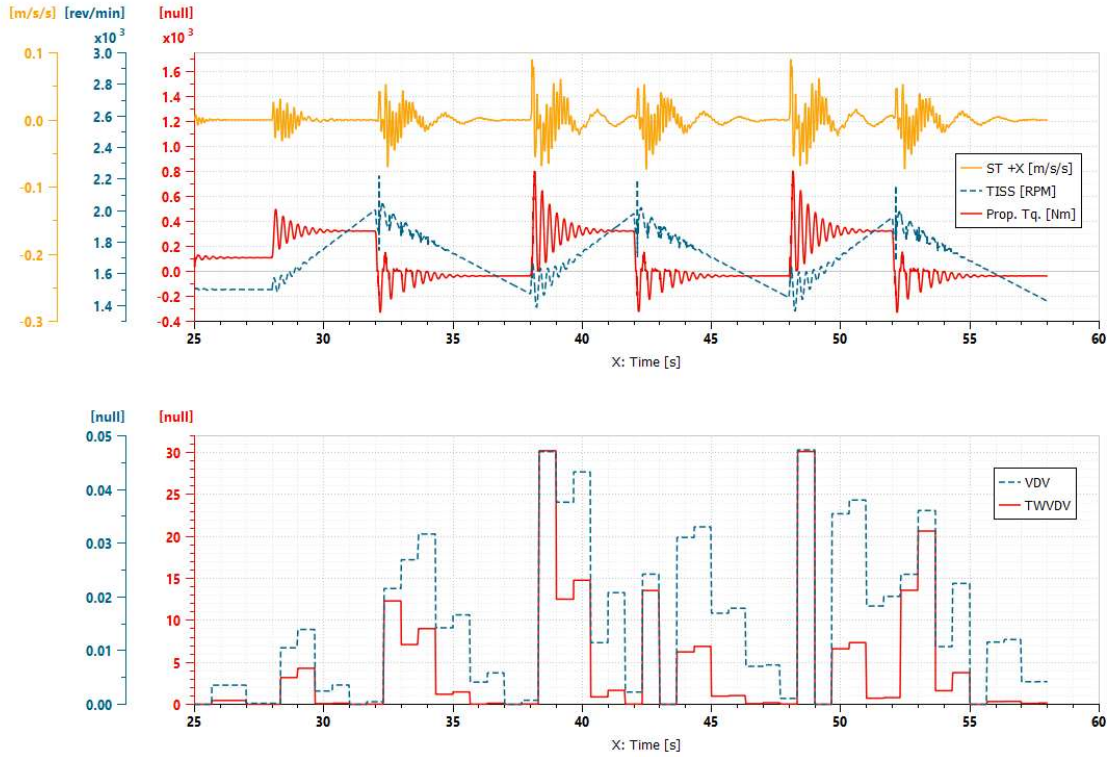

Figure 102: Digital Twin Simulation of Torque, TISS, and ST +X Response in the Top Subplot to TI and TO Events with VDV and TWVDV Estimates in the Bottom Subplot

Table 12 summarizes increases and decreases in system parameters and their changes to the digital twin TWVDV estimate. Each row indicates what parameter was changed in the first column, either a 10% increase or decrease in stiffness, damping, or both. The middle column designates the normalized TWVDV result (relative to the baseline). The third column represents the change of TWVDV as a percentage relative to the baseline. The best improvements were shown for decreased TC clutch stiffness and damping with increased equivalent transmission stiffness and damping. These two combined had even better results when based on the TWVDV and are highlighted with green to indicate a better TWVDV perception as opposed to red indicating worse perception. Changes in TC stiffness and/or damping could be realized physically with technologies described in [101]. Some of these options include modification to TC clutch hysteresis or modifications to the spring/damping architecture to achieve a lower effective spring rate. The Schaeffler document pushes toward reducing the TC clutch spring rate to drive the frequency response below idle excitation. These effects are explored with the parameter perturbation study summarized in Table 12.

Table 12: Parameter Perturbations of the Digital Twin with TWVDV Response and % Change for Improvements (Green) and non-Improvements (Red)

Parameter Changed	Tip Out TWVDV	Change
Original	1.00	0.00%
-10% TC Clutch K_{eq}	0.98	-2.25%
-10% TC Clutch K_{eq} & C_{eq}	0.98	-2.22%
+10% TC Clutch K_{eq}	1.02	2.14%
+10% TC Clutch K_{eq} & C_{eq}	1.02	2.14%
+10% Transmission K_{eq} & C_{eq}	0.99	-1.48%
-10% Transmission K_{eq} & C_{eq}	1.02	1.77%
+10% Prop. Shaft K_{eq} & C_{eq}	1.00	0.28%
-10% Prop. Shaft K_{eq} & C_{eq}	0.99	-0.73%
+10% Differential K_{eq} & C_{eq}	1.01	0.66%
-10% Differential K_{eq} & C_{eq}	0.99	-1.27%
+10% Half Shaft K_{eq} & C_{eq}	1.00	0.07%
-10% Half Shaft K_{eq} & C_{eq}	1.00	-0.38%
+10% Tire K_{eq} & C_{eq}	1.00	0.17%
-10% Tire K_{eq} & C_{eq}	1.00	0.08%
+225 kg & + 10% Body On Frame K_{eq}	0.93	-7.10%
-10% TC Clutch +10% Transmission K_{eq} & C_{eq}	0.96	-3.64%
+100% TC Clutch Hysteresis	0.99	-0.78%
+200% TC Clutch Hysteresis	0.97	-2.91%

Further modifications to the TC clutch stiffness and transmission stiffness (with proportional changes in damping) are depicted in Table 13. The results show that an increase in transmission stiffness with decrease in TC clutch stiffness are optimal from a TWVDV perception.

Table 13: Detailed Analysis of Transmission and TC Clutch Stiffness and Damping Increases

		Transmission Equivalent Stiffness (Nm/deg.)									
		310	330	350	370	390	410	430	450	470	490
TC Clutch Stiffness (Nm/deg.)	12.7	24.3	24.1	23.9	23.8	23.7	23.6	23.4	23.3	23.2	23.0
	22.7	27.0	26.8	26.5	26.3	26.1	25.9	25.7	25.5	25.3	25.1
	32.7	29.5	29.2	28.9	28.6	28.3	27.9	27.8	27.5	27.2	27.1
	42.7	31.1	31.1	30.6	30.3	30.1	29.7	29.4	28.9	28.5	28.2
	52.7	31.6	31.3	31.0	30.6	30.3	30.0	29.8	29.6	29.5	29.3
	62.7	32.3	32.0	31.7	31.3	30.9	31.1	30.6	30.4	30.3	30.0

The data shown in Figure 103 depicts five combinations of transmission and torque converter stiffness for comparison of their time domain response. The time domain data observes minimal change in the torque (dashed lines) or TOSS (dotted lines) signal while

the ST +X (solid lines) response is changing due to the perturbed parameters. This representation does not convey reasons for the change in TWVDV. However, the ST +X response is interrogated further in Figure 104 to include the spectral content truncated around the TI event.

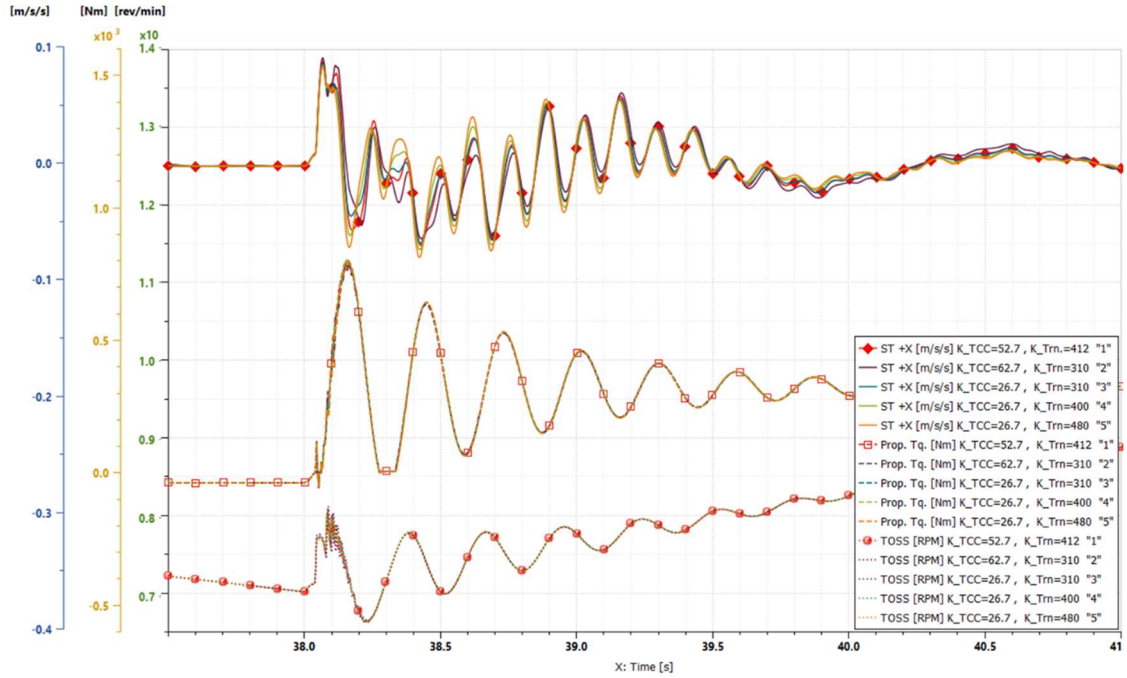

Figure 103: Simulated ST +X (Top Solid Lines) with Propeller Shaft Torque (Middle Dashed Lines) and TISS Speed (Bottom Dotted Lines) for TI Maneuver on the Digital Twin

Figure 104 has the time domain ST +X response in the top subplot along with linear spectra in the lower subplot. Each line denotes a perturbation of either the torque converter and/or transmission effective stiffness. The five values cover a range of high and low perturbations of each element. It is observed that decreasing the TC clutch while increasing the transmission stiffness causes the low frequency body on frame amplitude to decrease while the higher frequency (~8 Hz) transmission mode increases in amplitude. This is apparent from the spectral data on the bottom subplot. The reason this has a decrease in TWVDV is due to the BPF results applied from k-weighting based on ISO2631. This band pass weighting function has peak response near 1-2 Hz. Therefore, the powerplant pitch (PP Pitch) mode has minimal contribution in the TWVDV while the longitudinal body on frame mode is the key contributor. The shuffle mode is present in the spectral data but unchanged significantly based on the parameters perturbed.

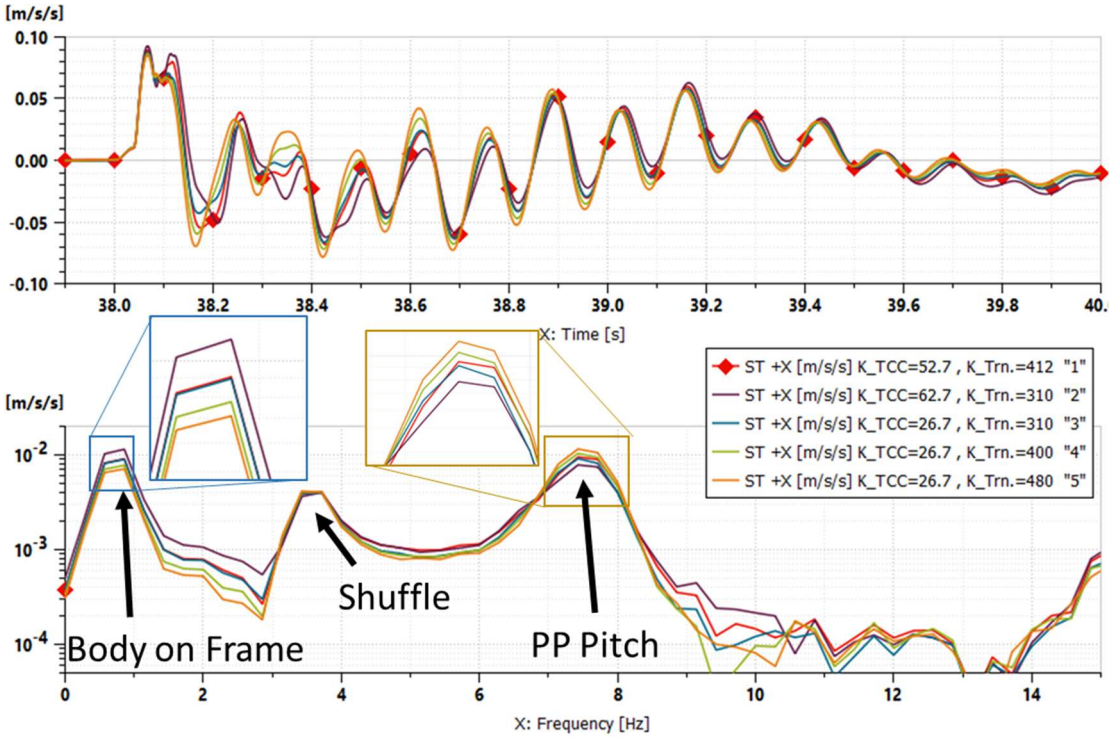

Figure 104: Top Subplot; Digital Twin Simulated ST +X Response to Changing Stiffness Parameters with Bottom Subplot; Linear Spectra of respective ST +X Response

4. Conclusions

A combination of known system parameters was used to build an analytical math model of the driveline for shuffle and clunk analysis. The math model, referred to as a digital twin, was developed using provided and estimated system parameters. The new model incorporated high accuracy driveline modeling with a reduced method for incorporating differential and powerplant pitching modes to induce longitudinal vibration estimates of the vehicle seat track (ST). The model achieved a correlation of <10% error in shuffle frequency relative to experimental estimates. It was unable to achieve the same error requirements for seat track response in the time domain due to estimated torque inputs with error based on CAN bus estimation.

The digital twin was used to confirm backlash propagation during TI and TO events. This verifies the assumption that the final backlash element to cross lash during a reversal is where the greatest impact is observed. This is attributed to the full traversal leading to a complete coupling of the lumped driveline response inducing clunk behavior where final crossing occurred.

The digital twin was further used to apply parameter perturbations on lumped driveline elements to understand their influence on calculated TWVDV during TO. Results of the parameter modifications concluded:

- An increase in the lumped transmission stiffness will decrease the TWVDV to TO.

- A decrease in TC Clutch stiffness and damping will decrease the TWVDV to TO.
- The improved TWVDV is understood by reduction in the body on frame mode (<1 Hz oscillation) with more energy input to the PP Pitch mode which does not contribute to the TWVDV measurement due to BPF roll off characteristics

Next Steps/Recommendations

There are several avenues within this work that can be further studied in future works. The experimental data was used to successfully extract an overall lash value from in-situ data. This data could be further interrogated to separate the major transmission contribution and differential lash contribution to overall. Additional studies could also evaluate the use of these backlash sizes for improved convergence time of EKF filters in reduced order modeling.

The dynamometer test rig can further be upgraded to include a feed forward control strategy. This will allow for improved TI and TO response on dyno and further backlash value extraction. Once the dyno response matches the experimental expectations, the digital twin model can be used with dyno data for real time performance and perturbation. To further improve the digital twin seat track estimates, the experimental seat track vs. propeller shaft torque FRF can be inserted for better prediction.

Based on the digital twin analysis, it is recommended that production models move towards a decrease in TC clutch stiffness and increase in transmission effective stiffness. These results can be evaluated by installing modified hardware on the dynamometer test vehicle to prove the digital twin results are valid.

References

[1] *Mechanical vibration and shock - Evaluation of human exposure to whole-body vibration*, Standard I. S. Organization, 07-15-1997 1997.

[2] R. A. Krenz, "Vehicle Response to Throttle Tip-In/Tip-Out," 1985. [Online]. Available: https://doi.org/10.4271/850967.

[3] T. Wellmann, K. Govindswamy, E. Braun, and K. Wolff, "Aspects of Driveline Integration for Optimized Vehicle NVH Characteristics," 2007. [Online]. Available: https://doi.org/10.4271/2007-01-2246.

[4] A. R. Crowther, N. Zhang, and R. Singh, "Development of a Clunk Simulation Model for a Rear Wheel Drive Vehicle With Automatic Transmission," 2005. [Online]. Available: https://doi.org/10.4271/2005-01-2292.

[5] Y. f. Xia, J. Pang, C. Hu, C. Zhou, and C. Wu, "Multi-Body Dynamic Analysis of Driveline Torsional Vibration for an RWD Vehicle," 2014. [Online]. Available: https://doi.org/10.4271/2014-01-2064.

[6] K. Govindswamy, M. Hueser, T. D'Anna, P. Diemer, and C. Roxin, "Study of Low-Frequency Driveline Clunk During Static Engagements," 2003. [Online]. Available: https://doi.org/10.4271/2003-01-1480.

[7] J. H. Elm, J. Viehöfer, and J.-W. Biermann, "Investigation of NVH Characteristics of a Downsizing Vehicle," ed: SAE International, 2014.

[8] A. Senatore, M. Pisaturo, and P. Dašić, "Frictional Torque Behavior in Actively-Closed Actuated Dry Clutch: The Temperature Influence," *Applied Mechanics and Materials,* vol. 806, pp. 240-248, 2016, doi:10.4028/www.scientific.net/AMM.806.240.

[9] B. Volinski, "Methodology: Automatic Transaxle Lash Study for Park Disengagement Clunk," 1999. [Online]. Available: https://doi.org/10.4271/1999-01-1765.

[10] D. A. Gilbert, M. F. O'Leary, and J. S. Rayce, "Integrating Test and Analytical Methods for the Quantification and Identification of Manual Transmission Driveline Clunk," 2001. [Online]. Available: https://doi.org/10.4271/2001-01-1502.

[11] N. Y. Wani and V. K. Singh, "Design Evaluations On IRS Axle System NVH Through Analytical Studies," 2005. [Online]. Available: https://doi.org/10.4271/2005-01-2289.

[12] R. Glover, H. Wang, and J. Koval, "Timing Gear Whine Noise Reduction Methodology and Application in Superchargers," 2005. [Online]. Available: https://doi.org/10.4271/2005-01-2450.

[13] J. S. P. Liu and J. T. Fox, "CAE Simulation and Experimental Testing of a CVT Vehicle Shuffle," 2006. [Online]. Available: https://doi.org/10.4271/2006-01-1308.

[14] Y. E. Lee, "Axle Gear Mesh Force Prediction, Correlation and Reduction," 2007. [Online]. Available: https://doi.org/10.4271/2007-01-2230.

[15] J. S. Gurm, W. J. Chen, A. Keyvanmanesh, T. Abe, A. R. Crowther, and R. Singh, "Transient Clunk Response of a Driveline System: Laboratory Experiment and

Analytical Studies," 2007. [Online]. Available: https://doi.org/10.4271/2007-01-2233.
[16] W. J. Chen, J. Gurm, A. Keyvanmanesh, and T. Abe, "Analytical Study for Transient Driveline Clunk Response Subject to Step Torque Input by a Mass Release System," 2007. [Online]. Available: https://doi.org/10.4271/2007-01-2244.
[17] A. Jahagirdar, R. Gehaney, P. K. Gupta, and S. Deshpande, "Probability Considerations in Design Case Study- Analysis of Multi Plate Wet Clutch for Judder and Rattling," 2007. [Online]. Available: https://doi.org/10.4271/2007-26-069.
[18] A. Gosain and M. Ravindran, "Refinement of Cabin Booming Noise In a Small Passenger Car Using Hybrid Numerical - Experimental Methodology," 2010. [Online]. Available: https://doi.org/10.4271/2010-01-0414.
[19] S. Sung, S. Chao, H. Lingala, and L. Mundy, "Structural-Acoustic Analysis of Vehicle Body Panel Participation to Interior Acoustic Boom Noise," 2011. [Online]. Available: https://doi.org/10.4271/2011-01-0496.
[20] Z. Sun, D. Schankin, W. Braun, and J. Ley, "Attenuation of Driveline Vibrations through Tuning of Propeller Shaft Liners," 2011. [Online]. Available: https://doi.org/10.4271/2011-01-1547.
[21] S. M. Jadhav, "Powertrain NVH Analysis Including Clutch and Gear Dynamics," 2014. [Online]. Available: https://doi.org/10.4271/2014-01-1680.
[22] M. Chen, D. Wang, H. Lee, C. Jiang, and J. Xin, "Application of CAE in Design Optimization of a Wet Dual Cutch Transmission and Driveline," ed: SAE International, 2014.
[23] V. Parmar, D. Di Rocco, M. Sopouch, and P. Albertini, "Multi-Physics Simulation Model for Noise and Vibration Effects in Hybrid Vehicle Powertrain," 2014. [Online]. Available: https://doi.org/10.4271/2014-01-2093.
[24] G. Wu and W. Luan, "The Impact of Gear Meshing Nonlinearities on the Vehicle Launch Shudder," ed: SAE International, 2015.
[25] D. Guo, Y. Wang, T. Lim, and P. Yi, "Tuning Axle Whine Characteristics with Emphasis on Gear Dynamics and Psychoacoustics," 2015. [Online]. Available: https://doi.org/10.4271/2015-01-2181.
[26] M. Krak, J. Dreyer, and R. Singh, "Development of a Non-Linear Clutch Damper Experiment Exhibiting Transient Dynamics," ed: SAE International, 2015.
[27] V. A. John Britto, S. Karmakar, M. Muthuveeraswamy, and B. Natarajasundaram, "High Speed Booming Noise Reduction in Passenger Car by Application of Cost Optimized NVH Solution," 2016. [Online]. Available: https://doi.org/10.4271/2016-28-0039.
[28] N. Pimpalkhare, G. Kumar, Y. K. Vaddi, and C. P. Jain, "Interior Noise Reduction in a Passenger Vehicle through Mode Modulation of Backdoor," 2016. [Online]. Available: https://doi.org/10.4271/2016-28-0058.
[29] J. Chatterjee, H. Talwar, and S. Garg, "An Experimental Study of Mechanism of Body Panel Vibration in Booming Noise Reduction of Passenger Vehicles," 2016. [Online]. Available: https://doi.org/10.4271/2016-28-0198.

[30] A. B. Shaik Mohammad, R. Vijayakumar, and N. rao.P, "Vibroacoustic Optimisation of Tractor Cabin and Correlation with Experimental Data," 2017. [Online]. Available: https://doi.org/10.4271/2017-01-1847.
[31] R. Yuan and G. Wu, "Investigation on Dry-clutch Transmissibility Characteristic for Vehicle Launch Shudder," 2018. [Online]. Available: https://doi.org/10.4271/2018-01-1225.
[32] P. Reddy *et al.*, "Control-Oriented Modeling of a Vehicle Drivetrain for Shuffle and Clunk Mitigation," 2019.
[33] T. Paygude and R. R. Joshi, "Modeling and Analysis of Clutch Engagement Judder in Commercial Vehicle Powertrain Systems," 2019. [Online]. Available: https://doi.org/10.4271/2019-01-0784.
[34] L. F. Gomez, J. Zeman, and J. Liu, "Integrated Multi-Physics Simulation for Full-Vehicle Low Frequency NVH Optimization in HEVs," 2019. [Online]. Available: https://doi.org/10.4271/2019-01-1455.
[35] P. Jawale, N. V. Karanth, A. A. Gaikwad, and K. Mutalik, "Low Frequency In-Cab Booming Noise Reduction in the Passenger Car," 2019. [Online]. Available: https://doi.org/10.4271/2019-26-0171.
[36] C. A. Joachim, D. J. Nefske, and J. A. Wolf, "Application of a Structural-Acoustic Diagnostic Technique to Reduce Boom Noise in a Passenger Vehicle," 1981. [Online]. Available: https://doi.org/10.4271/810398.
[37] D. L. Flanigan and S. G. Borders, "Application of Acoustic Modeling Methods for Vehicle Boom Analysis," 1984. [Online]. Available: https://doi.org/10.4271/840744.
[38] G. J. Fudala, T. C. Engle, and A. V. Karvelis, "A Systems Approach to Reducing Gear Rattle," 1987. [Online]. Available: https://doi.org/10.4271/870396.
[39] H. Petri and D. Heidingsfeld, "The Hydraulic Torsion Damper-A New Concept for Vibration Damping in Powertrains," 1989. [Online]. Available: https://doi.org/10.4271/892477.
[40] M. R. Khorrami, B. A. Singer, and M. A. Takallu, "Analysis of Flap Side-Edge Flowfield for Identification and Modeling of Possible Noise Sources," 1997. [Online]. Available: https://doi.org/10.4271/971917.
[41] S. Matsuyama and S. Maruyama, "Booming Noise Analysis Method Based On Acoustic Excitation Test," 1998. [Online]. Available: https://doi.org/10.4271/980588.
[42] M. Bartram, G. Mavros, and S. Biggs, "A study on the effect of road friction on driveline vibrations," (in English), *Proceedings of the Institution of Mechanical Engineers,* vol. 224, no. K4, pp. 321-340, Dec 2010 2012-03-19 2010. [Online]. Available: https://search.proquest.com/docview/862087715?accountid=28041_https://col-mtu.primo.exlibrisgroup.com/discovery/openurl?institution=01COL_MTU&vid=01COL_MTU:MTU&genre=article&atitle=A+study+on+the+effect+of+road+friction+on+driveline+vibrations&author=Bartram%2C+M%3BMavros%2C+G%3BBiggs%2C+S&volume=224&issue=K4&spage=321&date=2010&rft.btitle=&rft.jtitle=Proceedings+of+the+Institution+of+Mechanical+Engineers&issn=14644193&isbn=&sid=ProQ%3Asciencejournals_.

[43] J. Zhang, B. Chai, and X. Lu, "Active oscillation control of electric vehicles with two-speed transmission considering nonlinear backlash," (in English), *Proceedings of the Institution of Mechanical Engineers,* vol. 234, no. 1, pp. 116-133, Mar 2020 2020-02-01 2020, doi: http://dx.doi.org/10.1177/1464419319877332.

[44] W. Oh and R. Singh, "Examination of Clunk Phenomena Using a Non-Linear Torsional Model of a Front Wheel Drive Vehicle With Manual Transmission," 2005. [Online]. Available: https://doi.org/10.4271/2005-01-2291.

[45] A. Farshidianfar, M. K. Ebrahimi, H. Bartlett, and M. Moavenian, "Driveline shuffle in rear wheel vehicles," *International Journal of Heavy Vehicle Systems,* vol. 9, 01/01 2002, doi: 10.1504/IJHVS.2002.001170.

[46] T. D. Gillespie, *Fundamentals of Vehicle Dynamics*, 1 ed. Society of Automotive Engineers, 1992, p. 519.

[47] W. F. Milliken and D. L. Milliken, *Race Car Vehicle Dynamics*. SAE International, 1994.

[48] *Vehicle Dynamics Terminology*, 2008. [Online]. Available: https://doi.org/10.4271/J670_200801

[49] J. Furlich, J. Blough, and D. Robinette, "Torsional Vibration Analysis of Six Speed MT Transmission and Driveline from Road to Lab," 2017. [Online]. Available: https://doi.org/10.4271/2017-01-1845.

[50] M. Nordin, P. Bodin, and P.-O. Gutman, "New Models and Identification Methods for Backlash and Gear Play," *Adaptive Control of Nonsmooth Dynamic Systems. Springer, London,* 2001.

[51] M. Itoh, "Suppression of transient vibration for geared mechanical system with backlash using model-based control," (in English), *JSME International Journal, Series C: Mechanical Systems Machine Elements & Manufacturing,* vol. 47, no. 1, pp. 327-334, 2011-11-11 2004.

[52] J. Baumann, D. D. Torkzadeh, A. Ramstein, U. Kiencke, and T. Schlegl, "Model-Based Predictive Anti-Jerk Control," in *IFAC*, Salerno, Italy, 2004 2004: Elsevier, p. 6.

[53] D. Hao, C. Zhao, and Y. Huang, "A Reduced-Order Model for Active Suppression Control of Vehicle Longitudinal Low-Frequency Vibration," (in English), *Shock and Vibration,* vol. 2018, p. 22, 2018 2018-12-06 2018, doi: http://dx.doi.org/10.1155/2018/5731347.

[54] C. A. Malonga Makosi, S. Rinderknecht, R. Binz, F. Uphaus, and F. Kirschbaum, "Implementation of an Open-Loop Controller to Design the Longitudinal Vehicle Dynamics in Passenger Cars," 2017. [Online]. Available: https://doi.org/10.4271/2017-01-1107.

[55] *Serial Control and Communications Heavy Duty Vehicle Network - Top Level Document*, 2018. [Online]. Available: https://doi.org/10.4271/J1939_201808

[56] J. Furlich, J. Blough, and D. Robinette, "The Utilization of Onboard Sensor Measurements for Estimating Driveline Damping," 2019. [Online]. Available: https://doi.org/10.4271/2019-01-1529.

[57] W. Heylen, S. Lammens, and P. Sas, *Modal Analysis Theory and Testing*. Katholieke Universiteit Leuven, Faculty of Engineering, Department of Mechanical Engineering, Division of Production Engineering, Machine Design and Automation, 1998.

[58] F. J. Owens and M. S. Murphy, "A short-time Fourier transform," (in English), *Signal Processing,* vol. 14, no. 1, pp. 3-10, 2011-11-11 1988. [Online]. Available: https://search.proquest.com/docview/25023888?accountid=28041 https://col-mtu.primo.exlibrisgroup.com/discovery/openurl?institution=01COL_MTU&vid=01COL_MTU:MTU&genre=article&atitle=A+short-time+Fourier+transform.&author=Owens%2C+F+J%3BMurphy%2C+M+S&volume=14&issue=1&spage=3&date=1988&rft.btitle=&rft.jtitle=Signal+Processing&issn=01651684&isbn=&sid=ProQ%3Aelectronicscomms_1766307+%28CI%29.

[59] J. Furlich, J. Blough, and D. Robinette, "Analysis of experimental MT clunk with STFT and CWT to observe mode participation and reduction," in *ISMA 2018 and USD 2018*, Leuven Belgium, 2018: KU Leuven, pp. 4269-4282.

[60] D. Robinette, G. Gibson, D. Szpara, and E. Tehansky, "Performance Characterization of Automatic Transmission Upshifts with Reduced Shift Times," ed: SAE International, 2015.

[61] M. G. Donley, T. C. Lim, and G. C. Steyer, "Dynamic Analysis of Automotive Gearing Systems," 1992. [Online]. Available: https://doi.org/10.4271/920762.

[62] Z. A. Akbar, H. Ullah, F. M. Malik, A. Saeed, and A. Aziz, "PID Based Control of Electric Vehicle Drive Line with Backlash," in *2019 IEEE 10th International Conference on Mechanical and Aerospace Engineering (ICMAE)*, 22-25 July 2019 2019, pp. 590-595, doi: 10.1109/ICMAE.2019.8880955.

[63] M. Dub, O. Berka, F. Lopot, F. Starý, and V. Dynybyl, "Torsional Characteristics Measurement of a Gearbox," (in English), *Applied Mechanics and Materials,* vol. 827, pp. 87-90, Feb 2016 2019-08-30 2016, doi: http://dx.doi.org/10.4028/www.scientific.net/AMM.827.87.

[64] J. Roy R. Craig and A. J. Kurdila, *Fundamentals of Structural Dynamics*, 2 ed. Hoboken, New Jersey: John Wiley & Son's Inc., 1981.

[65] S. G. Kelly, *Fundamentals of Mechanical Vibrations*, 2 ed. Thomas Casson, McGraw-Hill Companies, Inc., 2000.

[66] P. Mistrot, P. Donati, J. P. Galmiche, and D. Florentin, "Assessing the discomfort of the whole-body multi-axis vibration: laboratory and field experiments," (in English), *Ergonomics,* vol. 33, no. 12, pp. 1523-1536, December 1990 2020-01-14 1990. [Online]. Available: https://search.proquest.com/docview/80254025?accountid=28041-https://col-mtu.primo.exlibrisgroup.com/discovery/openurl?institution=01COL_MTU&vid=01COL_MTU:MTU&genre=article&atitle=Assessing+the+discomfort+of+the+whole-body+multi-axis+vibration%3A+laboratory+and+field+experiments.&author=Mistrot%2C+P%3BDonati%2C+P%3BGalmiche%2C+J+P%3BFlorentin%2C+

D&volume=33&issue=12&spage=1523&date=1990&rft.btitle=&rft.jtitle=Ergonomics&issn=00140139&isbn=&sid=ProQ%3Amedline_2286198.

[67] A. Kjellberg, B. O. Wikström, and U. Dimberg, "Whole-body vibration: exposure time and acute effects--experimental assessment of discomfort," (in English), *Ergonomics,* vol. 28, no. 3, pp. 545-554, March 1985 2020-01-14 1985. [Online]. Available: https://search.proquest.com/docview/76213946?accountid=28041 https://col-mtu.primo.exlibrisgroup.com/discovery/openurl?institution=01COL_MTU&vid=01COL_MTU:MTU&genre=article&atitle=Whole-body+vibration%3A+exposure+time+and+acute+effects--experimental+assessment+of+discomfort.&author=Kjellberg%2C+A%3BWikstr%C3%B6m%2C+B+O%3BDimberg%2C+U&volume=28&issue=3&spage=545&date=1985&rft.btitle=&rft.jtitle=Ergonomics&issn=00140139&isbn=&sid=ProQ%3Amedline_4018007.

[68] A. Kjellberg and B. M. Wikstrom, "Subjective reactions to whole-body vibration of short duration," (in English), *Journal of Sound and Vibration,* vol. 99, pp. 415-424, 2011-11-11 1985. [Online]. Available: https://search.proquest.com/docview/24778021?accountid=28041-https://col-mtu.primo.exlibrisgroup.com/discovery/openurl?institution=01COL_MTU&vid=01COL_MTU:MTU&genre=article&atitle=Subjective+reactions+to+whole-body+vibration+of+short+duration.&author=Kjellberg%2C+A%3BWikstrom%2C+B+M&volume=99&issue=&spage=415&date=8+Apr.+1985&rft.btitle=&rft.jtitle=Journal+of+Sound+and+Vibration&issn=0022460X&isbn=&sid=ProQ%3Aante_AN8525763+%28AN%29.

[69] H. V. Howarth and M. J. Griffin, "The frequency dependence of subjective reaction to vertical and horizontal whole-body vibration at low magnitudes," (in English), *Journal of the Acoustical Society of America,* vol. 83, no. 4, pp. 1406-1413, Apr 1988 2017-09-25 1988, doi: http://dx.doi.org/10.1121/1.395947.

[70] M. J. Griffin and E. M. Whitham, "Discomfort produced by impulsive whole-body vibration," (in English), *Acoustical Society of America, Journal,* vol. 68, pp. 1277-1284, 2011-11-11 1980. [Online]. Available: https://search.proquest.com/docview/23699981?accountid=28041 https://col-mtu.primo.exlibrisgroup.com/discovery/openurl?institution=01COL_MTU&vid=01COL_MTU:MTU&genre=article&atitle=Discomfort+produced+by+impulsive+whole-body+vibration&author=Griffin%2C+M+J%3BWhitham%2C+E+M&volume=68&issue=&spage=1277&date=Nov.+1980&rft.btitle=&rft.jtitle=Acoustical+Society+of+America%2C+Journal&issn=&isbn=&sid=ProQ%3Aaerospace_A81-13212+%28AH%29.

[71] M. J. Griffin, "Evaluation of Vibration with Respect to Human Response," 1986. [Online]. Available: https://doi.org/10.4271/860047.

[72] M. J. Griffin, "Subjective Equivalence of Sinusoidal and Random Whole-Body Vibration," *Acoustical Society of America,* vol. 60, 5, pp. 1976-1976, 1976.

[73] T. E. Fairley and M. J. Griffin, "Predicting the discomfort caused by simultaneous vertical and fore-and-aft whole-body vibration," (in English), *Journal of Sound and Vibration,* vol. 124, pp. 141-156, 2011-11-11 1988. [Online]. Available: https://search.proquest.com/docview/24960653?accountid=28041 https://col-mtu.primo.exlibrisgroup.com/discovery/openurl?institution=01COL_MTU&vid=01COL_MTU:MTU&genre=article&atitle=Predicting+the+discomfort+caused+by+simultaneous+vertical+and+fore-and-aft+whole-body+vibration&author=Fairley%2C+T+E%3BGriffin%2C+M+J&volume=124&issue=&spage=141&date=8+July+1988&rft.btitle=&rft.jtitle=Journal+of+Sound+and+Vibration&issn=0022460X&isbn=&sid=ProQ%3Aaerospace_A88-48020+%28AH%29.

[74] P. Donati, A. Grosjean, P. Mistrot, and L. Roure, "The subjective equivalence of sinusoidal and random whole-body vibration in the sitting position (an experimental study using the "floating reference vibration" method)," (in English), *Ergonomics,* vol. 26, no. 3, pp. 251-273, March 1983 2020-01-14 1983. [Online]. Available: https://search.proquest.com/docview/80486828?accountid=28041 https://col-mtu.primo.exlibrisgroup.com/discovery/openurl?institution=01COL_MTU&vid=01COL_MTU:MTU&genre=article&atitle=The+subjective+equivalence+of+sinusoidal+and+random+whole-body+vibration+in+the+sitting+position+%28an+experimental+study+using+the+%22floating+reference+vibration%22+method%29.&author=Donati%2C+P%3BGrosjean%2C+A%3BMistrot%2C+P%3BRoure%2C+L&volume=26&issue=3&spage=251&date=1983&rft.btitle=&rft.jtitle=Ergonomics&issn=00140139&isbn=&sid=ProQ%3Amedline_6851997.

[75] M. J. Griffin and E. M. Whitham, "Assessing the discomfort of dual-axis whole-body vibration," (in English), *Journal of Sound and Vibration,* vol. 54, pp. 107-116, 2011-11-10 1977. [Online]. Available: https://search.proquest.com/docview/22957073?accountid=28041 https://col-mtu.primo.exlibrisgroup.com/discovery/openurl?institution=01COL_MTU&vid=01COL_MTU:MTU&genre=article&atitle=Assessing+the+discomfort+of+dual-axis+whole-body+vibration&author=Griffin%2C+M+J%3BWhitham%2C+E+M&volume=54&issue=&spage=107&date=8+Sept.+1977&rft.btitle=&rft.jtitle=Journal+of+Sound+and+Vibration&issn=0022460X&isbn=&sid=ProQ%3Aaerospace_A77-50196+%28AH%29.

[76] H. V. C. Howarth and M. J. Griffin, "Subjective reaction to vertical mechanical shocks of various waveforms," (in English), *Journal of Sound and Vibration,* vol.

147, pp. 395-408, 2011-11-11 1991. [Online]. Available: https://search.proquest.com/docview/25419942?accountid=28041 https://col-mtu.primo.exlibrisgroup.com/discovery/openurl?institution=01COL_MTU&vid=01COL_MTU:MTU&genre=article&atitle=Subjective+reaction+to+vertical+mechanical+shocks+of+various+waveforms.&author=Howarth%2C+H+V+C%3BGriffin%2C+M+J&volume=147&issue=&spage=395&date=22+June+1991&rft.btitle=&rft.jtitle=Journal+of+Sound+and+Vibration&issn=0022460X&isbn=&sid=ProQ%3Aante_AN9110807+%28AN%29.

[77] H.-K. Jang, S.-H. Choi, and K. Ruquet, "Evaluation of Discomfort Due to Vertical Feet Vibration at a Driver's Sitting Posture," 2007. [Online]. Available: https://doi.org/10.4271/2007-01-2395.

[78] A. Sorniotti, E. Galvagno, A. Morgando, M. Velardocchia, and F. Amisano, "An Objective Evaluation of the Comfort During the Gear Change Process," 2007. [Online]. Available: https://doi.org/10.4271/2007-01-1584.

[79] W. Huang and H. Liu, "Application of fuzzy dynamic weights drivability evaluation model in tip-in condition," *Journal of Vibration and Control,* vol. 25, no. 4, pp. 739-747, 2019, doi: 10.1177/1077546318795527.

[80] E. Johanning, "Vibration and shock exposure of maintenance-of-way vehicles in the railroad industry," *Applied Ergonomics,* vol. 42, pp. 555-562, 06-30-2010 2011, doi: 10.1016.

[81] D. Joshi, S. Kedia, and S. Muthiah, "A Study on the Repeatability of Vehicle Ride Performance Measurements," 2019. [Online]. Available: https://doi.org/10.4271/2019-26-0076.

[82] F. Buarque, P. M. C. L. Pacheco, L. de Souza Xavier, and P. P. Kenedi, "Experimental and Numerical Analysis of an Off-road Vehicle Suspension," 2003. [Online]. Available: https://doi.org/10.4271/2003-01-3650.

[83] M. Walber and A. Tamagna, "Evaluation of the Vibratory Effect Transmitted by Road Buses Bodyworks," 2008. [Online]. Available: https://doi.org/10.4271/2008-36-0208.

[84] S. Pawar, M. Bodla, R. Bhangale, and M. Kumbhar, "Tractor Operator Objective Response to Seat Vibration in Real World Usage Pattern," 2013. [Online]. Available: https://doi.org/10.4271/2013-26-0097.

[85] K. Horste, "Objective Measurement of Automatic Transmission Shift Feel Using Vibration Dose Value," 1995. [Online]. Available: https://doi.org/10.4271/951373.

[86] R. Hibino, T. Jimbo, H. Yamaguchi, Y. Tsurumi, H. Otsubo, and S. Kato, "Clarification of Transient Characteristics by Coupled Analysis of Powertrains and Vehicles," ed: SAE International, 2016.

[87] E. Little, P. Handrickx, P. Grote, M. Mergay, and J. Deel, "Ride Comfort Analysis: Practice and Procedures," 1999. [Online]. Available: https://doi.org/10.4271/990053.

[88] S.-J. Hwang, J. L. Stout, and C.-C. Ling, "Modeling and Analysis of Powertrain Torsional Response," 1998. [Online]. Available: https://doi.org/10.4271/980276.

[89] D. Wehrwein and Z. P. Mourelatos, "Modeling and Optimization of Vehicle Drivetrain Dynamic Performance Considering Uncertainty," 2005. [Online]. Available: https://doi.org/10.4271/2005-01-2371.
[90] D. Wehrwein and Z. P. Mourelatos, "Reliability Based Design Optimization of Dynamic Vehicle Performance Using Bond Graphs and Time Dependent Metamodels," 2006. [Online]. Available: https://doi.org/10.4271/2006-01-0109.
[91] D. Wehrwein and Z. P. Mourelatos, "Optimal Engine Torque Management for Reducing Driveline Clunk Using Time - Dependent Metamodels," 2007. [Online]. Available: https://doi.org/10.4271/2007-01-2236.
[92] P. Bingham, S. Theodossiades, T. Saunders, E. Grant, and R. Daubney, "A study on automotive drivetrain transient response to 'clutch abuse' events," *Proceedings of the Institution of Mechanical Engineers, Part D: Journal of Automobile Engineering,* vol. 230, no. 10, pp. 1403-1416, 2016, doi: 10.1177/0954407015611293.
[93] I. M. Khan, M. Datar, W. Sun, G. Festag, T. B. Juang, and N. Remisoski, "Multibody Dynamics Cosimulation for Vehicle NVH Response Predictions," ed: SAE International, 2017.
[94] G. R. Guercioni, E. Galvagno, A. Tota, A. Vigliani, and T. Zhao, "Driveline Backlash and Half-shaft Torque Estimation for Electric Powertrains Control," 2018. [Online]. Available: https://doi.org/10.4271/2018-01-1345.
[95] J. Xu, J. Zhu, and F. Xia, "Modeling and Analysis of Amplitude-Frequency Characteristics of Torsional Vibration for Automotive Powertrain," (in English), *Shock and Vibration,* vol. 2020, 2020 2020-09-07 2020, doi: http://dx.doi.org/10.1155/2020/6403413.
[96] J. Wang, T. C. Lim, and M. Li, "Dynamics of a hypoid gear pair considering the effects of time-varying mesh parameters and backlash nonlinearity," *Journal of Sound and Vibration,* vol. 308, no. 1, pp. 302-329, 2007/11/20/ 2007, doi: https://doi.org/10.1016/j.jsv.2007.07.042.
[97] T. Peng, "Coupled Multi-body Dynamic and Vibration Analysis of Hypoid and Bevel Geared Rotor System," Doctor of Philosophy, Mechanical Engineering, Cincinnati, 2010.
[98] J. Furlich, J. Blough, and D. Robinette, "Vehicle Driveline Benchmarking to Support Predictive CAE Modeling Development," 2020, pp. 141-148.
[99] J. Wang and T. C. Lim, "Effect of tooth mesh stiffness asymmetric nonlinearity for drive and coast sides on hypoid gear dynamics," *Journal of Sound and Vibration,* vol. 319, no. 3, pp. 885-903, 2009/01/23/ 2009, doi: https://doi.org/10.1016/j.jsv.2008.06.021.
[100] A. Crowther, C. Janello, and R. Singh, "Quantification of clearance-induced impulsive sources in a torsional system," *Journal of Sound and Vibration,* vol. 307, pp. 428-451, 11/01 2007, doi: 10.1016/j.jsv.2007.05.055.
[101] T. Heck, B. Zaugg, T. Krause, B. Vogtle, and M. Fub, "Efficient Solutions for Automatic Transmissions," presented at the Schaeffler Symposium: Mobility for Tomorrow, ---, 12/13/2018, 2018.

6. Appendix A: Test Vehicle and Instrumentation Figures

Figure 105: On Road Test Vehicle (right) and Laboratory Test Vehicle Before Disassembly (right)

Figure 106: Driver Side View of Laboratory Test Vehicle on Dyno

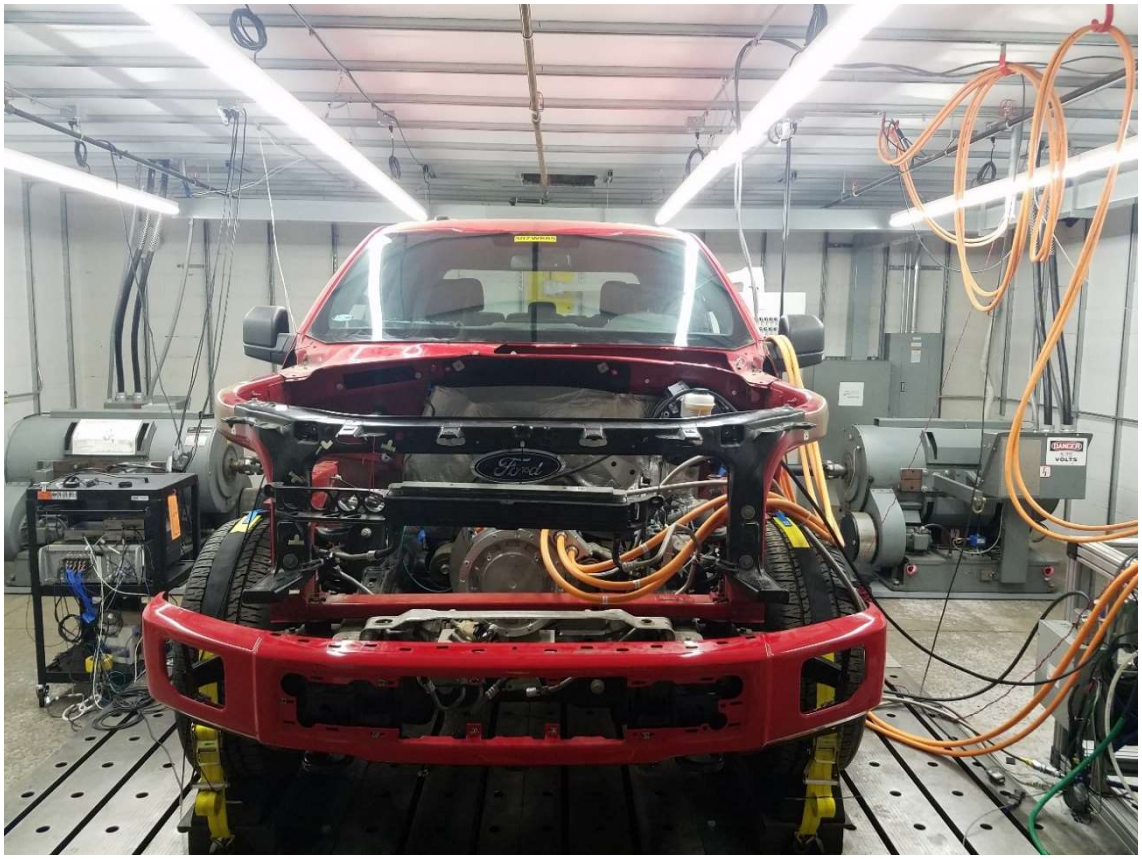

Figure 107: Front View of Laboratory Test Vehicle on Dyno

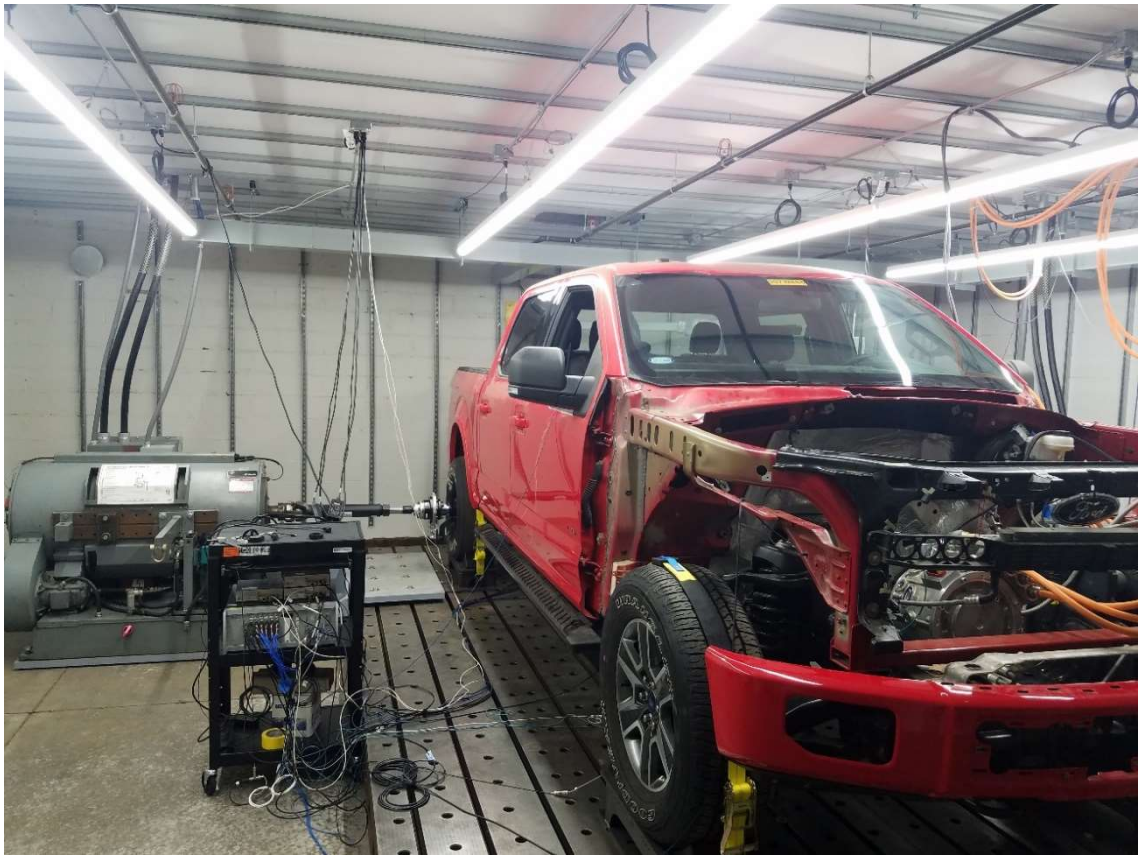

Figure 108: Passenger Side View of Laboratory Test Vehicle on Dyno

Figure 109: Top Down View of Cradle Assembly Coupled to the Transmission Bellhousing (top) and eMotor (bottom) Complete with Shafting and Torque Telemetry Mounting

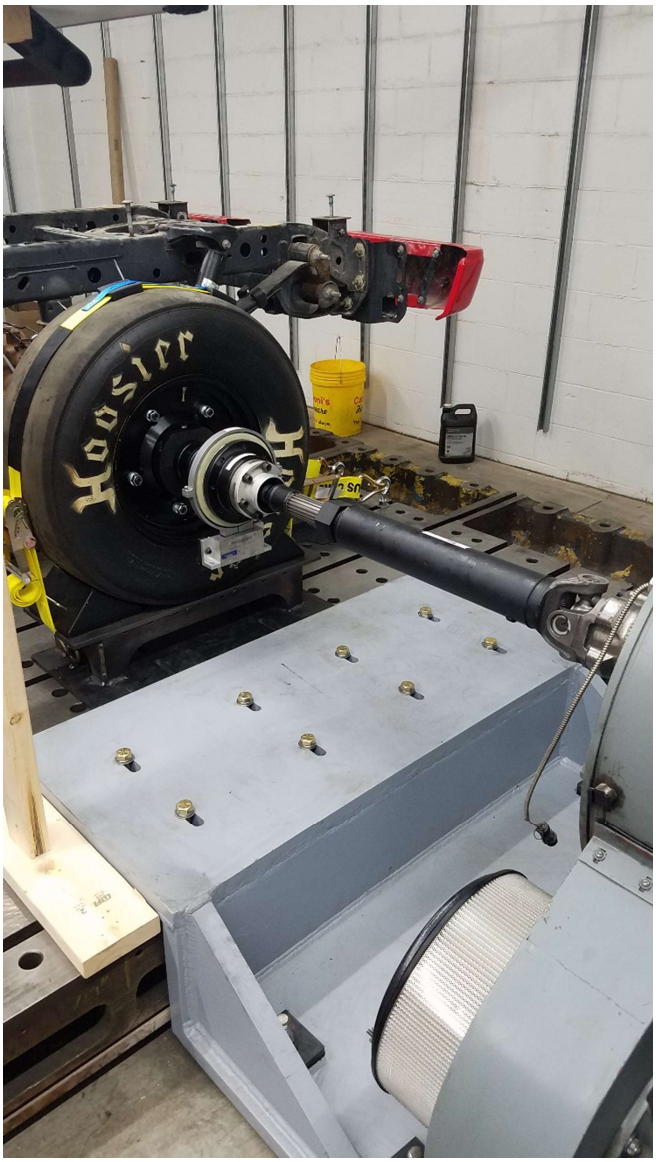

Figure 110: Wheel Hub Through Shaft Assembly and Coupling to Dyno (Driver Side)

Figure 111: Flexplate Magnetic Pickup Mounting through Transmission Bell Housing

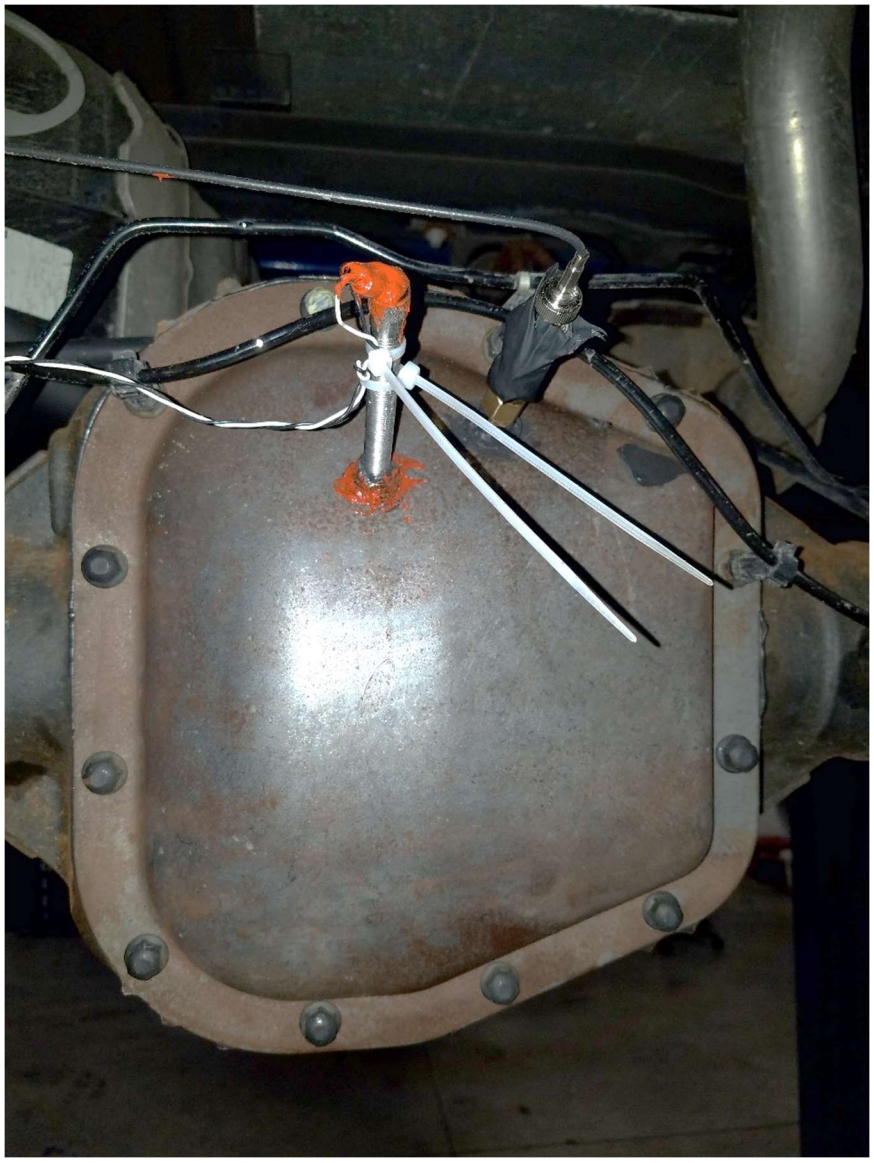

Figure 112: Differential Magnetic Pickup and Microphone Transducer Mounting Locations

Figure 113: Differential Accelerometer Mounting

Figure 114: Transmission Accelerometer Mounting

Figure 115: Chassis Accelerometer Mounting

Figure 116: Seat Track Accelerometer Mounting

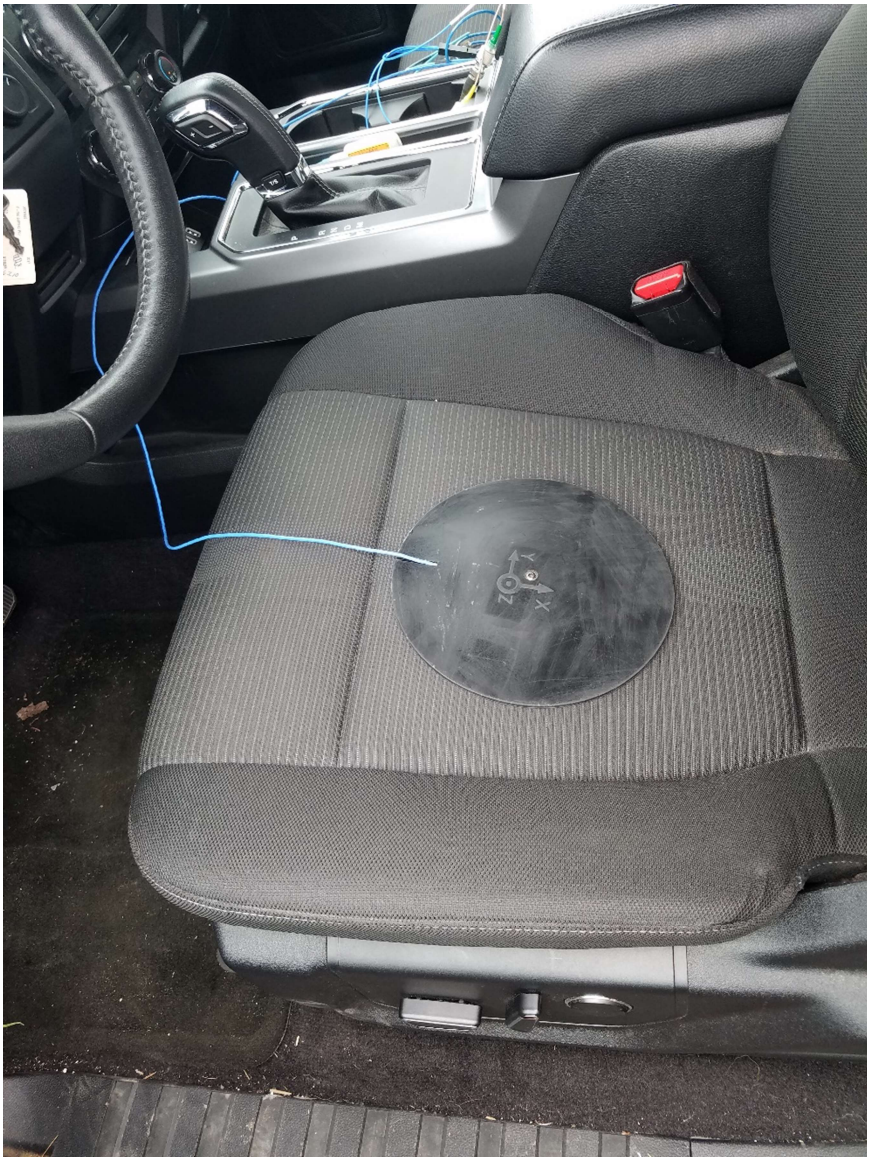

Figure 117: Seat Pad Accelerometer Mounting

7. Appendix B: Propeller Shaft Strain Gauge Installation

Propeller shaft torque was a desired measurement to acquire for road testing to compare with CAN bus measurements and to develop TWVDV methods. It was acquired by installing a balanced strain rosette in a torsion configuration as depicted by Figure 118. The signal was transferred using an Accumetrics AT5000 RF transmitter for bridge excitation according to the wiring diagram in Figure 119.

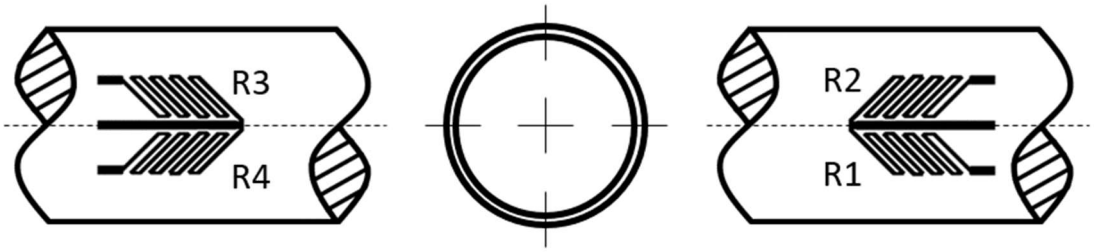

Figure 118: Torsion Bridge Installation Schematic

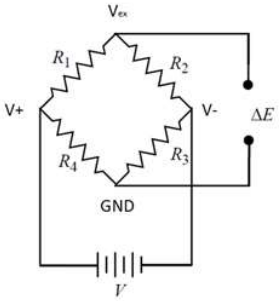

Figure 119: Bridge Excitation Circuit Schematic

The resulting torque measured across the bridge due to the change in output voltage is proportional to the torque based on the shaft material properties following Equation 23.

$$\varepsilon_1 = \frac{\gamma}{2} = \frac{2T}{E\pi(\frac{D}{2})^3}(1+\nu) \qquad \text{Equation 23}$$

The balanced bridge equation is simplified in pure torsion assuming $\varepsilon_1 = \varepsilon_3 = -\varepsilon_2 = -\varepsilon_4$ as described by Equation 24.

$$\frac{\Delta E}{V} = \frac{S_g}{4}[4\varepsilon_1] \qquad \text{Equation 24}$$

The gage factor, S_g, is determined by the strain gages used. For this application there were 350 Ohm resistors from Vishay Micro Measurement. They can be seen installed in Figure 120.

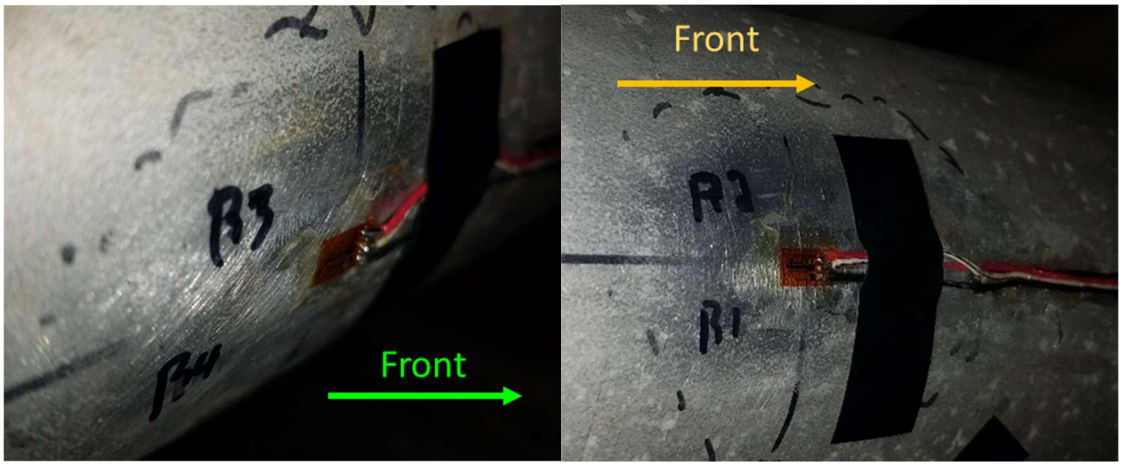

Figure 120: Installed Torsion Measurement Bridge with Front Arrow Indicating the Vehicle Front or +X Direction

8. Appendix C: Additional Analysis and Figures

The raw shaft speeds are depicted in Figure 121 while their projections onto the transmission input are depicted in Figure 122. Both figures show the engine, TIS, TOS, Differential, Driver Wheel, and Passenger Wheel speeds in solid blue, dotted red, solid yellow, purple with upper triangle markers, green with circle markers, and light blue with diamond markers respectively. The data once again shows a large spike in driveline speed following the TI and TO events as the dyno PID attempts to control the test system. Following each spike is the same low frequency (<1 Hz) control mode that can be filtered out as done in Figure 123.

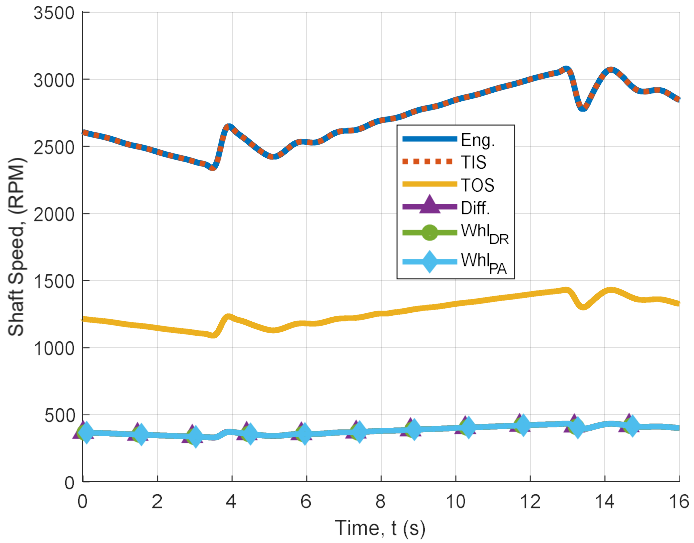

Figure 121: Dyno Thr/r Testing in 3rd Gear with TC Clutch Locked Including a TI and TO Event

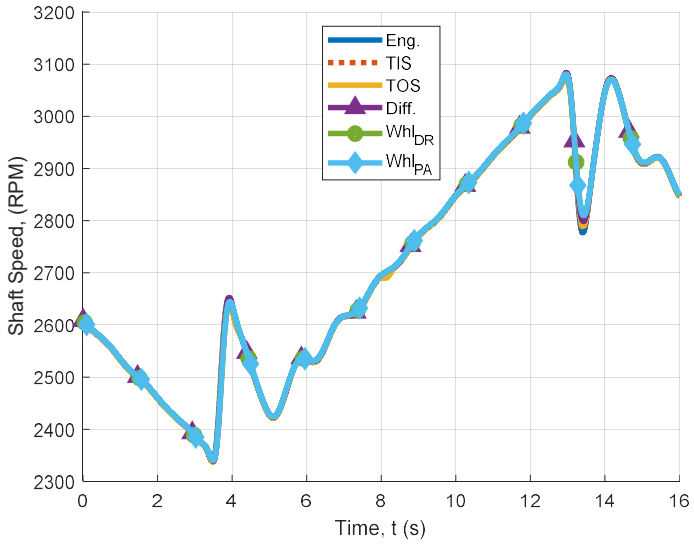

Figure 122: Dyno Thr/r Testing in 3rd Gear with TC Clutch Locked Including a TI and TO Event with All Shaft Speeds Reflected onto the TISS Plane

The BPF results in Figure 123 shows the engine, TIS, TOS, Differential, Driver Wheel, and Passenger Wheel speeds in solid blue, dotted red, solid yellow, purple with upper triangle markers, green with circle markers, and light blue with diamond markers respectively. The amplitude of oscillation in the locked torque converter example data is shown to have a lower peak-peak response than the unlocked torque converter data. This is due to the locked nature of the converter which doesn't allow the engine speed to flare at a higher amplitude than the downstream rotational elements. A major difference observed in the locked TC clutch data is that while the driveline is in a drive or coast condition between the TI and TO transients, there appears to be a constant frequency of oscillation close to that of the shuffle frequency. This steady state oscillation holds steady during all time and not just during transient events. The same peak response is observed in relative shaft speed amplitude where the peak amplitude is negative for a TI event and positive for a TO event. The overall response with microphones and accelerometers is shown in Figure 124.

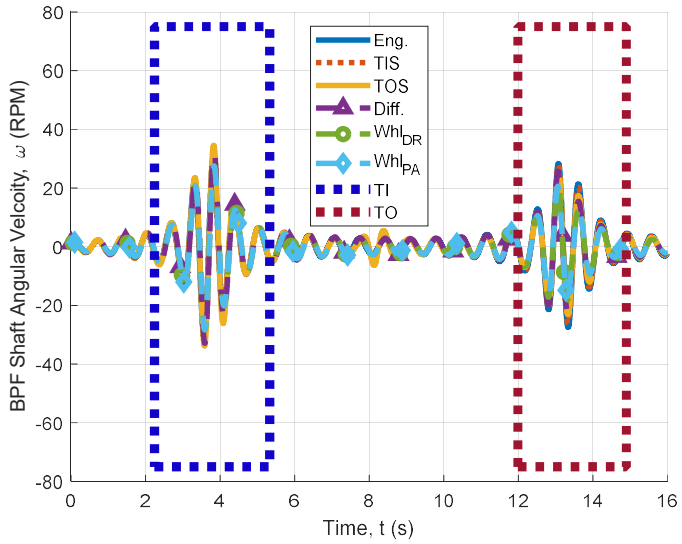

Figure 123: BPF Shaft Speeds During Dyno Thr/r Testing in 3rd Gear

The data in Figure 124 depicts from top subplot to bottom; the TIS speed in dashed red, the bridge measured propeller shaft torque in solid green, the longitudinal differential in solid red, the differential microphone in dashed blue, the longitudinal transmission acceleration in solid blue and the longitudinal seat track acceleration in solid purple. The behavior with a locked torque converter is similar in the propeller shaft torque where during the flare in shaft speeds, the torque amplitude plateaus at a higher amplitude than the settling torque before oscillating with the dyno control mode. The longitudinal acceleration in the differential and seat track exhibit impulsive events at both the TI ad TO locations in the example data while the differential microphone once again does not. The longitudinal transmission accelerometer does not show any impulsive events for the TI and TO in locked or unlocked states and differs in this nature from the road test data. The data traces can further be processed like the road data for shuffle frequency, lash size, and other metrics for ramp rate, slip factor, and peak-peak response for all runs combined on the dyno test vehicle.

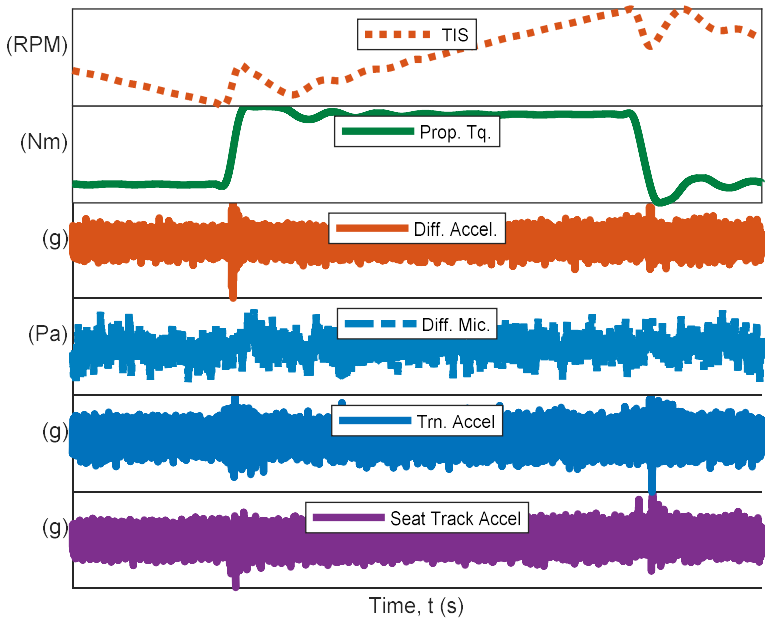

Figure 124: Summary of Dyno Thr/r Testing in 3rd Gear with TC Clutch Locked from Top to Bottom; TIS Speed (RPM), Propeller Shaft Torque (Nm), D1 +X (g), M2 (Pa), Tr1 +X (g), and ST +X (g).

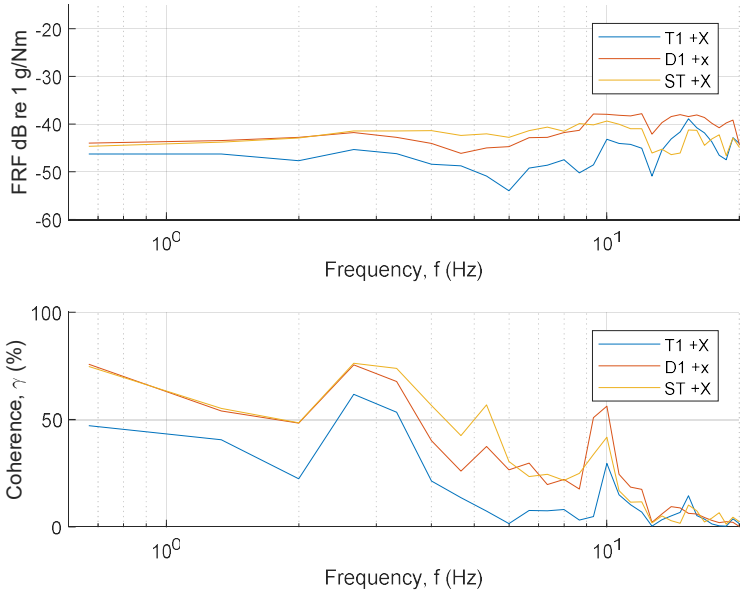

Figure 125: Longitudinal Accelerometer Response for T1, D1, ST vs. Propeller Shaft Torque FRF and Coherence in 3rd Gear for Road Data Normal Mode 2WD

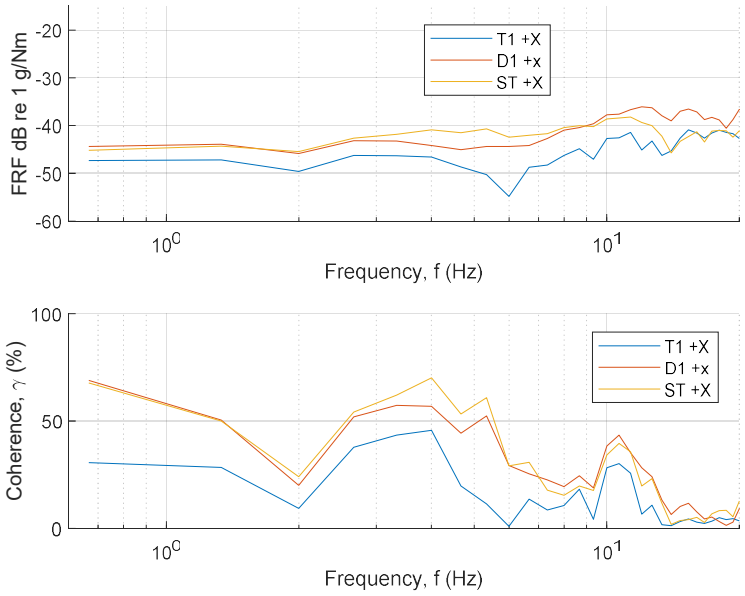

Figure 126: Longitudinal Accelerometer Response for T1, D1, ST vs. Propeller Shaft Torque FRF and Coherence in 4th Gear for Road Data Normal Mode 2WD

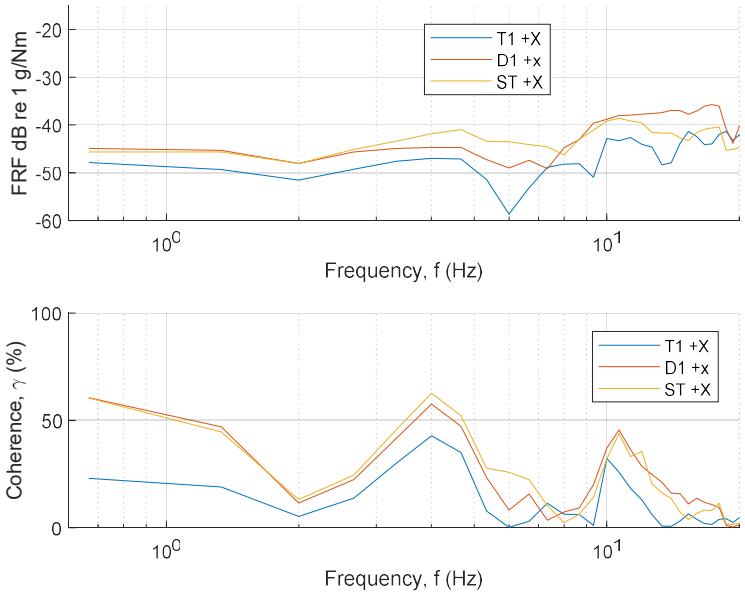

Figure 127: Longitudinal Accelerometer Response for T1, D1, ST vs. Propeller Shaft Torque FRF and Coherence in 5th Gear for Road Data Normal Mode 2WD

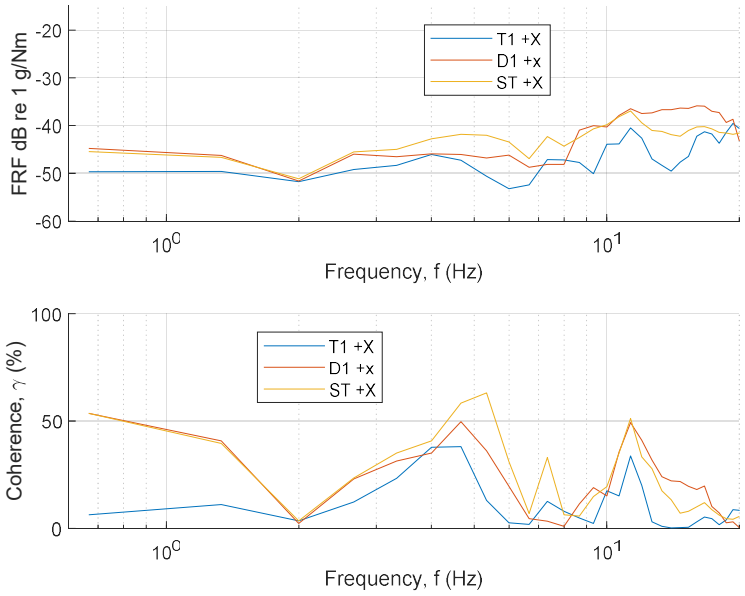

Figure 128: Longitudinal Accelerometer Response for T1, D1, ST vs. Propeller Shaft Torque FRF and Coherence in 6th Gear for Road Data Normal Mode 2WD

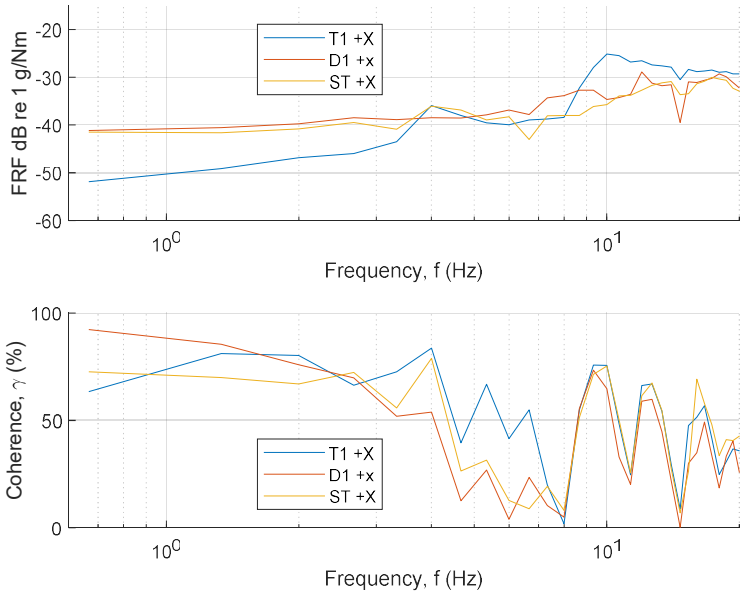

Figure 129: Longitudinal Accelerometer Response for T1, D1, ST vs. Propeller Shaft Torque FRF and Coherence in 3rd Gear for Unlocked TC Clutch Data from Dyno Thr/r Testing

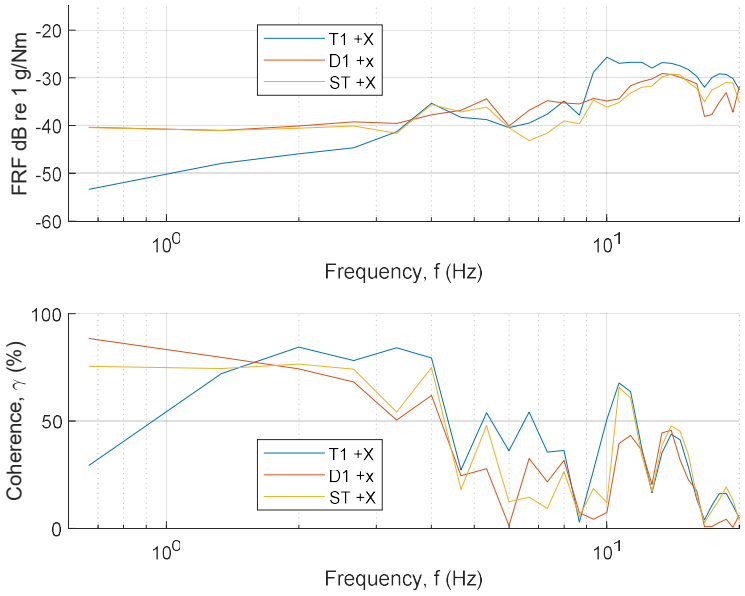

Figure 130: Longitudinal Accelerometer Response for T1, D1, ST vs. Propeller Shaft Torque FRF and Coherence in 4th Gear for Unlocked TC Clutch Data from Dyno Thr/r Testing

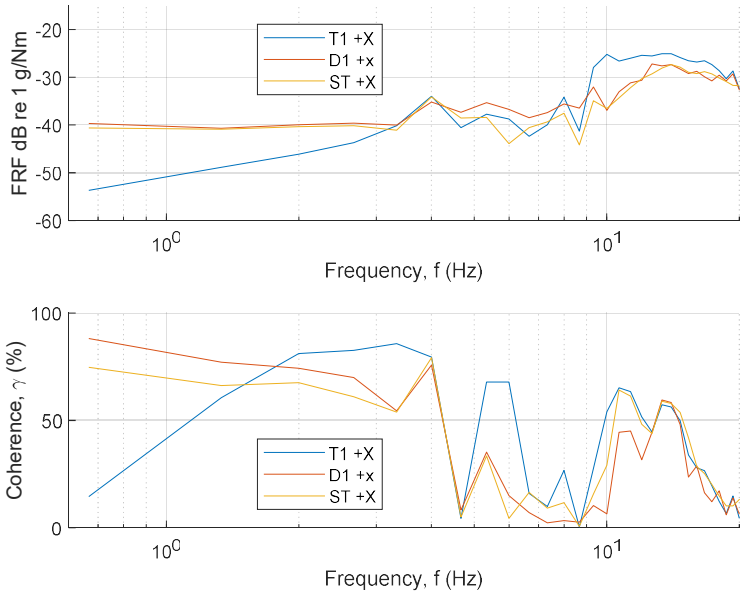

Figure 131: Longitudinal Accelerometer Response for T1, D1, ST vs. Propeller Shaft Torque FRF and Coherence in 5th Gear for Unlocked TC Clutch Data from Dyno Thr/r Testing

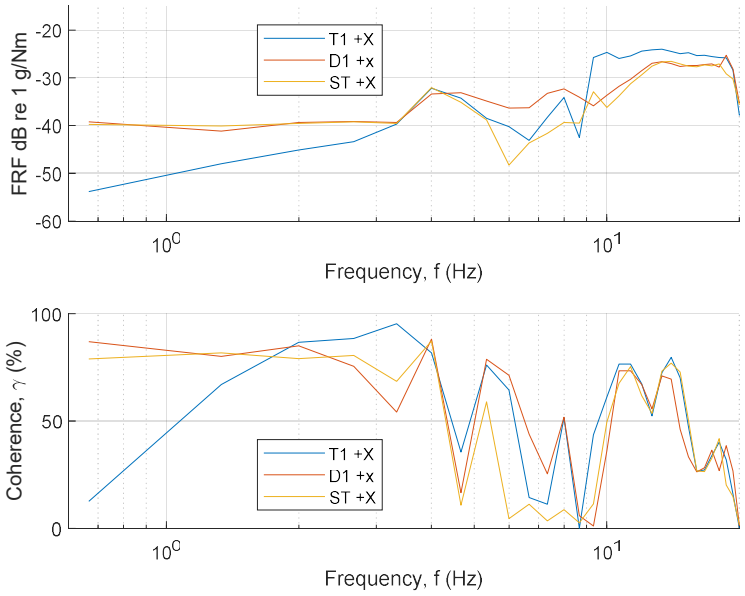

Figure 132: Longitudinal Accelerometer Response for T1, D1, ST vs. Propeller Shaft Torque FRF and Coherence in 6th Gear for Unlocked TC Clutch Data from Dyno Thr/r Testing

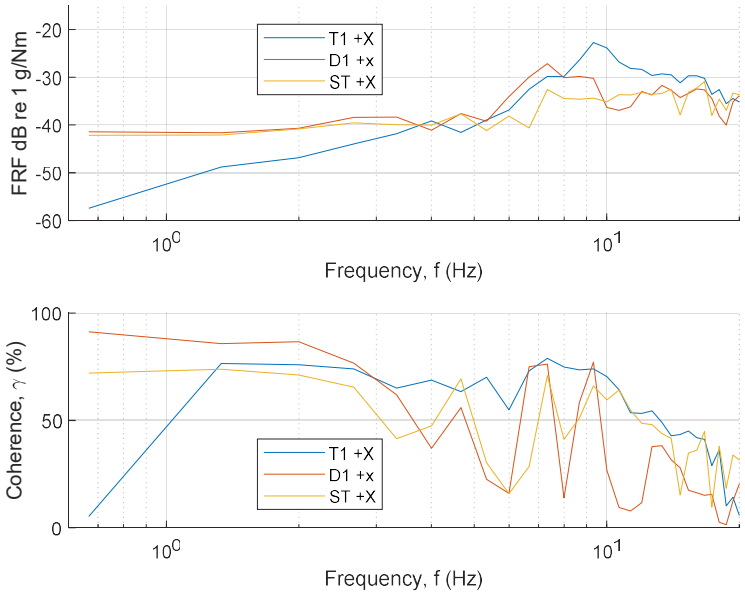

Figure 133: Longitudinal Accelerometer Response for T1, D1, ST vs. Propeller Shaft Torque FRF and Coherence in 3rd Gear for Locked TC Clutch Data from Dyno Thr/r Testing

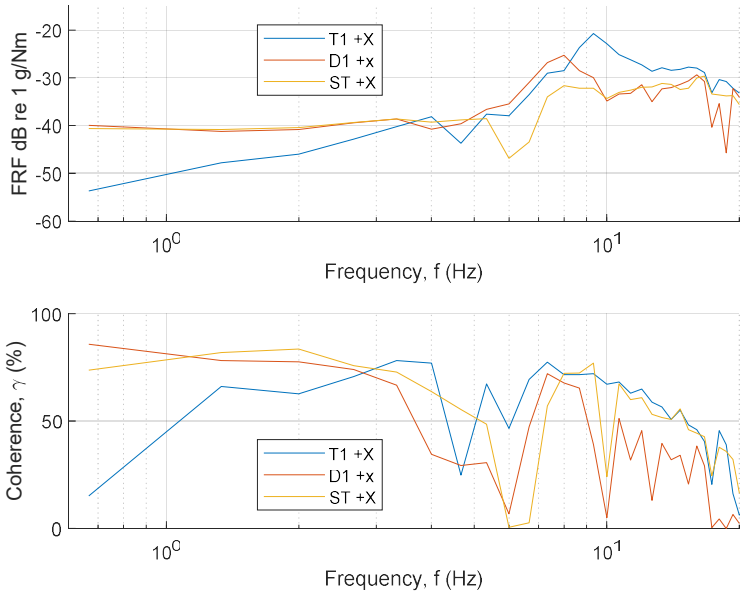

Figure 134: Longitudinal Accelerometer Response for T1, D1, ST vs. Propeller Shaft Torque FRF and Coherence in 4th Gear for Locked TC Clutch Data from Dyno Thr/r Testing

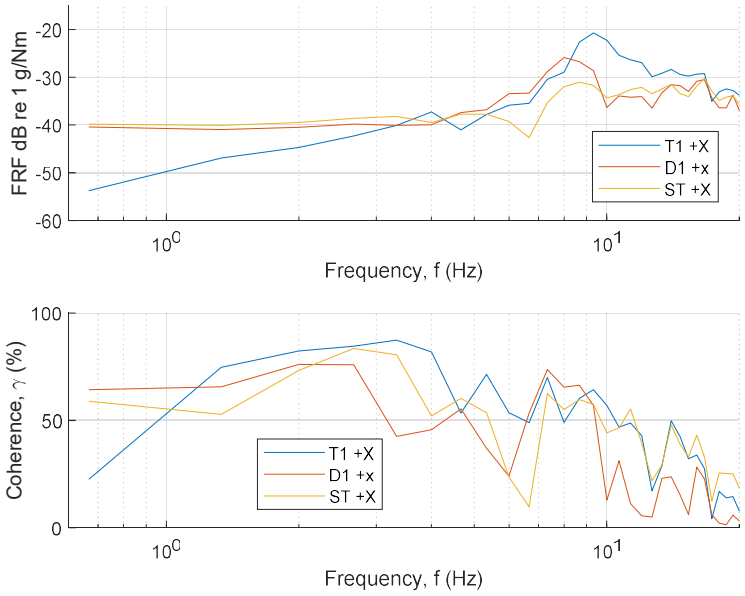

Figure 135: Longitudinal Accelerometer Response for T1, D1, ST vs. Propeller Shaft Torque FRF and Coherence in 5th Gear for Locked TC Clutch Data from Dyno Thr/r Testing

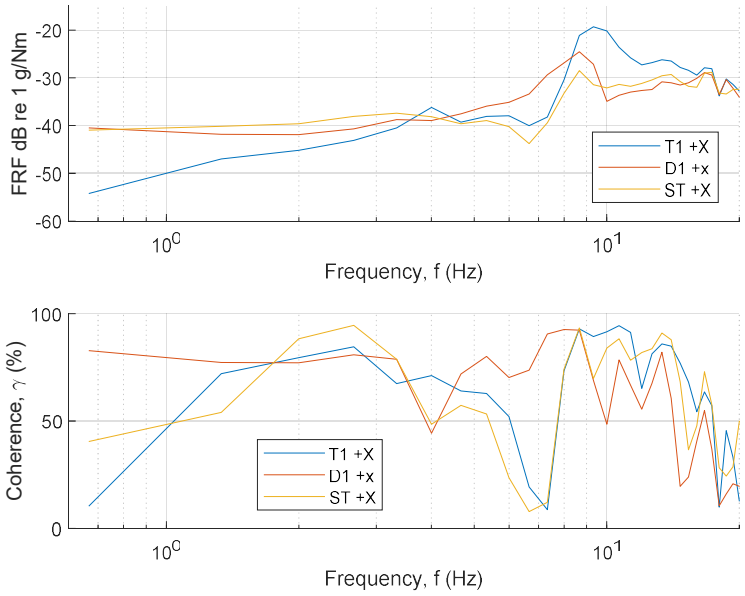

Figure 136: Longitudinal Accelerometer Response for T1, D1, ST vs. Propeller Shaft Torque FRF and Coherence in 6th Gear for Locked TC Clutch Data from Dyno Thr/r Testing

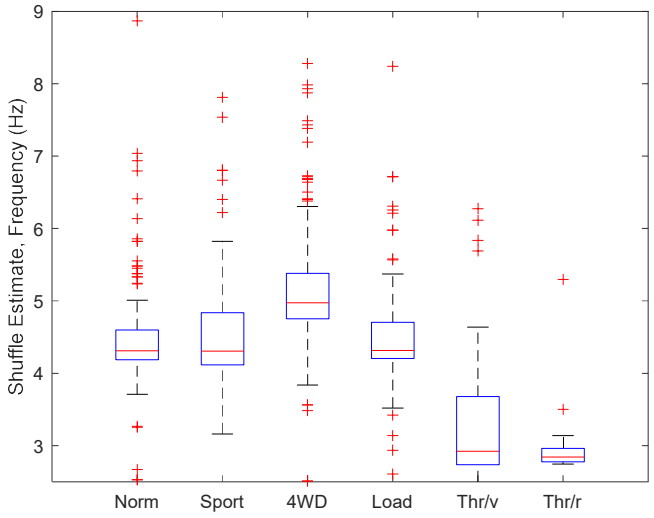

Figure 137: Fourth Gear TI Shuffle Frequency Estimates for Road (Normal Mode 2WD [Norm], Sport Mode 4WD [Sport], Sport Mode 4WD [4WD], Loaded Sport Mode 2WD [Load]) and Dyno Data (Thr/v and Thr/r) Extracted from TOSS Signal Data

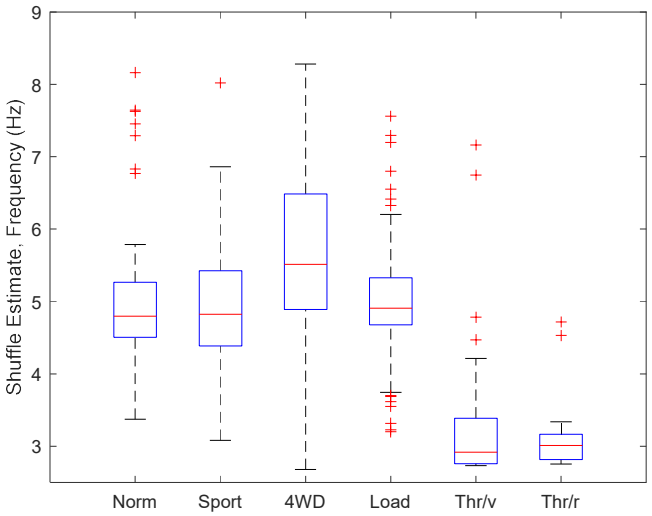

Figure 138: Fifth Gear TI Shuffle Frequency Estimates for Road (Normal Mode 2WD [Norm], Sport Mode 4WD [Sport], Sport Mode 4WD [4WD], Loaded Sport Mode 2WD [Load]) and Dyno Data (Thr/v and Thr/r) Extracted from TOSS Signal Data

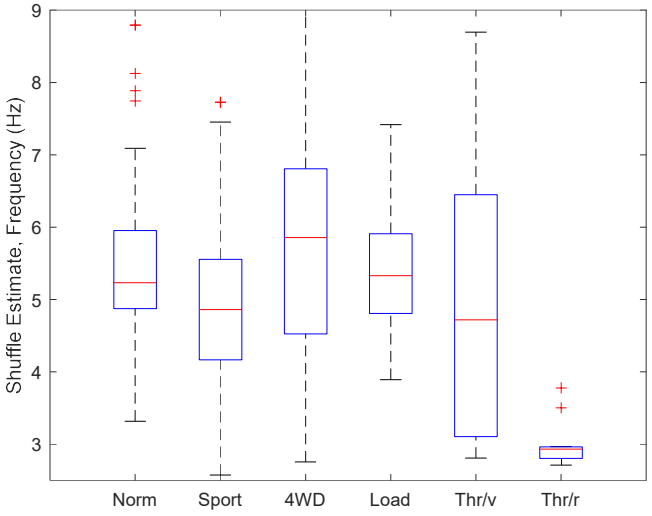

Figure 139: Sixth Gear TI Shuffle Frequency Estimates for Road (Normal Mode 2WD [Norm], Sport Mode 4WD [Sport], Sport Mode 4WD [4WD], Loaded Sport Mode 2WD [Load]) and Dyno Data (Thr/v and Thr/r) Extracted from TOSS Signal Data

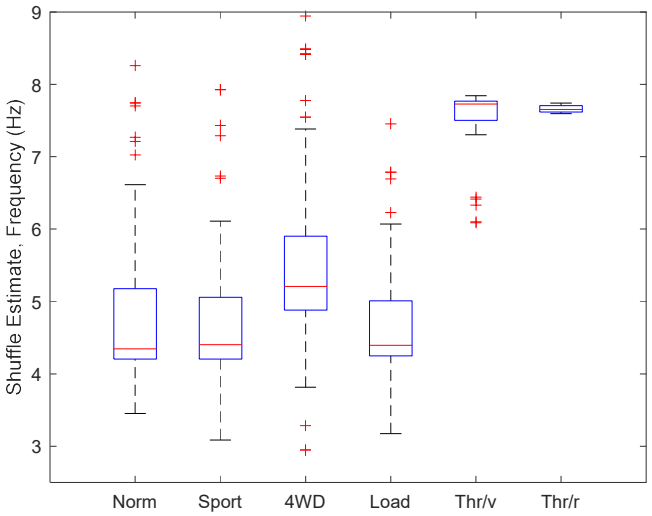

Figure 140: Fourth Gear TI Shuffle Frequency Estimates for Road (Normal Mode 2WD [Norm], Sport Mode 4WD [Sport], Sport Mode 4WD [4WD], Loaded Sport Mode 2WD [Load]) and Dyno Data (Thr/v and Thr/r) Extracted from Torque Signal Data

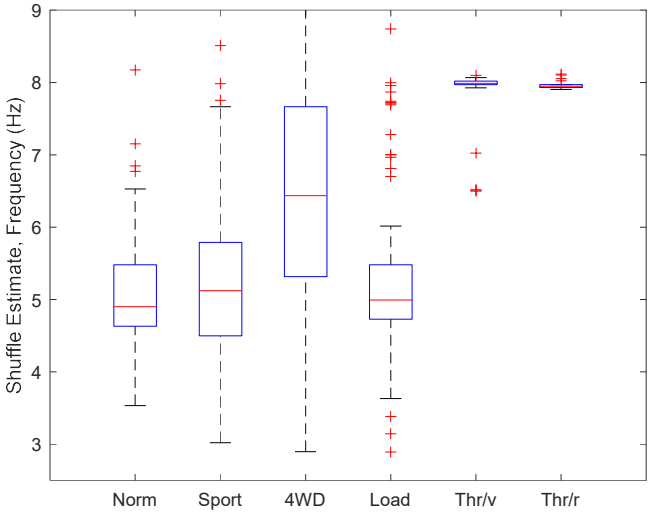

Figure 141: Fifth Gear TI Shuffle Frequency Estimates for Road (Normal Mode 2WD [Norm], Sport Mode 4WD [Sport], Sport Mode 4WD [4WD], Loaded Sport Mode 2WD [Load]) and Dyno Data (Thr/v and Thr/r) Extracted from Torque Signal Data

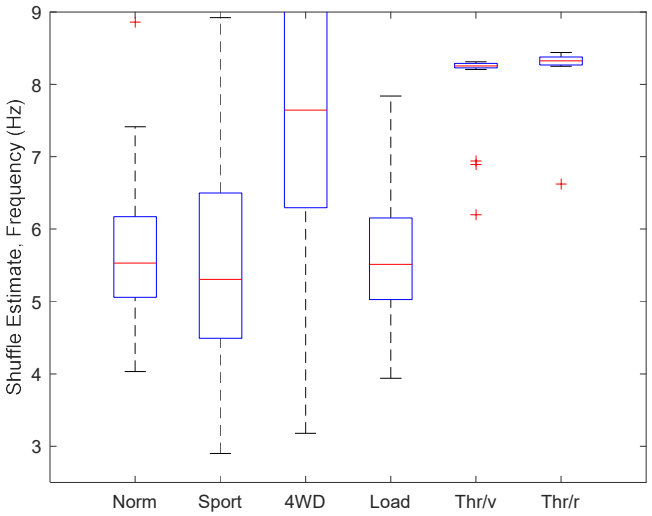

Figure 142: Sixth Gear TI Shuffle Frequency Estimates for Road (Normal Mode 2WD [Norm], Sport Mode 4WD [Sport], Sport Mode 4WD [4WD], Loaded Sport Mode 2WD [Load]) and Dyno Data (Thr/v and Thr/r) Extracted from Torque Signal Data

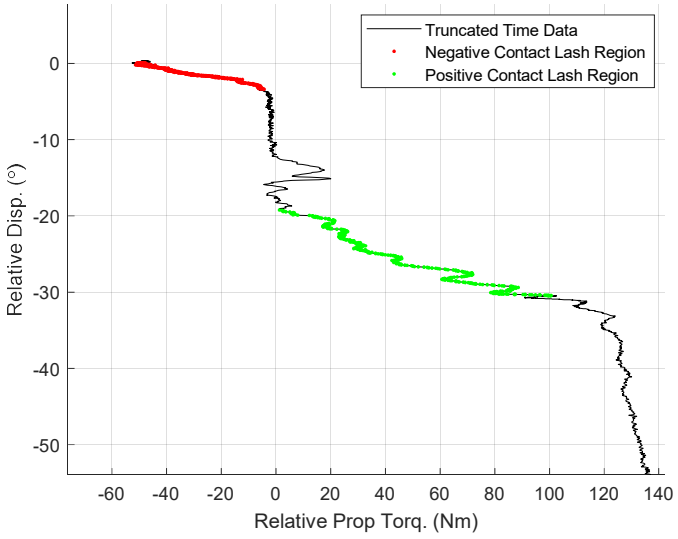

Figure 143: Sport 2WD Lash Estimation Data with Highlighted Negative Contact Lash Region in Red and Positive Contact Lash Region in Green

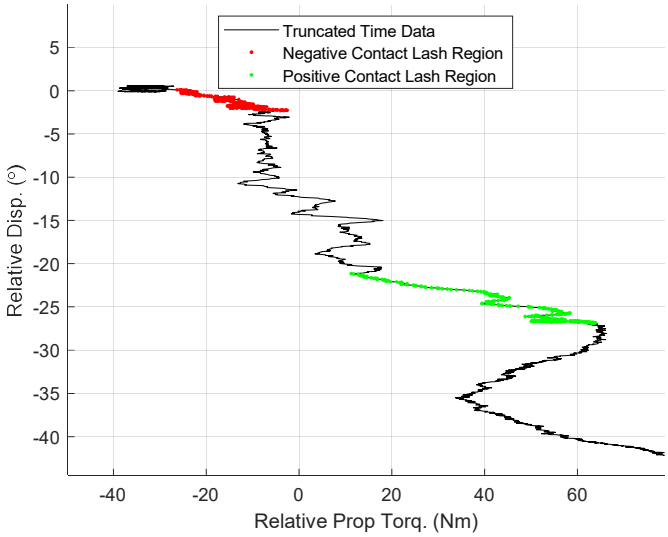

Figure 144: Sport 4WD Lash Estimation Data with Highlighted Negative Contact Lash Region in Red and Positive Contact Lash Region in Green

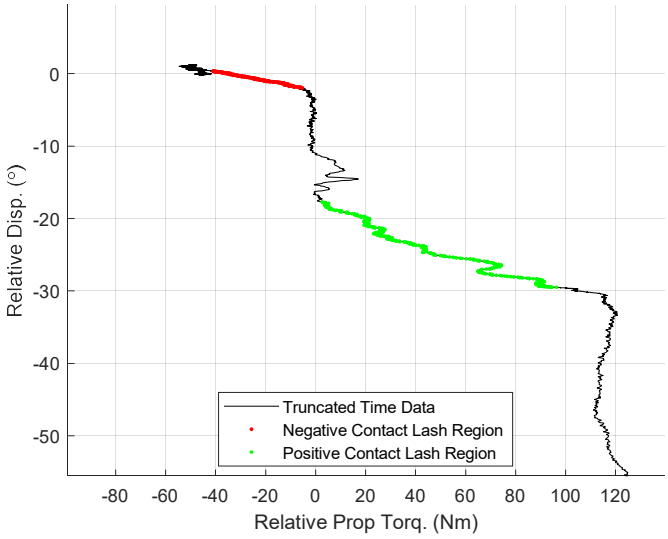

Figure 145: Loaded Sport 2WD Lash Estimation Data with Highlighted Negative Contact Lash Region in Red and Positive Contact Lash Region in Green

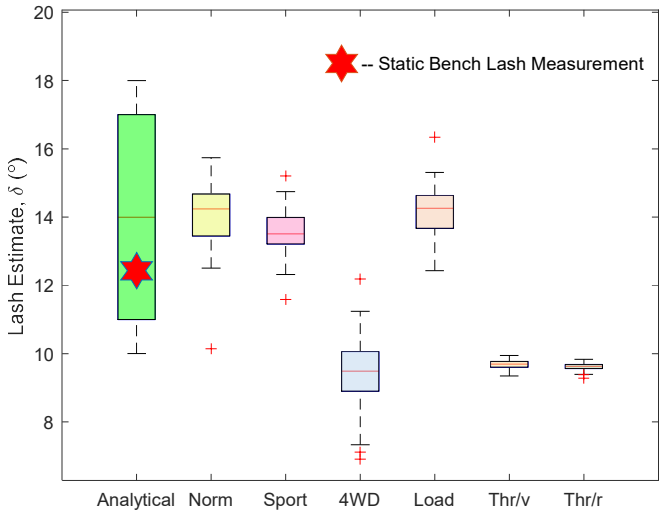

Figure 146: Lash Estimation Comparison in 4th Gear for Road (Normal Mode 2WD [Norm], Sport Mode 4WD [Sport], Sport Mode 4WD [4WD], Loaded Sport Mode 2WD [Load]) and Dyno Data (Thr/v and Thr/r) Extracted from Torque and Relative Displacement Signal Data

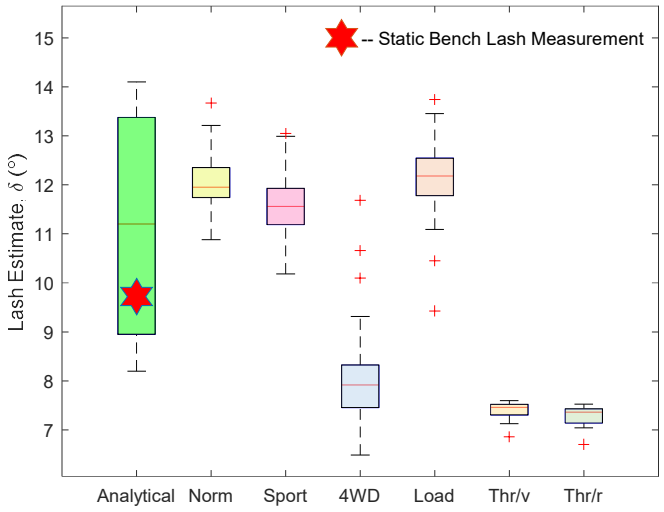

Figure 147: Lash Estimation Comparison in 5th Gear for Road (Normal Mode 2WD [Norm], Sport Mode 4WD [Sport], Sport Mode 4WD [4WD], Loaded Sport Mode 2WD [Load]) and Dyno Data (Thr/v and Thr/r) Extracted from Torque and Relative Displacement Signal Data

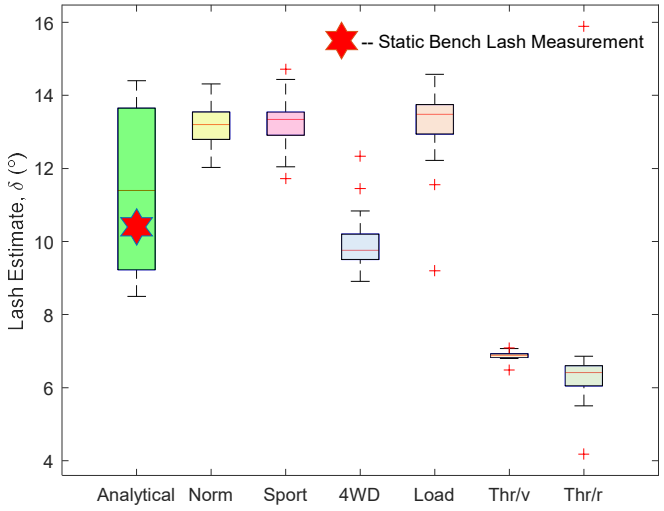

Figure 148: Lash Estimation Comparison in 6th Gear for Road (Normal Mode 2WD [Norm], Sport Mode 4WD [Sport], Sport Mode 4WD [4WD], Loaded Sport Mode 2WD [Load]) and Dyno Data (Thr/v and Thr/r) Extracted from Torque and Relative Displacement Signal Data

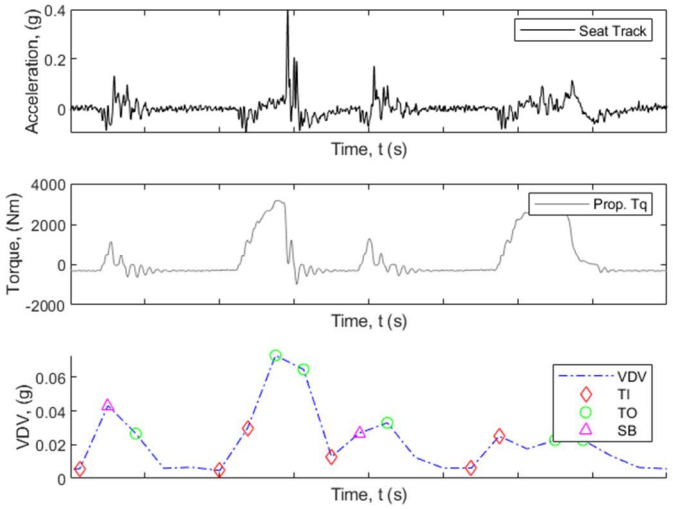

Figure 149: Fourth Gear Processed Data in Normal 2WD for Seat Track +X Acceleration vs. Time in Subplot 1, Propeller Shaft Torque Projected on the Transmission Input Plane in Subplot 2, and the Corresponding Shifted VDV Calculation vs. Time in Subplot 3 With Indicators for TI, TO, and SB.

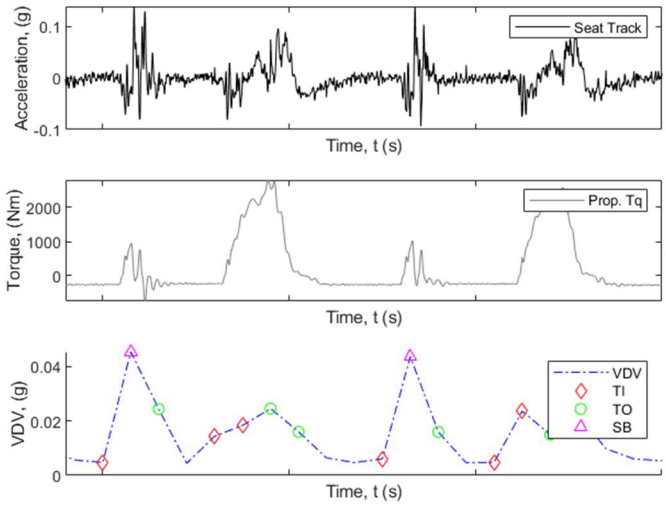

Figure 150: Fifth Gear Processed Data in Normal 2WD for Seat Track +X Acceleration vs. Time in Subplot 1, Propeller Shaft Torque Projected on the Transmission Input Plane in Subplot 2, and the Corresponding Shifted VDV Calculation vs. Time in Subplot 3 With Indicators for TI, TO, and SB.

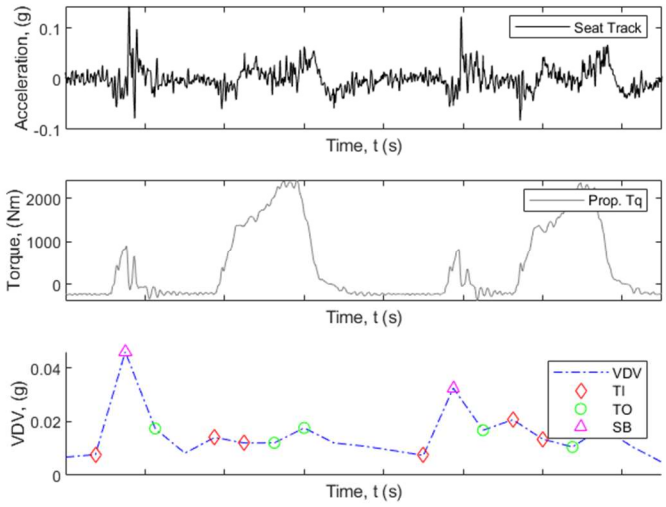

Figure 151: Sixth Gear Processed Data in Normal 2WD for Seat Track +X Acceleration vs. Time in Subplot 1, Propeller Shaft Torque Projected on the Transmission Input Plane in Subplot 2, and the Corresponding Shifted VDV Calculation vs. Time in Subplot 3 With Indicators for TI, TO, and SB.

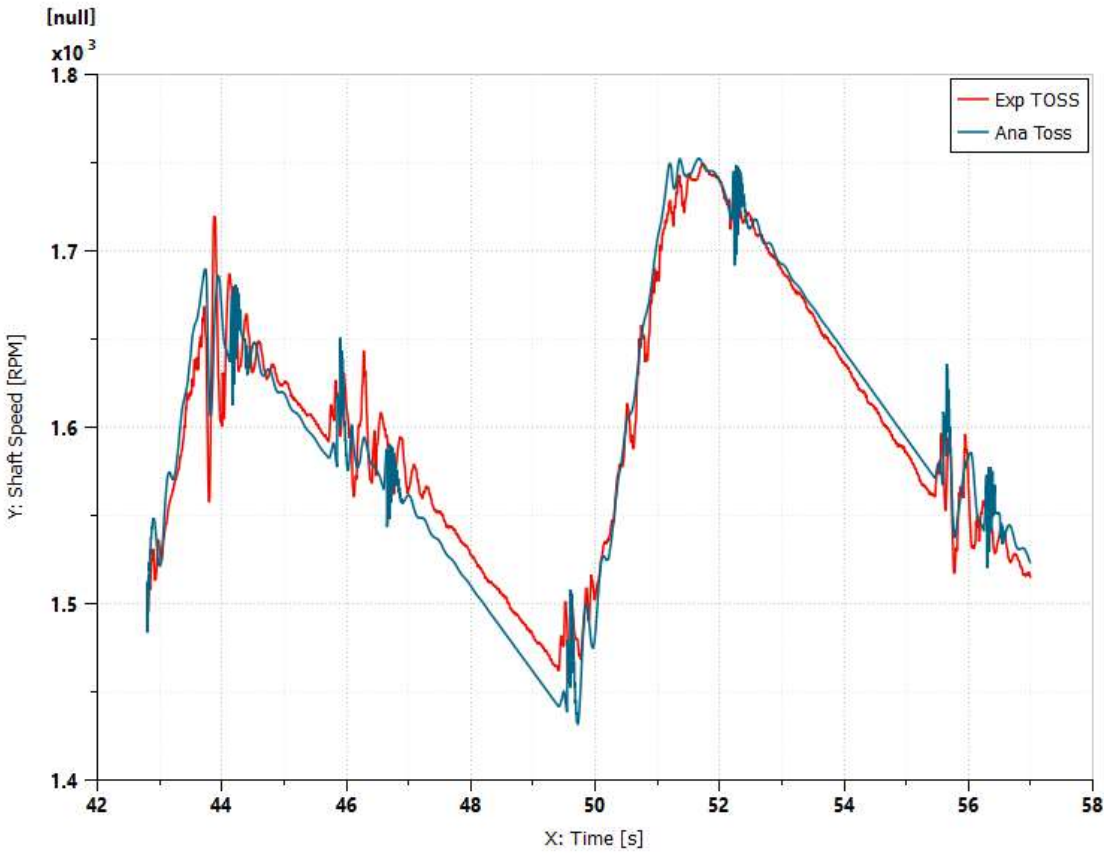

Figure 152: Experimental (Solid Red) vs. Analytical (Solid Blue) TOS Signal Results from TITO Testing in 4th Gear

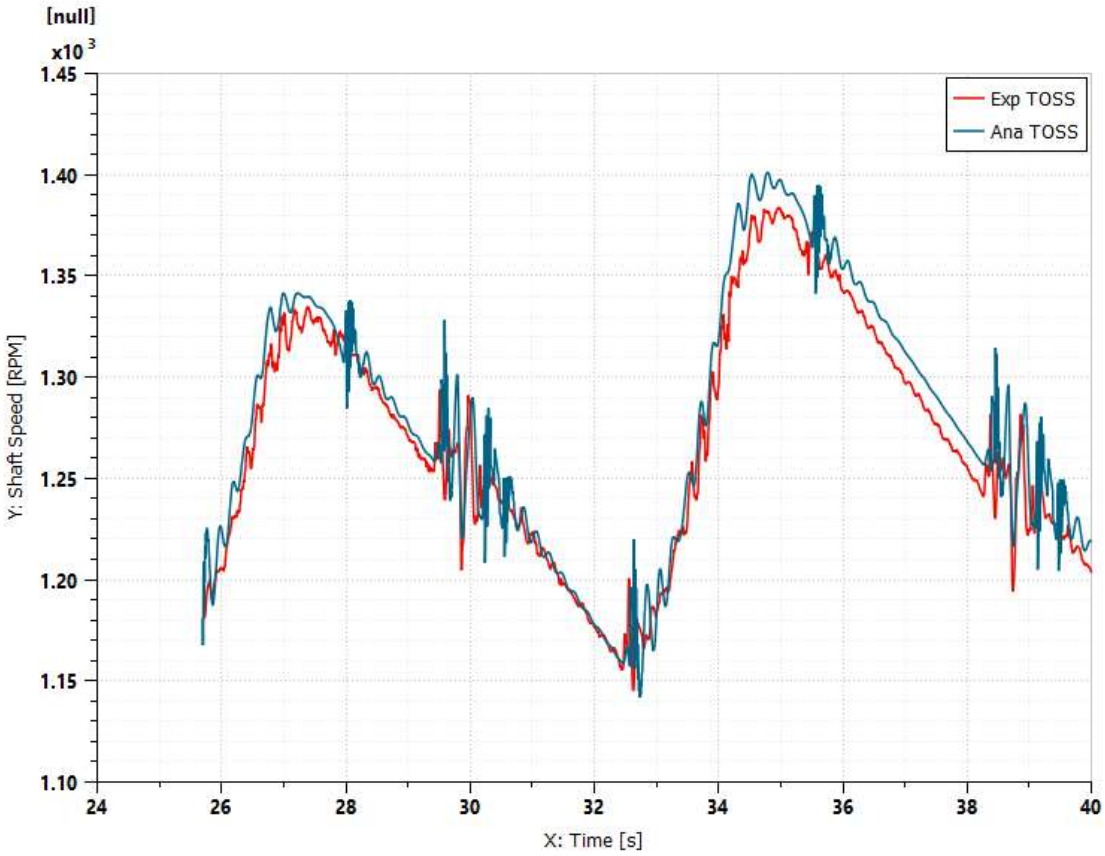

Figure 153: Experimental (Solid Red) vs. Analytical (Solid Blue) TOS Signal Results from TITO Testing in 5th Gear

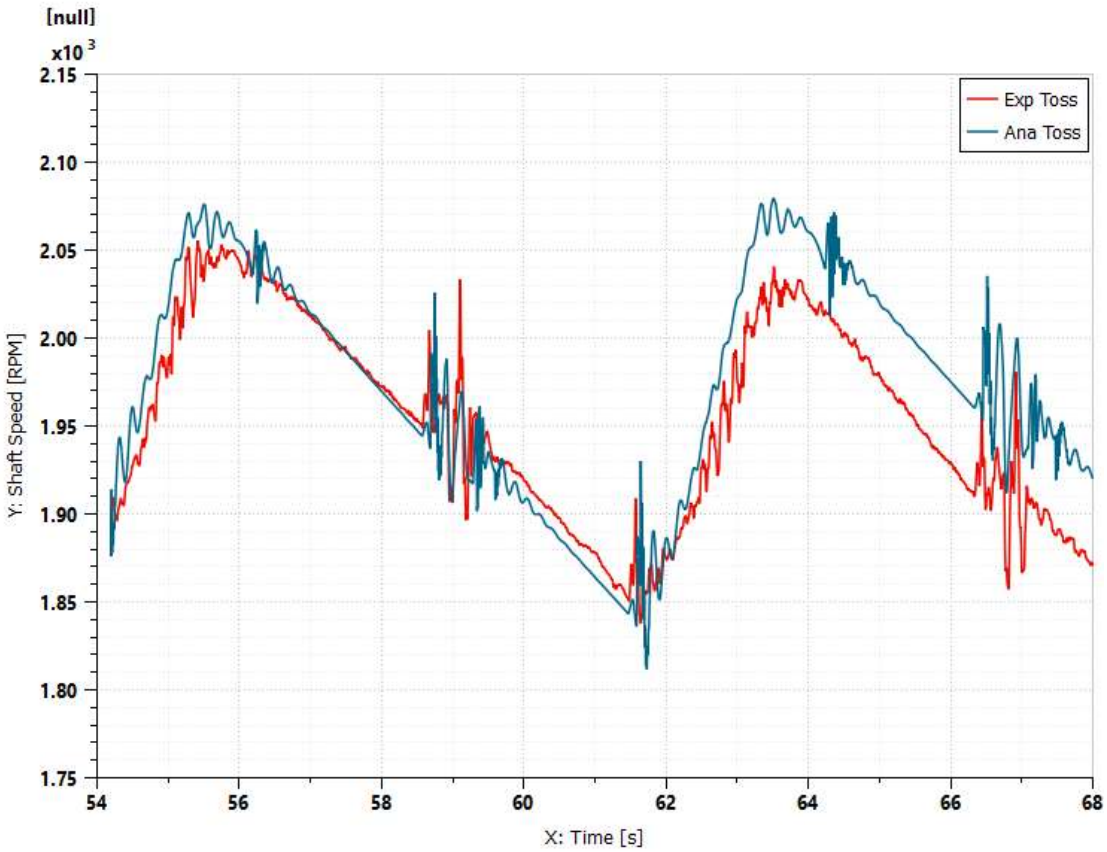

Figure 154: Experimental (Solid Red) vs. Analytical (Solid Blue) TOS Signal Results from TITO Testing in 6th Gear

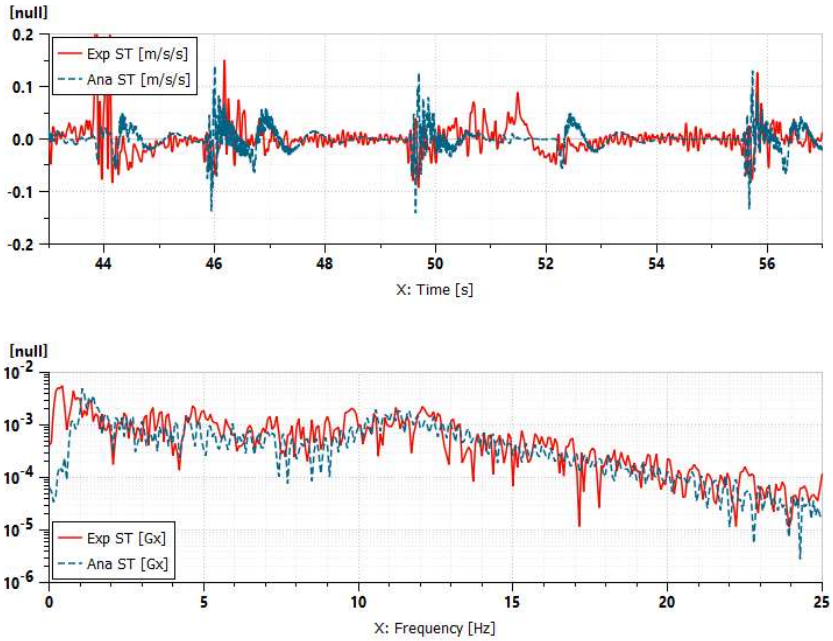

Figure 155: Fourth Gear ST +X from Experimental Data (Solid Red) and Analytical Estimate (Dashed Blue) for Digital Twin Estimate in Top Subplot and Linear Spectra in Bottom Subplot

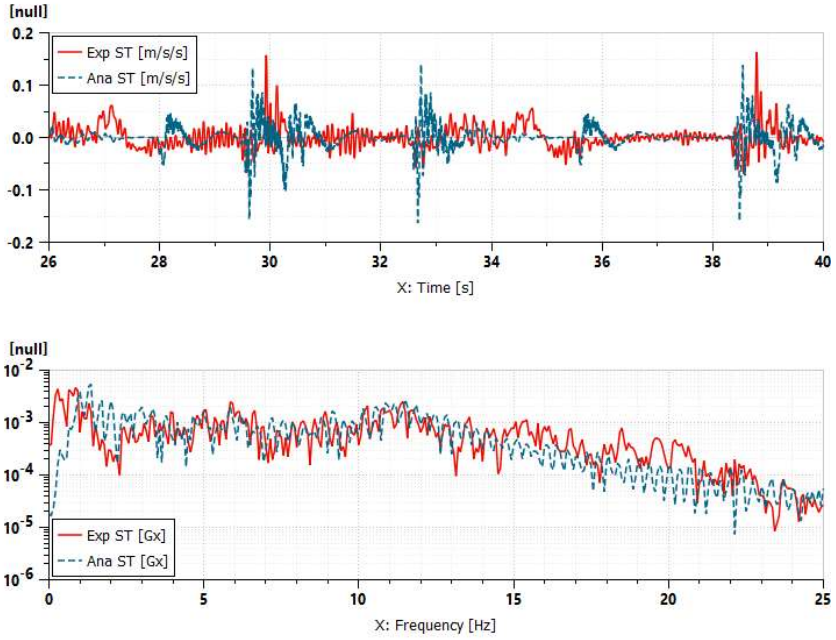

Figure 156: Fifth Gear ST +X from Experimental Data (Solid Red) and Analytical Estimate (Dashed Blue) for Digital Twin Estimate in Top Subplot and Linear Spectra in Bottom Subplot

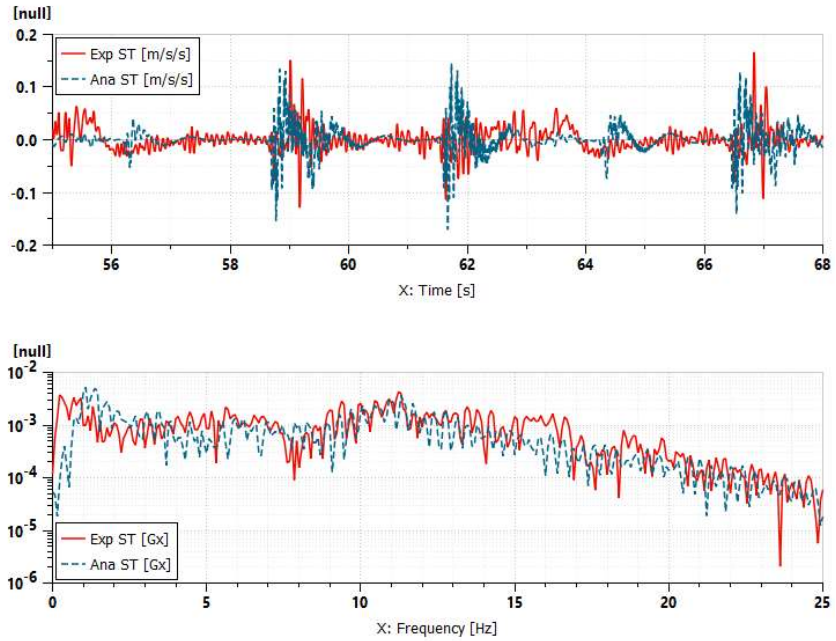

Figure 157: Sixth Gear ST +X from Experimental Data (Solid Red) and Analytical Estimate (Dashed Blue) for Digital Twin Estimate in Top Subplot and Linear Spectra in Bottom Subplot

9. Appendix D: Additional Shuffle Frequency Processed Data

The Shuffle Frequency Data was extracted as indicated in Chapter 3 Section 2. Additional signals were used to extract the shuffle frequency and are depicted here for comparison and completeness. The data includes the mean estimated frequency along with the standard deviation. The data included in the body of the dissertation included the most well behaved in terms of lower standard deviation in post processing.

Table 14: Tip In Data Results for Shuffle Frequency and (Standard Deviation) Gear and Center Target Speed Extracted from the Engine Speed Signal

Normal 2WD Eng. *'Hz (Std. Dev.)'*		Transmission Forward Gear Number			
		3	4	5	6
Target Center Velocity (kph)	56	'3.5 (1.4)'	'4.0 (0.4)'	'4.4 (0.6)'	[]
	73	'3.6 (0.1)'	'3.9 (0.8)'	'4.2 (1.1)'	'4.9 (0.9)'
	88	[]	'4.5 (0.2)'	'4.4 (0.9)'	'4.3 (1.1)'

Loaded 2WD Eng. *'Hz (Std. Dev.)'*		Transmission Forward Gear Number			
		3	4	5	6
Target Center Velocity (kph)	56	'2.8 (0.6)'	'3.9 (0.6)'	'3.9 (0.7)'	[]
	73	'3.5 (0.2)'	'3.8 (0.6)'	'4.2 (0.6)'	'3.9 (0.7)'
	88	[]	'4.7 (0.5)'	'4.8 (0.6)'	'4.0 (0.7)'

Sport 4WD Eng. *'Hz (Std. Dev.)'*		Transmission Forward Gear Number			
		3	4	5	6
Target Center Velocity (kph)	56	'4.2 (0.7)'	'3.9 (1.0)'	'4.2 (1.0)'	[]
	73	'4.4 (0.4)'	'4.9 (0.7)'	'4.8 (0.6)'	'4.3 (0.7)'
	88	[]	'5.0 (0.2)'	'5.4 (0.6)'	'4.8 (0.5)'

Loaded 2WD Eng. *'Hz (Std. Dev.)'*		Transmission Forward Gear Number			
		3	4	5	6
Target Center Velocity (kph)	56	'3.3 (0.6)'	'3.9 (0.5)'	'4.0 (0.6)'	[]
	73	'3.8 (0.4)'	'4.1 (0.5)'	'4.0 (0.8)'	'4.4 (0.8)'
	88	[]	'4.5 (0.5)'	'4.5 (0.5)'	'5.0 (0.4)'

Table 15: Tip In Data Results for Shuffle Frequency and (Standard Deviation) focused on Center Target Speed when processing different measurement locations and sensor locations

9

Normal 2WD *'Hz (Std. Dev.)'*		Sensor			
		Eng.	TIS	TOS	Diff
Target Center Velocity (kph)	56	'3.9 (1.0)'	'5.3 (1.3)'	'5.4 (1.1)'	'5.3 (1.2)'
	73	'4.3 (0.9)'	'5.1 (1.2)'	'5.7 (1.1)'	'5.3 (1.2)'
	88	'4.5 (0.9)'	'5.1 (1.1)'	'5.1 (1.1)'	'5.1 (1.1)'

Sport 2WD *'Hz (Std. Dev.)'*		Sensor			
		Eng.	TIS	TOS	Diff
Target Center Velocity (kph)	56	'3.5 (0.8)'	'4.4 (0.8)'	'4.5 (0.9)'	'4.3 (0.8)'
	73	'3.8 (0.6)'	'4.7 (0.9)'	'4.8 (0.8)'	'4.7 (0.8)'
	88	'4.7 (0.7)'	'5.1 (0.6)'	'5.3 (0.8)'	'5.1 (0.7)'

Sport 4WD *'Hz (Std. Dev.)'*		Sensor			
		Eng.	TIS	TOS	Diff
Target Center Velocity (kph)	56	'4.2 (0.9)'	4.9 (1.0)'	'5.6 (1.0)'	'4.9 (1.1)'
	73	'4.5 (0.6)'	'5.1 (0.9)'	'5.9 (1.1)'	'5.4 (1.0)'
	88	'5.0 (0.5)'	'5.2 (0.7)'	'5.5 (1.0)'	'5.4 (0.8)'

Loaded 2WD *'Hz (Std. Dev.)'*		Sensor			
		Eng.	TIS	TOS	Diff
Target Center Velocity (kph)	56	'3.9 (0.7)'	'4.5 (0.9)'	'4.6 (1.1)'	'4.4 (1.0)'
	73	'4.1 (0.7)'	'4.4 (0.8)'	'4.6 (0.8)'	'4.5 (0.7)'
	88	'4.5 (0.5)'	'5.0 (0.8)'	'4.9 (0.5)'	'5.0 (0.7)'

Table 16: Tip In Data Results for Shuffle Frequency and (Standard Deviation) focused on Forward Transmission Gear when processing different measurement locations and sensor locations

Normal 2WD 'Hz (Std. Dev.)'		Sensor			
		Eng.	TIS	TOS	Diff
Forward Gear Number	3	'3.5 (1.1)'	'4.5 (1.5)'	'5.0 (1.1)'	'4.7 (1.2)'
	4	'4.1 (0.6)'	'5.2 (1.2)'	'5.3 (1.2)'	'5.1 (1.2)'
	5	'4.3 (0.9)'	'5.4 (1.0)'	'5.6 (1.0)'	'5.4 (1.0)'
	6	'4.6 (1.0)'	'6.0 (1.0)'	'6.2 (1.0)'	'6.1 (1.0)'

Sport 2WD 'Hz (Std. Dev.)'		Sensor			
		Eng.	TIS	TOS	Diff
Forward Gear Number	3	'3.2 (0.6)'	'3.9 (1.0)'	'4.3 (0.8)'	'4.3 (0.8)'
	4	'4.1 (0.7)'	'4.7 (0.6)'	'4.8 (0.7)'	'4.8 (0.7)'
	5	'4.3 (0.8)'	'5.1 (0.7)'	'5.3 (0.8)'	'5.3 (0.8)'
	6	'4.0 (0.7)'	'5.0 (0.7)'	'5.6 (0.9)'	'5.6 (0.9)'

'4.7 (0.7)'

Sport 4WD 'Hz (Std. Dev.)'		Sensor			
		Eng.	TIS	TOS	Diff
Forward Gear Number	3	'4.3 (0.6)'	'4.5 (0.7)'	'5.3 (0.9)'	'4.7 (1.1)'
	4	'4.7 (0.8)'	'5.1 (0.7)'	'5.6 (0.9)'	'5.2 (0.9)'
	5	'4.8 (0.9)'	'5.5 (0.8)'	'5.8 (0.9)'	'5.5 (0.8)'
	6	'4.5 (0.7)'	'5.7 (1.0)'	'6.6 (1.2)'	'6.1 (0.8)'

Loaded 2WD 'Hz (Std. Dev.)'		Sensor			
		Eng.	TIS	TOS	Diff
Forward Gear Number	3	'3.6 (0.5)'	'4.0 (0.9)'	'4.1 (0.7)'	'3.9 (0.6)'
	4	'4.2 (0.6)'	'4.6 (0.8)'	'4.7 (0.6)'	'4.7 (0.7)'
	5	'4.2 (0.7)'	'5.1 (0.6)'	'5.1 (0.7)'	'5.1 (0.7)'
	6	'4.6 (0.8)'	'5.2 (0.8)'	'5.3 (0.9)'	'5.3 (0.9)'

Table 17: Tip Out Data Results for Shuffle Frequency and (Standard Deviation) Gear and Center Target Speed Extracted from the Engine Speed Signal

Normal 2WD Eng. 'Hz (Std. Dev.)'		Transmission Forward Gear Number			
		3	4	5	6
Target Center Velocity (kph)	56	'3.7 (0.5)'	'4.5 (0.6)'	'4.9 (0.8)'	[]
	73	'3.5 (0.7)'	'4.2 (0.6)'	'4.7 (0.3)'	'5.3 (0.9)'
	88	[]	'4.5 (0.5)'	'4.7 (0.6)'	'4.8 (0.9)'

Sport 2WD Eng. 'Hz (Std. Dev.)'		Transmission Forward Gear Number			
		3	4	5	6
Target Center Velocity (kph)	56	'3.5 (0.7)'	'4.3 (0.3)'	'4.8 (0.5)'	[]
	73	'3.7 (0.3)'	'4.5 (0.7)'	'4.7 (0.7)'	'5.0 (1.1)'
	88	[]	'4.6 (0.7)'	'4.9 (0.7)'	'4.6 (1.1)'

Sport 4WD Eng. 'Hz (Std. Dev.)'		Transmission Forward Gear Number			
		3	4	5	6
Target Center Velocity (kph)	56	'3.8 (0.8)'	'4.8 (0.6)'	'5.6 (1.2)'	[]
	73	'4.4 (0.5)'	'4.8 (0.8)'	'5.5 (0.4)'	'5.4 (0.5)'
	88	[]	'5.2 (0.5)'	'5.4 (0.4)'	'5.6 (0.7)'

Loaded 2WD Eng. 'Hz (Std. Dev.)'		Transmission Forward Gear Number			
		3	4	5	6
Target Center Velocity (kph)	56	'3.7 (0.5)'	'4.5 (0.5)'	'4.8 (0.5)'	[]
	73	'4.0 (1.1)'	'4.5 (0.5)'	'5.0 (0.6)'	'5.2 (0.7)'
	88	[]	'4.4 (0.4)'	'5.1 (0.3)'	'5.2 (0.5)'

Table 18: Tip Out Data Results for Shuffle Frequency and (Standard Deviation) focused on Center Target Speed when processing different measurement locations and sensor locations

Normal 2WD 'Hz (Std. Dev.)'		Sensor			
		Eng.	TIS	TOS	Diff
Target Center Velocity (kph)	56	'4.3 (0.8)'	'4.3 (1.0)'	'4.8 (0.8)'	'4.3 (0.9)'
	73	'4.5 (0.9)'	'4.7 (1.0)'	'4.9 (0.9)'	'4.8 (0.9)'
	88	'4.6 (0.6)'	'4.7 (0.7)'	'5.2 (0.7)'	'4.8 (0.9)'

Sport 2WD 'Hz (Std. Dev.)'		Sensor			
		Eng.	TIS	TOS	Diff
Target Center Velocity (kph)	56	'4.2 (0.7)'	'4.4 (0.9)'	'4.8 (0.7)'	'4.6 (0.8)'
	73	'4.3 (0.8)'	'4.3 (0.9)'	'4.7 (1.0)'	'4.6 (1.0)'
	88	'4.6 (0.8)'	'4.7 (0.8)'	'5.3 (1.0)'	'5.1 (0.8)'

Sport 4WD 'Hz (Std. Dev.)'		Sensor			
		Eng.	TIS	TOS	Diff
Target Center Velocity (kph)	56	'4.6 (1.2)'	'4.9 (1.2)'	'5.6 (1.1)'	'5.1 (1.0)'
	73	'5.1 (0.7)'	'5.1 (0.8)'	'5.7 (1.0)'	'5.2 (0.9)'
	88	'5.2 (0.6)'	'5.3 (0.7)'	'5.5 (0.8)'	'5.5 (0.7)'

Loaded 2WD 'Hz (Std. Dev.)'		Sensor			
		Eng.	TIS	TOS	Diff
Target Center Velocity (kph)	56	'4.4 (0.7)'	'4.4 (0.8)'	'4.5 (0.8)'	'4.4 (0.7)'
	73	'4.6 (0.9)'	'4.6 (0.9)'	'4.8 (0.9)'	'4.7 (0.9)'
	88	'4.8 (0.5)'	'4.8 (0.5)'	'5.1 (0.6)'	'4.9 (0.5)'

Table 19: Tip Out Data Results for Shuffle Frequency and (Standard Deviation) focused on Forward Transmission Gear when processing different measurement locations and sensor locations

Normal 2WD *'Hz (Std. Dev.)'*		Sensor			
		Eng.	TIS	TOS	Diff
Forward Gear Number	3	'3.6 (0.6)'	'3.7 (0.6)'	'4.3 (0.7)'	'4.0 (0.6)'
	4	'4.4 (0.6)'	'4.5 (0.5)'	'4.7 (0.6)'	'4.4 (0.5)'
	5	'4.8 (0.6)'	'5.0 (0.9)'	'5.3 (0.7)'	'5.2 (0.8)'
	6	'5.1 (0.9)'	'5.4 (0.5)'	'5.7 (0.7)'	'5.6 (0.7)'

Sport 2WD *'Hz (Std. Dev.)'*		Sensor			
		Eng.	TIS	TOS	Diff
Forward Gear Number	3	'3.6 (0.5)'	'3.7 (0.6)'	'4.2 (0.5)'	'4.1 (0.6)'
	4	'4.5 (0.6)'	'4.5 (0.7)'	'4.9 (0.6)'	'4.6 (0.7)'
	5	'4.8 (0.6)'	'4.9 (0.6)'	'5.3 (0.8)'	'5.0 (0.6)'
	6	'4.8 (1.1)'	'5.1 (1.1)'	'6.1 (1.0)'	'5.8 (1.0)'

Sport 4WD *'Hz (Std. Dev.)'*		Sensor			
		Eng.	TIS	TOS	Diff
Forward Gear Number	3	'4.1 (0.8)'	'4.3 (0.8)'	'5.1 (0.9)'	'4.3 (0.6)'
	4	'4.9 (0.7)'	'5.0 (0.6)'	'5.6 (0.7)'	'5.2 (0.7)'
	5	'5.5 (0.8)'	'5.6 (0.7)'	'6.1 (0.8)'	'5.7 (0.6)'
	6	'5.5 (0.6)'	'5.9 (0.8)'	'6.4 (1.2)'	'6.0 (0.8)'

Loaded 2WD *'Hz (Std. Dev.)'*		Sensor			
		Eng.	TIS	TOS	Diff
Forward Gear Number	3	'3.9 (0.9)'	'3.7 (0.6)'	'4.0 (0.4)'	'3.9 (0.6)'
	4	'4.5 (0.5)'	'4.5 (0.6)'	'4.7 (0.5)'	'4.6 (0.5)'
	5	'5.0 (0.5)'	'5.0 (0.5)'	'5.2 (0.6)'	'5.0 (0.5)'
	6	'5.2 (0.7)'	'5.5 (0.7)'	'5.7 (0.8)'	'5.7 (0.7)'

10. Appendix E: Cradle Assembly Engine Swap Verification

The laboratory test vehicle swapped an eMotor for the ICE originally installed in the production vehicle. An eMotor "cradle" was designed to take place of the ICE while still supporting the transmission and housing the new eMotor and input coupling shaft. FEA was performed to ensure proper function and durability of the cradle based on peak loading of the eMotor. The HVH250 090SWM motor installed in the laboratory test vehicle was capable of a peak torque of 310 Nm at 2400 RPM. A safety factor was applied to the peak torque and distributed on the cradle FEA as shown in Figure 158.

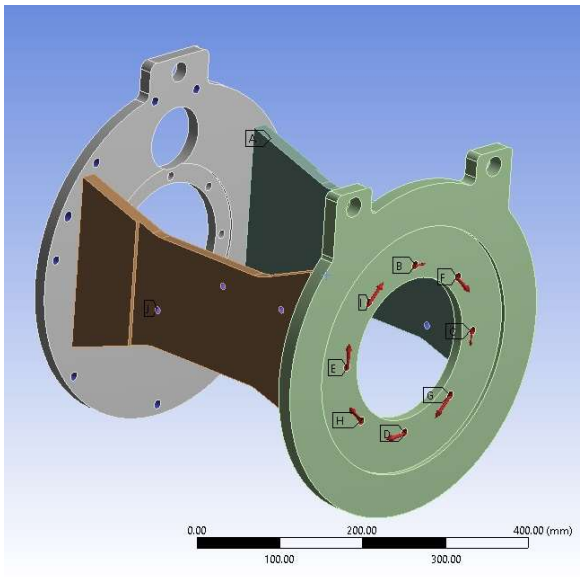

Figure 158: eMotor Cradle FEA Load Distribution

The cradle assembly was fixed at one end where the transmission bellhousing and cradle meet. The distributed torque loading was applied to the other end where the eMotor is installed on each bolt hole. The FEA first checked for von-Misses stress distribution due to the loading to ensure no plastic deformation would occur. It was assumed and verified that no stress exceeds the material Young's modulus thus no plastic deformation during testing is expected according to Figure 159.

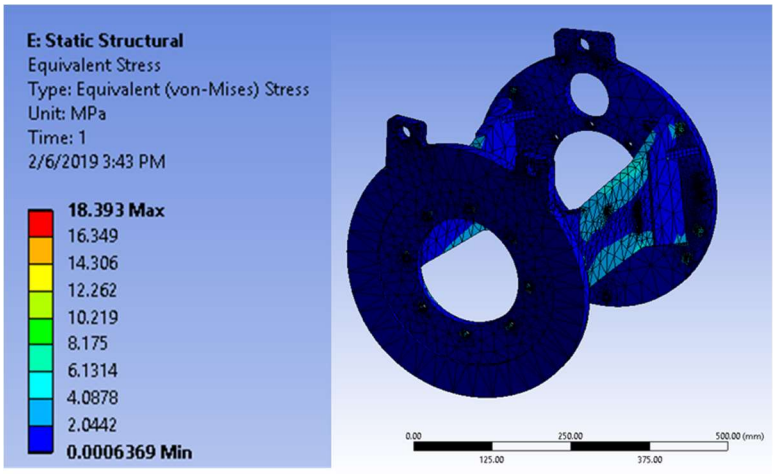

Figure 159: Static Testing for von-Mises Stress Distribution

A dynamic solver was applied to the FEA model to extract the first eight structural modes of the cradle assembly. It was assumed there were unknown cradle mount stiffness and material properties in the design phase. Material properties for both Aluminum and Steel were applied in various loading conditions with elastomer mount rates to estimate the first eight modes. A summary of this analysis is shown in Table 20. The conclusions were that the first Mode may be excited if engine speeds exceed 5000 RPM based on first order excitation. All other modes were not of concern therefore the cradle manufacturing proceeded with additional gussets installed to stiffen the breathing mode solved for as Mode 1.

Table 20: eMotor Cradle Dynamic FEA Results for Various Materials and Assumed Elastomer Mounts

Material	**Steel**	**Steel**	**Steel**	**Steel**	**Steel***	**Aluminum**		**Aluminum**
BC	**Free-Free**	**Fixed-Clamped**	**Fixed-Clamped**	**Fixed-Clamped**	**Fixed-Clamped**	**Free-Free**	**Fixed-Clamped**	**Fixed-Clamped**
Mount Stiffness (N/mm^3)	**100**	**100**	**500**	**500000**	**500**	**- -**	**100**	**500**
Mode 1	166.1	76.672	77.773	191.9	82.437	166.26	77.575	80.335
Mode 2	181.82	307.71	382.09	441.03	385.15	182.27	358.27	394.97
Mode 3	289.27	339.14	417.23	559.77	420.87	290.11	399.6	466.03
Mode 4	464.12	399.49	483.67	738.41	487.21	465.92	439.35	567.19
Mode 5	530.42	525.11	577.16	800.46	602.91	532.29	556.24	589.11
Mode 6	543.62	571.4	591.07	996.56	610.82	545.78	576.9	648.53
Mode 7	586.31	631.51	690.76	1189.9	702.48	587.61	654.04	885.26
Mode 8	651.07					653.74		

11. Appendix F: Sample Post Processing MATLAB® Scripts

The following is code written in MATLAB® R2018a to post process Shuffle Frequency Estimates

```
function [frqdat] = frqest(tq,aped,w,Fs)
%FRQEST is a function that analyzes the torque signal for tip in and tip
%out events. It classifies them as such then analyzes the wheel speed data
%using an output only analysis assuming an sdof
%
% (c) Jon Furlich 2020
%
% ------------------------------------------------------------------------
%    IMPORTANT: This function assumes that tq, w, and r are reflected
%               on the same torsional plane. It also assumes that they
%               are input with units rpm
% ------------------------------------------------------------------------
%
% ***************** Function Inputs ***********************************
%   tq - contains a torque signal with tip in and/or tip out maneuvers
%
%   w - contains the reference shaft speed signal in rev/min
%
%   Fs - is the sample frequency of the data input in tq, wr, and wl
%
% ************************************************************************
%
% ++++++++++++++++ Function Outputs ++++++++++++++++++++++++++++++++++++
%
% frqdat - this is a structure file that holds the tip in and tip out data
%
% ++++++++++++++++++++++++++++++++++++++++++++++++++++++++++++++++++++++++

% check input consistancy
tql = numel(tq); wl = numel(w);
if tql ~= wl
    error('Improper vector lengths')
else

    % Here are some "useful" conversions that may be used
    rtd = 180/pi; %radians to degrees
    dtr = pi/180; %degrees to radians
    rpm2rds = 2*pi/60; % rev/min to rad/sec

    % Low pass filter the troque data to remove high frequency noise and
    % know that tip in or out signals contain high frequency content
    % necessary to make them happen but can contain lower information
    if Fs > 64
        [bl,al] = cheby2(5,10,32/(Fs/2),'low');
    else
        [bl,al] = cheby2(5,10,0.85,'low');
    end

    % lowpass filter the torque signal
    tq = filtfilt(bl,al,tq);

    %%% ------------------------------------------------------------------
    % look for tip in and or tip out increments in the torque signal
        [ind] = torqtrigz(aped,Fs);
%         [min(ind.tipin),max(ind.tipin)]
%         [min(ind.tipot),max(ind.tipot)]
%         numel(tq)
%         dbstop
    %%% ------------------------------------------------------------------
```

```
    % Bandpass filter the shaft speed signal
    if Fs > 24
        [bl,al] = cheby2(5,20,12/(Fs/2),'low');
    else
        [bl,al] = cheby2(5,20,0.85,'low');
    end

    % high pass filter coefficients
    [bh,ah] = cheby2(5,20,1/(Fs/2),'high');
    % combine filters for bandpass filter effect
    w = filtfilt(bl,al,filtfilt(bh,ah,w));


    %%% find the peaks
    [fitdat] = decfit(w,ind,Fs);
end

%% Combine all the data into one output structure
frqdat.ind = ind;
frqdat.fit = fitdat;

end

function [ind] = torqtrigz(torq,Fs)
%TORQTRIG evaluates a torque signal assuming the torque oscillates from
%positive to negative. It will search for a trigger condition based on the
%difference from the maximum to minimum torque observed.
% (c) Jon Furlich 2020

% ---------------------------------------------------------------------
%    IMPORTANT:
% ---------------------------------------------------------------------
%
% ********** Function Inputs ***************************************
%   tq - contains a torque signal with tip in and/or tip out maneuvers
%
%   Fs - is the sample frequency of the data input in tq
%
% *********************************************************************
%
% ++++++++++++++++ Function Outputs ++++++++++++++++++++++++++++++++++
%
% ind - contains indices relative to the torq vector where either a tip in
%       or a tip out event occurred. It is a structure variable
%
% +++++++++++++++++++++++++++++++++++++++++++++++++++++++++++++++++++++


% 1111 The function defines a threshold based on a medium between the
% maximum and minimum torque values

% 2222 It then finds all of those locations and declares if the slope is
% positive it knows that is a tip in condition and searches backwards for
% when the tip in was initiated

% 3333 if the slope is negative it knows that a tip out occured and it
% also searches backwards for when the tip out was initiated.

% 4444 the function knows that the tip in or out occured searching
% backwards if the slope changes to zero or near zero.

%%%% Due to high sample rates, I will calculate the slope or difference
%%%% based off a down sample rate to 1 Hz.

    ti = zeros(1,10000); %prealocate zeros for in and out
    to = zeros(1,10000);
```

```
    %%% create a slope vector
    % use a lpf to improve differentiation results
    [b,a] = butter(4,32/Fs/2,'low');
    tqd = diff(filtfilt(b,a,torq));
    tqdm = mean(tqd);

    movingnum = 50;

    %1111 Create Threshold
%     threshold = (max(torq)-min(torq))/2;
    threshold = 15;
    tipinct = 1; % initialize tip in counter
    tipotct = 1;
    for jj = movingnum+1:movingnum:numel(torq)-movingnum
        %2222 Check if tip in occurs
        if mean(torq(jj-movingnum:jj))<threshold && mean(torq(jj:jj+movingnum))>threshold
            ctmax = numel(torq)-jj-movingnum-1;
            ct = 1;
            ii = jj+movingnum;
            %3333 itterate backwards for when tip in occured, meaning when
            %3333 the slope settles back to ~zero
            while ct < ctmax
                if ii-Fs-1 <= 0 || ii-Fs <= 0
                    break
                end
                %4444 check if it settles back to the mean slope (zero) and
                %also that the mean slope for the past second has been
                %close to the mean, this ensure's "steady state" has been
                %achieved at the current torque level
                if tqd(ii) < 0.1 && mean(tqd(ii-Fs:ii)) <= 0.1
                    ti(tipinct) = ii;
                    tipinct = tipinct +1;
%                     disp('tip in')
                    break
                else
                end
                ct = ct+1; % increase counter
                ii = ii-1; % decrease time itteration

            end
%         ++++++++++++++++++++++++++++++++++++++++++++++++++++++++++++++++
        %2222 Check if tip out occurs
        elseif mean(torq(jj-movingnum:jj))>threshold &&
mean(torq(jj:jj+movingnum))<threshold
            ctmax = numel(torq);
            ct = 1;
            ii = jj+movingnum;
            %3333 itterate forwards to the end of tip out because that is
            %when the system will start to free vibrate due to the torque
            %crossing near zero
            while ct < ctmax
                %4444 check if it settles back to the mean slope (zero) and
                %also that the mean slope for the past second has been
                %close to the mean, this ensure's "steady state" has been
                %achieved at the current torque level
                if tqd(ii) > -0.1
                    to(tipotct) = ii;
                    tipotct = tipotct +1;
                    break
                else
                end
                ct = ct+1; % increase counter
                ii = ii+1; % decrease time itteration
            end
        end
    end

    ti = ti(ti>0);if numel(ti)>=1,ind.tipin = ti;else,ind.tipin = NaN;end
```

```
    to = to(to>0);if numel(to)>=1,ind.tipot = to;else,ind.tipot = NaN;end

end

function [fitdat] = decfit(x,ind,Fs)
% DECFIT is a function that will analyze output only vibration data that
% appears to follow a SDOF decay response.
% (c) Jon Furlich 2020.

% ------------------------------------------------------------------------
%    IMPORTANT: This function assumes that x has already been band pass
%    filtered to the desired outcome removing DC components.
% ------------------------------------------------------------------------
%
% *************** Function Inputs ***************************************
%   x - contains the filtered data with log decrement behavior
%
%   ind - is a structure variable that contains both tip in and tip out
%           events based on trigger criteria.
%
% ***********************************************************************
%
% ++++++++++++++++ Function Outputs +++++++++++++++++++++++++++++++++++++
%
% fitdat - this is a structure file that holds the frequency and damping
%           values relative to the tip in and tip out data
%
% +++++++++++++++++++++++++++++++++++++++++++++++++++++++++++++++++++++++

% This function is in step with tip in and tip out function where you send
% the function time data along with indices in the data where you believe
% there is a log decrement.

% The function will then find the first five positive and netgative peaks.
% It will then attempt to fit a logarithmic curve to those peaks and return
% the frequency associated along with damping value.

% to include 0.66s of data, Fs = 1/dt therefore N = 0.66*Fs;
proj = round(1*Fs); %projection of data

%%% first analyze the tip in indicees. Assuming all frequencies are below
%%% twelve Hz then it should include ~0.66 seconds of data
    % initialize frequency estimate vector
    freqest = zeros(1,numel(ind.tipin)); zetaest = freqest; rest = freqest;
    frqtmpest = [0,0]; zeta = [0,0];
    dim = ceil(sqrt(numel(ind.tipin)));
    for ii = 1:1:numel(ind.tipin(ind.tipin+2*proj<numel(x)))
        rng = ind.tipin(ii):ind.tipin(ii)+proj;
        [~,maxind] = max(x(rng)); % find the maximum indice, use as start
        rng = ind.tipin(ii)+maxind-25:ind.tipin(ii)+maxind-25+proj;
%         [~,maxind] = max(x(rng)); % find the maximum indice, use as start

        % find the first five positive peaks assuming Fs = 1024
        % min dist 800 ~ 10 Hz (1/10*1024)
        % max dist 4096 = 2 Hz (1/2*1024)
        [pkpos,locpos] =
findpeaks(x(rng),'NPeaks',5,'MinPeakDistance',100,'MinPeakHeight',0,'MaxPeakWidth',512);
        % find the first six negative peaks by multiplying by -1 knowing
        % that the first peak is a filter ring artifact
        [pkneg,locneg] = findpeaks(-
1*x(rng),'NPeaks',5,'MinPeakDistance',100,'MinPeakHeight',0,'MaxPeakWidth',512);
        r = [0,0];
        if numel(pkpos)>1&&numel(locpos)>1&&numel(pkneg)>1&&numel(locneg)>1
            frq = zeros(4,2); %first column positive decay, second column negative decay
            for jj = numel(locpos):-1:2
                frq(jj-1,1) = Fs/(locpos(jj)-locpos(jj-1));
            end
```

```
            for jj = numel(locneg):-1:2
                frq(jj-1,2) = Fs/(locneg(jj)-locneg(jj-1));
            end
            frqtmpest(1) = mean(frq(frq(:,1)~=0,1)); % average positive frequency
            frqtmpest(2) = mean(frq(frq(:,2)~=0,2)); % average negative frequency

            % use least square fit to calculate the decrement
            [copos] = polyfit(locpos/Fs,log(pkpos),1);
            [coneg] = polyfit(locneg/Fs,log(pkneg),1);
            % note that the first coefficient is -sigma
            zeta(1) = -1*copos(1)/2/pi/frqtmpest(1)*100;
            zeta(2) = -1*coneg(1)/2/pi/frqtmpest(2)*100;
            %estimate the correlation
            corp = corrcoef(locpos/Fs,log(pkpos));
            r(1) = corp(2,1).^2;
            corn = corrcoef(locneg/Fs,log(pkneg));
            r(2) = corn(2,1).^2;
        end
        freqest(ii) = mean(frqtmpest(r>0.5));
        zetaest(ii) = mean(zeta(r>0.5));
        rest(ii) = mean(min(r(r>0.5)));

    end

fitdat.tipin.frqest = freqest;
fitdat.tipin.zetaest = zetaest;
fitdat.tipin.corr = rest;

%%% first analyze the tip in indicees. Assuming all frequencies are below
%%% twelve Hz then it should include ~0.66 seconds of data
    % initialize frequency estimate vector
    freqest = zeros(1,numel(ind.tipot)); zetaest = freqest; rest = freqest;
    frqtmpest = [0,0]; zeta = [0,0];
    dim = ceil(sqrt(numel(ind.tipot)));
    for ii = 1:1:numel(ind.tipot(ind.tipot+2*proj<numel(x)))
        rng = ind.tipot(ii):ind.tipot(ii)+proj;
        [~,maxind] = max(x(rng)); % find the maximum indice, use as start
        rng = ind.tipot(ii)+maxind-25:ind.tipot(ii)+maxind-25+proj;
        [~,maxind] = max(x(rng)); % find the maximum indice, use as start
        % find the first five positive peaks
        [pkpos,locpos] =
findpeaks(x(rng),'NPeaks',5,'MinPeakDistance',100,'MinPeakHeight',0,'MaxPeakWidth',512);
        % find the first six negative peaks by multiplying by -1 knowing
        % that the first peak is a filter ring artifact
        [pkneg,locneg] = findpeaks(-
1*x(rng),'NPeaks',5,'MinPeakDistance',100,'MinPeakHeight',0,'MaxPeakWidth',512);
        r = [0,0];
        if numel(pkpos)>1&&numel(locpos)>1&&numel(pkneg)>1&&numel(locneg)>1
            frq = zeros(4,2); %first column positive decay, second column negative decay
            for jj = numel(locpos):-1:2
                frq(jj-1,1) = Fs/(locpos(jj)-locpos(jj-1));
            end
            for jj = numel(locneg):-1:2
                frq(jj-1,2) = Fs/(locneg(jj)-locneg(jj-1));
            end
            frqtmpest(1) = mean(frq(frq(:,1)~=0,1)); % average positive frequency
            frqtmpest(2) = mean(frq(frq(:,2)~=0,2)); % average negative frequency

            % use least square fit to calculate the decrement
            [copos] = polyfit(locpos/Fs,log(pkpos),1);
            [coneg] = polyfit(locneg/Fs,log(pkneg),1);
            % note that the first coefficient is -sigma
            zeta(1) = -1*copos(1)/2/pi/frqtmpest(1)*100;
            zeta(2) = -1*coneg(1)/2/pi/frqtmpest(2)*100;
            %estimate the correlation
            corp = corrcoef(locpos/Fs,log(pkpos)); r(1) = corp(2,1).^2;
            corn = corrcoef(locneg/Fs,log(pkneg)); r(2) = corn(2,1).^2;
        end
```

```
        freqest(ii) = mean(frqtmpest(r>0.5));
        zetaest(ii) = mean(zeta(r>0.5));
        rest(ii) = mean(min(r(r>0.5)));

    end

fitdat.tipot.frqest = freqest;
fitdat.tipot.zetaest = zetaest;
fitdat.tipot.corr = rest;

end
```

The following is code written in MATLAB®R2018a to post process Lash Estimates

```
function [lshdat,lshdat2,fitdat] = lashest(tq,wr,wl,Fs,mva,ttrig,trncrng,indic)
%LASHEST is a function that compares two wheel speed signals and a torque
%signal to estimate the lash in a total driveline.
%
% (c) Jon Furlich 2020
%
% ------------------------------------------------------------------------
%    IMPORTANT: This function assumes that tq, w, and r are reflected
%               on the same torsional plane. It also assumes that they
%               are input with units rpm
% ------------------------------------------------------------------------
%
% ***************** Function Inputs **********************************
%   tq - contains a torque signal with base units for integration etc.
%
%   wr - contains the reference shaft speed signal in rev/min
%
%   wl - contains a relative shaft speed which has been reflected onto the
%        same rotational plane as the reference shaft speed. It is also in
%        units of rev/min
%
%   Fs - is the sample frequency of the data input in tq, wr, and wl
%
% ********************************************************************
%
% ++++++++++++++++ Function Outputs ++++++++++++++++++++++++++++++++++++
%
%
% ++++++++++++++++++++++++++++++++++++++++++++++++++++++++++++++++++++++++

% check input consistancy
tql = numel(tq); wrl = numel(wr); wll = numel(wl);
if tql ~= wrl || tql ~= wll
    error('Improper vector lengths')
else

    % Here are some "useful" conversions that may be used
    rtd = 180/pi; %radians to degrees
    dtr = pi/180; %degrees to radians
    rpm2rds = 2*pi/60; % rev/min to rad/sec

    % First step is to convert rpm to rad/s for consistent integration and
    % differentiation. Must be in base units
    wr = wr*rpm2rds;
    wl = wl*rpm2rds;

    % As proposed, my second order of business is to low pass filter the
    % wheel speed data before integration and differentiation. From past
    % trial and error I found best results when filtering at 32 hz but this
    % can be modified

    N = numel(wr);    T = N/Fs;    df = 1/T;    hz = 0:df:Fs/2;
    fftflt = zeros(1,numel(hz));  fftflt(hz<15) = 1;   fftflt(hz<2.75) = 0;
%     fftflt = zeros(1,numel(hz));  fftflt(hz<15) = 1;   fftflt(hz<4.5) = 0;
    if rem(N,2) == 0,fftflt = [fftflt,fliplr(fftflt(2:end-1))];else,fftflt =
[fftflt,fliplr(fftflt(2:end))];end

    % I need to do this filtering first because the lowpass filter below is
    % causing error in the frequency estimate.
%     spd = ifft(fft(tq).*fftflt);
    spd = ifft(fft(wr).*fftflt);
    tqe = ifft(fft(tq).*fftflt);

    if Fs > 32,[b,a] = cheby2(5,20,32/(Fs/2),'low');end
    wr = filter(b,a,wr);
```

```
    wl = filter(b,a,wl);

%     wr = ifft(fft(wr).*fftflt);
%     wl = ifft(fft(wr).*fftflt);

%     [b,a] = butter(4,0.2,'low');
    tqf = filter(b,a,tq);

    % Due to turning or other instabilities in the integration algorithm I
    % will implement reset integration which will use a moving average
    % calculation of the theta for use in lash estimates.

        % initialize moving average lash vector
        lsh = zeros(1,numel(wr)-mva-1);
        % initialize moving average torque value
        tqa = lsh; tqaf = lsh;
        slptqth = lsh;
        for ii = 1:1:numel(wr)-mva-1
            lsh(ii) = (trapz(wl(ii:ii+mva))/Fs-trapz(wr(ii:ii+mva))/Fs)*rtd;
            tqa(ii) = (tq(ii+mva)); %use the last value
            tqaf(ii) = (tqf(ii+mva)); %use the last value
            if ii <= 5
                slptqth(ii) = 0;
            else
                slptqth(ii) = (lsh(ii)-lsh(ii-5))/(tqaf(ii)-tqaf(ii-5));
            end
        end
end

%% Look for an increment for tip ins in a seperate function
[inc.tipin] = torqtrig(tq,Fs,ttrig);
inc.tipin = unique(inc.tipin);

    % based on this algorithm I need at least 1 second of data pre and post
    % tip in based on the torqtrig location therefore I will filter out any
    % data points that are too close to the start and end.
    inc.tipin = inc.tipin(inc.tipin-1.5*Fs>1);
    inc.tipin = inc.tipin(inc.tipin+1.5*Fs<numel(tqa));

% 07/27/2020
% I realized that the use of arbitrary tip in triggers based on assumed
% locations isn't working for the data I want to process. I need to have
% better criteria for truncating data and now think I should take arbitrary
% length pieces of data as long as they follow appropriate results.

%% First iteration of estimating the lash based on arbitrary trucation

% [lshdat] = lashleadlag(tqa,lsh,inc,mva,Fs,trncrng);
[lshdat2] = lashestimator(tqa,lsh,slptqth,inc,Fs,indic);

%% Calculate Log-decriment of data

[ind] = torqtrigz(tqa,Fs);
[fitdat.wr] = decfit(spd,ind,Fs);
[fitdat.tq] = decfit(tqe,ind,Fs);

%% Combine all the data into one output structure
lshdat.inc = inc;
lshdat.tqa = tqa;
lshdat.lsh = lsh;
lshdat.tq = tq;
lshdat.wl = wl;
lshdat.wr = wr;

lshdat2.inc = inc;
lshdat2.tqa = tqa;
lshdat2.lsh = lsh;
lshdat2.tq = tq;
```

```
lshdat2.wl = wl;
lshdat2.wr = wr;

end

function [tipinind] = torqtrig(torq,Fs,ttrig)
%TORQTRIG evaluates a torque signal assuming the torque oscillates from
%positive to negative
    tipinind = zeros(1,10000); %prealocate zeros

%     filter the signal for better results
    [b,a] = butter(4,8/Fs/2,'low');
    torq = filtfilt(b,a,torq);

    movingnum = 50;
    tipinct = 1; threshold = mean(torq);
    for jj = movingnum+1:movingnum:numel(torq)-movingnum
        if mean(torq(jj-movingnum:jj))<threshold && mean(torq(jj:jj+movingnum))>threshold
            ctmax = 10000;
            ct = 1;
            ii = jj+movingnum;
            while ct < ctmax
                if torq(ii) < ttrig && torq(ii+1) > ttrig
                    tipinind(tipinct) = ii;
                    tipinct = tipinct +1;
                    break
                else
                end
                ct = ct+1; % increase counter
                ii = ii-1; % decrease
                if ii <= 0
                    break
                end
            end
        end
    end

    tipinind = tipinind(tipinind~=0);
end

function [lshdat] = lashleadlag(tqa,lsh,inc,mva,Fs,trncrng)
% LASHLEADLAG is a function that utilizes triggered events based on torque
% tip in data previously solved for

    %%% define a structure that will output the lash estimates and the
    %%% relevant data to those lash estimates
    lshdat = struct;
    raw = struct;

    lshrng = [trncrng(1),trncrng(2)];
    lag = zeros(numel(inc.tipin),2); lead = lag;
    lagr = zeros(numel(inc.tipin),1); leadr = lagr;
    ct = 1; %initialize counter of good lash crossings
    for kk = 1:1:numel(inc.tipin)
        x = tqa(inc.tipin(kk)+lshrng(1):inc.tipin(kk)+lshrng(2));
        y = (lsh(inc.tipin(kk)+lshrng(1):inc.tipin(kk)+lshrng(2))-...
                    mean(lsh(2*mva:20:end)));
                    % note, the mean calculation removes an
                    % offset due to hysteresis
        y = y-y(1);
            lagx = x(trncrng(3):trncrng(4));
            lagy = y(trncrng(3):trncrng(4));
            leadx = x(trncrng(5):trncrng(6));
            leady = y(trncrng(5):trncrng(6));
        xx = fliplr(x); yy = fliplr(y);
        precriteria = 0; pstcriteria = 0;
%%% ------------------------------------------- slope evaluation bit
%%% ---------------------------------------------------------------------
```

```
            % I will use the following criteria;
                % 1.) slope must be negative
                % 2.) stiffness must be within 10-1000 Nm/deg
                % 3.) correlation coefficient must be >50%
                % 4.) will grow sample size assuming correlation stays high
                % 4.) will attempt to reset up to five times
                % 5.) will attempt to unsucessfully grow up to five times
%                 resetmax = 10;
%                 rstmv = 25; rstrng = 50; growrt = 25;
                rstmv = 10; rstrng = 20; growrt = 10;
                resetmax = floor(numel(x)/rstrng)-1;
                if resetmax > 10
                    resetmax =10;
                end
        %%% ++++++++++++++++++++++++++++++++++++++ Pre Lash Processing
        reset = 1; grow = 1;  prerng = 1:rstrng;
        while reset <= resetmax
            xpre = x(prerng); ypre = y(prerng);
            preft = polyfit(xpre,ypre,1); precmp = preft(1); prestf = 1/precmp;
                rpre = corrcoef(xpre,ypre); rpre = rpre(2,1)^2;
            if precmp < 0 && abs(prestf) < 200 && abs(prestf) >10 && rpre > 0.6
                % if all criteria were met, attempt to grow
                lstrng = prerng;
                prerng = [prerng,prerng(end)+1:prerng(end)+growrt];
                grow = grow + 1;
%                 fprintf('\n Grow number %1.0f',grow-1)
                % if successfully grew 5 times or correlation is high break
                if grow == 6 || rpre > 0.9
%                     fprintf('\n Achieved Pre Lash Criteria kk=%2.0f',kk)
                    lagx = xpre;
                    lagy = ypre;
                    precriteria = 1;
                    break
                end
            elseif grow == 1
                % if not all criteria were met and no growth was attempted
                % then shift the data
                prerng = [1:rstrng] + reset*rstmv;
%                 fprintf('\n Reset number %1.0f',reset)
                reset = reset + 1; grow = 1;
            elseif grow ~= 1
                % if criteria were not met but had attempted to grow at
                % some point, then take that data
%                 fprintf('\n Partially Acheived Pre Lash Criteria kk=%2.0f',kk)
                lagx = x(lstrng);
                lagy = y(lstrng);
                precriteria = 2;
                break
            end
        end

        %%% ++++++++++++++++++++++++++++++++++++++ post lash processing
        reset = 1; grow = 1; pstrng = 1:rstrng;
        while reset <= resetmax
            xpst = xx(pstrng); ypst = yy(pstrng);
            pstft = polyfit(xpst,ypst,1); pstcmp = pstft(1); pststf = 1/pstcmp;
                rpst = corrcoef(xpst,ypst); rpst = rpst(2,1)^2;
            if pstcmp < 0 && abs(pststf) < 200 && abs(pststf) > 10 && rpst > 0.6
                % if all criteria were met, attempt to grow
                lstrng = pstrng;
                pstrng = [pstrng,pstrng(end)+1:pstrng(end)+growrt];
                grow = grow + 1;
                % if successfully grew 5 times or correlation is high break
                if grow == 6 || rpre > 0.9
                    leadx = xpst;
                    leady = ypst;
                    pstcriteria = 1;
%                     fprintf('\n Achieved Post Lash Criteria kk=%2.0f',kk)
```

```
                    break
                end
            elseif grow == 1
                % if not all criteria were met and no growth was attempted
                % then shift the data
                pstrng = [1:rstrng] + reset*rstmv;
%                 fprintf('\n Reset number %1.0f',reset)
                reset = reset + 1; grow = 1;
            elseif grow ~= 1
                % if criteria were not met but had attempted to grow at
                % some point, then take that data
%                 fprintf('\n Partially Acheived Post Lash Criteria kk=%2.0f',kk)
                leadx = xx(lstrng);
                leady = yy(lstrng);
                pstcriteria = 2;
                break
            end
        end


%%% ------------------------------------------------------------------------
        % variable stating if criteria were met
        crit(kk,:) = [precriteria,pstcriteria];

        % lag estimate is the pre-lash crossing
        lag(kk,:) = polyfit(lagx,lagy,1);
        r = corrcoef(lagx,lagy); lagr(kk) = abs(r(2,1))^2;
        % lead estimate is the post-lash crossing
        lead(kk,:) = polyfit(leadx,leady,1);
        r = corrcoef(leadx,leady); leadr(kk) = abs(r(2,1))^2;
        % assume that lead displacement value should be lower than the lag
        % value thus filter as such
        if precriteria >= 1 && pstcriteria >= 1 && lead(kk,2) < lag(kk,2)
            tqlsh(ct,:) = x;%good torque data
            thlsh(ct,:) = y;%good theta data
            pre(ct) = lag(kk,2);
            post(ct) = lead(kk,2);
            stiff(ct,:) = [1/lag(kk,1),1/lead(kk,1)];
            rs(ct,:) = [lagr(kk),leadr(kk)];
            lshest(ct) = abs(post(ct)-pre(ct));
            ct = ct+1;
        elseif exist('tqlsh','var') ~= 1 && kk == numel(inc.tipin)
            % the criteria failed all the way through the last iteration
            tqlsh(ct,:) = [Inf];%good torque data
            thlsh(ct,:) = [Inf];%good theta data
            pre(ct) = [0];
            post(ct) = [0];
            stiff(ct,:) = [0,0];
            rs(ct,:) = [0,0];
            lshest(ct) = [0];
        end
            % all crappy data selected
        raw.x = x;
        raw.y = y;
        raw.lag = lag(kk,:);
        raw.lead = lead(kk,:);
        raw.lagr = lagr(kk);
        raw.leadr = leadr(kk);
        lshdat = setfield(lshdat,strcat('raw',num2str(kk)),raw);
    end

    %good data
    lshdat.tqlsh = tqlsh;
    lshdat.thlsh = thlsh;
    lshdat.pre = pre;
    lshdat.post = post;
    lshdat.stiff = stiff;
    lshdat.lshest = lshest;
```

```
    lshdat.rs = rs;
    lshdat.crit = crit;


end

function [lshdat] = lashestimator(tqa,lsh,slptqth,inc,Fs,indic)
% LASHLEADLAG is a function that utilizes triggered events based on torque
% tip in data previously solved for. It then determines where to truncate
% the data and then finds the pre and post lash stiffness locations.

%%%%%%%%%%%%%%%%%%%%% INPUTS %%%%%%%%%%%%%%%%%%%%%%%%%%%%%%%%%%%%%%%%%%%
    %
    % tqa - This is a vector of torque data in Nm
    %
    % lsh - This is a vector of lash data in degrees
    %
    % inc - This is a vector of calculated tip in locations
    %
    % Fs - This is a scalor of the data sample frequency
    %
%%%%%%%%%%%%%%%%%%%%%%%%%%%%%%%%%%%%%%%%%%%%%%%%%%%%%%%%%%%%%%%%%%%%%%%5

    %%% define a structure that will output the lash estimates and the
    %%% relevant data to those lash estimates
    lshdat = struct;
    raw = struct;

%% Look back for lash accumulation start and forward to minimum
lshlow = inc.tipin-0.25*Fs; %auto 1 second rewind before tip in.
lshhigh = ones(numel(inc.tipin),1);

for ii = 1:numel(inc.tipin)
    %%%% Look forwards to the end of the lash crossing by finding the
    %%%% peaks, or really the minima and knowing that the indicator is at
    %%%% the very first pks.
    [~,locs] = findpeaks(-1*lsh(inc.tipin(ii):inc.tipin(ii)+Fs));
%     isempty(locs)
    if isempty(locs) == 1
        [~,locs] = min(lsh(inc.tipin(ii):inc.tipin(ii)+Fs));
    end

    lshhigh(ii) = locs(1)+inc.tipin(ii);
    if lshhigh(ii)-inc.tipin(ii) < 1024
        lshhigh(ii) = inc.tipin(ii) + 800;
    end
end

%% Find where the key knee points are in the lash data.

% to find these key points we can look at the slope vector of the lash
% data. I'm thinking of looking for a trigger. start from the inside near
% the trigger condition and move outward to find spot 2 then 1, 3 then 4.
%   spot 1 - no more data points ahead greater than 5
%   spot 2 - no more data points behind greater than 5
%   spot 3 - no more data points ahead greater than 5
%   spot 4 - no more data points behind greater than 5

% spot = ones(numel(inc.tipin),4);
spot = indic;
% numel(indic(:,1))
% numel(inc.tipin)
% lshhigh-inc.tipin
    % note that the spot data was collected from flexplate comparisons,
    % therefore it may miss on other data sets....correct this later
```

```
ct = 1; pre=Inf; post=Inf;stiff=[Inf,Inf];lshest=Inf;rs=[0,0];

lennn = numel(inc.tipin);
lenn = numel(spot(:,1));

for kk = 1:numel(inc.tipin)

        % I am choosing to extend lshhigh to the length of spot(kk,4) to
        % grab more data rather than less... could do the other way around
        % and observe better ideas

%%% ++++++++++++++++++++++++++++++++++++++++++++++++++++++++++++++++++++++
            % Extend range to conform with Flexplate data
%         if lshhigh(kk)-inc.tipin(kk) < spot(kk,4)
%             lshhigh(kk) = spot(kk,4)+inc.tipin(kk);
%         end
%%% ++++++++++++++++++++++++++++++++++++++++++++++++++++++++++++++++++++++
%             % Truncate range to conform with new length
%         if spot(kk,4) < lshhigh(kk)
%             spot(kk,4) = lshhigh(kk);
%         end
%%% ++++++++++++++++++++++++++++++++++++++++++++++++++++++++++++++++++++++

    x = tqa(lshlow(kk):lshhigh(kk));
    y = lsh(lshlow(kk):lshhigh(kk))-mean(lsh(2:20:end));

%         note, the mean calculation removes an
%         offset due to hysteresis


    % the ADAPT data doesn't cross near zero therefore the data appears to
    %
    tqadj = mean(x(spot(kk,2):spot(kk,3)));
    x = x-tqadj;

    y = y-y(1); % force the first torque value to zero
    lagx = x(spot(kk,1):spot(kk,2));
    lagy = y(spot(kk,1):spot(kk,2));

    leadx = x(spot(kk,3):spot(kk,4));
    leady = y(spot(kk,3):spot(kk,4));



%%% ------------------------------------------------ slope evaluation bit
%%% ------------------------------------------------------------------------
        % I will use the following criteria;
            % 1.) slope must be negative
            % 2.) stiffness must be within 10-1000 Nm/deg
            % 3.) correlation coefficient must be >50%



    % lag estimate is the pre-lash crossing
    lag(kk,:) = polyfit(lagx,lagy,1);
    r = corrcoef(lagx,lagy); lagr(kk) = abs(r(2,1))^2;
    % lead estimate is the post-lash crossing
    lead(kk,:) = polyfit(leadx,leady,1);
    r = corrcoef(leadx,leady); leadr(kk) = abs(r(2,1))^2;
    % only take good correlation coefficient data
    if lagr(kk) >= 0.2 && leadr(kk) >= 0.2
        keep.tqlsh = x;
        keep.thlsh = y;
        keep.rng = spot(kk,:);
        pre(ct) = lag(kk,2);
        post(ct) = lead(kk,2);
```

```
        stiff(ct,:) = [1/lag(kk,1),1/lead(kk,1)];
        rs(ct,:) = [lagr(kk),leadr(kk)];
        lshest(ct) = abs(lead(kk,2)-lag(kk,2));

        lshdat = setfield(lshdat,strcat('keep',num2str(ct)),keep);

        ct = ct+1;
    end

%%%%%%%%%%%%%%%%%%%%%%%%%%%%%%%%%%%%%%%%%%%%%%%%%%%%%%%%%%%%%%%%%%%%%%%%%%%%%%%

    % all crappy data selected
    raw.x = x;
    raw.y = y;
    raw.lag = lag(kk,:);
    raw.lead = lead(kk,:);
    raw.lagr = lagr(kk);
    raw.leadr = leadr(kk);

%%%%%%%%%%%%%%%%%%%%%%%%%%%%%%%%%%%%%%%%%%%%%%%%%%%%%%%%%%%%%%%%%%%%%%%%%%%%%%%

    lshdat = setfield(lshdat,strcat('raw',num2str(kk)),raw);

    clear x y lag lead r lagr leadr
end

%%%%%%%%%%%%%%%%%%%%%%%%%%%%%%%%%%%%%%%%%%%%%%%%%%%%%%%%%%%%%%%%%%%%%%%%%%%%%%%
    %good data
    lshdat.pre = pre;
    lshdat.post = post;
    lshdat.stiff = stiff;
    lshdat.lshest = lshest;
    lshdat.rs = rs;
    lshdat.ct = ct-1;
%%%%%%%%%%%%%%%%%%%%%%%%%%%%%%%%%%%%%%%%%%%%%%%%%%%%%%%%%%%%%%%%%%%%%%%%%%%%%%%

end

function [ind] = torqtrigz(torq,Fs)
%TORQTRIG evaluates a torque signal assuming the torque oscillates from
%positive to negative. It will search for a trigger condition based on the
%difference from the maximum to minimum torque observed.
% (c) Jon Furlich 2020

% ---------------------------------------------------------------------------
%    IMPORTANT:
% ---------------------------------------------------------------------------
%
% ***************** Function Inputs ************************************
%   tq - contains a torque signal with tip in and/or tip out maneuvers
%
%   Fs - is the sample frequency of the data input in tq
%
% ***************************************************************************
%
% +++++++++++++++++ Function Outputs +++++++++++++++++++++++++++++++++++++
%
% ind - contains indices relative to the torq vector where either a tip in
%       or a tip out event occurred. It is a structure variable
%
% +++++++++++++++++++++++++++++++++++++++++++++++++++++++++++++++++++++++++


% 1111 The function defines a threshold based on a medium between the
% maximum and minimum torque values

% 2222 It then finds all of those locations and declares if the slope is
% positive it knows that is a tip in condition and searches backwards for
```

```
% when the tip in was initiated

% 3333 if the slope is negative it knows that a tip out occured and it
% also searches backwards for when the tip out was initiated.

% 4444 the function knows that the tip in or out occured searching
% backwards if the slope changes to zero or near zero.

%%%% Due to high sample rates, I will calculate the slope or difference
%%%% based off a down sample rate to 1 Hz.

    ti = zeros(1,10000); %prealocate zeros for in and out
    to = zeros(1,10000);

    %%% create a slope vector
    % use a lpf to improve differentiation results
    [b,a] = butter(4,32/Fs/2,'low');
    tqd = diff(filtfilt(b,a,torq));
    tqdm = mean(tqd);

    movingnum = 50;

    %1111 Create Threshold
%     threshold = (max(torq)-min(torq))/2;
    threshold = 15;
    tipinct = 1; % initialize tip in counter
    tipotct = 1;
    for jj = movingnum+1:movingnum:numel(torq)-movingnum
        %2222 Check if tip in occurs
        if mean(torq(jj-movingnum:jj))<threshold && mean(torq(jj:jj+movingnum))>threshold
            ctmax = numel(torq)-jj-movingnum-1;
            ct = 1;
            ii = jj+movingnum;
            %3333 itterate backwards for when tip in occured, meaning when
            %3333 the slope settles back to ~zero
            while ct < ctmax
                if ii-Fs-1 <= 0 || ii-Fs <= 0
                    break
                end
                %4444 check if it settles back to the mean slope (zero) and
                %also that the mean slope for the past second has been
                %close to the mean, this ensure's "steady state" has been
                %achieved at the current torque level
                if tqd(ii) < 0.1 && mean(tqd(ii-Fs:ii)) <= 0.1
                    ti(tipinct) = ii;
                    tipinct = tipinct +1;
%                     disp('tip in')
                    break
                else
                end
                ct = ct+1; % increase counter
                ii = ii-1; % decrease time itteration

            end
%         ++++++++++++++++++++++++++++++++++++++++++++++++++++++++++++++++
        %2222 Check if tip out occurs
        elseif mean(torq(jj-movingnum:jj))>threshold &&
mean(torq(jj:jj+movingnum))<threshold
            ctmax = numel(torq);
            ct = 1;
            ii = jj+movingnum;
            %3333 itterate forwards to the end of tip out because that is
            %when the system will start to free vibrate due to the torque
            %crossing near zero
            while ct < ctmax
                %4444 check if it settles back to the mean slope (zero) and
                %also that the mean slope for the past second has been
                %close to the mean, this ensure's "steady state" has been
```

```
                %achieved at the current torque level
                if tqd(ii) > -0.1
                    to(tipotct) = ii;
                    tipotct = tipotct +1;
                    break
                else
                end
                ct = ct+1; % increase counter
                ii = ii+1; % decrease time itteration
            end
        end
    end

    ti = unique(ti);
    to = unique(to);

    ti = ti(ti>0);if numel(ti)>=1,ind.tipin = ti;else,ind.tipin = NaN;end
    to = to(to>0);if numel(to)>=1,ind.tipot = to;else,ind.tipot = NaN;end


end

function [fitdat] = decfit(x,ind,Fs)
% DECFIT is a function that will analyze output only vibration data that
% appears to follow a SDOF decay response.
% (c) Jon Furlich 2020.

% ---------------------------------------------------------------------
%    IMPORTANT: This function assumes that x has already been band pass
%    filtered to the desired outcome removing DC components.
% ---------------------------------------------------------------------
%
% ***************** Function Inputs ***************************************
%   x - contains the filtered data with log decrement behavior
%
%   ind - is a structure variable that contains both tip in and tip out
%           events based on trigger criteria.
%
% *************************************************************************
%
% ++++++++++++++++ Function Outputs +++++++++++++++++++++++++++++++++++++
%
% fitdat - this is a structure file that holds the frequency and damping
%           values relative to the tip in and tip out data
%
% +++++++++++++++++++++++++++++++++++++++++++++++++++++++++++++++++++++++

% This function is in step with tip in and tip out function where you send
% the function time data along with indices in the data where you believe
% there is a log decrement.

% The function will then find the first five positive and netgative peaks.
% It will then attempt to fit a logarithmic curve to those peaks and return
% the frequency associated along with damping value.

% to include 0.66s of data, Fs = 1/dt therefore N = 0.66*Fs;
proj = round(1*Fs); %projection of data

%%% first analyze the tip in indicees. Assuming all frequencies are below
%%% twelve Hz then it should include ~0.66 seconds of data
    % initialize frequency estimate vector
    freqest = zeros(1,numel(ind.tipin)); zetaest = freqest; rest = freqest;
    frqtmpest = [0,0]; zeta = [0,0];
    dim = ceil(sqrt(numel(ind.tipin)));
    for ii = 1:1:numel(ind.tipin(ind.tipin+2*proj<numel(x)))
        rng = ind.tipin(ii):ind.tipin(ii)+proj;
        [~,maxind] = max(x(rng)); % find the maximum indice, use as start
        rng = ind.tipin(ii)+maxind-25:ind.tipin(ii)+maxind-25+proj;
```

```
%         [~,maxind] = max(x(rng)); % find the maximum indice, use as start

        % find the first five positive peaks assuming Fs = 1024
        % min dist 800 ~ 10 Hz (1/10*1024)
        % max dist 4096 = 2 Hz (1/2*1024)
        [pkpos,locpos] =
findpeaks(x(rng),'NPeaks',5,'MinPeakDistance',floor(Fs/15),'MinPeakHeight',0);%,'MaxPeakW
idth',512);
        % find the first six negative peaks by multiplying by -1 knowing
        % that the first peak is a filter ring artifact
        [pkneg,locneg] = findpeaks(-
1*x(rng),'NPeaks',5,'MinPeakDistance',floor(Fs/15),'MinPeakHeight',0);%,'MaxPeakWidth',51
2);
        r = [0,0];
        if numel(pkpos)>1&&numel(locpos)>1&&numel(pkneg)>1&&numel(locneg)>1
            frq = zeros(4,2); %first column positive decay, second column negative decay
            for jj = numel(locpos):-1:2
                frq(jj-1,1) = Fs/(locpos(jj)-locpos(jj-1));
            end
            for jj = numel(locneg):-1:2
                frq(jj-1,2) = Fs/(locneg(jj)-locneg(jj-1));
            end
            frqtmpest(1) = mean(frq(frq(:,1)~=0,1)); % average positive frequency
            frqtmpest(2) = mean(frq(frq(:,2)~=0,2)); % average negative frequency

            %%%% Troubleshooting Figure

            % use least square fit to calculate the decrement
            [copos] = polyfit(locpos/Fs,log(pkpos),1);
            [coneg] = polyfit(locneg/Fs,log(pkneg),1);
            % note that the first coefficient is -sigma
            zeta(1) = -1*copos(1)/2/pi/frqtmpest(1)*100;
            zeta(2) = -1*coneg(1)/2/pi/frqtmpest(2)*100;
            %estimate the correlation
            corp = corrcoef(locpos/Fs,log(pkpos));
            r(1) = corp(2,1).^2;
            corn = corrcoef(locneg/Fs,log(pkneg));
            r(2) = corn(2,1).^2;
        end
        freqest(ii) = mean(frqtmpest(r>0.5));
        zetaest(ii) = mean(zeta(r>0.5));
        rest(ii) = mean(min(r(r>0.5)));

    end

fitdat.tipin.frqest = freqest;
fitdat.tipin.zetaest = zetaest;
fitdat.tipin.corr = rest;

%%% first analyze the tip in indicees. Assuming all frequencies are below
%%% twelve Hz then it should include ~0.66 seconds of data
    % initialize frequency estimate vector
    freqest = zeros(1,numel(ind.tipot)); zetaest = freqest; rest = freqest;
    frqtmpest = [0,0]; zeta = [0,0];
    dim = ceil(sqrt(numel(ind.tipot)));
    for ii = 1:1:numel(ind.tipot(ind.tipot+2*proj<numel(x)))
        rng = ind.tipot(ii):ind.tipot(ii)+proj;
        [~,maxind] = max(x(rng)); % find the maximum indice, use as start
        rng = ind.tipot(ii)+maxind-25:ind.tipot(ii)+maxind-25+proj;
        [~,maxind] = max(x(rng)); % find the maximum indice, use as start
        % find the first five positive peaks
        [pkpos,locpos] =
findpeaks(x(rng),'NPeaks',5,'MinPeakDistance',floor(Fs/15));%,'MinPeakHeight',0,'MaxPeakW
idth',512);
        % find the first six negative peaks by multiplying by -1 knowing
        % that the first peak is a filter ring artifact
        [pkneg,locneg] = findpeaks(-
1*x(rng),'NPeaks',5,'MinPeakDistance',floor(Fs/15));%,'MaxPeakWidth',512);
```

```
        r = [0,0];
        if numel(pkpos)>1&&numel(locpos)>1&&numel(pkneg)>1&&numel(locneg)>1
            frq = zeros(4,2); %first column positive decay, second column negative decay
            for jj = numel(locpos):-1:2
                frq(jj-1,1) = Fs/(locpos(jj)-locpos(jj-1));
            end
            for jj = numel(locneg):-1:2
                frq(jj-1,2) = Fs/(locneg(jj)-locneg(jj-1));
            end
            frqtmpest(1) = mean(frq(frq(:,1)~=0,1)); % average positive frequency
            frqtmpest(2) = mean(frq(frq(:,2)~=0,2)); % average negative frequency

            % use least square fit to calculate the decrement
            [copos] = polyfit(locpos/Fs,log(pkpos),1);
            [coneg] = polyfit(locneg/Fs,log(pkneg),1);
            % note that the first coefficient is -sigma
            zeta(1) = -1*copos(1)/2/pi/frqtmpest(1)*100;
            zeta(2) = -1*coneg(1)/2/pi/frqtmpest(2)*100;
            %estimate the correlation
            corp = corrcoef(locpos/Fs,log(pkpos)); r(1) = corp(2,1).^2;
            corn = corrcoef(locneg/Fs,log(pkneg)); r(2) = corn(2,1).^2;
        end
        freqest(ii) = mean(frqtmpest(r>0.5));
        zetaest(ii) = mean(zeta(r>0.5));
        rest(ii) = mean(min(r(r>0.5)));

    end
fitdat.tipot.frqest = freqest;
fitdat.tipot.zetaest = zetaest;
fitdat.tipot.corr = rest;
end
```

The following is sample code written in MATLAB® R2018a to post process TWVDV.

```
function [ trunc ] = jefvdvat(t,f,T,ov,iv,vdvs,vdvci,tqi)
%jefvdvat is a function that will take the input data t and f and mine it for
%all time simliar to STFT
%
% ------------------------------------------------------------------------
%   t  -    is an input time vector with dimensions 1xN. The dimension N
%           should match that of f
%
%   f  -    is a matrix of all the response signals and assumed to be an
%           MxN matrix where M is the number of response signals and N is
%           the time dimension
%
%   T -     is the period of time T (s) that will be used to calculate the
%           VDV
%
%   ov -    is the percentage overlap to use.
%
%   gs -    is the row location in f where the gear position vector lies
%
%   spd -   is the row location in f where the vehicle brake speed lies
%
%   tq -    is the row location in f where the telemetry torque lies
%
%   iv -    is a two column matrix that contains the rows in f that will be
%           compared to one another when computing the impact velocity
%
%   vdvci - are the rows in ft that correspond to accelerometers that we
%           wish to analyze for VDV metrics
%
%   vdvs -  scaling factor from iso 2631
%
% ------------------------------------------------------------------------

% First, perform some checks on the inputs
a = size(t); b = size(f);
if a(2) == b(2)

    % +++++++++++++++++ FUNCTION IS HERE ++++++++++++++++++++++++++
        % This function of all time will calculate the VDV function over
        % all time. It will take blocks of 4 seconds worth of data with a
        % 75% overlap of the data and decimate it down to 256 hz

%         ov = 0.75; % 75% overlap
%         T = 4; % four seconds of time
        tt = t(end); % total amount of time available
        dt = t(2)-t(1); %time increment
        Nov = floor((T*(1-ov))/dt);%number of increments for overlap
        Nts = floor((t(end)-(T*ov))/(T*(1-ov))); %number of points to calculate
        N = round(T/dt);
         % decimate the dater, knowing its at 8192 want 256
            orig = round(1/dt); newsa = 256;
            decrate = orig/newsa; ny = newsa/orig;
%             [bb,aa] = cheby1(8,2,ny);
            n = 8;[bb,aa] = fir1(n,ny,'low',hamming(n+1));clear n
    for ii = 1:1:Nts
%         Nov
%         N
        rng = 1+(ii-1)*Nov:1+(ii-1)*Nov+N;
%         numel(rng)
        trunc.ti(ii,:) = downsample(t(rng),decrate);
        trunc.tq(ii,:) = filtfilt(bb,aa,downsample(f(tqi,rng),decrate));

            if (f(tqi,rng(1)))<10 && (f(tqi,rng(end)))>10,trunc.tin(ii) = 1;
                else,trunc.tin(ii) = 0;end
            if (f(tqi,rng(end)))<10 && (f(tqi,rng(1)))>10,trunc.tot(ii) = 1;
```

```
                else,trunc.tot(ii) = 0;end
            if (f(tqi,rng(1)))<10 && max(f(tqi,rng(:)))>10 && trunc.tin(ii) ~=
1,trunc.sb(ii) = 1;
                else,trunc.sb(ii) = 0;end
        for kk = 1:1:numel(vdvci)
            trunc.xi(kk,:,ii) = filtfilt(bb,aa,downsample(f(vdvci(kk),rng),decrate));
            [trunc.vdv(kk,:,ii),~] = VDV(trunc.ti(ii,:),...
                        squeeze(trunc.xi(kk,:,ii))',squeeze(trunc.tq(ii,:))',vdvs(kk));
            trunc.meantime(ii) = mean(t(rng));
        end
        for jj = 1:1:numel(iv.row(:,1))
            if numel(f(:,1)) > 30
            % determine the gear state
            trunc.gear(ii) = floor(mean(f(65,rng))); %gear position in f
            if trunc.gear(ii) == 0, trunc.gear(ii) = 1;end
                % Run this line of code if you want m/s
    %             trunc.iv(jj,:,ii) = trunc.ft(iv.row(jj,1),:,ii)*iv.rad(jj,1) - ...
    %                                 trunc.ft(iv.row(jj,2),:,ii)*iv.rad(jj,2);
%calculate impact delta velocity
                % Run this line of code if you want (rpm) reflected on trans
                % out
    %             trunc.iv(jj,:,ii)
                ivtemp = f(iv.row(jj,1),rng)*...
                    iv.proj(iv.prow(jj,1),trunc.gear(ii)) - ...
                                f(iv.row(jj,2),rng)*...
                    iv.proj(iv.prow(jj,2),trunc.gear(ii)); %calculate impact delta
velocity

                [trunc.ivmax(jj,ii),trunc.ind(jj,ii)] = max(ivtemp); %max delta velocity
                trunc.drtqatmax(jj,ii) = f(64,rng(1)+trunc.ind(jj,ii));%driverrqtorque
                trunc.ivmin(jj,ii) = min(ivtemp); %min delta velocity
            end
        end
    end

elseif a(1) > 1
    error('Incorrect input time vector t, must be size 1xM')
else
    error('Time and Response Channel lengths differ')
end

end

function [ metrics,xw ] = VDV(t,x,tq,s)
% t - time vector
% x - truncated set of data to process
% tq - torque vector, is a DC coupled signal or should be
% s - weighitng factor to apply according to ISO2631

%VDV calculates ISO 2631 metrics relevant to VDV
%   Metrics for x as a function of time are calculated such as
%   Crest Factor - ratio of max transient to rms value in time domain
%
%   rms - root mean squared
%
%   rmq - root mean quad
%
%   VDV - vibration dose value
%
%   MTVV - max transient value

N = numel(x);
dt = t(2)-t(1);
T = N*dt;
Fs = 1/dt;
df = 1/T;
hz = 0:df:Fs/2;
```

```
% fft the data, weight it, then ifft back
wf = wfiso(hz,s);
if rem(numel(x),2) == 0
    sf = abs([wf,fliplr(wf(2:end-1))]);
else
    sf= abs([wf,fliplr(wf(2:end))]);
end
xw = ifft((fft(x.*hann(numel(x)))'.*sf)');
tq = [diff(tq);0];
tqw = ifft((fft(tq.*hann(numel(tq)))'.*sf)');
% disp('size xw'),size(xw)
% calculate max value
mtvv = max(abs(xw));
% disp('size mtvv'),size(mtvv)

% calculate rms value
xrms = rms(xw);
% disp('size xrms'),size(xrms)

% calculate the crest factor
cf = mtvv/xrms;
% disp('size cf'),size(cf)

% frequency domain crest factor
% cff = max(abs(2/N*fft(xw)))/rms(abs(2/N*fft(xw)))*df;
% cff = max(abs(2/N*fft(xw)))/xrms;

% calculate weighted rms
% twrms = sqrt(1/T*trapz(xw.*xw)*dt);

% calculate time weighted rmq
twrmq = sqrt(sqrt(1/T*trapz(xw.*xw.*xw.*xw)*dt));
% disp('size twrmq'),size(twrmq)

% calculate time weighted VDV
twvdv = sqrt(sqrt(trapz(xw.*xw.*xw.*xw)*dt));
% disp('size twvdv'),size(twvdv)

% calculate VDV/a_w*T^0.25 ratio, equates to 1.75
ratvdv = twvdv/(xrms*T^0.25);
% disp('size ratvdv'),size(ratvdv)

% calculate torque weighted vdv
tqvdv = sqrt(sqrt(trapz(tqw.*tqw.*tqw.*tqw)*dt));
tqwvdv = sqrt(twvdv.*tqvdv);

% metrics = [cf,cff,twrms,twrmq,twvdv];
metrics = [cf,xrms,twrmq,twvdv,ratvdv,mtvv,tqwvdv,tqvdv];

end

function [wf] = wfiso(p,s)
%wfiso is a function that returns the weighting coefficents according to
%ISO 2631
%
%   p   - is a discrete frequency vector
%
%   s   - is the weighting designation options are k, d, f, c, e, or j
%

if strcmp(s,'k') == 1
    w = [0.4,100,12.5,12.5,2.37,3.35];
    q = [0.63,0.91,0.91];
elseif strcmp(s,'d') == 1
    w = [0.4,100,2,2,0.63,10000,10000];
    q = [0.63,1,1];
elseif strcmp(s,'f') == 1
    w = [0.08,0.63,Inf,0.25,0.0625,0.1];
```

```
    q = [0.86,0.8,0.8];
elseif strcmp(s,'c') == 1
    w = [0.4,100,8,8,100000,100000];
    q = [0.63,1,1];
elseif strcmp(s,'e') == 1
    w = [0.4,100,1,1,100000,100000];
    q = [0.63,1,1];
elseif strcmp(s,'j') == 1
    w = [0.4,100,Inf,Inf,3.75,5.32];
    q = [1,0.91,0.91];
else
    error('Incorrect weighting designation s')
end

% High pass filters
gh = (1./(1+sqrt(2)*w(1)./(1j.*p)+(w(1)./(1j.*p)).^2));

% Low Pass Filter
gl = (1./(1+sqrt(2).*1j.*p./(w(2))+(1j.*p/(w(2))).^2));

% Acceleration-velocity transition
gt = ((1+1j.*p./w(3))./...
    (1+1j.*p./(q(1)*w(4))+(1j.*p./w(4)).^2));

% Upward Step (proportionality to jerk)
gs = ((1+1j.*p./(q(2).*w(5))+(1j.*p./w(5)).^2)./...
    (1+1j.*p./(q(2).*w(6))+(1j.*p./w(6)).^2).*...
    (w(5)/w(6)).^2);

% Total Weighting Function
wf = gh.*gl.*gt.*gs;

% clip weighting function for out of band elements.
if strcmp(s,'k') == 1
    wf(p<0.1) = 0;
    wf(p>400) = 0;
elseif strcmp(s,'d') == 1
    wf(p<0.1) = 0;
    wf(p>400) = 0;
elseif strcmp(s,'f') == 1
    wf(p<0.02) = 0;
    wf(p>4) = 0;
elseif strcmp(s,'c') == 1
    wf(p<0.02) = 0;
    wf(p>400) = 0;
elseif strcmp(s,'e') == 1
    wf(p<0.02) = 0;
    wf(p>400) = 0;
elseif strcmp(s,'j') == 1
    wf(p<0.02) = 0;
    wf(p>400) = 0;
end

end

function [ metrics,xw ] = VDVButter(t,x,s)
%VDV calculates ISO 2631 metrics relevant to VDV
%   Metrics for x as a function of time are calculated such as
%   Crest Factor - ratio of max transient to rms value in time domain
%
%   rms - root mean squared
%
%   rmq - root mean quad
%
%   VDV - vibration dose value
%
%   MTVV - max transient value
```

```
N = numel(x);
dt = t(2)-t(1);
T = N*dt;
Fs = 1/dt;
df = 1/T;
hz = 0:df:Fs/2;

% apply butterworth filter
if strcmp(s,'k') == 1
    bpf = [0.4,100];
elseif strcmp(s,'d') == 1
    bpf = [0.4,100];
elseif strcmp(s,'f') == 1
    bpf = [0.08,0.63];
elseif strcmp(s,'c') == 1
    bpf = [0.4,100];
elseif strcmp(s,'e') == 1
    bpf = [0.4,100];
elseif strcmp(s,'j') == 1
    bpf = [0.4,100];
end

[b,a] = butter(2,bpf/Fs,'bandpass');

xw = filtfilt(b,a,x);

% calculate max value
mtvv = max(abs(xw));

% calculate rms value
xrms = rms(xw);

% calculate the crest factor
cf = mtvv/xrms;

% frequency domain crest factor
% cff = max(abs(2/N*fft(xw)))/rms(abs(2/N*fft(xw)))*df;
% cff = max(abs(2/N*fft(xw)))/xrms;

% calculate weighted rms
% twrms = sqrt(1/T*trapz(xw.*xw)*dt);

% calculate weighted rmq
twrmq = sqrt(sqrt(1/T*trapz(xw.*xw.*xw.*xw)*dt));

% calculate weighted VDV
twvdv = sqrt(sqrt(trapz(xw.*xw.*xw.*xw)*dt));

% calculate VDV/a_w*T^0.25 ratio, equates to 1.75
ratvdv = twvdv/(xrms*T^0.25);

% metrics = [cf,cff,twrms,twrmq,twvdv];
metrics = [cf,xrms,twrmq,twvdv,ratvdv,mtvv];

end

function [ alpha,td ] = omega2alpha(w,t,decra,Fs,lpcf)
%omega2alpha converts a shaft rotational speed to acceleration
%
%   w       - omega represents a vector of shaft speed
%
%   t       - this is the respective time vector to omega
%
%   decra   - this is the decimation rate
%
%   Fs      - this is the sample frequency of omega, should equal
%               1/(t(2)-t(1)) and thus may be unneccesary
%
```

```
%   lpcf    - this is the low pass cuttoff frequency

Fn = Fs/2/decra; % Nyquist frequency at decimated rate for LPF

if lpcf < Fn
    [b,a] = butter(4,lpcf/Fn,'low');
else
    [b,a] = butter(4,0.85,'low');
    disp('Selected Cuttoff Frequency is too high for decimation rate')
    disp('Cuttoff frequency defaulted to 85% nyquist')
end

% decimate the data
tmp = decimate(w,decra); %temporary decimated vector
td = downsample(t,decra); %new time vector, use downsample not decimate
td = td(1:end-1); %because the first difference loses a data point, the
        % time vector must also neglect one data point

% compute the first difference
alpha = diff(tmp,1)*Fn*2; % multiplied by Fn to normalize by time resolution

% low pass filter to desired frequency
alpha = filtfilt(b,a,alpha);

end
```

12. Appendix G: Copyright Use Permissions

Copyright Clearance Center Marketplace™

SAE International - License Terms and Conditions

This is a License Agreement between Jon Furlich - Michigan Technological University ("You") and SAE International ("Publisher") provided by Copyright Clearance Center ("CCC"). The license consists of your order details, the terms and conditions provided by SAE International, and the CCC terms and conditions.

All payments must be made in full to CCC.

Order Date	18-Sep-2020	Type of Use	Republish in a thesis/dissertation
Order license ID	1064043-2		
ISBN-13	9781560911999	Publisher	SOCIETY OF AUTOMOTIVE ENGINEERS, INCORPORATED
		Portion	Image/photo/illustration

LICENSED CONTENT

Publication Title	Fundamentals of vehicle dynamics	Country	United States of America
		Rightsholder	SAE International
Author/Editor	GILLESPIE, T. D.	Publication Type	Book
Date	01/01/1992		
Language	English		

REQUEST DETAILS

Portion Type	Image/photo/illustration	Distribution	United States
Number of images / photos / illustrations	1	Translation	Original language of publication
Format (select all that apply)	Print, Electronic	Copies for the disabled?	No
		Minor editing privileges?	No
Who will republish the content?	Academic institution	Incidental promotional use?	No
Duration of Use	Life of current edition	Currency	USD
Lifetime Unit Quantity	Up to 499		
Rights Requested	Main product		

NEW WORK DETAILS

Title	Experimental Evaluation of a RWD Vehicle with Parameter Extraction for Analytical Modeling and Evaluation	Institution name	Michigan Technological University
		Expected presentation date	2020-09-25
Instructor name	Jon Furlich		

ADDITIONAL DETAILS

Order reference number	N/A

The requesting person / organization to appear on the license	Jon Furlich - Michigan Technological University

REUSE CONTENT DETAILS

Title, description or numeric reference of the portion(s)	Figure 2.11	Title of the article/chapter the portion is from	Chapter 2 - Acceleration Performance
Editor of portion(s)	N/A	Author of portion(s)	GILLESPIE, T. D.
Volume of serial or monograph	N/A	Issue, if republishing an article from a serial	N/A
Page or page range of portion	37	Publication date of portion	1992-01-01

CCC Republication Terms and Conditions

1. Description of Service; Defined Terms. This Republication License enables the User to obtain licenses for republication of one or more copyrighted works as described in detail on the relevant Order Confirmation (the "Work(s)"). Copyright Clearance Center, Inc. ("CCC") grants licenses through the Service on behalf of the rightsholder identified on the Order Confirmation (the "Rightsholder"). "Republication", as used herein, generally means the inclusion of a Work, in whole or in part, in a new work or works, also as described on the Order Confirmation. "User", as used herein, means the person or entity making such republication.

2. The terms set forth in the relevant Order Confirmation, and any terms set by the Rightsholder with respect to a particular Work, govern the terms of use of Works in connection with the Service. By using the Service, the person transacting for a republication license on behalf of the User represents and warrants that he/she/it (a) has been duly authorized by the User to accept, and hereby does accept, all such terms and conditions on behalf of User, and (b) shall inform User of all such terms and conditions. In the event such person is a "freelancer" or other third party independent of User and CCC, such party shall be deemed jointly a "User" for purposes of these terms and conditions. In any event, User shall be deemed to have accepted and agreed to all such terms and conditions if User republishes the Work in any fashion.

3. Scope of License; Limitations and Obligations.

   3.1. All Works and all rights therein, including copyright rights, remain the sole and exclusive property of the Rightsholder. The license created by the exchange of an Order Confirmation (and/or any invoice) and payment by User of the full amount set forth on that document includes only those rights expressly set forth in the Order Confirmation and in these terms and conditions, and conveys no other rights in the Work(s) to User. All rights not expressly granted are hereby reserved.

   3.2. General Payment Terms: You may pay by credit card or through an account with us payable at the end of the month. If you and we agree that you may establish a standing account with CCC, then the following terms apply: Remit Payment to: Copyright Clearance Center, 29118 Network Place, Chicago, IL 60673-1291. Payments Due: Invoices are payable upon their delivery to you (or upon our notice to you that they are available to you for downloading). After 30 days, outstanding amounts will be subject to a service charge of 1-1/2% per month or, if less, the maximum rate allowed by applicable law. Unless otherwise specifically set forth in the Order Confirmation or in a separate written agreement signed by CCC, invoices are due and payable on "net 30" terms. While User may exercise the rights licensed immediately upon issuance of the Order Confirmation, the license is automatically revoked and is null and void, as if it had never been issued, if complete payment for the license is not received on a timely basis either from User directly or through a payment agent, such as a credit card company.

   3.3. Unless otherwise provided in the Order Confirmation, any grant of rights to User (i) is "one-time" (including the editions and product family specified in the license), (ii) is non-exclusive and non-transferable and (iii)

is subject to any and all limitations and restrictions (such as, but not limited to, limitations on duration of use or circulation) included in the Order Confirmation or invoice and/or in these terms and conditions. Upon completion of the licensed use, User shall either secure a new permission for further use of the Work(s) or immediately cease any new use of the Work(s) and shall render inaccessible (such as by deleting or by removing or severing links or other locators) any further copies of the Work (except for copies printed on paper in accordance with this license and still in User's stock at the end of such period).

3.4. In the event that the material for which a republication license is sought includes third party materials (such as photographs, illustrations, graphs, inserts and similar materials) which are identified in such material as having been used by permission, User is responsible for identifying, and seeking separate licenses (under this Service or otherwise) for, any of such third party materials; without a separate license, such third party materials may not be used.

3.5. Use of proper copyright notice for a Work is required as a condition of any license granted under the Service. Unless otherwise provided in the Order Confirmation, a proper copyright notice will read substantially as follows: "Republished with permission of [Rightsholder's name], from [Work's title, author, volume, edition number and year of copyright]; permission conveyed through Copyright Clearance Center, Inc. " Such notice must be provided in a reasonably legible font size and must be placed either immediately adjacent to the Work as used (for example, as part of a by-line or footnote but not as a separate electronic link) or in the place where substantially all other credits or notices for the new work containing the republished Work are located. Failure to include the required notice results in loss to the Rightsholder and CCC, and the User shall be liable to pay liquidated damages for each such failure equal to twice the use fee specified in the Order Confirmation, in addition to the use fee itself and any other fees and charges specified.

3.6. User may only make alterations to the Work if and as expressly set forth in the Order Confirmation. No Work may be used in any way that is defamatory, violates the rights of third parties (including such third parties' rights of copyright, privacy, publicity, or other tangible or intangible property), or is otherwise illegal, sexually explicit or obscene. In addition, User may not conjoin a Work with any other material that may result in damage to the reputation of the Rightsholder. User agrees to inform CCC if it becomes aware of any infringement of any rights in a Work and to cooperate with any reasonable request of CCC or the Rightsholder in connection therewith.

4. Indemnity. User hereby indemnifies and agrees to defend the Rightsholder and CCC, and their respective employees and directors, against all claims, liability, damages, costs and expenses, including legal fees and expenses, arising out of any use of a Work beyond the scope of the rights granted herein, or any use of a Work which has been altered in any unauthorized way by User, including claims of defamation or infringement of rights of copyright, publicity, privacy or other tangible or intangible property.

5. Limitation of Liability. UNDER NO CIRCUMSTANCES WILL CCC OR THE RIGHTSHOLDER BE LIABLE FOR ANY DIRECT, INDIRECT, CONSEQUENTIAL OR INCIDENTAL DAMAGES (INCLUDING WITHOUT LIMITATION DAMAGES FOR LOSS OF BUSINESS PROFITS OR INFORMATION, OR FOR BUSINESS INTERRUPTION) ARISING OUT OF THE USE OR INABILITY TO USE A WORK, EVEN IF ONE OF THEM HAS BEEN ADVISED OF THE POSSIBILITY OF SUCH DAMAGES. In any event, the total liability of the Rightsholder and CCC (including their respective employees and directors) shall not exceed the total amount actually paid by User for this license. User assumes full liability for the actions and omissions of its principals, employees, agents, affiliates, successors and assigns.

6. Limited Warranties. THE WORK(S) AND RIGHT(S) ARE PROVIDED "AS IS". CCC HAS THE RIGHT TO GRANT TO USER THE RIGHTS GRANTED IN THE ORDER CONFIRMATION DOCUMENT. CCC AND THE RIGHTSHOLDER DISCLAIM ALL OTHER WARRANTIES RELATING TO THE WORK(S) AND RIGHT(S), EITHER EXPRESS OR IMPLIED, INCLUDING WITHOUT LIMITATION IMPLIED WARRANTIES OF MERCHANTABILITY OR FITNESS FOR A PARTICULAR PURPOSE. ADDITIONAL RIGHTS MAY BE REQUIRED TO USE ILLUSTRATIONS, GRAPHS, PHOTOGRAPHS, ABSTRACTS, INSERTS OR OTHER PORTIONS OF THE WORK (AS OPPOSED TO THE ENTIRE WORK) IN A MANNER CONTEMPLATED BY USER; USER UNDERSTANDS AND AGREES THAT NEITHER CCC NOR THE RIGHTSHOLDER MAY HAVE SUCH ADDITIONAL RIGHTS TO GRANT.

7. Effect of Breach. Any failure by User to pay any amount when due, or any use by User of a Work beyond the scope of the license set forth in the Order Confirmation and/or these terms and conditions, shall be a material breach of the license created by the Order Confirmation and these terms and conditions. Any breach not cured within 30 days of written notice thereof shall result in immediate termination of such license without further notice. Any unauthorized (but licensable) use of a Work that is terminated immediately upon notice thereof may be liquidated by payment of the Rightsholder's ordinary license price therefor; any unauthorized (and unlicensable) use that is not terminated immediately for any reason (including, for example, because materials containing the Work cannot reasonably be recalled) will be subject to all remedies available at law or in equity, but in no event to a payment of less than three times the Rightsholder's ordinary license price for the most closely analogous licensable use plus Rightsholder's and/or CCC's costs and expenses incurred in collecting such payment.

8. Miscellaneous.

   8.1. User acknowledges that CCC may, from time to time, make changes or additions to the Service or to these terms and conditions, and CCC reserves the right to send notice to the User by electronic mail or otherwise for the purposes of notifying User of such changes or additions; provided that any such changes or additions shall not apply to permissions already secured and paid for.

   8.2. Use of User-related information collected through the Service is governed by CCC's privacy policy, available online here:https://marketplace.copyright.com/rs-ui-web/mp/privacy-policy

   8.3. The licensing transaction described in the Order Confirmation is personal to User. Therefore, User may not assign or transfer to any other person (whether a natural person or an organization of any kind) the license created by the Order Confirmation and these terms and conditions or any rights granted hereunder; provided, however, that User may assign such license in its entirety on written notice to CCC in the event of a transfer of all or substantially all of User's rights in the new material which includes the Work(s) licensed under this Service.

   8.4. No amendment or waiver of any terms is binding unless set forth in writing and signed by the parties. The Rightsholder and CCC hereby object to any terms contained in any writing prepared by the User or its principals, employees, agents or affiliates and purporting to govern or otherwise relate to the licensing transaction described in the Order Confirmation, which terms are in any way inconsistent with any terms set forth in the Order Confirmation and/or in these terms and conditions or CCC's standard operating procedures, whether such writing is prepared prior to, simultaneously with or subsequent to the Order Confirmation, and whether such writing appears on a copy of the Order Confirmation or in a separate instrument.

   8.5. The licensing transaction described in the Order Confirmation document shall be governed by and construed under the law of the State of New York, USA, without regard to the principles thereof of conflicts of law. Any case, controversy, suit, action, or proceeding arising out of, in connection with, or related to such licensing transaction shall be brought, at CCC's sole discretion, in any federal or state court located in the County of New York, State of New York, USA, or in any federal or state court whose geographical jurisdiction covers the location of the Rightsholder set forth in the Order Confirmation. The parties expressly submit to the personal jurisdiction and venue of each such federal or state court.If you have any comments or questions about the Service or Copyright Clearance Center, please contact us at 978-750-8400 or send an e-mail to support@copyright.com.

v 1.1

Copyright Clearance Center Marketplace™

SAE International - License Terms and Conditions

This is a License Agreement between Jon Furlich - Michigan Technological University ("You") and SAE International ("Publisher") provided by Copyright Clearance Center ("CCC"). The license consists of your order details, the terms and conditions provided by SAE International, and the CCC terms and conditions.

All payments must be made in full to CCC.

Order Date	18-Sep-2020	Type of Use	Republish in a thesis/dissertation
Order license ID	1064043-1		
System ID	920762	Publisher	SAE International
		Portion	Image/photo/illustration

LICENSED CONTENT

Publication Title	Dynamic Analysis of Automotive Gearing Systems	Country	United States of America
		Rightsholder	SAE International
Author/Editor	Donley, Mark G.	Publication Type	Report
Date	01/01/1992		

REQUEST DETAILS

Portion Type	Image/photo/illustration	Distribution	United States
Number of images / photos / illustrations	1	Translation	Original language of publication
Format (select all that apply)	Print, Electronic	Copies for the disabled?	No
		Minor editing privileges?	No
Who will republish the content?	Academic institution	Incidental promotional use?	No
Duration of Use	Life of current edition	Currency	USD
Lifetime Unit Quantity	Up to 499		
Rights Requested	Main product		

NEW WORK DETAILS

Title	Experimental Evaluation of a RWD Vehicle with Parameter Extraction for Analytical Modeling and Evaluation	Institution name	Michigan Technological University
		Expected presentation date	2020-09-25
Instructor name	Jon Furlich		

ADDITIONAL DETAILS

Order reference number	N/A	The requesting person / organization to appear on the license	Jon Furlich - Michigan Technological University

REUSE CONTENT DETAILS

Title, description or numeric reference of the portion(s)	Figure 6/ Reaction forces acting on the gear teeth at the mesh for drive and coast conditions	Title of the article/chapter the portion is from	Dynamic analysis of automotive gearing systems/Bevel and hypoid gear sets
Editor of portion(s)	N/A	Author of portion(s)	Donley, Mark G.
Volume of serial or monograph	N/A	Issue, if republishing an article from a serial	N/A
Page or page range of portion	8	Publication date of portion	1992-01-01

CCC Republication Terms and Conditions

1. Description of Service; Defined Terms. This Republication License enables the User to obtain licenses for republication of one or more copyrighted works as described in detail on the relevant Order Confirmation (the "Work(s)"). Copyright Clearance Center, Inc. ("CCC") grants licenses through the Service on behalf of the rightsholder identified on the Order Confirmation (the "Rightsholder"). "Republication", as used herein, generally means the inclusion of a Work, in whole or in part, in a new work or works, also as described on the Order Confirmation. "User", as used herein, means the person or entity making such republication.

2. The terms set forth in the relevant Order Confirmation, and any terms set by the Rightsholder with respect to a particular Work, govern the terms of use of Works in connection with the Service. By using the Service, the person transacting for a republication license on behalf of the User represents and warrants that he/she/it (a) has been duly authorized by the User to accept, and hereby does accept, all such terms and conditions on behalf of User, and (b) shall inform User of all such terms and conditions. In the event such person is a "freelancer" or other third party independent of User and CCC, such party shall be deemed jointly a "User" for purposes of these terms and conditions. In any event, User shall be deemed to have accepted and agreed to all such terms and conditions if User republishes the Work in any fashion.

3. Scope of License; Limitations and Obligations.

   3.1. All Works and all rights therein, including copyright rights, remain the sole and exclusive property of the Rightsholder. The license created by the exchange of an Order Confirmation (and/or any invoice) and payment by User of the full amount set forth on that document includes only those rights expressly set forth in the Order Confirmation and in these terms and conditions, and conveys no other rights in the Work(s) to User. All rights not expressly granted are hereby reserved.

   3.2. General Payment Terms: You may pay by credit card or through an account with us payable at the end of the month. If you and we agree that you may establish a standing account with CCC, then the following terms apply: Remit Payment to: Copyright Clearance Center, 29118 Network Place, Chicago, IL 60673-1291. Payments Due: Invoices are payable upon their delivery to you (or upon our notice to you that they are available to you for downloading). After 30 days, outstanding amounts will be subject to a service charge of 1-1/2% per month or, if less, the maximum rate allowed by applicable law. Unless otherwise specifically set forth in the Order Confirmation or in a separate written agreement signed by CCC, invoices are due and payable on "net 30" terms. While User may exercise the rights licensed immediately upon issuance of the Order Confirmation, the license is automatically revoked and is null and void, as if it had never been issued, if complete payment for the license is not received on a timely basis either from User directly or through a payment agent, such as a credit card company.

   3.3. Unless otherwise provided in the Order Confirmation, any grant of rights to User (i) is "one-time" (including the editions and product family specified in the license), (ii) is non-exclusive and non-transferable and (iii) is subject to any and all limitations and restrictions (such as, but not limited to, limitations on duration of use or circulation) included in the Order Confirmation or invoice and/or in these terms and conditions. Upon completion of the licensed use, User shall either secure a new permission for further use of the

Work(s) or immediately cease any new use of the Work(s) and shall render inaccessible (such as by deleting or by removing or severing links or other locators) any further copies of the Work (except for copies printed on paper in accordance with this license and still in User's stock at the end of such period).

3.4. In the event that the material for which a republication license is sought includes third party materials (such as photographs, illustrations, graphs, inserts and similar materials) which are identified in such material as having been used by permission, User is responsible for identifying, and seeking separate licenses (under this Service or otherwise) for, any of such third party materials; without a separate license, such third party materials may not be used.

3.5. Use of proper copyright notice for a Work is required as a condition of any license granted under the Service. Unless otherwise provided in the Order Confirmation, a proper copyright notice will read substantially as follows: "Republished with permission of [Rightsholder's name], from [Work's title, author, volume, edition number and year of copyright]; permission conveyed through Copyright Clearance Center, Inc. " Such notice must be provided in a reasonably legible font size and must be placed either immediately adjacent to the Work as used (for example, as part of a by-line or footnote but not as a separate electronic link) or in the place where substantially all other credits or notices for the new work containing the republished Work are located. Failure to include the required notice results in loss to the Rightsholder and CCC, and the User shall be liable to pay liquidated damages for each such failure equal to twice the use fee specified in the Order Confirmation, in addition to the use fee itself and any other fees and charges specified.

3.6. User may only make alterations to the Work if and as expressly set forth in the Order Confirmation. No Work may be used in any way that is defamatory, violates the rights of third parties (including such third parties' rights of copyright, privacy, publicity, or other tangible or intangible property), or is otherwise illegal, sexually explicit or obscene. In addition, User may not conjoin a Work with any other material that may result in damage to the reputation of the Rightsholder. User agrees to inform CCC if it becomes aware of any infringement of any rights in a Work and to cooperate with any reasonable request of CCC or the Rightsholder in connection therewith.

4. Indemnity. User hereby indemnifies and agrees to defend the Rightsholder and CCC, and their respective employees and directors, against all claims, liability, damages, costs and expenses, including legal fees and expenses, arising out of any use of a Work beyond the scope of the rights granted herein, or any use of a Work which has been altered in any unauthorized way by User, including claims of defamation or infringement of rights of copyright, publicity, privacy or other tangible or intangible property.

5. Limitation of Liability. UNDER NO CIRCUMSTANCES WILL CCC OR THE RIGHTSHOLDER BE LIABLE FOR ANY DIRECT, INDIRECT, CONSEQUENTIAL OR INCIDENTAL DAMAGES (INCLUDING WITHOUT LIMITATION DAMAGES FOR LOSS OF BUSINESS PROFITS OR INFORMATION, OR FOR BUSINESS INTERRUPTION) ARISING OUT OF THE USE OR INABILITY TO USE A WORK, EVEN IF ONE OF THEM HAS BEEN ADVISED OF THE POSSIBILITY OF SUCH DAMAGES. In any event, the total liability of the Rightsholder and CCC (including their respective employees and directors) shall not exceed the total amount actually paid by User for this license. User assumes full liability for the actions and omissions of its principals, employees, agents, affiliates, successors and assigns.

6. Limited Warranties. THE WORK(S) AND RIGHT(S) ARE PROVIDED "AS IS". CCC HAS THE RIGHT TO GRANT TO USER THE RIGHTS GRANTED IN THE ORDER CONFIRMATION DOCUMENT. CCC AND THE RIGHTSHOLDER DISCLAIM ALL OTHER WARRANTIES RELATING TO THE WORK(S) AND RIGHT(S), EITHER EXPRESS OR IMPLIED, INCLUDING WITHOUT LIMITATION IMPLIED WARRANTIES OF MERCHANTABILITY OR FITNESS FOR A PARTICULAR PURPOSE. ADDITIONAL RIGHTS MAY BE REQUIRED TO USE ILLUSTRATIONS, GRAPHS, PHOTOGRAPHS, ABSTRACTS, INSERTS OR OTHER PORTIONS OF THE WORK (AS OPPOSED TO THE ENTIRE WORK) IN A MANNER CONTEMPLATED BY USER; USER UNDERSTANDS AND AGREES THAT NEITHER CCC NOR THE RIGHTSHOLDER MAY HAVE SUCH ADDITIONAL RIGHTS TO GRANT.

7. Effect of Breach. Any failure by User to pay any amount when due, or any use by User of a Work beyond the scope of the license set forth in the Order Confirmation and/or these terms and conditions, shall be a material breach of

the license created by the Order Confirmation and these terms and conditions. Any breach not cured within 30 days of written notice thereof shall result in immediate termination of such license without further notice. Any unauthorized (but licensable) use of a Work that is terminated immediately upon notice thereof may be liquidated by payment of the Rightsholder's ordinary license price therefor; any unauthorized (and unlicensable) use that is not terminated immediately for any reason (including, for example, because materials containing the Work cannot reasonably be recalled) will be subject to all remedies available at law or in equity, but in no event to a payment of less than three times the Rightsholder's ordinary license price for the most closely analogous licensable use plus Rightsholder's and/or CCC's costs and expenses incurred in collecting such payment.

8. Miscellaneous.

8.1. User acknowledges that CCC may, from time to time, make changes or additions to the Service or to these terms and conditions, and CCC reserves the right to send notice to the User by electronic mail or otherwise for the purposes of notifying User of such changes or additions; provided that any such changes or additions shall not apply to permissions already secured and paid for.

8.2. Use of User-related information collected through the Service is governed by CCC's privacy policy, available online here:https://marketplace.copyright.com/rs-ui-web/mp/privacy-policy

8.3. The licensing transaction described in the Order Confirmation is personal to User. Therefore, User may not assign or transfer to any other person (whether a natural person or an organization of any kind) the license created by the Order Confirmation and these terms and conditions or any rights granted hereunder; provided, however, that User may assign such license in its entirety on written notice to CCC in the event of a transfer of all or substantially all of User's rights in the new material which includes the Work(s) licensed under this Service.

8.4. No amendment or waiver of any terms is binding unless set forth in writing and signed by the parties. The Rightsholder and CCC hereby object to any terms contained in any writing prepared by the User or its principals, employees, agents or affiliates and purporting to govern or otherwise relate to the licensing transaction described in the Order Confirmation, which terms are in any way inconsistent with any terms set forth in the Order Confirmation and/or in these terms and conditions or CCC's standard operating procedures, whether such writing is prepared prior to, simultaneously with or subsequent to the Order Confirmation, and whether such writing appears on a copy of the Order Confirmation or in a separate instrument.

8.5. The licensing transaction described in the Order Confirmation document shall be governed by and construed under the law of the State of New York, USA, without regard to the principles thereof of conflicts of law. Any case, controversy, suit, action, or proceeding arising out of, in connection with, or related to such licensing transaction shall be brought, at CCC's sole discretion, in any federal or state court located in the County of New York, State of New York, USA, or in any federal or state court whose geographical jurisdiction covers the location of the Rightsholder set forth in the Order Confirmation. The parties expressly submit to the personal jurisdiction and venue of each such federal or state court.If you have any comments or questions about the Service or Copyright Clearance Center, please contact us at 978-750-8400 or send an e-mail to support@copyright.com.

v 1.1